



**DOCTORAL THESIS**

**Can two wrongs make a right?**

Investigating F508del-CFTR rescue with second-site  
mutations using a new fluorescence assay for high content  
CFTR screening

*Author*  
Stella Prins

*Supervisor*  
Dr Paola Vergani

submitted to  
**University College London**  
for the degree of  
**Doctor of Philosophy**

Department of Neuroscience, Physiology and Pharmacology  
University College London  
July 2020

*I, Stella Prins, confirm that the work presented in this thesis is my own. Where information has been derived from other sources, this has been indicated in the thesis.*

## Abstract

The cystic fibrosis transmembrane conductance regulator (CFTR) is an anion channel that is primarily expressed in epithelial cells where it regulates the transepithelial transport of salt and water. Mutations in the *CFTR* gene can cause cystic fibrosis, and a deletion of the phenylalanine at site 508, F508del, is the most common mutation associated with cystic fibrosis. F508del impairs both biogenesis and gating of CFTR. Instead of being trafficked to the cell membrane, F508del-CFTR is almost completely retained at the endoplasmic reticulum (ER) where it is eventually degraded. The little F508del-CFTR that makes it to the cell membrane has decreased stability and defective gating.

This thesis describes the development and validation of a fluorescence-based assay capable of fast and simultaneous quantification of CFTR channel function and membrane proximity in live human embryonic kidney (HEK-293) cells. We constructed a pIRES2-mCherry-YFPCFTR plasmid that directs co-expression of mCherry and CFTR with a halide-sensitive YFP (YFP(H148Q/I152L)) tagged to its N-terminal. The mCherry expression makes it possible to identify the borders of cells, corresponding to the location of the cell membrane. YFP(H148Q/I152L)-CFTR that colocalises with the border, is used to estimate the amount of CFTR in close proximity of the membrane. Function of CFTR is quantified by analysis of the rate of YFP quenching in response to the influx of iodide.

We used the assay to systematically search for mutations in *cis* with F508del that have the potential to rescue F508del-CFTR biogenesis and function. Scanning of a section of intracellular loop 4 (ICL4) with 61 second-site mutations, validates R1070W (Thibodeau et al., 2010) as a particularly effective revertant. Furthermore, we tested the effects of two mutations corresponding to revertant mutations for F670del-Yor1p, a yeast homolog to F508del-CFTR in which the deletion of F670 causes defects in Yor1p similar to those caused by F508del in CFTR.

# Acknowledgements

Working on this thesis has been a very rewarding and humbling experience. I am incredibly grateful for having had the opportunity to do my PhD at University College London in a stimulating environment that has allowed me to learn, broaden my view, and grow both academically and personally. This thesis would not have been possible without the support of others, and I want to express my gratitude and appreciation to all the people who have helped and inspired me during my doctoral studies.

First and foremost, I want to thank my supervisor, Dr Paola Vergani, for her continuous support and inspiration. Her critical view and expertise have been invaluable, and it has been a great pleasure to work in her group. A special thanks to Dr Emily Langron for showing me the ropes in the lab. A heartfelt thanks as well, to all other past and present members and project students in the Vergani and Moss labs for their help, conversations, and input. Furthermore, I am grateful for the support I have received from the staff and PhD students in the NPP department. Also, a very warm thanks to Professor David Sheppard and the other members of the F508del Strategic Research Centre for their encouragement and enthusiasm about this project.

Dealing with cancer during my PhD has been challenging, and I owe great thanks to everyone who offered support and care. Furthermore, I want to thank my friends in London, Utrecht, and elsewhere, for their companionship. Felipe, thanks for your love and support during the final year of my PhD. Of course, I also want to thank my parents, Jan and Mariet. You have always encouraged me to be creative and pursue my interests, and I cannot express enough gratitude for your support throughout my life. And finally, I want to profoundly thank Lucas and my sister Myrthe. You guys are incredible and, as always, your support during my studies has been immense.

*I gratefully acknowledge the generous funding received from the Cystic Fibrosis Trust UK, and the additional one-year fellowship received from the UCL Doctoral School.*

## Impact Statement

The assay we developed is the first available method that allows simultaneous assessment of biogenesis as well as channel function of the cystic fibrosis transmembrane conductance regulator (CFTR). Being able to monitor, within the same population of cells, how a perturbation (like a mutation or incubation with pharmacological compounds) affects both CFTR conductance and the amount of CFTR near the membrane, allows separation of effects on biogenesis from those on permeation or gating. This can provide advantages for drug development as well as for structure/function studies.

So far, the search for effective CFTR modulators has involved separate assays to screen compounds, looking for either potentiators that increase CFTR function, or correctors that promote biogenesis. This drug discovery strategy makes a sharp distinction between potentiators and correctors which might act as an obstacle for discovery of effective drugs (Rowe & Verkman, 2013). For example, effective rescue of the most common CFTR variant, F508del-CFTR, requires a combination of corrector and potentiator compounds. Orkambi, an approved combination treatment for patients who are homozygous for F508del, has limited clinical efficacy, likely because of interference between the two compounds. Implementation of our assay in the early stages of drug development could promote the search for dual-acting compounds, circumventing the problem of adverse drug-drug interactions associated with combination treatment. This all could be of great benefit to people affected by cystic fibrosis.

We believe our assay will also accelerate discovery in CFTR structure-function studies. The method does not require expensive antibodies and provides a reliable and informative description of CFTR molecular characteristics. While convenient to use, the information content of the readouts is higher than that obtained by most other medium or high throughput methods. In combination with other techniques, the assay provides a powerful tool for investigation of CFTR ion channel biophysics. For example, mutagenesis can be used to investigate plausible molecular mechanisms, or to target residues in putative drug-binding sites in mechanistic studies and hypotheses can be generated and tested easily, identifying directions for further investigation by more labour-intensive techniques like

patch-clamping or molecular dynamics. In this study we demonstrate this by screening 61 second-site mutations in intracellular loop 4 (ICL4), and two equivalents to second-site mutations that were identified as revertants for F670del-Yor1p, a yeast homologue of F508del-CFTR, generating testable hypotheses about mechanisms of F508del-CFTR rescue.

Cystic fibrosis is a rare disease which only affects ~100,000 people worldwide. CFTR however, is emerging as a potential target for other, more prevalent, diseases. Recent studies suggest that CFTR dysfunction may play a role in airways diseases such as chronic obstructive pulmonary disease (COPD) and asthma which are a common causes of morbidity and mortality (Solomon et al., 2017). Furthermore, CFTR has been the target in drug development programmes for diarrheal disease (Thiagarajah et al., 2015) and anti-secretory therapy for people with polycystic kidney disease which can cause kidney failure requiring dialysis and kidney transplantation (Snyder et al., 2011). Our assay can be employed in CFTR modulator development programmes for diseases beyond cystic fibrosis.

# Contents

List of figures .....	12
List of tables .....	13
List of abbreviations .....	14
List of symbols .....	17
1. Introduction .....	19
<b>1.1 ABC transporter superfamily</b> .....	<b>19</b>
<b>1.2 CFTR</b> .....	<b>20</b>
1.2.1 Structure .....	20
<i>Domain swapping</i> .....	20
<i>Inward-facing apo structure</i> .....	21
<i>Outward-facing ATP-bound structure</i> .....	21
1.2.2 Gating .....	22
<i>CFTR's permeation pathway</i> .....	22
<i>Gating mechanism</i> .....	24
1.2.3 Physiological role of CFTR .....	27
<i>CFTR's expression in epithelial tissues</i> .....	27
<i>Fluid secretion</i> .....	28
1.2.4 Involvement of CFTR in diseases .....	29
<b>1.3 Cystic fibrosis</b> .....	<b>29</b>
1.3.1 Pathophysiology .....	30
<b>1.4 F508del-CFTR</b> .....	<b>31</b>
1.4.1 Structural changes .....	32
1.4.2 Biogenesis .....	32
1.4.3 Gating defect .....	33
1.4.4 Correcting F508del-CFTR .....	34
<i>Pharmacological compounds</i> .....	34
<i>Low temperature</i> .....	35
<i>Revertant mutations</i> .....	36
<b>1.5 Methods for CFTR assessment</b> .....	<b>37</b>
1.5.1 Channel function .....	37
<i>Patch clamp technique</i> .....	37
<i>Ussing chamber</i> .....	37
<i>Radiotracer flux</i> .....	38
<i>Iodide influx assays using halide sensitive YFP</i> .....	38

<i>FRET based membrane potential assay</i> .....	38
<i>Organoids</i> .....	39
1.5.2 Biogenesis .....	40
<i>Western blot</i> .....	40
<i>Extracellular epitope tagging</i> .....	40
<i>Horseradish Peroxidase tag</i> .....	41
<i>Fluorogen activating protein tag</i> .....	41
<i>pH-sensitive tag</i> .....	42
<b>1.6 Aims of this research</b> .....	<b>42</b>
1.6.1 Enabling rapid and simultaneous assessment of CFTR function and biogenesis .....	42
1.6.2 Investigating F508del-CFTR rescue by second site mutations .....	43
<b>2. Methods</b> .....	<b>44</b>
<b>2.1 Molecular Biology</b> .....	<b>44</b>
2.1.1 pIRES2-mCherry-YFPCFTR construction .....	44
2.1.2 Introduction of second-site mutations in <i>cis</i> with F508del .....	46
<i>Site directed mutagenesis</i> .....	46
<i>Transformation of chemically competent E. coli</i> .....	47
<i>Mini prep</i> .....	48
<i>Gel electrophoresis</i> .....	48
<i>Fluorescence-based cycle sequencing</i> .....	49
<i>Midi prep</i> .....	50
<b>2.2 HEK-293 cell culture and transfection</b> .....	<b>50</b>
2.2.1 HEK-293 cell line .....	50
2.2.2 Maintenance HEK-293 culture .....	51
2.2.3 Plating HEK-293 cells .....	52
2.2.4 Transient cationic lipid mediated transfection .....	52
2.2.5 Temperature correction and chronic drug treatment .....	52
<b>2.3 Fluorescence image acquisition</b> .....	<b>53</b>
2.3.1 ImageXpress .....	53
2.3.2 MetaXpress image acquisition protocols .....	54
<i>CFTR membrane proximity</i> .....	54
<i>The I<sup>-</sup> first protocol</i> .....	54
<i>The I<sup>-</sup> last protocol</i> .....	55
<b>2.4 Pharmacology</b> .....	<b>55</b>
2.4.1 Forskolin .....	55
2.4.2 VX-770 .....	56
2.4.3 VX-809 .....	56

<b>2.5 Image analysis</b> .....	<b>56</b>
2.5.1 Membrane proximity .....	56
<i>Binarisation and noise reduction</i> .....	57
<i>Watershed based segmentation</i> .....	57
<i>Background correction</i> .....	58
<i>Cell filtering</i> .....	59
2.5.2 CFTR function .....	59
<b>2.6 Statistics</b> .....	<b>59</b>
<b>3. Development of the mCherry-YFPCFTR assay</b> .....	<b>60</b>
<b>3.1 Introduction</b> .....	<b>60</b>
<b>3.2 Fluorescence imaging</b> .....	<b>62</b>
3.2.1 YFP(H148Q/I152L).....	63
3.2.2 mCherry .....	64
3.2.3 Bicistronic expression system .....	64
<b>3.3 The pIRES2-mCherry-YFPCFTR plasmid</b> .....	<b>65</b>
<b>3.4 Quantification of CFTR Channel function</b> .....	<b>67</b>
3.4.1 The <i>I<sup>-</sup> first protocol</i> : maximal rate of iodide entry .....	67
3.4.2 The <i>I<sup>-</sup> last protocol</i> : estimation of G and V <sub>m</sub> .....	69
<i>Equilibrium potentials</i> .....	71
<i>Ionic currents and conductance</i> .....	71
<i>Intracellular ion concentrations</i> .....	73
<i>The proportion of anion-bound and anion-free YFP(H148Q/I152L)</i> .....	74
<i>The membrane capacitance</i> .....	76
<i>The membrane potential</i> .....	76
3.4.3 Normalisation to control for transfection efficiency .....	77
<b>3.5 CFTR membrane proximity</b> .....	<b>77</b>
3.5.1 WT-CFTR: normalisation .....	77
3.5.2 mCherry: membrane localisation and normalisation .....	80
3.5.3 Defining CFTR membrane proximity ( $\rho$ ) .....	81
<b>3.6 Discussion</b> .....	<b>83</b>
3.6.1 Membrane proximity .....	83
3.6.2 pH sensitivity YFP(H148Q/I152L) .....	84
3.6.3 K <sub>i</sub> .....	85
3.6.4 Relevance .....	86

4. Validating the mCherry-YFPCFTR assay.....	87
4.1 Introduction.....	87
4.2 Results .....	88
4.2.1 mCherry accounts for variability due to unequal transfection efficiency .....	88
4.2.2 Ability to reach the membrane .....	89
<i>VX-809</i> .....	89
<i>Rescue by R1070W</i> .....	89
<i>VX-770 destabilisation</i> .....	90
<i>Temperature rescue</i> .....	91
4.2.3 CFTR function .....	91
<i>DMSO control</i> .....	93
<i>WT-CFTR</i> .....	93
<i>F508del-CFTR: VX-770 potentiation</i> .....	93
<i>F508del-CFTR: VX-809 correction</i> .....	94
<i>F508del-CFTR: Rescue by R1070W</i> .....	95
<i>F508del-CFTR: Temperature rescue</i> .....	95
4.3 Relationship between channel function and membrane proximity.....	95
4.4 Discussion .....	97
4.4.1 Validation of membrane proximity quantification .....	97
4.4.2 Background noise in $\rho$ measurements .....	97
4.4.3 Channel function: upper limit of the dynamic range .....	99
4.4.4 Channel function: <i>I<sup>-</sup> first protocol</i> .....	99
4.4.5 Simultaneous assessment of membrane proximity and channel function for pharmacology .....	100
4.4.6 Correlation results rare mutant panel with existing datasets .....	100
5. Second-site mutations in <i>cis</i> with F508del.....	101
5.1 Introduction.....	101
5.1.1 ICL4 .....	102
<i>The TMD-NBD interfaces</i> .....	102
<i>Flexibility of the ICL-NBD interfaces</i> .....	102
<i>Role of the ICL4-NBD1 interface</i> .....	103
<i>F508del-CFTR rescue by targeting the ICL4</i> .....	103
5.1.2 F670del-Yor1 revertants .....	104
<i>Yeast models</i> .....	104
<i>F670del-Yor1p</i> .....	105
<i>Rescue of F670del-Yor1p by second site-mutations</i> .....	105

<b>5.2 Results</b>	<b>106</b>
5.2.1 The CFTR equivalents to the F670del-Yor1p revertants	107
5.2.2 mCherry fluorescence	107
5.2.3 Membrane proximity	111
5.2.4 Channel function	111
<i>Conductance</i>	113
<i>Membrane potential</i>	116
5.2.5 Relating ion channel function and membrane proximity	117
<i>F1068 substitutions</i>	118
<i>R1070 substitutions</i>	118
<i>F1074 substitutions</i>	119
<i>A141S and R1097T</i>	120
<b>5.3 Discussion</b>	<b>120</b>
5.3.1 R1070Y	120
5.3.2 Why is R1070W such an effective rescue mutation?	121
5.3.3 Window for optimal ICL4-NBD1 interface flexibility	122
5.3.4 Methionine substitutions at sites F1068 and F1074 partially rescue F508del-CFTR	124
5.3.5 F670del-Yor1p revertants	124
<i>A141S</i>	124
<i>R1097T</i>	125
<b>6. Conclusion</b>	<b>126</b>
<b>6.1 Assay development</b>	<b>126</b>
<b>6.2 F508del-CFTR revertant mutations</b>	<b>127</b>
6.2.1 ICL4	127
6.2.2 F670del-Yor1p revertants in F508del-CFTR	128
<b>6.3 Limitations of our study</b>	<b>128</b>
6.3.1 Expression system	128
6.3.2 Image acquisition system	129
6.3.3 Inability to directly measure CFTR surface expression	129
6.3.4 Unwanted secondary mutations	130
<b>6.4 Future directions</b>	<b>130</b>
6.4.1 Single cell analysis for CFTR function	130
6.4.2 R1070W rescue mechanism	131
Supplementary information	133
References	141

## List of figures

<i>Figure 1</i> Schematic organisation of the CFTR domains.....	20
<i>Figure 2</i> CFTR molecular structure.....	22
<i>Figure 3</i> Model of the gating mechanism of CFTR.....	25
<i>Figure 4</i> Problems caused by F508del .....	29
<i>Figure 5</i> Representation of the ICL4-NBD1 interface in WT-CFTR, F508del-CFTR, and F508del/R1070W-CFTR .....	36
<i>Figure 6</i> ICL4-NBD1 molecular structure .....	43
<i>Figure 7</i> Construction of the pIRES2-mCherry-YFPCFTR plasmid .....	45
<i>Figure 8</i> Thermal cycling protocols.....	46
<i>Figure 9</i> Layout of a filter cube .....	53
<i>Figure 10</i> Automated cell boundary detection with MATLAB.....	58
<i>Figure 11</i> Co-expression of soluble mCherry and YFP(H148Q/I152L)-CFTR.....	66
<i>Figure 12</i> Fitting of the fluorescence quenching to a simple mathematical model .....	70
<i>Figure 13</i> Effect of normalisation on mCherry fluorescence.....	78
<i>Figure 14</i> Effect of normalisation on YFP(H148Q/I152L) fluorescence .....	79
<i>Figure 15</i> Quantification of CFTR membrane proximity ( $\rho$ ).....	81
<i>Figure 16</i> The relationship between $\hat{f}_{mCherry\ cell}$ and $\hat{f}_{YFP\ cell}$ , $\hat{f}_{YFP\ membrane}$ , and $\rho$ .....	88
<i>Figure 17</i> WT-CFTR, F508del-CFTR, and F508del/R1070W-CFTR membrane proximity in various experimental conditions .....	90
<i>Figure 18</i> Effect of temperature, genotype, acute potentiation with VX-770 and chronic VX-809 treatment on the rate of iodide entry .....	94
<i>Figure 19</i> Relationship between $\rho$ and the maximal rate of iodide entry .....	96
<i>Figure 20</i> Linear regression on VX-809 rescued F508del-CFTR.....	98
<i>Figure 21</i> Positions of F508, A141, R1097 and N1148 in CFTR molecular models .....	108
<i>Figure 22</i> Boxplots of the normalised mCherry fluorescence intensity.....	110
<i>Figure 23</i> Effect of ICL4 mutations in cis with F508del on membrane proximity.....	112
<i>Figure 24</i> Effect of ranking on normalised conductance distributions in the control condition.....	113
<i>Figure 25</i> Effect of second-site mutations in cis with F508del on CFTR conductance and membrane potential.....	115
<i>Figure 26</i> Relationship between conductance and membrane proximity in genotypes with second-site mutations that alleviate F508del related impairments .....	119
<i>Figure 27</i> ICL4-NBD1 interface.....	122

## List of tables

<i>Table 1</i> Specifications of the ImageXpress filter cubes used for imaging of YFP(H148Q/I152L) and mCherry .....	54
<i>Table 2</i> Assay validation: Statistical test results $\log_{10}p$ .....	133
<i>Table 3</i> Assay validation: $d[I^-]/dt$ in the control condition.....	133
<i>Table 4</i> Assay validation: statistical test results $d[I^-]/dt$ (Forskolin vs. DMSO) .....	134
<i>Table 5</i> Assay validation: statistical test results $d[I^-]/dt$ after addition of forskolin .....	135
<i>Table 6</i> Descriptive statistics: normalised mCherry fluorescence intensity .....	136
<i>Table 7</i> Descriptive statistics: assay readouts for WT-CFTR and F508del-CFTR with and without second-site mutations .....	137
<i>Table 8</i> Paired t-tests comparing $\log_{10}p$ of F508del without vs. with second-site mutations.....	138
<i>Table 9</i> One-tailed Wilcoxon Rank Sum tests (DMSO vs. forskolin) .....	139
<i>Table 10</i> Two-tailed Wilcoxon Rank Sum tests comparing F508del without vs. with second-site mutations.....	140

## List of abbreviations

ABC	ATP-binding cassette
ABCx	ATP-binding cassette subfamily x
ABCxn	ATP-binding cassette subfamily x member number n
ANOVA	Analysis of variance
ASL	Airway surface liquid
ATP	Adenosine triphosphate
ATP12A	Nongastric H <sup>+</sup> /K <sup>+</sup> adenosine triphosphatase
AU	Arbitrary unit
cAMP	Cyclic adenosine monophosphate
CF	Cystic fibrosis
CFBE	Cystic fibrosis bronchial epithelium
CFTR	Cystic fibrosis transmembrane conductance regulator
<i>CFTR</i> gene	Gene encoding the cystic fibrosis transmembrane conductance regulator (CFTR)
CH	Coupling helix
CI	Confidence interval
COPD	Chronic Obstructive Pulmonary Disease
COPII	Coat protein complex II
cryo-EM	Cryo-electron microscopy
ddNTP	2'-3'dideoxynucleotide triphosphate
DMEM	Dulbecco's Modified Eagle's medium
DMSO	Dimethylsulfoxide
DNA	Deoxyribonucleic acid
dNTP	Deoxyribonucleotide triphosphate
DTT	Dithiothreitol
ECL	Extracellular loop
ECLn	Extracellular loop number n
ECMV	Encephalomyocarditis virus
EDTA	Ethylenediaminetetraacetic acid
ENaC	Epithelial sodium channel
ER	Endoplasmic Reticulum
ERAD	Endoplasmic-reticulum-associated protein degradation
FAP	Fluorogen activating protein

FBS	Fetal bovine serum
FDA	Food and Drug Administration
FRET	Fluorescence resonance energy transfer
FRT	Fisher rat thyroid
FRTL-5	Fischer Rat Thyroid Cell Line number 5
FSK	Forskolin
GFP	Green fluorescent protein
HA	Human influenza hemagglutinin
HBSS	Hank's Balanced Salt Solution
HEK-293	Human embryonic kidney 293
HEPES	Hydroxyethyl piperazineethanesulfonic acid
HRP	Horseradish peroxidase
ICL	Intracellular loop
ICLn	Intracellular loop number n
IRES	Internal ribosome entry site
LB broth	Luria Bertani broth
McjD	Microcin-J25 export ATP-binding/permease protein
MD	Mean difference
mFRP	Monomeric red fluorescent protein
mRFP1	Monomeric red fluorescent protein number 1
mRNA	Messenger ribonucleic acid
MsbA	Lipid A export ATP-binding/permease protein
NBD	Nuclear binding domain
NBDn	Nuclear binding domain number n
NKCC1	Na <sup>+</sup> K <sup>+</sup> 2Cl <sup>-</sup> cotransporter
NTP	Nucleoside triphosphate
PCR	Polymerase chain reaction
PDL	Poly-D-lysine
PKA	cAMP-dependent protein kinase
RFP	Red fluorescent protein
RNA	Ribonucleic acid
Sav1866	Putative multidrug export ATP-binding/permease protein
SD	Standard deviation
SEM	Standard error of the mean

SOC medium	Super Optimal broth with Catabolite repression
<i>STE6</i>	Gene encoding Alpha-factor-transporting ATPase (Ste6p)
Ste6p	Alpha-factor-transporting ATPase
SUR1	Sulfonylurea receptor 1 (ABCC8)
SUR2	Sulfonylurea receptor 2 (ABCC9)
TE	Ethylenediaminetetraacetic acid (Tris-EDTA)
TM287/288	Thermotoga maritima heterodimeric ABC transporter TM287-TM288
TMD	Transmembrane domain
TMDn	Transmembrane domain number n
TMn	Transmembrane helix number n
TMs	Transmembrane helices
WT	Wild type
YFP	Yellow fluorescent protein
<i>YOR1</i>	Gene encoding the yeast oligomycin resistance protein (Yor1p)
Yor1p	Yeast oligomycin resistance protein
R domain	Regulatory domain
AU	Arbitrary units

## List of symbols

$[i]_{\text{sym}}$	The concentration of ion $i$ which is symmetrical extracellularly and intracellularly
$[L]$	Free ligand concentration
$A_m$	Area surface of the membrane
$C_m$	Membrane capacitance in farads
$E_i$	Equilibrium potential for ion $i$
$F$	Faraday's constant (96485.332 C·mol <sup>-1</sup> )
$f$	YFP(H148Q/I152L) fluorescence intensity in the cell selection normalised to the timepoint before iodide addition
$f_{\text{mCherry}}$	mCherry fluorescence intensity
$f_{\text{mCherry cell}}$	Average mCherry fluorescence intensity over a single entire cell
$\hat{f}_{\text{mCherry cell}}$	Average mCherry fluorescence intensity over a single entire cell normalised to WT, $\frac{f_{\text{mCherry cell}}}{\text{Mdn}(\text{WT } f_{\text{mCherry cell}})}$
$f_{\text{mCherry cells}}$	Average mCherry fluorescence intensity inside the area of the image containing cells
$\hat{f}_{\text{mCherry cells}}$	Average mCherry fluorescence intensity inside the area of the image containing cells normalised to WT, $\frac{f_{\text{mCherry cells}}}{\text{WT } f_{\text{mCherry cells}}}$
$f_{\text{YFP}}$	YFP(H148Q/I152L) fluorescence intensity
$\hat{f}_{\text{YFP}}$	YFP(H148Q/I152L) fluorescence intensity normalised to WT
$f_{\text{YFP cell}}$	Average YFP(H148Q/I152L) fluorescence intensity over a single entire cell
$\hat{f}_{\text{YFP cell}}$	Average YFP(H148Q/I152L) fluorescence intensity over a single entire cell normalised to WT, $\frac{f_{\text{YFP cell}}}{\text{Mdn}(\text{WT } f_{\text{YFP cell}})}$
$f_{\text{YFP membrane}}$	Average YFP(H148Q/I152L) fluorescence intensity within the membrane-proximal zone
$\hat{f}_{\text{YFP membrane}}$	Average normalised YFP(H148Q/I152L) fluorescence intensity within the membrane-proximal zone, $\frac{f_{\text{YFP membrane}}}{\text{Mdn}(\text{WT } f_{\text{YFP cell}})}$
$G$	CFTR mediated chloride conductance in the presence of 140 mM symmetrical $[\text{Cl}^-]$
$\hat{G}$	Normalised CFTR mediated chloride conductance, $\frac{G}{\hat{f}_{\text{mCherry cells}}}$
$G_{\text{CFTR-}i}$	CFTR mediated conductance for ion $i$
$G_i$	Conductance for ion $i$
$G_{\text{leak-K}}$	An endogenous leak conductance for $\text{K}^+$ set to 2.5 nS (Rapedius et al., 2005)
$G_{\text{trans}}$	A CFTR independent transient conductance probably caused by endogenous anion permeabilities of the HEK-293

$I_{cap}$	the capacitive current
$I_i$	Ionic current across a cell membrane for ion $i$ (in $A \cdot m^{-2}$ )
$I_{ion}$	Net ionic current
$K_d$	Equilibrium dissociation constant
$K_i$	Dissociation equilibrium constants
$nH$	Hill coefficient
$P_{free}$	Fraction unbound YFP(H148Q/I152L)
$\hat{P}_{free}$	Normalised fraction unbound YFP(H148Q/I152L) to the fraction unbound YFP(H148Q/I152L) at the timepoint just before addition of iodide, $\frac{P_{free}}{P_{free}(t_0)}$
$p_i$	The permeability of the membrane to ion $i$
$P_i$	Fraction YFP(H148Q/I152L) bound to ion $i$
$P_o$	Open probability
$Q_m$	Charge stored in the membrane in coulombs
$R$	Ideal gas constant ( $8.314 J \cdot K^{-1} \cdot mol^{-1}$ )
$r$	Radius
$T$	Absolute temperature in Kelvin (K)
$t$	Timepoint in seconds
$t_0$	Timepoint zero
$V_{cell}$	Cell volume
$V_m$	Membrane potential in mV
YFP	YFP(H148Q/I152L)
YFPCl <sup>-</sup>	Chloride bound YFP(H148Q/I152L)
YFPI <sup>-</sup>	Iodide bound YFP(H148Q/I152L)
$z_i$	Valence of ion $i$
$\gamma$	Single-channel conductance
$\theta$	Fraction of ligand-bound macromolecules
$\rho$	Membrane proximity, $\frac{\hat{f}_{YFP \text{ membrane}}}{\hat{f}_{mCherry \text{ cell}}}$
$\tau_{trans}$	A single exponential decay that represents the time in seconds after which the transient conductance ( $G_{trans}$ ) is reduced to $1/e$ ( $\approx 0.368$ ) times its initial value.

# 1. Introduction

## 1.1 ABC transporter superfamily

The ATP-binding cassette (ABC) transporter family is a large superfamily of ATP-binding proteins that mediate a wide variety of processes (Davidson et al., 2008). ABC transporters are ubiquitous in all domains of life (Locher, 2016). They are classified as ABC transporters based on sequence analysis. All ABC transporters share highly conserved sequence motifs in their nucleotide binding domains (NBDs): Walker A and B which are found in a wide variety of ATP-binding proteins, and signature C motif which is characteristic for ABC transporters (Dean et al., 2001). Based on domain organization and phylogenetic analysis seven subfamilies of ABC transporters (ABCA to ABCG) have been defined in the human genome (Dean & Annilo, 2005). Most of these proteins are active transporters that transport substrates across the cell membrane against their electrochemical gradient at the expense of ATP hydrolysis.

Within the entire ABC transporter superfamily, CFTR (ABCC7) is thought to be the only protein that functions as an ion channel (Csanády et al., 2019), allowing ions to cross the membrane down their electrochemical gradient. The only other type of eukaryotic ABC transporters that are not involved in active transmembrane transport, are the soluble ABCE and ABCF subfamily members, as well as SUR1 (ABCC8) and SUR2 (ABCC9) which function as regulatory subunits of ATP-sensitive potassium channels (Dean & Annilo, 2005). With exception of the ABCE and ABCF subfamilies that lack transmembrane domains (TMDs), functional units of ABC transporters are typically composed of four domains: two TMDs and two NBDs. While prokaryotic ABC transporters are formed by either four individual polypeptides or two TMD-NBD half transporters that are coassembled posttranslationally, in eukaryotes the domains are organised as half transporters or full transporters in which all 4 domains are linked in a single polypeptide chain (Hyde et al., 1990).

## 1.2 CFTR

### 1.2.1 Structure

CFTR is one of the 48 human ABC transporters and is formed by two homologous TMD-NBD halves that are connected by a cytosolic regulatory domain (R domain) that is thought to be unique to CFTR (Riordan et al., 1989); see **Figure 1**. Major breakthroughs have been achieved in the last few years with the publication of the first three-dimensional atomic resolution structures of full-length CFTR obtained by cryo-electron microscopy (cryo-EM): two from zebrafish CFTR (Zhang et al., 2017; Zhang & Chen, 2016), two from chicken (Fay et al., 2018), and four from human CFTR (Liu et al., 2017, 2019; Zhang et al., 2018b).

#### *Domain swapping*

As had been predicted by homology modelling and confirmed by cross-linking studies (He et al., 2008; Mense et al., 2006; Serohijos et al., 2008), the overall structure of CFTR features the domain-swapping found in ABC exporter structures such as those of bacterial Sav1866 (Dawson & Locher, 2006, 2007), MsbA (Ward et al., 2007), TM287/288 (Hohl et al., 2012), mammalian P-glycoprotein (Aller et al., 2009), human ABCB10 (Shintre et al., 2013), and McjD (Choudhury et al., 2014). As in other ABC exporters, each TMD consists of six transmembrane helices (TMs) that are connected by intracellular and extracellular loops (ICLs and ECLs) and form two wings composed of helices from each TMD.

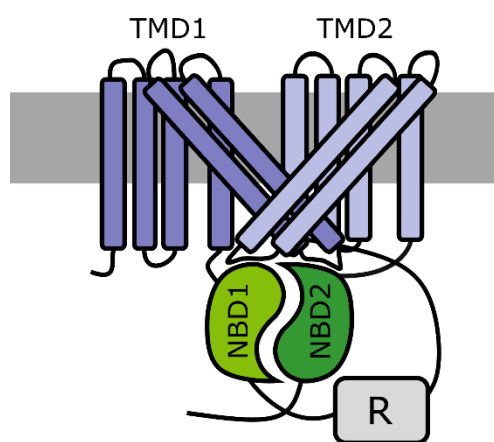


**Figure 1 Schematic organisation of the CFTR domains**

CFTR consists of two transmembrane domains (TMD1, dark purple; TMD2, light purple) each made up of 6 transmembrane helices (TM1-12) connected to each other by extracellular loops (ECL1-6) and intracellular loops (ICL1-4). Furthermore, there are two nucleotide binding domains (NBD1, light green; NBD2, dark green) and a regulatory domain (R domain, light grey). Individual TMs, ECLs and ICLs are numbered from the N terminus (tail of the TMD1) to the C terminus (tail of the NBD2). In each TMD, two ICLs extended into the cytoplasm, and interact with the NBDs in a domain-swapped fashion: ICL2 from TMD1 swaps over to NBD2 and ICL4 from TMD2 swaps over to the NBD1.

One wing consists of TMD1 TM 1, 2, 3, 6 plus TMD2 TM 10 and 11, and the other one consists of TMD2 TM 7, 8, 9, 12 plus TMD1 TM 4 and 5. Interactions between TMDs and NBDs are mediated through four intracellular loops (ICLs) each including a short coupling helix (CH) on the cytosolic side of the TMDs. Each NBD is connected to the TMDs by an interface involving a pair of ICLs. The units formed by a surface depression in each NBD and the two ICLs that contact it, have been described as 'ball-and-socket joints' (Csanády et al., 2019). NBD1 forms a relatively shallow socket that interfaces with ICL1 and ICL4, and NBD2 forms a deeper socket that contacts ICL2 and ICL3. So ICL2 and ICL4 cross over to the NBD linked to the opposite TMD, which is referred to as domain swapping.

#### *Inward-facing apo structure*

As observed for other ABC exporters, with structures obtained in the absence of ATP (Aller et al., 2009; Hohl et al., 2012; Shintre et al., 2013; Ward et al., 2007), in the dephosphorylated apo state CFTR adopts an inward-facing conformation with the extracellular portion of the TMs tightly bundled but their cytosolic extensions spread apart (**Figure 2a**) (Liu et al., 2017; Zhang & Chen, 2016). In the resolved apo structures of zebrafish (Zhang & Chen, 2016) as well as human (Liu et al., 2017) CFTR, the R domain is clearly visible but largely unstructured. Except for an  $\alpha$ -helix that likely corresponds to the C-terminal of the R domain and interacts with the TMD2, its density is too weak to assign secondary structure, suggesting a high degree of flexibility. In agreement with its inhibitory role (Csanády et al., 2000), the density attributed to the unphosphorylated R domain is observed between the two halves of the molecule, sterically preventing NBD dimerization and therefore channel opening.

#### *Outward-facing ATP-bound structure*

In the phosphorylated ATP-bound structure of CFTR which includes a mutation (E1371Q) that prevents ATP hydrolysis, the TMDs adopt an outward-facing orientation in which the cytosolic extensions of the TMs are bundled together, and the NBDs are tightly dimerized (**Figure 2b**) (Zhang et al., 2017, 2018b). In ATP-bound ABC exporters the arrangement of the ECLs and of the extracellular ends of the TMDs can vary a lot. In some of them the ECLs are widely separated from each other (Dawson & Locher, 2006; Ward et al., 2007). In phosphorylated ATP-bound CFTR however, there is a tight bundling of the

ECLs similar to what is seen in McjD's outward occluded state (Choudhury et al., 2014). In the human as well as the zebrafish ATP-bound outward-facing CFTR structure, the R domain is no longer inserted in between the two halves of CFTR, permitting NBD dimerization. Although no density corresponding to the R domain was observed in zebrafish CFTR, in human CFTR a density that likely corresponds to part of the phosphorylated R domain is observed relocated away from the NBD dimer interface, interacting instead with the lasso domain at the cytosol/membrane interface.

### 1.2.2 Gating

#### *CFTR's permeation pathway*

Many studies have attempted to predict which TM segments line the pore of CFTR (Bai et al., 2010; Beck et al., 2008; El Hiani & Linsdell, 2010; Fatehi & Linsdell, 2009; Gao et al., 2013; Ge et al., 2004;

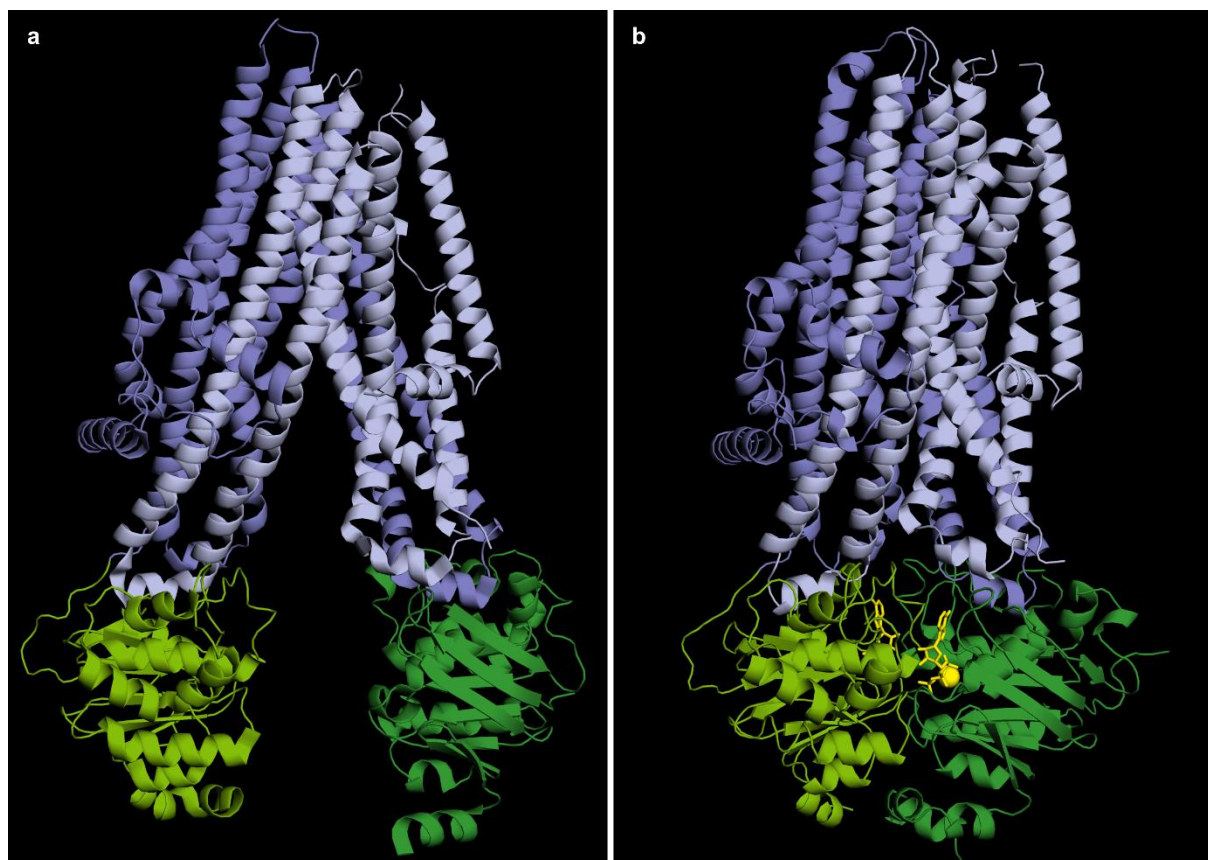


**Figure 2 CFTR molecular structure**

Ribbon representation from the cryo-EM structure of the apo structure of human CFTR (5UAK; Liu et al., 2017) in the inward conformation where the NBDs are separated and the TMDs are spread open to the cytosol (a) and of the phosphorylated, ATP-bound form of human CFTR (6MSM; Zhang et al., 2018b) in the outward facing configuration which is characterised a parallel orientation of the TMDs and formation of a NBD dimer with Mg-ATP (yellow) molecules bound buried within the interface (b).

Qian et al., 2011; Wang et al., 2011, 2014; Zhang & Hwang, 2015). While the currently available cryo-EM structures agree with most of these predictions, they also reveal an unexpected contribution of TM8 to the outer part of the pore. A subsequent study by Linsdell and colleagues confirms that the outer part of the TM8 plays a critical role in channel gating and permeation (Negoda et al., 2019).

The outer part of the pore has been suggested as the location of the selectivity filter that allows discrimination between different anions (Linsdell, 2016; Linsdell et al., 2000; McCarty & Zhang, 2001; Negoda et al., 2017; Wei et al., 2016). It must be noted that CFTR, like other anion channels, is only weakly selective. Experimentally obtained anion permeability sequences indicate that CFTR exhibits lyotropic selectivity; the permeability of an ion tends to be higher for ions with a lower change in free energy upon dehydration of the ion (Linsdell et al., 2000; McCarty & Zhang, 2001; Smith et al., 1999). For example, anions that are more easily dehydrated compared to chloride, like  $\text{SCN}^-$  and nitrate, have a reduced barrier to enter the pore and therefore display higher permeabilities (Linsdell et al., 2000; McCarty & Zhang, 2001). At the same time, these high permeability-anions also bind more tightly inside the pore, resulting in a lower throughput rate compared to chloride (defined by a lower relative conductance). The pore of CFTR seems to be optimise for maximal chloride conductance (Linsdell, 2001).

In addition to comprising the selectivity filter, the outer part of the pore region is also believed to be the location of the gate that opens and closes the permeation pathway (Corradi et al., 2015; Gao & Hwang, 2015; Wei et al., 2016). Interestingly, even in the phosphorylated, ATP-bound state, the cryo-EM structures of CFTR show that the permeation pathway is closed at its extracellular end, suggesting that some further structural rearrangement is required to allow anion conduction. While active transporters require two “gates”, never simultaneously open, only the extracellular gate appears conserved in the ion-channel CFTR. The intracellular gate formed by tight bundling of TMs at the tight NBD/TMD interfaces, seen in outward-facing ABC exporter structures, is cracked open in CFTR: a cytosolic portal between TM4 and 6 forms an entrance to the pore vestibule, which remains open in NBD-dimerised conformations. This portal was predicted (Corradi et al., 2015; Mornon et al.,

2015), and later confirmed by both cryo-EM structures (Zhang et al., 2017, 2018b) and functional measurements (Li et al., 2018).

### *Gating mechanism*

Gating of CFTR is regulated by the following two processes: phosphorylation of the R domain (**Figure 3a**) and interaction of ATP at the NBDs (**Figure 3b**). For a CFTR channel to become activated, its cytosolic R domain must be phosphorylated by cAMP-dependent protein kinase (PKA). Once CFTR is phosphorylated, channel opening is mediated by binding of ATP to the NBDs. Both Phosphorylation of the R domain and binding of ATP to the NBDs are required for pore opening (Aleksandrov et al., 2001; Berger et al., 2005; Cheng et al., 1991; Rich et al., 1991; Vergani et al., 2003, 2005b).

### Phosphorylation of the R domain by PKA

The presence of ATP is required for CFTR channel gating, but because ATP is abundantly present in living cells in a concentration that saturates the ATP-binding sites on CFTR channels, it is probably not the *in vivo* regulator of channel activity (Csanády et al., 2019). Even before CFTR was identified, it was hypothesised that the anion permeability involved in cystic fibrosis was regulated by a cAMP dependent phosphorylation (Frizzell et al., 1986; Schoumacher et al., 1987; Welsh & Liedtke, 1986).

When the CFTR gene was first cloned and characterised a high density of phosphorylation sites for protein kinases A and C was found in the R domain, suggesting that this domain may serve to regulate the activity of the channel (Riordan et al., 1989). Although PKA appears to be the main regulator of CFTR activity (Anderson et al., 1991; Berger et al., 1991), CFTR phosphorylation by protein kinase C (PKC) also causes some channel activity (Berger et al., 1993; Tabcharani et al., 1991). It is not totally clear whether PKC phosphorylation itself is responsible for activation of CFTR, or whether PKC phosphorylation permits activation by PKA. Some studies indicate that basal PKC phosphorylation might be a prerequisite for full channel activation by PKA (Chappe et al., 2003; Jia et al., 1997).

In the cryo-EM structures of unphosphorylated CFTR, density likely corresponding to the R domain has been observed sandwiched between the cytosolic extensions of the TMDs (Liu et al., 2017; Zhang & Chen, 2016) which is consistent with its regulatory role, as such an arrangement is sterically

incompatible with an outward-facing TMD conformation and with NBD dimerization, both of which are believed to be required for channel opening. The occluded location of the unphosphorylated R domain in the resolved cryo-EM structures is unlikely to be accessible to PKA.

It has been proposed that there might be an infrequent spontaneous disengagement of the unphosphorylated R domain from its position between the NBDs making it accessible to PKA which then locks the R domain in its released state by phosphorylating a number of serines (**Figure 3a**, Liu et al., 2017). Consistent with this view, dephosphorylated CFTR still gates with a very low open probability and displays some ATPase activity (Li et al., 1996; Liu et al., 2017); both these observations are incompatible with the position of the R domain (wedged between the two NBDs) in the unphosphorylated cryo-EM structures. On top of that, the sigmoidal time course of macroscopic currents upon addition of PKA, suggests that there are at least two sequential steps in the activation

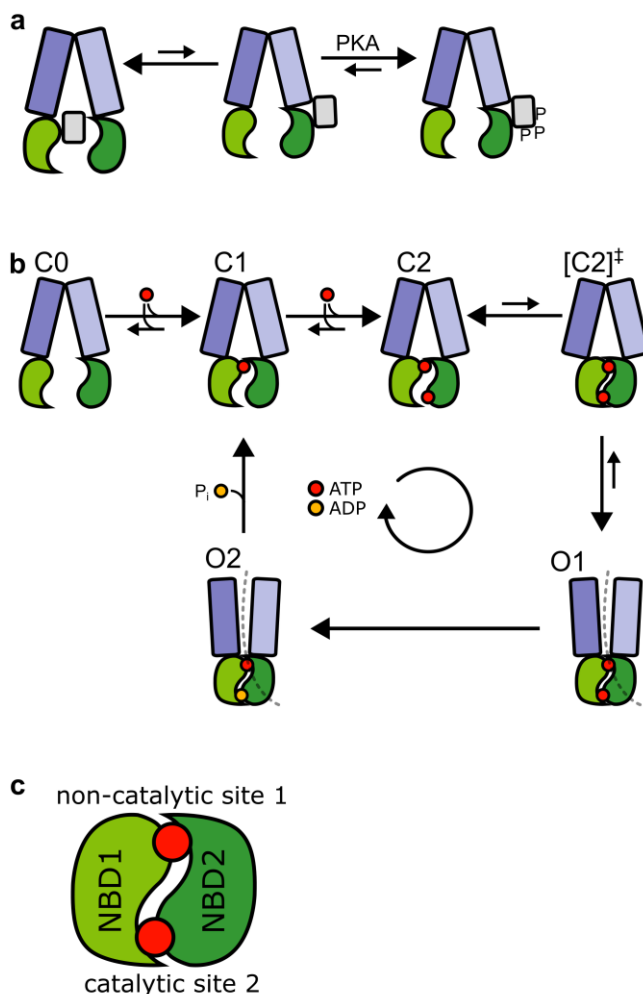


**Figure 3 Model of the gating mechanism of CFTR**

**a)** Infrequent disengagement of the unphosphorylated R domain (grey) from its position between the NBDs (green) makes the R domain accessible to PKA. PKA phosphorylates the R domain (phosphoryl groups; P) which then locks the R domain in its position. **b)** After phosphorylation of the R domain (omitted in **b** for clarity), the NBDs are able to form a 'head-to-tail' dimer with the two ATP-binding sites at their interface (**c**). Only upon ATP binding at catalytic site 2, tight dimerization of the NBDs occurs (C1→C2). The conformational change spreads towards the pore and visits a very transient and unstable conformation before entering a stable open state (C2→[C2]<sup>‡</sup>→O1). Eventually, hydrolysis of ATP at catalytic site 2 disrupts the NBD dimer. Before entering a stable closed state (C1), the channel enters a short-lived, post-hydrolytic open state (O2). An alternative route for channel closure is via a non-hydrolytic closing pathway. However, the O1 to O2 transition is much faster than that of the O1 to C2 transition, so hardly any channel openings terminate via this route, at least in WT-CFTR. ATP at non-catalytic site 1 remains bound for many gating cycles.

process: a slow step that is thought to correspond to the spontaneous R domain release, followed by faster subsequent R domain phosphorylation and channel opening (Liu et al., 2017).

#### ATP mediated NBD dimerisation

The gating of CFTR seems to exploit the same molecular mechanism that drives uphill transport by ABC transporters: a cycle of ATP binding and hydrolysis at the NBDs is linked to NBD dimer formation or disruption and coupled movements of the TMDs. NBD dimerization flips the TMDs from the inward-facing conformation to outward-facing conformation, and dimer disruption resets them facing inward (Hollenstein et al., 2007). While the TMDs among ABC transporters are structurally diverse to accommodate the transport of different substrates, the NBDs are highly conserved. The NBDs share a common architecture, each consisting of the following two subdomains: a core subdomain (referred to as the head) which contains motifs important for ATP binding, and a smaller helical subdomain (referred to as the tail) containing the ABC signature sequence (LSGGQ; involved in nucleotide binding) characteristic for ABC transporters (Davidson & Chen, 2004; Oswald et al., 2006).

In the presence of ATP, the NBDs form a head-to-tail dimer, creating two ATP-binding sites at the interface, each between the Walker motifs of one NBD and the signature sequence of the other NBD. As for the other ABCC family members, CFTR's ATP binding sites are asymmetric (Procko et al., 2009); one site is capable of catalysing ATP hydrolysis, while the other site contains mutations in conserved motifs rendering it catalytically inactive. The degenerate, non-catalytic site, referred to as site 1, is formed by the head of NBD1 and the tail of NBD2 and is not capable of ATP hydrolysis although it still binds ATP tightly for many gating cycles without dissociation (Aleksandrov et al., 2002; Basso et al., 2003; Tsai et al., 2010). The catalytic site (site 2) is formed by the head of NBD2 and the tail of NBD1.

ATP binding to site 2 triggers NBDs dimerization which transmits the conformational changes to the TMDs that are responsible for opening CFTR's gate. Eventually, hydrolysis of the ATP at catalytic site 2 disrupts the NBD dimer and closes the pore (Vergani et al., 2005). Just after hydrolysis and before the pore closes, the channel enters a short-lived, post-hydrolytic open state which, in specific

conditions, can be differentiated from the pre-hydrolytic open state by a larger conductance (Gunderson & Kopito, 1995). An alternative route for channel closure is via the reversal of the opening transition, via the so-called non-hydrolytic closing pathway; however, because the rate of this pathway is very slow compared to the hydrolytic pathway, almost no channel openings terminate via this route (Csanády et al., 2010), at least for WT CFTR (**Figure 3b**).

### 1.2.3 Physiological role of CFTR

#### *CFTR's expression in epithelial tissues*

CFTR is primarily expressed in epithelial cells in various tissues like the airway submucosal glands and surface epithelium (Engelhardt et al., 1992), the intestinal crypts, the epithelium of the pancreatic ducts, the salivary glands (Trezise & Buchwald, 1991), the epithelium of sweat glands (Kartner et al., 1992), the intrahepatic bile ducts (Yang et al., 1993), and the gall bladder (Kulaksiz et al., 2004). Various non-epithelial tissues, such as neurons in the brain (Guo et al., 2009) and endothelial tissue in the lungs (Tousson et al., 1998) have also been reported to express CFTR, albeit at generally lower levels (Bush et al., 2005).

Epithelial tissues, in which CFTR is mostly expressed, are composed of one or several layers of closely packed cells that cover surfaces or line cavities in the body. Epithelial cells have three different plasma membrane regions: the apical, the basolateral, and the lateral membranes (Salas et al., 1988). The apical membrane is in contact with the external environment, or luminal spaces equivalent to it, and it serves as a barrier to prevent potential pathogens or toxic substances from entering the blood. The basolateral membrane on the other hand, faces away from the lumen toward the extracellular matrix and is responsible for the disposal of cellular waste products and uptake of nutrients, ions and oxygen from the blood. Reflecting the different functions of the apical and basolateral membrane, epithelial cells establish apical-basal polarity, with different phospholipids and protein complexes harboured in each membrane region. The lateral membrane is oriented perpendicularly to the basolateral and apical membranes and is the region of the plasma membrane that contacts neighbouring epithelial cells, enabling them to interact through tight junctions that also act as

diffusion barriers separating the apical and basolateral sides so that polarity can be maintained (Wills et al., 1996).

The lipid raft hypothesis postulates that preferential interactions between sterols and certain phospholipids can drive the formation of dynamic patches within the plasma membrane that have different protein and lipid compositions from the surrounding membrane domains. Although there are still unresolved controversies about the composition, properties, and even the very existence of lipid rafts, there is abundant evidence that supports the existence of rafts *in vivo* (reviewed in Levental, Levental, & Heberle, 2020). Several studies have indicated that CFTR is situated in lipid rafts (e.g. Abu-Arish et al., 2015; Bajmoczy, Gadjeva, Alper, Pier, & Golan, 2009; Kowalski & Pier, 2004; Zaidi, Bajmoczy, Zaidi, Golan, & Pier, 2008) where CFTR is thought to initiate raft dependent epithelial cytokine and chemokine release critical for innate immune reaction to infections (Bajmoczy et al., 2009; Dudez et al., 2008; Kowalski & Pier, 2004; Vij et al., 2009). Lack of this reaction in people with cystic fibrosis could play a role in their susceptibility to chronic infections.

### *Fluid secretion*

For any organism, the necessity to regulate fluid absorption, secretion and composition, is a major challenge requiring precise regulation of ions and non-electrolytes, like sugars and water, to be absorbed from, or excreted into, the external environment (Wills et al., 1996). Fluid homeostasis is tightly regulated in epithelial tissues where fluid secretion is mainly controlled by the transport of chloride ions. Chloride secretion by CFTR expressing epithelial cells involves the active accumulation of chloride ions across the basolateral membrane: the electrochemical gradient of sodium is established by the Na<sup>+</sup>/K<sup>+</sup>-ATPase and used by Na<sup>+</sup>-K<sup>+</sup>-2Cl<sup>-</sup> cotransporter (NKCC1) to accumulate Cl<sup>-</sup> above its electrochemical equilibrium (Saint-Criq & Gray, 2017). Within some epithelial tissues, a basolateral Cl<sup>-</sup>/HCO<sub>3</sub><sup>-</sup> anion exchanger together with an Na<sup>+</sup>-bicarbonate cotransporter (NBC) also results in the accumulation of intracellular Cl<sup>-</sup> (Shan et al., 2012). CFTR is located at the apical surface of epithelial cells where its role is to coordinate electrolyte and fluid transport across the epithelium. CFTR mediated chloride secretion differentially depolarizes the apical membrane, and thus drives the

passive transport of sodium through a cation-selective paracellular route, enabling water to osmotically follow (Saint-Criq & Gray, 2017).

#### 1.2.4 Involvement of CFTR in diseases

Several human diseases are linked to changes in CFTR channel function. While overactivation of CFTR has been associated with polycystic kidney disease (Hanaoka & Guggino, 2000) and diarrhoea (Zhang et al., 2012), loss of CFTR activity due to mutations in the *CFTR* gene underlies cystic fibrosis. Furthermore, CFTR dysfunction also possibly plays a role in common airway diseases like chronic obstructive pulmonary disease (COPD) and asthma (Solomon et al., 2017). Even though the focus of this thesis is on cystic fibrosis, some of the work in this study will also be relevant for other conditions linked to CFTR dysfunction.

### 1.3 Cystic fibrosis

Cystic fibrosis is the most common lethal genetic disease among Caucasian populations, affecting 1 in ~2500 new-borns in Europe (Davies et al., 2007). In 1989, the gene mutated in cystic fibrosis patients was identified (Riordan et al., 1989). Although it was initially unclear whether the encoded CFTR protein was directly responsible for chloride transport in epithelial cells, or responsible for the regulation of one or more other chloride channels, it soon became clear that CFTR itself was

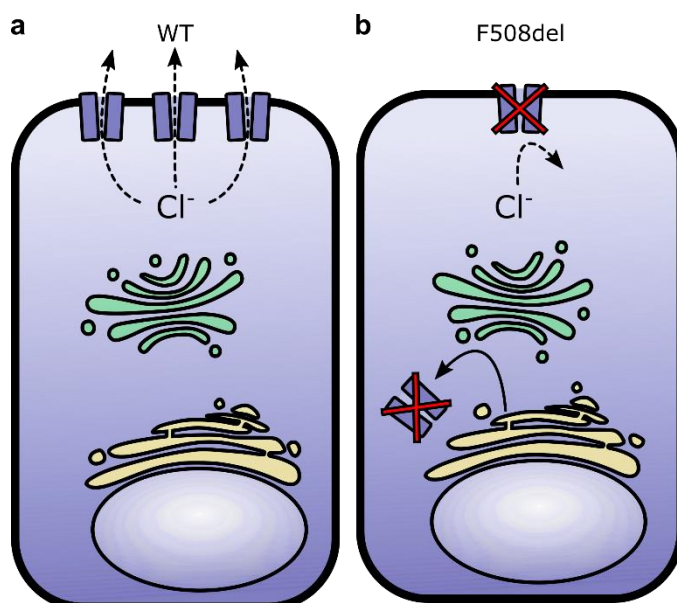


**Figure 4 Problems caused by F508del**

WT-CFTR (a) is located at the apical surface of epithelial cells where its activity allows chloride to move out of the cell, regulating transepithelial water transport which is necessary for the production of a layer of thin, hydrated mucus. Because F508del-CFTR (b) is misfolded, it is almost completely retained at the endoplasmic reticulum from where it is degraded instead of trafficked to the Golgi. Of the few proteins that reach the apical membrane, channel function is severely disrupted. These problems result in a decreased whole-cell chloride conductance, causing dehydration of the mucus layer on top of the cells.

responsible for chloride transport across epithelial surfaces (**Figure 4a**) (Bear et al., 1992). Mutations in the CFTR gene (such as F508del, **Figure 4b**) are responsible for a decrease or total loss of CFTR activity, leading to a range of problems in multiple organs. Deterioration of lung function, triggered by bacterial infection and exacerbated inflammation of the airways, is currently the primary cause of morbidity, causing 70 % of the deaths (Cystic Fibrosis Foundation, 2013). In the 1940s, children with cystic fibrosis died in early infancy but significant improvements in treatment have greatly prolonged the life expectancy of people with cystic fibrosis. In the UK median survival of children with cystic fibrosis born in 2010 is estimated to be 37 and 40 years for females and males respectively if the level of mortality does not change (MacKenzie et al., 2014).

### 1.3.1 Pathophysiology

Healthy airways are lined by ciliated epithelial cells which are covered with an airway surface liquid (ASL), consisting of a mucus layer that entraps pathogens and sits on top of a periciliary layer that has a low viscosity and facilitates ciliary beating for efficient mucus clearance (Knowles & Boucher, 2002). Mucociliary clearance serves as defence mechanism of the lung, protecting it from infection by removing inhaled particles. The way in which mutations in the *CFTR* gene contribute to the pathological problems in the airways of people with cystic fibrosis is not entirely clear. While there is consensus that impairment of CFTR, because of mutations, disrupts the control of fluid homeostasis across the bronchial epithelia, there are several hypotheses regarding the way in which subsequent changes contribute to the disease.

It is thought that decreased apical secretion of chloride ions via CFTR and increased apical sodium absorption via epithelial Na<sup>+</sup> channels (ENaC) dehydrates the ASL in people with cystic fibrosis, making their mucus difficult to clear and leaving their lungs vulnerable to infection (Boucher, 2007). Another aspect that may contribute to disease progression is the inflammatory state of the cystic fibrosis lungs which contain large quantities of pro-inflammatory mediators like neutrophils, macrophages, and T-lymphocytes (Roesch et al., 2018). The inflammation begins early in life and contributes to progressive damage to the lungs. It is unclear whether chronic inflammation is a

secondary symptom caused by increased pathogen exposure, or a primary defect in cystic fibrosis. Some studies report inflammation in the absence of bacterial infection in infants with cystic fibrosis, suggesting a primary effect of CFTR dysfunction on the inflammatory response, while other studies point towards recurrent infection as the main determinant for inflammation (reviewed in Nichols & Chmiel, 2015).

Furthermore, a reduced ability to regulate the pH of the ASL may also contribute to the vulnerability of cystic fibrosis lungs to persistent microbial infections. CFTR is permeable to bicarbonate ( $\text{HCO}_3^-$ ) which has an important role in modulating the pH of the secreted fluids and could influence the ASL pH (Linsdell et al., 1997). Genetically modified Pigs, lacking CFTR activity, that develop airway disease similar to cystic fibrosis in humans (Rogers et al., 2008; Stoltz et al., 2010), display an abnormally low pH of the ASL. This correlates with lower bactericidal activity of the cystic fibrosis ASL. When ASL pH is restored to normal values, antibacterial properties of the ASL improve (Pezzulo et al., 2012). Moreover, limited ASL acidification in cystic fibrosis mice who, unlike cystic fibrosis pigs or humans with cystic fibrosis, secrete minimal  $\text{H}^+$  through the nongastric  $\text{H}^+/\text{K}^+$  adenosine triphosphatase (ATP12A), could explain why cystic fibrosis mice do not develop airway infections (Shah et al., 2016). Although the loss of CFTR activity was also found to reduce ASL pH in cultures of human airway epithelia (Coakley et al., 2003) and in newborn humans with cystic fibrosis (Abou Alaiwa et al., 2014), studies in children and adults with cystic fibrosis have produced conflicting results (Abou Alaiwa et al., 2014; Garland et al., 2013; McShane et al., 2003).

#### 1.4 F508del-CFTR

Almost 300 cystic fibrosis-causing mutations in the *CFTR* gene have been confirmed (The Clinical and Functional TRanslation of CFTR (CFTR2); available at <http://cftr2.org>). Based on how they affect CFTR they are grouped in six different classes (Rowe et al., 2005). Class I mutations introduce premature stop codons producing mRNA strands incapable of undergoing translation, class II mutations impair folding and maturation of the protein, class III mutations impair channel gating, class IV mutations affect anion permeation, class V mutations mostly cause splicing defects reducing the amount CFTR

that is being produced, and finally, class VI mutations reduce stability of the protein at the membrane. The most common mutation is a deletion of phenylalanine at site 508 (F508del), present on at least one allele in 90 percent of the people with cystic fibrosis (Cystic Fibrosis Foundation, 2013). The F508del mutation impairs folding, maturation, trafficking, membrane stability, and channel gating of CFTR.

#### 1.4.1 Structural changes

X-ray structures of the human F508del NBD1 show that there are only small local changes in the conformation of the loop comprising residues 507 to 511 (Lewis et al., 2010). Zhang and Cheng (2016) have pointed out that cystic fibrosis causing mutations are unequally distributed between the two NBD-ICL interfaces. These important “transmission interfaces” are responsible for coupling phosphorylation and ATP binding and hydrolysis to channel gating by transmission of conformational changes from the NBDs to the TMDs. While thirteen mutations, including F508del, are located the NBD1-TMD interface, only two are located at the NBD2-TMD interface. They argue that the structural differences between these two interfaces could explain this imbalance. CFTR lacks a short helix in NBD1 (present in CFTR’s NBD2 and in most other NBDs) leading to a weaker NBD1-ICL4 interaction. This might underlie the observation that the NBD1-ICL4 interface is particularly vulnerable to mutations and might explain the severe defects caused by deletion of F508, since this phenylalanine normally contributes the NBD1-ICL4 interface.

#### 1.4.2 Biogenesis

It has been proposed that wild-type CFTR’s folding is inherently inefficient, which makes the protein vulnerable to mutations (Lukacs & Verkman, 2012). Misfolded proteins are recognized by the quality control system in the ER where they will be retained and undergo ER associated degradation (ERAD). The amount of CFTR escaping the ERAD system, can be determined by quantifying the extent of maturation. CFTR becomes core-glycosylated in the ER after which it matures in the Golgi system where it undergoes complex glycosylation; the shift in molecular weight corresponding to complex glycosylation can be observed by western blot or pulse-chase experiments.

Most studies show that only 20 to 40 % of translated wild-type CFTR undergoes complex glycosylation in the Golgi which is a requirement for transport of the channel to the cell membrane (Lukacs et al., 1994; Marshall et al., 1994; Pind et al., 1994; Ward & Kopito, 1994). These findings suggest that, even without being perturbed by mutations, a large proportion of CFTR appears to be misfolding. However, others have reported that complex glycosylation takes place in 80 % of heterologously expressed CFTR (Denning et al., 1992a) and up to 100 % of endogenously expressed CFTR (Varga et al., 2004), indicating that inefficient folding might not be inherent to CFTR but dependent on cell-type specific components involved in biogenesis.

Whether maturation of WT CFTR is inherently inefficient or not, it is clear that mutations can severely disrupt maturation. When the F508del mutation is present, the protein does not undergo any detectable complex glycosylation at 37 °C (Cheng et al., 1990; Denning et al., 1992a; Lukacs et al., 1994; Marshall et al., 1994; Pind et al., 1994; Varga et al., 2004; Ward & Kopito, 1994). Instead, F508del-CFTR becomes trapped in the ER and is subsequently degraded by the proteasome in an ubiquitin depended process (Ward et al., 1995). The little F508del-CFTR that escapes to the cell membrane has a decreased membrane stability (Lukacs et al., 1993; Okiyoneda et al., 2018; Varga et al., 2008) and a severe gating impairment.

#### 1.4.3 Gating defect

The deletion of F508 severely affects channel gating, characterised by a reduction in the open probability of CFTR (Cai & Sheppard, 2002; Dalemans et al., 1991; Denning et al., 1992a; Haws et al., 1996; Hwang et al., 1997; Kopeikin et al., 2014; Schultz et al., 1999) caused by a prolonged closed time interval between bursts and possibly also a small reduction in the average duration of the bursts (Cai & Sheppard, 2002; Haws et al., 1996). The reduction in opening rate of F508del-CFTR reflects destabilization of the transition state to channel opening relative to the closed state. Various studies show that the F508del mutation does not affect the pore properties such as single-channel conductance, the single-channel current-voltage relationship, and anion selectivity (reviewed in Z. W. Cai, Liu, Li, & Sheppard, 2011).

#### 1.4.4 Correcting F508del-CFTR

##### *Pharmacological compounds*

CFTR pharmacology made huge breakthroughs in the last decade with the identification of a number of compounds that act as potentiators that enhance channel gating, and correctors that rescue protein folding, alleviate processing defects and increase plasma-membrane stability. Because F508del impairs both gating and biogenesis, effective rescue of F508del-CFTR to treat patients, will likely require a combination of corrector and potentiator compounds, or effective dual-activity compounds. Below follows a brief overview of some of the recent developments.

VX-770 (ivacaftor) was the first CFTR potentiator evaluated in clinical trials and was identified by Vertex Pharmaceuticals (Van Goor et al., 2009). The compound has been approved for the treatment of patients carrying a number of gating mutations approximately 5 % of the people with CF (Gentzsch & Mall, 2018). VX-770 also increases activity of F508del-CFTR *in vitro* (Van Goor et al., 2009). However, potentiation of F508del-CFTR function by VX-770 on its own, is not sufficient for effective treatment of patients homozygous for the F508del mutation (Flume et al., 2012).

The corrector compound VX-809 (lumacaftor) partially rescues the processing and trafficking defects exhibited by F508del-CFTR (Van Goor et al., 2011). Orkambi, a combination of VX-770 and VX-809, has been approved for the treatment of patients who are homozygous for F508del. The idea is that VX-770 enhances the activity of the VX-809-corrected F508del-CFTR that has reached the membrane. However, the clinical success of this combination treatment has been limited. One explanation for this underwhelming clinical outcome is thought to be linked to the observation that, *in vitro*, VX-770 has a negative impact on F508del-CFTR biogenesis and thereby counteracts the action of VX-809 and other corrector compounds like VX-661 (Cholon et al., 2014; Veit et al., 2014). A number of other potentiators, structurally different from VX-770, were also found to have a negative impact on F508del-CFTR biogenesis (Veit et al., 2014). Last year a triple-combination therapy called Trikafta, combining the correctors elexacaftor (VX-445) and tezacaftor (VX-661) with ivacaftor (VX-770), was FDA approved for patients with at F508del on at least one of their alleles, after it was shown improve

clinical outcomes in people with cystic fibrosis who were heterozygous for F508del (Middleton et al., 2019), and in people homozygous for F508del (Heijerman et al., 2019).

Furthermore, a new potentiator, GLPG1837, was developed by Galapagos (Van der Plas et al., 2018) and has recently entered clinical trials (Davies et al., 2019). The compound appears to be more effective on class III gating mutants (G551D and G1349D) and seems to be less detrimental to the folding and trafficking of corrected F508del-CFTR than VX-770 (Gees et al., 2018). Efforts have been made to identify potentiators that do not impair F508del-CFTR biogenesis and corrector action (Phuan et al., 2015). The difficulties associated with the combination corrector-potentiator therapies have led to the identification of several dual-acting molecules that appear to both correct and potentiate F508del-CFTR and might eventually abolish the need for combination treatment (Favia et al., 2014; Knapp et al., 2012; Pedemonte et al., 2011; Phuan et al., 2011), although no high-potency dual-acting modulators have emerged so far.

### *Low temperature*

The folding defect of F508del-CFTR is temperature sensitive and, in the laboratory, a common strategy to promote trafficking of F508del-CFTR to the cell surface involves incubating cells at low temperatures, generally between 26 and 30 °C (Denning et al., 1992a; Rennolds et al., 2008; Varga et al., 2008; Wang et al., 2008; Yang et al., 2003). Low temperature is thought to provide an energetically favourable folding environment leading to a decrease in F508del-CFTR misfolding and increase of F508del-CFTR being trafficked to the Golgi and subsequently to the cell membrane. A study by Rennolds *et al.* (2008) suggests low temperature also promotes trafficking of core-glycosylated immature in addition to complex-glycosylated mature F508del-CFTR, the first depending on a nonconventional trafficking pathway that by-passes the Golgi. It has been suggested that the stress associated with low temperature evokes a response during which the cell alters its protein expression in a way that promotes F508del-CFTR processing and trafficking through alternative pathways (Gomes-Alves et al., 2009). However, the exact mechanism by which low temperature rescues F508del-CFTR biogenesis has yet to be elucidated.

### Revertant mutations

Rescue of F508del-CFTR can be achieved by introducing second-site mutations in *cis* with F508del. Identified rescue mutations located in the NBD1 include V510D/E/A (Loo et al., 2010; Ren et al., 2013; Wang et al., 2007), I539T (Decarvalho et al., 2002; He et al., 2010), G550E (Decarvalho et al., 2002), R553M/Q (Teem et al., 1993) and R555K (He et al., 2010; John L Teem, Carson, & Welsh, 1996; although these findings could initially not be replicated by Chang et al., 1999). Whereas some of these mutations restore either maturation (V510D/E, R555K) or channel opening (V510A), others promote both (I539T, G550E, R553M/Q).

The NBD1 has been particularly well studied with regards to the effects of second-site rescue mutations in *cis* with F508del. This is probably because most rescue mutations have been identified using the yeast chimera system developed by Teem and colleagues (1993). This system exploits the modular structure of ABC transporters and the high degree of conservation among their NBDs. Incorporation of the NBD1 sequence from the human *CFTR* gene into the *STE6* gene of *Saccharomyces cerevisiae* (which translates into Ste6p), allowed thousands of random second-site mutations in *cis* with F508del to be screened. The system is limited to investigating the NBD1 because this is the only part of CFTR present in the STE6-CFTR hybrid

R1070W, located in the ICL4 (**Figure 5**), partially corrects both function and trafficking of F508del-CFTR (Mendoza et al., 2013; Rabeh et al., 2012; Thibodeau et al., 2010). While mutations like G550E, R553Q and R555K appear to rescue F508del-CFTR by partially reducing F508del-NBD1 thermodynamic and kinetic instability (Rabeh et al., 2012; Roxo-Rosa et al., 2006), R1070W is thought to act by repairing the impaired interaction between the NBD1 and ICL4.

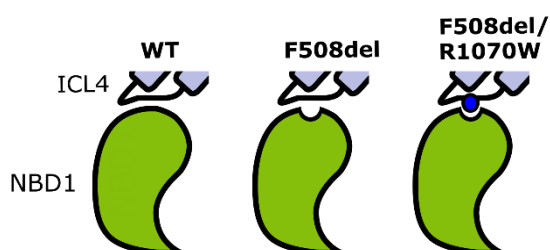


**Figure 5 Representation of the ICL4-NBD1 interface in WT-CFTR, F508del-CFTR, and F508del/R1070W-CFTR**  
F508del causes the deletion of F508 on the NBD1 side of the ICL4-NBD1 interface. The defects caused by F508del, can be partially reverted by R1070W (blue circle), located in the ICL4 side of the interface.

## 1.5 Methods for CFTR assessment

### 1.5.1 Channel function

#### *Patch clamp technique*

In 1976, Neher and Sakmann developed the patch-clamp technique. The technique involves forming a seal between a glass micropipette and the lipids surrounding a small patch of the cell membrane. The micropipette is filled with an electrolyte solution and connects to a recording electrode, allowing direct measurement of the current flow through individual, or groups of channels present in the membrane patch (Neher & Sakmann, 1976). Patch clamping can provide detailed kinetic information on ion channel function and is regarded as a gold standard for ion channel research. Despite its high information content, the technique is time consuming and requires a high level of experience and technical skills making it difficult to adapt for screening for drug development. Automated patch clamp techniques have been found to be suitable for investigation of CFTR pharmacology, providing a medium throughput screening method (Billet et al., 2017). However, only whole cell records can be obtained with these techniques, precluding detection of single-channel gating events and therefore providing only limited information on ion channel function.

#### *Ussing chamber*

The Ussing chamber system is named after the Danish zoologist Hans Ussing, who developed a device capable of measuring the short-circuit current reflecting ion transport across frog skin (Ussing & Zerahn, 1951). The Ussing chamber consists of two halves filled with a physiological solution separated by a monolayer of epithelial cells across which ion transport takes place. Current and voltage electrodes at the apical and basolateral side of the chamber allow the measurement of resistance, current, voltage, capacitance across the layer of cells (Li et al., 2004). The method allows a direct electrophysiological assessment of CFTR function in the apical membrane of primary airway epithelial cultures. While the Ussing chamber allows investigation of CFTR within a physiologically relevant system, it does not allow simultaneous evaluation of a large number of samples, making this technique relatively low throughput.

### *Radiotracer flux*

Radiotracer flux methods allow the determination of anion permeability using an appropriate radiotracer ( $^{36}\text{Cl}$  or  $^{125}\text{I}$  for chloride channels; Norez et al., 2004). Cells expressing CFTR are washed with a physiological buffer and then loaded with the radiotracer. After the radiotracer has diffused into the cells the loading buffer is replaced with a radiotracer-free buffer and the efflux of radiotracer is quantified by sampling the buffer at determined time intervals and counting the radioactivity in each sample with a gamma counter for  $^{125}\text{I}$  or beta scintillation counter for  $^{36}\text{Cl}$ . Radiotracer flux methods provide high throughput and have been used in several studies for quantification of CFTR mediated ion flux (e.g. Becq et al., 1999; Dormer et al., 2001; Vachel, Norez, Becq, & Vandebrouck, 2013). Another similar but nonradioactive method uses an iodide-sensitive electrode for quantification of CFTR mediated ion transport (Long & Walsh, 1997). In addition to not requiring the use of radioactive isotopes, this method allows continuous measurements.

### *Iodide influx assays using halide sensitive YFP*

The development of a halide sensitive YFP with a high affinity for iodide and a low affinity for chloride (Galiotta et al., 2002, 2001b), has allowed assessment of CFTR-mediated conductance by analysis of the rate of YFP quenching related to iodide influx. The halide sensitive YFP serves as an iodide sensor that quenches when iodide binds to it (see section 3.2.1 *YFP(H148Q/I152L)*). A modified version of this assay in which the halide sensitive YFP is tagged onto the N terminal, instead of co-expressed with CFTR, has been developed in our group (Langron et al., 2017). Linking the fluorophore to CFTR has reduced variability and has allowed more accurate quantification of CFTR function.

### *FRET based membrane potential assay*

Vertex Pharmaceuticals has employed a high throughput screening assay that enables monitoring of the transmembrane voltage using fluorescence resonance energy transfer (FRET) (Van Goor et al., 2006). FRET refers to the energy transfer between two fluorophores: a fluorescent donor that is excited, may transfer its energy to another fluorescent molecule, the acceptor, which then emits within a distinct emission wavelength range. The assay uses a membrane-soluble dye that is

positioned in the outer leaflet of the membrane and acts as donor, and a voltage-sensitive dye which is also located in the outer leaflet of the membrane at resting membrane potential. When the membrane depolarises, the voltage-sensitive acceptor flips to the inner leaflet of the membrane, reducing the FRET signal (González et al., 1999). Being able to monitor the changes in membrane potential allows indirect quantification of CFTR channel function. Vertex Pharmaceuticals has used this method to screen hundreds of thousands of compounds, eventually leading to the development of VX-770 and VX-809 (Van Goor et al., 2009, 2011).

### *Organoids*

An organoid is a three-dimensional culture, developed from stem cells or organ progenitors, that contains several cell types and recapitulates the histological organisation and function specific to that organ (Lancaster & Knoblich, 2014). Intestinal organoids cultured from intestinal stem cells possess essential features of the *in vivo* tissue function and anatomical architecture. They can be used as models to study altered transepithelial fluid movement in cystic fibrosis (Dekkers et al., 2013). Dekkers and colleagues (2013) found that forskolin mediated activation of intestinal CFTR – which is mainly expressed at the apical membrane of the crypt cells – induced a rapid swelling of intestinal organoids that entirely depends on CFTR. While organoids from healthy subjects swell in response to forskolin, the swelling is severely reduced or absent in organoids derived from people with cystic fibrosis. The swelling of the intestinal organoids correlates with clinical responses of patients with corresponding genotypes (Dekkers et al., 2016). Organoid forskolin-induced swelling can therefore assess the impact of CFTR mutations and other patient-specific genetic factors that may contribute to disease phenotype, and the response to pharmacological intervention. Testing of drug combinations on patient-derived organoids has been proposed as the basis of “n-of-one” clinical trials to help patients with rare mutations get faster access to treatment.

## 1.5.2 Biogenesis

### *Western blot*

CFTR is synthesized in the ER where core-oligosaccharide chains are attached to the protein co-translationally (Chang et al., 1994). After this, if it is not degraded, it is transported to the Golgi where it undergoes post-translational modifications producing the fully glycosylated mature form. CFTR maturation is most often studied using Western blot techniques, allowing assessment of intracellular processing of CFTR. Western blot allows proteins to be separated based on molecular weight through gel electrophoresis after which they are transferred to a solid support and labelled using antibodies for visualisation of the protein of interest through methods such as staining or immunofluorescence (Bass et al., 2017). The intensity of the band corresponds to the amount of labelled protein present in the sample and the distance migrated through the gel is related to its molecular weight.

According to its glycosylation status, three different forms of the CFTR can be distinguished. CFTR can be non-glycosylated CFTR (band A, 130 kDa), ER core-glycosylated (band B, 150 kDa) and fully glycosylated (band C, 170–180 kDa). Band A can only be detected following treatment with glycosidases. CFTR maturation is often quantified using the ratio of band C over band C plus band B. This technique is technically challenging and it is hard to convert Western blotting from a qualitative technique to a quantitative technique; violations of assumptions underpinning sample comparison in Western blot data can lead to incorrect inferences and may contribute to poor reproducibility of research (Butler et al., 2019).

### *Extracellular epitope tagging*

An epitope refers to the unique binding region of a molecule to an antibody. Antibodies directed against extracellular epitopes – either endogenous (Denning et al., 1992b) or exogenous generated by in-frame insertion of non-CFTR coding sequences in the CFTR gene (Howard et al., 1995) – allow detection of the CFTR located on the plasma membrane in non-permeabilised cells. An engineered CFTR gene, with introduction of 3 copies of a human influenza hemagglutinin epitope tag in a row into

ECL4 (CFTR-3HA), has been used in several studies for quantification of CFTR cell surface density, internalization rate, and cell surface stability (Barriere et al., 2009; Glozman et al., 2009; Pedemonte et al., 2005a; Phuan et al., 2014; Sharma et al., 2004) and has been successfully modified for high throughput screening for F508del-CFTR correctors (Carlile et al., 2007).

A double-tagged CFTR with an extracellular exogenous FLAG epitope, or FLAG-tag, added to ECL4 and an intracellular mCherry tag linked to the N-terminal of CFTR was developed by Botelho and colleagues (Botelho et al., 2015). This recombinant protein enables detection of the total amount of CFTR via mCherry fluorescence intensity, and membrane CFTR detection via antibodies directed to the FLAG epitope. While the other image-based assays discussed here only allow quantification of membrane bound CFTR, this assay is capable of measuring both total CFTR and membrane CFTR.

#### *Horseradish Peroxidase tag*

Chemiluminescence refers to the release of photons at a specific wavelength from chemical reactions. The process involves the formation of an unstable chemical species that decomposes, leaving one or more of its reaction products in an electronically excited state. These finally emit a photon as they relax to their ground state (Baldwin, 2013). One of the most exploited chemiluminescent reactions is the oxidation of luminol, which can be catalysed by horseradish peroxidase (HRP), generating a bright blue luminescence. Quantification of CFTR membrane density has been achieved by tagging HRP to ECL4 (Phuan et al., 2014; Veit et al., 2014). When Luminol is added to the extracellular medium it is oxidised by the HRP tag of membrane localised CFTR, and the rate of chemiluminescence emission is used to quantify the membrane density of CFTR. The method has been employed for synergy-based screening to identify corrector combinations that are effective in increasing cell surface expression of F508del-CFTR (Phuan et al., 2014) and potentiator-corrector combinations that do not reduce corrector efficacy (Phuan et al., 2015).

#### *Fluorogen activating protein tag*

Fluorogen activating proteins (FAPs) do not fluoresce unless bound to specific small-molecule fluorogens. Membrane proteins that have an extracellular FAP tag are detected with cell membrane

impermeable fluorogens, whereas proteins within intracellular compartments can only be visualised with membrane permeable fluorogens (Xu & Hu, 2018). Malachite Green FAP tags have been fused to the N-terminus of CFTR (with an additional membrane-spanning segment) or the fourth extracellular loop of CFTR, making it possible to rapidly detect CFTR at the cell surface (Holleran et al., 2012). The authors concluded that although glycosylation of the ECL4 FAP-tagged CFTR was impaired and had a generally lower membrane density compared to WT-CFTR, both FAP tags produced functional CFTR fusion proteins with qualitatively similar behaviour.

### *pH-sensitive tag*

To enable fast quantification of both membrane localised CFTR and internal CFTR in living cells, a fluorescence assay was developed in our group (Langron et al., 2017). A pH sensitive red fluorescent protein, pH-tomato, was tagged to the fourth extracellular loop of CFTR. Only the deprotonated form of pH-tomato is fluorescent, so as the pH increases more of the pH-tomato proteins exist in their deprotonated form, increasing the fluorescence (Li & Tsien, 2012). First, using a non-permeant buffer, the pH of the extracellular environment is lowered to 6.5, then raised to ~9. The corresponding change in pH-tomato fluorescence intensity represents membrane localised CFTR. After this, NH<sub>3</sub> is added to permeate the membrane and internal vesicles, raising the intracellular pH. The increase in fluorescence associated with NH<sub>3</sub> addition is used to estimate the level of immature CFTR that is localized along the biosynthetic pathway. The assay allows rapid quantification of membrane localised and internal CFTR without involving multiple washes or incubations with expensive antibodies.

## **1.6 Aims of this research**

1.6.1 Enabling rapid and simultaneous assessment of CFTR function and biogenesis  
Many CFTR variants associated with cystic fibrosis, including F508del-CFTR, are characterized by processing as well as functional defects. Rescue of either ion channel function or CFTR biogenesis alone appears to be insufficient for effective treatment of patients (Clancy et al., 2012; Flume et al., 2012). On top of that, potentiators can negatively interfere with corrector action (Cholon et al., 2014; Veit et al., 2014). Monitoring of CFTR biogenesis in addition to channel function provides a clear

advantage for drug development as well as for structure/function studies. Until now, no assay has been available for simultaneous assessment of CFTR biogenesis and function. Instead, assays for CFTR screening report on either CFTR biogenesis or CFTR function. One of the aims of this research was to develop a method that allows rapid and simultaneous assessment of both CFTR biogenesis and channel function in live cells.

### 1.6.2 Investigating F508del-CFTR rescue by second site mutations

The second aim of this research was to identify revertant mutations in *cis* with F508del. In addition to helping us understand why F508del-CFTR is not functioning correctly, identification of revertant mutations could help us find targets for pharmacological intervention. Furthermore, the use of revertant mutations alongside pharmacological compounds can help elucidate their mechanism of action; the extent to which a compound can synergise with a certain revertant is information that can be used to make inferences on the compound mechanism. Using this strategy, Okiyoneda and colleagues (2013) were able to demonstrate that most corrector compounds identified to date target the NBD1-ICL4 interface (**Figure 6**). Increased understanding of the molecular mechanisms underlying both the efficacy of these correctors and the importance of the NBD1-ICL4 interface for CFTR folding and gating, could help guide the development of more effective modulators.

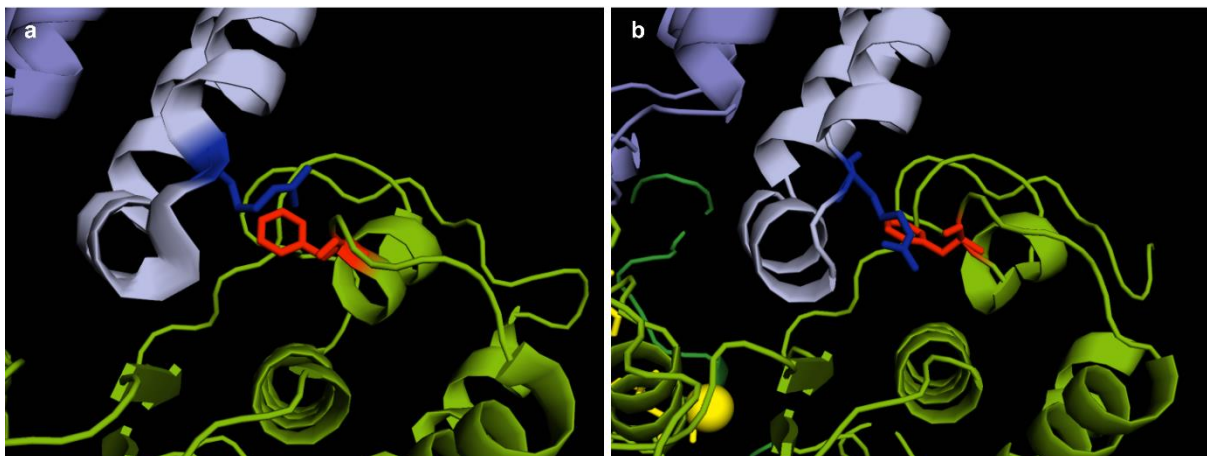


**Figure 6** ICL4-NBD1 molecular structure

Ribbon representation of the ICL4-NBD1 interface from the cryo-EM structure of apo human CFTR, 5UAK (**a**) and of the phosphorylated, ATP-bound form of human CFTR, 6MSM (**b**). The NBD1 is depicted in green and the ICL4 in purple. Deletion of F508 (red sticks), impairs the interactions at the interface. This impairment can be partially restored by changing the arginine (R) at site 1070 (blue sticks) to a tryptophan (W).

## 2. Methods

### 2.1 Molecular Biology

#### 2.1.1 pIRES2-mCherry-YFPCFTR construction

Subcloning is a technique used to move a DNA fragment from one plasmid into another plasmid. Restriction enzymes are capable of recognising short DNA sequences, referred to as restriction sites, and cleave the DNA backbone at specific positions within or next to the restriction site. They can be used to simultaneously excise plasmid fragments in the donor and destination plasmids. After isolation of the fragments, they can be ligated by an enzyme called DNA ligase which covalently binds the plasmid fragments together.

The pIRES2-mCherry-YFPCFTR plasmid with the IRES2 positioned between the two open reading frames for mCherry and YFP-CFTR was obtained with two sequential subcloning steps and was a joint effort involving Dr Emily Langron and me. First the pIRES2-eGFP-YFPCFTR plasmid was constructed by subcloning a 1.727kb region of pcDNA3.1-YFP-CFTR, containing the YFP(H148Q/I152L) coding segment, into eGFP-pIRES2-CFTR (a gift from David Gadsby, Rockefeller University) using the *Nhe1* and *Blp1* restriction sites (**Figure 7a**). Subsequently a 0.737kb region from pIRES2-mCherry-p53 deltaN, containing the mCherry-coding segment and part of the ECMV IRES (Lin, Karoly, & Taatjes, 2013, Plasmid #49243 from Addgene), was subcloned into the pIRES2-eGFP-YFPCFTR plasmid using the *Not1* and *BmgB1/Btr1* restriction sites (**Figure 7b**).

Double digests with *Nhe1* and *Blp1* restriction enzymes (step 1 **Figure 7a**) and with *Not1* and *BmgB1/Btr1* restriction enzymes (step 3 **Figure 7b**) were carried out at 37 °C for 3 h, after which preparative 0.8 % agarose gels were used to separate the fragments by gel electrophoresis. After confirming that the fragments had the expected molecular weight, the bands containing the relevant DNA fragments were cut out of the gel and purified using the Wizard® SV Gel and PCR Clean-up System (Promega UK Ltd., Southampton, UK).

For the ligation (step 2 and 4 **Figure 7**), the isolated DNA fragments (1:1 molar ratio) were mixed in ATP-containing ligation buffer and T4 DNA ligase (New England Biolabs) was added. T4 DNA ligase is the ligase most commonly used for ligation in molecular biology applications and requires ATP as a cofactor. The mixtures were incubated at 16 °C overnight after which the T4 DNA ligase was heat inactivated at 65°C for 10 minutes. Subsequently the mixture was chilled on ice and transformed into 5-alpha Competent *E. coli* (New England Biosciences) that were plated on LB agar containing 50 µg/ml kanamycin. Colonies were inoculated in 50 ml LB broth with 50 µg/ml kanamycin, to maintain selection for the plasmid, and incubated at 37 °C overnight in a shaking incubator (250 rpm). Finally, the plasmids were purified using Qiagen midi prep kits, according to the instructions of the manufacturer (Qiagen Ltd., Manchester, UK).

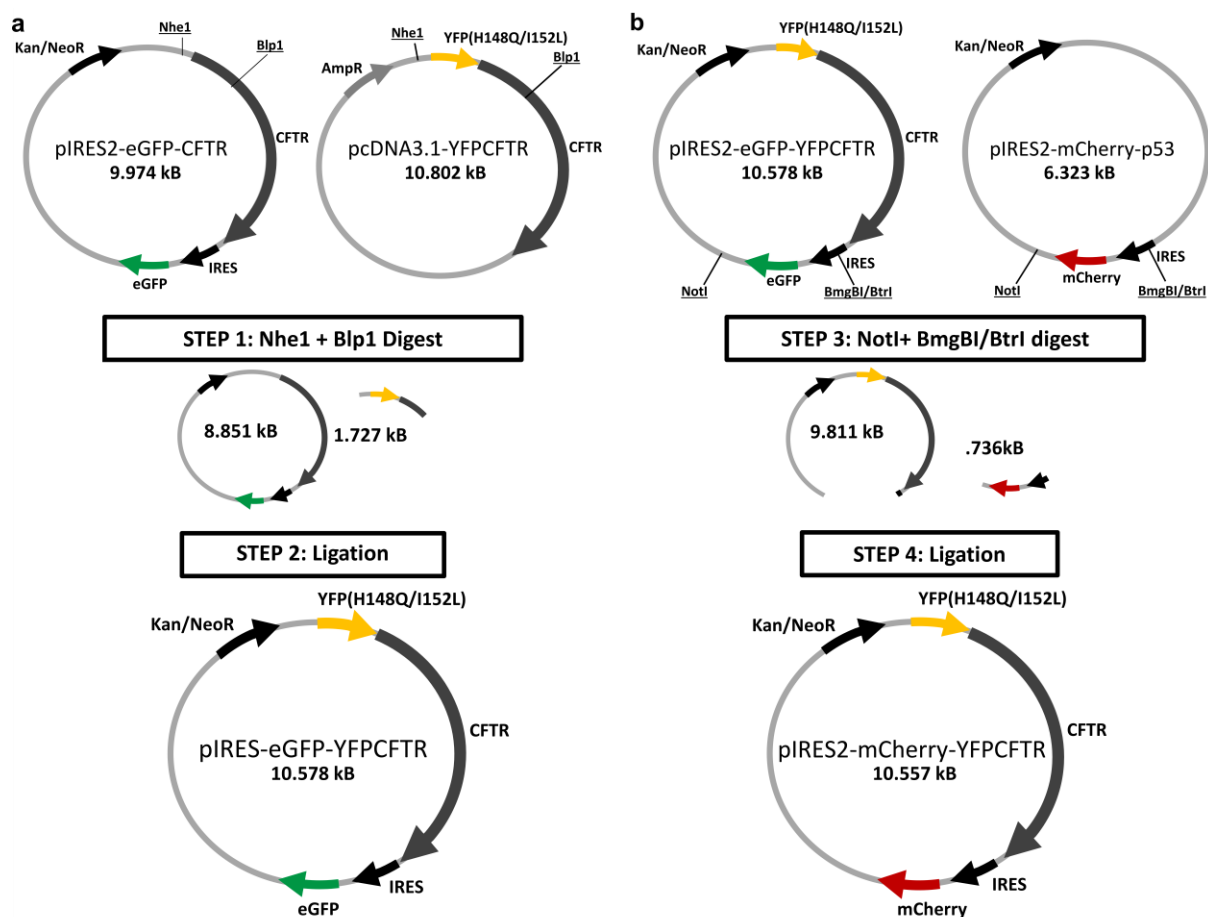


**Figure 7 Construction of the pIRES2-mCherry-YFPCFTR plasmid**

a) The pcDNA3.1-YFP-CFTR plasmid and the pIRES2-eGFP-CFTR plasmid were digested (step 1) and ligated (step 2) to construct an pIRES2-eGFP-YFPCFTR plasmid. b) The pIRES2-eGFP-YFPCFTR plasmid and the pIRES2-mCherry-p53 plasmid were digested (step 3) and ligated (step 2) to create the pIRES2-mCherry-YFPCFTR plasmid.

## 2.1.2 Introduction of second-site mutations in *cis* with F508del

### *Site directed mutagenesis*

To introduce second-site mutations in *cis* with F508del, site-directed mutagenesis was performed on pcDNA3.1-YFP-CFTR template and the pIRES2-mCherry-YFPCFTR template using a modified version of the QuikChange protocol (Stratagene). QuikChange allows the introduction of site-specific mutations in double-stranded plasmids. The protocol makes use of complementary primers in which the desired mutation is incorporated. Following initial denaturation, the temperature is lowered to a temperature that allows the primers to anneal to the template. After this, the temperature is raised and the primer is extended by a thermostable DNA polymerase that copies the rest of the plasmid. This temperature cycle protocol is repeated 18 times. To separate the mutated plasmid from the template parent plasmid, the PCR product is digested by *DpnI*, which is a restriction enzyme that digests methylated DNA. In this way only the newly synthesized, unmethylated, mutant DNA remains uncut.

Forward and reverse complementary primers containing each mutation flanked by approximately 15 complementary bases (Eurofins MWG Operon, Germany) were incorporated in single-strand, nicked plasmid replicates by thermal cycling, as described above. Each reaction mixture (100  $\mu$ l) contained 100 ng F508del-CFTR-YFP(H148Q/I152L) template DNA, 0.5  $\mu$ M of each primer (forward and reverse), 80  $\mu$ M of each deoxyribonucleotide triphosphate (dNTP) (New England Biolabs), 2 units Phusion polymerase enzyme (New England Biolabs) in Phusion High-Fidelity (HF) buffer with 5 % dimethyl sulfoxide (DMSO) to minimise the formation of secondary structures. To denature the template plasmid, and to anneal and extend the oligonucleotide primers, the reaction mixtures were cycled in a Thermal Cycler (model 2720, Applied Biosciences, see **Figure 8a** for the cycling parameters).

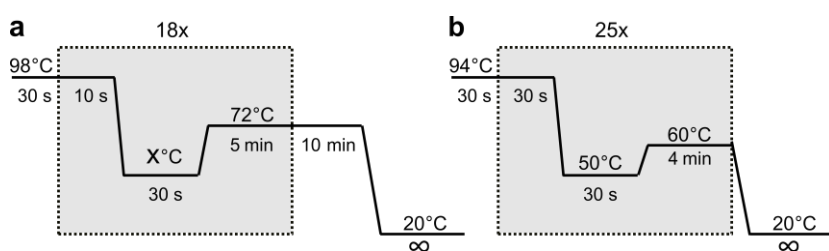


**Figure 8 Thermal cycling protocols**

**a)** Parameters used for mutant strand synthesis. Temperature X ranged from 52°C to 56°C. **b)** Parameters used for sanger sequencing.

After the temperature reached 20 °C in the final hold segment, the methylated parental template DNA was digested with 2 µl *Dpn1* (20U/µl) at 37 °C for two hours, or overnight at room temperature. To precipitate the DNA, sodium acetate (NaOAc) and ethanol (EtOH) were added to each sample (to reach a final concentration of 83.3 mM and 70 % respectively) after which they were kept for 20 min at -20 °C. Subsequently the mixture was centrifuged twice at 24,000 × *g* (20 min, 4 °C). After the first centrifugation, the supernatant was removed, and 100 µl 70 % EtOH added to the pellet. After the second centrifugation, the supernatant was removed, and the sample resuspended in 10 µl 10 mM tris(hydroxymethyl)aminomethane 1 mM ethylenediaminetetraacetic acid (Tris-EDTA or TE) buffer (pH 8) to protect the DNA from degradation. The Tris helps maintain a constant pH and the EDTA chelates metal ions whereby it inhibits metal ion-dependent activities of DNases that would otherwise degrade the DNA by catalysing the hydrolytic cleavage of phosphodiester bonds in the DNA backbone.

#### *Transformation of chemically competent E. coli*

*Escherichia coli* (*E. coli*) is a widely used host for molecular biology procedures. Transformation is defined as the transfer of genetic information into a recipient bacterium and competence refers to its ability to take up and propagate plasmids. *E. coli* are pre-treated with inorganic ions, DMSO and dithiothreitol (DTT), rendering them chemically competent, then incubated with the exogenous DNA on ice and given a brief heat shock to favour DNA uptake (Hanahan, 1983). 1 µL of the site-directed mutagenesis product was chilled on ice in a 13 ml culture tube (Sarstedt). 18 µL of competent *E. coli* (New England Biosciences, 5-alpha Competent *E. coli*, High Efficiency) were added, and incubated on ice for 20 - 30 min. The mixture was heat shocked at 42 °C for 41 s, then returned to ice for ~2 min. Super Optimal broth with catabolite repression (SOC, Life Technologies) was added and the mixture was incubated at 37 °C in a shaking incubator (250 rpm) for 60 minutes, allowing recovery of the *E. coli*. To select the *E. coli* that have incorporated the desired plasmid, 200 µl of the *E. coli* / SOC mixture was spread on Luria Bertani broth (LB broth, Sigma-Aldrich Company Ltd., Dorset, UK) agar plates (1.5 % (w/v) agar), containing 100 µg/ml ampicillin or 50 µg/ml kanamycin. The plates were incubated overnight at 37 °C.

### *Mini prep*

*E. coli* colonies were inoculated in 5 ml LB broth (Sigma-Aldrich Company Ltd., Dorset, UK) containing 100 µg/ml ampicillin or 50 µg/ml kanamycin, and the cultures were grown for ~8 hours in a 37 °C swirling incubator (250 rpm). After this, the *E. coli* were spun at 1,811 *g* for 20 min in a centrifuge (5810R Eppendorf centrifuge). The supernatant was discarded, and for isolation of plasmids from *E. coli* cells mini preps were carried out using a Qiagen mini prep kit according to the instructions of the manufacturer (Qiagen Ltd., Manchester, UK). This kit is designed for purification of up to 20 µg high-purity plasmid. Alkaline lysis of bacteria cells is followed by adsorption of the DNA onto a spin column that contains a silica gel membrane that selectively, binds DNA, after which the DNA is washed and eluted in low salt solution using a microcentrifuge (5415R Eppendorf centrifuge, Eppendorf UK Ltd, UK).

### *Gel electrophoresis*

To estimate the concentration of the purified plasmids and DNA fragments, and confirm their approximate size in base pairs, mini and midi prep samples were visualised using gel electrophoresis. Gel electrophoresis makes use of an electrical field to move DNA (which is negatively charged) through an agarose gel towards a positive electrode. Shorter DNA fragments migrate through the gel more quickly than larger ones. The distance migrated on the gel is inversely related to the logarithm of the molecular weight of the DNA fragment. The concentration and size of the DNA fragments can be determined by calibrating the gel, using known amounts of size standards, and comparing band brightness (to estimate concentration) and the migration distance of the fragment (to estimate size).

To create the gel, 0.32 g agarose (0.8%, Starlab) was dissolved in 40 ml Tris-Acetate-EDTA (TAE) buffer (Life Technologies), followed by 1 min of heating in a standard microwave at 800 W. 1 µl of 10 mg/ml ethidium bromide solution (Sigma-Aldrich) was added to the gel after which it was poured into a gel casting tray and left to set for ~40 min. The ethidium bromide allows visualisation of the DNA. When exposed to UV light it emits an orange fluorescence which intensifies ~20-fold when the compound is intercalated between paired bases in the DNA helix.

After the gel had set, combs to create wells were removed and 260 ml TAE buffer was poured over it to submerge it. 2 or 1  $\mu\text{l}$  of 6x Gel Loading Dye, Purple (New England Biolabs) was added to 10 or 5  $\mu\text{l}$  of plasmid sample respectively (depending on the well sizes in the gel). The loading dye helps the sample sink to the bottom of the well, and it gives a colour indication for following the migration of the DNA sample. Once the DNA and dye were loaded in the wells, an electrical potential difference of 100 V was applied to opposite sides of the gel chamber. The potential difference attracts the negatively charged DNA to the positive end of the chamber. Each gel was run for 40 min. A 1kb DNA ladder (Quick-Load Purple, New England Biolabs) was run alongside each set of samples. This ladder is composed of DNA fragments of known size and concentration, so that the concentration and size of the DNA fragments in the sample can be inferred.

#### *Fluorescence-based cycle sequencing*

The preparation for sequencing involved repeated cycles of denaturation, annealing of primers and extension (see **Figure 8b** on p. 46 for the thermal cycling parameters) in the presence of BigDye Terminator v1.1 mix (Life Technologies). Primers approximately 20 bases long (Eurofins) complementary to the DNA sequence between 100 and 500 bases upstream of the region of interest were used. BigDye Terminator v1.1 (Life Technologies) contains thermostable polymerase, dNTPs for strand elongation, and fluorescently labelled 2'-3'dideoxynucleotide triphosphates (ddNTPs), each ddNTP labelled with a dye emitting at a different wavelength. The ddNTPs lack the 3' OH group to which the  $\alpha$ -phosphate of the next dNTP of the growing DNA chain would normally be covalently linked. Therefore, the ddNTPs terminate strand elongation when they are incorporated, resulting in a mixture of DNA chains of different lengths.

2  $\mu\text{l}$  of Big Dye 1.1, 0.3  $\mu\text{M}$  primer, and  $\sim 100$  ng mini or midi prep sample were mixed in a 0.2 ml thin-walled PCR tube and water ( $\text{dH}_2\text{O}$ ) was added to reach a volume of 10  $\mu\text{l}$ . After temperature cycling, 10  $\mu\text{l}$   $\text{dH}_2\text{O}$ , 50  $\mu\text{l}$  EtOH (to reach a concentration of  $\sim 70$  %) and 2  $\mu\text{l}$  3M NaOAc (to reach a concentration of 83.3 mM) were added to precipitate the DNA and it was chilled on ice for  $\sim 10$  min and centrifuged at 16,100  $g$  for 15 min at 4  $^\circ\text{C}$ . After removing the supernatant, the pellet was washed

with 100  $\mu$ l 70 % EtOH, and centrifuged again at 16,100  $g$  for 15 min. The pellet was left to dry for at least 2 h before analysis.

Laser detection was used to detect the fluorescence-tag labelled ddNTPs after capillary electrophoresis to separate and sort the chains according to length, generating a sequence chromatogram with fluorescent peaks corresponding to the different nucleotides in the DNA sequence. The chromatograms were generated by the UCL Sequencing Facility using a 3100-Avant Genetic Analyzer (Applied Biosystems), or outsourced to SourceBioscience (Nottingham UK).

### *Midi prep*

Single *E. coli* colonies were inoculated in 50 ml LB broth (Sigma-Aldrich Company Ltd., Dorset, UK) containing 100  $\mu$ g/mL ampicillin or 50  $\mu$ g/mL kanamycin, and the cultures were grown overnight (~15 hours) in a 37 °C rotating incubator (250 rpm). The culture was spun at 1,811  $g$  for 20 min in a centrifuge (5810R Eppendorf centrifuge) and the supernatant was discarded. Midi preps were carried out according to the instructions of the manufacturer using a Qiagen midi prep kit (Qiagen Ltd., Manchester, UK). The kit uses gravity-flow, anion-exchange tips for purification of the DNA. After this, the DNA (eluted in 5 ml elution buffer) was precipitated by addition of 3.5 ml isopropanol (30%), and centrifuged at 24,000  $\times g$  (30 min, 4 °C), in a Beckman J2-M1 centrifuge (Beckman Coulter (UK) Ltd., High Wycombe, UK). The supernatant was discarded after which the pellet was washed with 2 ml 70 % EtOH and centrifuged for 10 min at 24,000  $\times g$  (4 °C). After centrifuging, the EtOH was discarded and the pellet was air-dried. The pellet was resuspended in 100  $\mu$ l 10 mM TE-buffer (pH 8) and the yield was estimated using gel electrophoresis.

## 2.2 HEK-293 cell culture and transfection

### 2.2.1 HEK-293 cell line

Human Embryonic Kidney 293 (HEK-293) cells were created nearly two decades ago by transformation and culture of human embryonic kidney cells with sheared fragments of human adenovirus type 5 DNA (Graham et al., 1977). They are widely used in cell biology and biotechnology because they are amenable to transfection, faithfully express exogenous proteins and are easy to maintain and

propagate (Thomas & Smart, 2005). Although CFTR potentiator action appears to be independent of cell-type, corrector action has been found to be cell-type specific (Pedemonte et al., 2010). Unfortunately, even CFBE or A549 cell lines derived from human bronchial epithelia, do not fully predict the effectiveness of many correctors in primary human bronchial epithelia derived from patients (Phuan et al., 2014). For our assay we chose to use HEK-293 cells because this cell line offers advantages over more native cell lines, like ease of culture and molecular manipulation. Although they do not form monolayers suitable for measurements of transepithelial currents, they provide a useful system for molecular characterization of the CFTR protein and are widely used to study CFTR biogenesis and function (Domingue et al., 2014)

### 2.2.2 Maintenance HEK-293 culture

We cultured HEK-293 cells at 37 °C in a 5 % CO<sub>2</sub> : 95 % air humidified tissue culture incubator. The cells were kept in T25 flasks (Nunc, Fisher Scientific Ltd., Leicestershire, UK) in the presence of Dulbecco's Modified Eagle Medium (DMEM) supplemented with 2 mM L-glutamine (Life Technologies), 100 U/ml penicillin and streptomycin (Thermo Fischer) and 10 % foetal bovine serum (FBS, Life Technologies). Confluent flasks were passaged every 2-3 days. To passage cells, the DMEM medium was discarded and cells were rinsed with 5 ml Hank's Buffered Salt Solution (HBSS, Life Technologies) after which 1,5 ml 0.05 % trypsin disodium ethylenediaminetetraacetic acid (trypsin-EDTA, Life Technologies) was added for ~3 min to lift the cells. The EDTA chelates calcium and magnesium from the cell surface, disrupting cell-to-cell adhesion and allowing trypsin to cleave peptides on the C-terminal side of lysine and arginine residues, removing adherent cells from a culture surface. To deactivate the trypsin, 9 ml DMEM medium was added before transferring the cell suspension to a 15 ml tube (Falcon, Fisher Scientific). The 10 ml cell suspension was centrifuged for 2 min at 180 g after which the supernatant was removed and the pellet with cells resuspended in 10 ml medium. For passage, 2 ml of the cell suspension was added to 8 ml fresh DMEM medium in a T25 flask.

### 2.2.3 Plating HEK-293 cells

For fluorescence imaging, cells were seeded on black walled 96-well plates (Costar, Fisher Scientific). Before seeding, the wells were coated with poly-D-lysine (PDL). To achieve this, the surface of each well was covered with 45  $\mu$ l PDL for 5 min after which the PDL was removed and then wells were rinsed with 50  $\mu$ l cell culture water. Plates were left to dry for at least 2 hours. HEK-293 cells suspended in DMEM medium were transferred to each well (100  $\mu$ l/well) and the plate was stored overnight in the tissue culture incubator at 37 °C.

### 2.2.4 Transient cationic lipid mediated transfection

When the HEK-293 cells were at least ~30% confluent, a mixture of 500 ng lipofectamine2000 (Life Technologies) and 150 ng plasmid DNA in 50  $\mu$ l Opti-MEM (a minimum essential medium (MEM), buffered with HEPES and NaHCO<sub>3</sub>, and supplemented with hypoxanthine, thymidine, sodium pyruvate, L-glutamine, trace elements, and growth factors) was prepared according to the instructions of the manufacturer and added to each well in order to transiently transfect the cells. Lipofectamine 2000 contains cationic lipids that can form liposomes in an aqueous environment. The positively charged head groups facilitate interaction between the lipids with negatively charged sugar-phosphate backbone of nucleic acids, entrapping the transfection load in liposomes. The positive charge on the surface of the liposomes enables interaction with the negative plasma membrane and fusion is mediated by neutral co-lipids in the lipofectamine 2000 formulation making it possible for the nucleic acids to enter the cell. After adding the transfection reagent, the plates were kept 1-2 day at 37 °C in the tissue culture incubator.

### 2.2.5 Temperature correction and chronic drug treatment

24 hours after cells were transfected, they underwent another 24 hours of incubation at either 37 °C or at 28 °C to temperature correct the expressed CFTR molecules. Some conditions involved chronic treatment (which was 24 hours in this study, during the second incubation) with 10  $\mu$ l VX-809 alone or in combination with 10  $\mu$ l VX-770. For the drug treatments, Opti-MEM solution with the transfection reagents was removed 24 hours after cells were transfected, and the drug(s) or DMSO

(control) were added on top of the cells in 100 µl DMEM medium for 24 hours. Just before imaging, the wells were washed 2 times with 100 µl standard buffer after which 100 µl of standard buffer was added to each well.

## 2.3 Fluorescence image acquisition

In this study we made use of an epifluorescence microscope, in which the same objective is used for illumination of the sample with the excitation light and to detect the fluorescence emitted from the sample. The filter cube contains three filters: an excitation filter, a dichromatic mirror and an emission filter (**Figure 9**). The filters enable separation of light belonging to a certain wavelength band so that an image of the emitted light can be captured without interference from the excitation light. Inverted fluorescence microscopes, where the sample is imaged from below, are most commonly used to image live cells because it allows imaging of cells grown in petri dishes or multi-well plates from below, while media with or without compounds can be left on top of the cells (Murphy & Davidson, 2012).

### 2.3.1 ImageXpress

The ImageXpress (ImageXpress Micro XLS, Molecular Devices) is an image acquisition system that employs an inverted wide-field fluorescence microscope using epifluorescence illumination and contains a temperature-controlled chamber in which cell plates can be loaded. A robotic arm allows

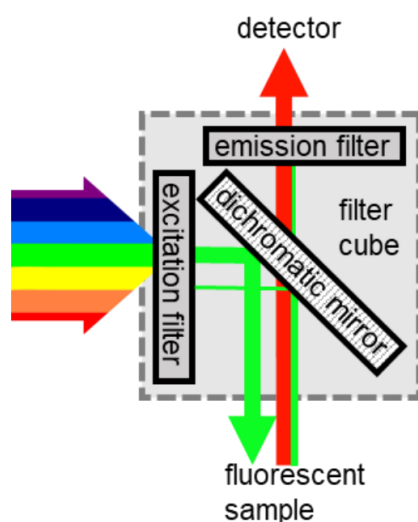


**Figure 9** Layout of a filter cube

A dichroic mirror, an excitation filter and an emission filter, joined in a filter cube, allow the separation of light in bands of certain wavelengths so that the emitted fluorescence can be captured by the detector and imaged. The excitation filter selectively transmits a band of wavelengths to excite the fluorescent sample. The dichromatic mirror reflects the shorter wavelength of the excitation light towards the sample while transmitting the longer emission wavelength of the fluorescence towards the detector. Shorter wavelengths reflected by the sample are directed back towards the excitation filter. The emission filter blocks any residual short excitation wavelengths reflected by the sample and transmits the sample fluorescence. The fluorescence can then be detected and forms an image.

the addition of fluids to the wells in the plate. Protocols for fluid additions were created using MetaXpress software (Molecular Devices). The specifications of the filter cubes used for imaging of YFP-CFTR and mCherry are listed in **Table 1**.

**Table 1** Specifications of the ImageXpress filter cubes used for imaging of YFP(H148Q/I152L) and mCherry

	Excitation filter	Emission filter	Dichroic mirror	
			Reflection	Transmission
YFP(H148Q/I152L)	472 ± 30 nm	520 ± 35 nm	350-488 nm	502-950 nm
mCherry	531 ± 20 nm	593 ± 20 nm	350-555 nm	569-950 nm

### 2.3.2 MetaXpress image acquisition protocols

Three different protocols were created in MetaXpress for imaging: one for measuring CFTR membrane proximity and two protocols for quantifying CFTR function. Both CFTR quenching experiments for function required two “compound” plates – one for the first and one for the second fluid addition – in addition to the “cell” plate. Each well with cells contained 100 µl standard buffer at the start of the experiments

#### *CFTR membrane proximity*

For quantification of CFTR membrane proximity, images of YFP-CFTR as well as mCherry fluorescence were acquired. This was done with either a 60× objective used to take a grid of 9 16-bit binned (2x2 pixels), or unbinned images per well for each fluorophore (4. *Validating the mCherry-YFPCFTR assay*), or with the 20× objective to take a single unbinned image per well for each fluorophore (5. *Second-site mutations in cis with F508del*).

#### *The I<sup>-</sup> first protocol*

A 20× objective was used to take 16-bit images of mCherry and YFP-CFTR fluorescence and images were binned (5x5 pixels). Only two images of mCherry were taken, one at the start and one at the end of the protocol. In contrast, the YFP fluorescence was imaged every 2 seconds over 150 seconds. After acquiring a baseline reading for 20 s, 50 µl of 300 mM I<sup>-</sup> buffer (300 mM NaI, 4.7 mM KCl, 1.2 mM MgCl<sub>2</sub>, 5 mM HEPES, 2.5 mM CaCl<sub>2</sub>, 1mM glucose, pH 7.4) were added from the first compound plate

to the wells in the cell plate, already containing 100  $\mu\text{l}$  of standard buffer, making the final concentration of  $\text{I}^-$  100 mM. 40 s later, another 50  $\mu\text{l}$  of a 100 mM  $\text{I}^-$  buffer containing 40  $\mu\text{M}$  forskolin (100 mM NaI, 4.7 mM KCl, 1.2 mM  $\text{MgCl}_2$ , 5 mM HEPES, 2.5 mM  $\text{CaCl}_2$ , 1 mM glucose, 40  $\mu\text{M}$  forskolin, pH 7.4) were added from the second compound plate, so that the final concentration of forskolin in the extracellular medium was 10  $\mu\text{M}$  while concentration of  $\text{I}^-$  and other components remained the same.

### *The $\text{I}^-$ last protocol*

For this protocol too, a 20 $\times$  objective was used to take 16-bit images (5x5 binning) of both fluorophores, every 2 seconds. After a baseline of 20 s, 50  $\mu\text{l}$  standard buffer containing either 30  $\mu\text{M}$  forskolin or 30  $\mu\text{M}$  forskolin in combination with 30  $\mu\text{M}$  VX-770 (all to reach final concentrations of 10  $\mu\text{M}$ ) were added to wells to activate CFTR in the absence of iodide. After a further 230 s during which no images were obtained and CFTR is assumed to have reached a steady state activation level (Langron et al., 2018), 50  $\mu\text{l}$  of 400 mM iodide buffer (400 mM NaI, 4.7 mM KCl, 1.2 mM  $\text{MgCl}_2$ , 5 mM HEPES, 2.5 mM  $\text{CaCl}_2$ , 1 mM glucose, 40  $\mu\text{M}$  forskolin, pH 7.4) containing either 10  $\mu\text{M}$  forskolin, or 10  $\mu\text{M}$  forskolin in combination with 10  $\mu\text{M}$  VX-770 (to keep the extracellular concentrations of the activating compounds unchanged), was added to achieve an extracellular iodide concentration of 100 mM. Images were taken for 40 more seconds.

## 2.4 Pharmacology

### 2.4.1 Forskolin

We used a high concentration of forskolin, a well-known activator of adenylate cyclase, to evaluate CFTR gating. Forskolin is found in the *Plectranthus barbatus*, a plant used for traditional medicinal practices in India East and Central Africa, China and Brazil (Alasbahi & Melzig, 2010). Forskolin rapidly and reversibly activates adenylyl cyclase, an enzyme that converts ATP into cyclic-adenosine mono phosphate (cAMP), resulting in the increase in intracellular cAMP concentration (Seamon et al., 1981). When cAMP is present, the PKA enzyme is activated and it phosphorylates CFTR. PKA-mediated phosphorylation of the R domain of CFTR, regulates ATP-dependent gating (Anderson et al., 1991).

### 2.4.2 VX-770

In some experiments we used the potentiator VX-770 (Vertex Pharmaceuticals); cells were either exposed chronically (24 h) or acutely together with forskolin to achieve maximal activation of CFTR. VX-770, also known as Ivacaftor, is a FDA-approved drug for treatment of patients carrying the G551D gating mutation and a number of other mutations impairing channel function (Gentsch & Mall, 2018).

### 2.4.3 VX-809

We used chronic (24 hour) incubation with VX-809 (Selleck Chemicals) to investigate the capability of our assay to measure improvements in F508del-CFTR biogenesis. The use of VX-809 alongside VX-770 has been an FDA approved combination for treatment of patients carrying mutations affecting biogenesis (including two copies of F508del) under the name of Orkambi. In addition to enhancing the stability of F508del-CFTR in the ER which allows the protein to exit the ER and subsequently traffic to the plasma membrane, it has been reported that chronic treatment but not acute treatment with VX-809, substantially increases  $P_o$  of the F508del-CFTR that has reached the cell surface (Van Goor et al., 2011). Others, however, have reported that in combination with temperature correction, chronic VX-809 treatment of BHK cells expressing F508del-CFTR only slightly increases the mean burst duration, but does not affect other channel characteristics such as  $P_o$  and interburst intervals (Wang et al., 2018).

## 2.5 Image analysis

Image analysis was automated using MATLAB mathematical computing software (MathWorks). Separate analysis protocols were implemented for estimation of CFTR membrane proximity and channel function

### 2.5.1 Membrane proximity

To assess CFTR biogenesis, we quantified the amount of CFTR located in close proximity of the plasma membrane. A 1.08  $\mu\text{m}$  band within the boundary of each cell was defined as the membrane proximal

zone. The membrane proximity analysis relied on the automated detection of the cell boundaries and was made possible by a combination of morphological operations and image transformations.

#### *Binarisation and noise reduction*

First mCherry images were binarized using a locally adaptive threshold chosen based on the local mean intensity of surrounding pixels. The pixels with values higher than this threshold were assigned the value 1 and all other pixels the value 0 (panel 2, row 1; **Figure 10**). After this, basic morphological operations (i.e. opening, closing, area opening, and dilation) were carried out to reduce noise (panel 3-5, row 1; **Figure 10**). Morphological operations adjust the pixels in an image based on the values of neighbouring pixels. The most basic operations are dilation and erosion. The first adds pixels to the boundaries of objects while the latter removes pixels from object boundaries. Morphological opening of an image is defined by an erosion followed by a dilation. Morphological closing on the other hand, is defined by a dilation followed by an erosion. While opening removes small objects turning them into background, closing removes small holes from objects.

#### *Watershed based segmentation*

To prepare the image for watershed segmentation, a distance transform was performed; assigning to each pixel the value of its distance to the nearest pixel with value 0 (panel 1, row 2; **Figure 10**). Oversegmentation, caused by shallow local minima, was prevented by locating and imposing deep local minima, using the *imextendedmin* and *imimposemin* functions respectively (MATLAB Image Processing Toolbox) (panel 2-3, row 2; **Figure 10**).

The watershed transformation enables boundary detection by treating the image as a topological surface where pixel intensity represents the level of elevation. A drop of water would follow the gradient of the image until it reaches a local minimum. The watershed transform identifies catchment basins corresponding to the areas that would collect water and drain it into a common minimum (panel 4, row 2; **Figure 10**). The ridges that separate the catchment basins from each other are used (white lines panel 4, row 2; **Figure 10**) to draw the boundaries between the cells (panel 5,

row 2; **Figure 10**) enabling segmentation of the image so that separate analysis of individual cells is possible. Cells that were touching the edge of the image were removed from the analysis.

### *Background correction*

Background selection was achieved by inverting the binarized and preprocessed mCherry images (**Figure 10**, panel 5, row 1) after which it was morphologically closed using a large structuring element to prevent cells being mistaken as background. To correct for noise in the signal, the average background fluorescence intensity was subtracted from each pixel. If the average fluorescence intensity inside the cell selection fell below 0 because of low transfection efficiency and high background noise, cells were removed from analysis.

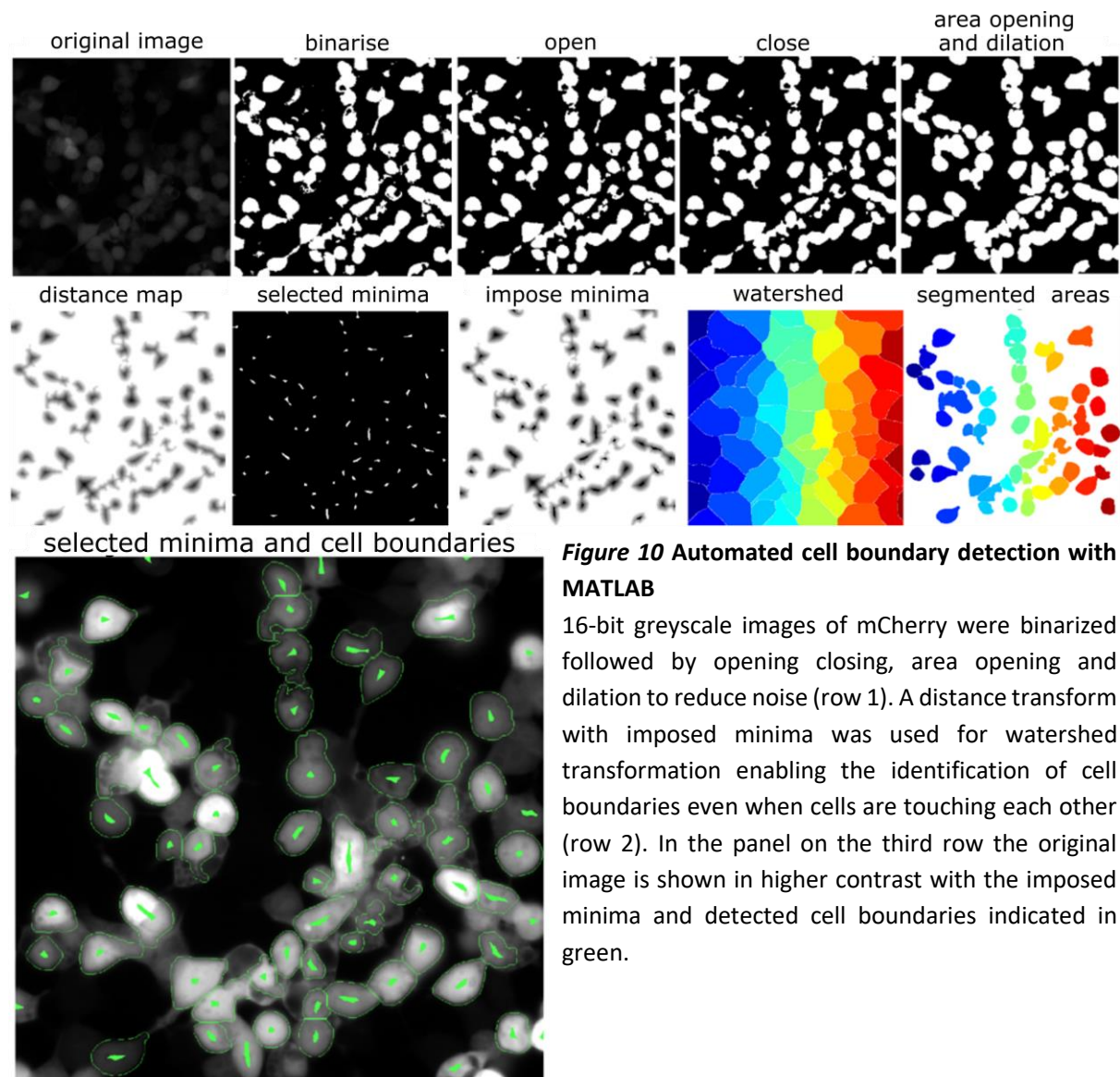


**Figure 10 Automated cell boundary detection with MATLAB**

16-bit greyscale images of mCherry were binarized followed by opening closing, area opening and dilation to reduce noise (row 1). A distance transform with imposed minima was used for watershed transformation enabling the identification of cell boundaries even when cells are touching each other (row 2). In the panel on the third row the original image is shown in higher contrast with the imposed minima and detected cell boundaries indicated in green.

### *Cell filtering*

To minimise the inclusion of image features incorrectly identified as cells in the analysis, cells were excluded if they had an area of under  $108 \mu\text{m}^2$  or over  $5400 \mu\text{m}^2$ , if their longest axis was over  $32.4 \mu\text{m}$ , or if their area over perimeter was less than 25 or over 300.

### 2.5.2 CFTR function

For assessment of CFTR function, two different protocols were used (see 3.4 *Quantification of CFTR Channel function*, p. 67). For both protocols, a cell mask was created using mCherry images obtained before fluid addition and at the end of the experiment. The images were binarized using an adaptive threshold after which they were dilated and combined to account for possible movement of cells over the time course due to fluid additions. The cell mask was used to determine the mean mCherry and YFP(H148Q/I152L) fluorescence intensity inside and outside the cell selection. To correct for fluorescence unrelated to fluorescent protein expression, for each fluorophore the background fluorescence (i.e. the mean fluorescence intensity outside the cell selection) was subtracted from that inside the cell selection. The background-subtracted mean YFP(H148Q/I152L) fluorescence intensity was used for monitoring iodide-dependent YFP quenching and the background-subtracted mean mCherry fluorescence intensity measured at the beginning of the protocol was used to correct estimates for G and for the maximal rate of iodide entry according to transfection efficacy.

## 2.6 Statistics

Statistical analysis was carried out in MATLAB (MathWorks) using the MATLAB Statistics Toolbox. Before statistical tests were performed, distributions were examined to assess whether they approximated normal distributions and whether there was homogeneity of variances. If the normality and homogeneity assumptions for parametric testing were not met, data was transformed to meet the assumptions or non-parametric tests were used to analyse the data. When *post hoc* tests consisted of all possible pairwise comparisons between groups, the Tukey-Kramer procedure was applied to prevent inflation of the type I error rate (using the *multcompare* function in Matlab). On the other hand, when comparisons were planned, either the Bonferroni adjustment or the Benjamini-Hochberg

procedure with a false discovery rate of 10 % was applied to control the family-wise error rate. When only few groups were compared, the Bonferroni adjustment was used. However, because this adjustment is overly conservative when a large number of comparisons are made, the Benjamini-Hochberg was used when many (>60) planned comparisons were made. Statistical tests were performed two-sided unless otherwise specified. Data in graphs represent mean  $\pm$  SEM, and the significance level was pre-specified as  $\alpha = 0.05$ .

### 3. Development of the mCherry-YFPCFTR assay

#### 3.1 Introduction

Like many other CF-causing mutations, the F508del mutation results not only in ion channel dysfunction, but also in a reduction of the number of channels present at the cell surface. It is becoming clear that both defects need to be restored in order to see a significant improvement in lung function in CF patients homozygous for F508del. To get a complete idea of how CFTR variants, like F508del-CFTR, are affected by second-site mutations, drugs, temperature, or other conditions, both ion channel function and biogenesis have to be quantified.

The most informative way to measure CFTR channel function is with single channel patch clamp recordings to fully describe channel properties like gating kinetics, which can be summed up using open probability ( $P_o$ ), and permeation properties, such as single-channel conductance ( $\gamma$ ) and selectivity. However, this method is hard to scale up. The development of a halide sensitive YFP (Galiotta et al., 2001b) has made high throughput screening possible (Galiotta et al., 2001a; Ma et al., 2002; Pedemonte et al., 2005a, 2005b; Yang et al., 2003). Later, Vertex Pharmaceuticals employed a high throughput assay for CFTR channel function based on changes in membrane potential (Van Goor et al., 2006, 2009). Furthermore, the automated patch clamp technique has recently been validated as a medium throughput method for investigation of whole-cell CFTR currents (Billet et al., 2017).

However, the medium and high throughput assays mentioned above do not give any information on the capacity of CFTR to reach the plasma membrane. For this reason, they cannot

discriminate between whether an increase in CFTR conductance reflects an increased number of CFTR channels on the membrane, an improvement in channel function, or both. Potentially promising compounds could be missed because of this, for example when compounds do not potentiate but correct, or when they do potentiate but decrease membrane stability. For these reasons multi-assay approaches have been implemented in drug development, sequentially monitoring the effects of compounds on CFTR channel function and CFTR biogenesis.

Biogenesis and stability at the membrane are often monitored using biochemistry, especially protein immunoblots using the Western Blot technique to compare the proportion of CFTR protein appearing in complex-glycosylated (mature) vs. core-glycosylated (immature) bands. However, this technique is time consuming and several high-throughput assays have been developed to quantify CFTR membrane density independently from channel function. All these exploit tags, fused to the CFTR protein, and exposed on the extracellular side: HA tagged CFTR (Carlile et al., 2007), HRP tagged CFTR (Phuan et al., 2014), FAP tagged CFTR (Larsen et al., 2016), double tagged mCherry/FLAG CFTR (Botelho et al., 2015) and pH-tomato tagged CFTR (Langron et al., 2017).

We developed an assay that makes it possible to simultaneously monitor CFTR channel function and biogenesis in live HEK-293 cells. We constructed the pIRES2-mCherry-YFPCFTR plasmid to enable co-expression of mCherry with YFP(H148Q/I152L) tagged CFTR. The YFP(H148Q/I152L)-CFTR fluorescence quenching in response to iodide influx is used to monitor CFTR function. Depending on the protocol used, the readouts for function are either the maximal rate of iodide entry ( $d[I^-]/dt$  in mM/s) or conductance ( $G$  in nS) and membrane potential ( $V_m$  in mV). CFTR biogenesis is monitored by quantifying the YFP(H148Q/I152L)-CFTR fluorescence that localises at the boundary of the areas of cytosolic mCherry fluorescence. To assess the capacity of CFTR to reach the plasma membrane, we quantified the amount of CFTR in close proximity to the membrane (membrane proximity as  $\rho$ ). The total mCherry fluorescence intensity inside the cell was used as an internal standard to account for different levels of expression.

## 3.2 Fluorescence imaging

The amount of energy carried by a photon is inversely proportional to its wavelength; the more energy it carries and the shorter its wavelength. Molecules can absorb photons if the energy provided by the photon is equal to the energy that is required to promote a molecule from the ground state to a higher energy excited state. Following absorption of a photon, the molecule exists in an excited state before returning to the ground state. There are different ways by which an excited molecule can return to the ground state. The pathway can involve the emission of a photon, which is the process that underlies fluorescence (see Lakowicz, 2006). However, for most molecules alternative nonradiative processes are so efficient that they emit little if any fluorescence.

Because a small amount of energy usually dissipates during the lifetime of an excited molecule, the energy of the photon emitted as fluorescence never exceeds, and is usually less than, the energy of the absorbed photon. For this reason, the wavelength of the emitted fluorescence will be typically longer than the wavelength of the light absorbed and the emission spectrum for a fluorescent molecule will be shifted to longer wavelengths with respect to the excitation spectrum. This shift in wavelength is what makes it possible for fluorescence microscopes to, with the help of optical filters (see **Figure 9**, p. 53), separate the emitted light from the light used for excitation (Murphy & Davidson, 2012; Sanderson, 2019).

Molecules that have fluorescent properties are usually called fluorescent probes or fluorophores. Some of these are proteins, that living organisms have evolved for diverse functions, of which the coding sequence has been cloned. There has been a dramatic growth in the use of these genetically encoded fluorophores in cell biology. A wide and diverse range of fluorophores have been developed many of them with well-separated absorption and emission spectra which makes simultaneous observation of multiple probes within a sample possible. Fluorophores can be tagged to proteins of interest to reveal the intracellular localization of molecules or changes in gene expression through fluorescence imaging. Moreover, fluorophores can be used in living cells to report on changes in their environment like changes in pH, ionic concentrations, or membrane potential (Thorn, 2017)

### 3.2.1 YFP(H148Q/I152L)

Green fluorescent protein (GFP), first observed in the light-emitting jellyfish *Aequorea victoria*, was the first fluorescent protein to be isolated (Shimomura et al., 1962), cloned, biochemically and structurally characterised (Prasher et al., 1992) and used as an endogenous biological marker (Chalfie et al., 1994). Yellow fluorescent protein (YFP) is a variant of GFP that contains the point mutations S65G/V68L/S72A/T203Y. The mutation T203Y is responsible for the red shift in the excitation and emission spectra of the protein (Ormö et al., 1996) and the additional mutations enhance the brightness of the protein (Wachter & Remington, 1999).

YFP exists in a protonated state with an excitation peak at 416 nm, and a deprotonated state with its excitation peak at 514 nm. The relative magnitudes of the excitation peaks are dependent on the  $pK_a$  for protonation and the pH of the environment (Mcananey et al., 2005; Wachter et al., 1998); YFP will be deprotonated if the pH is higher than the  $pK_a$ . While the excited deprotonated YFP emits fluorescence when it returns to ground state, the excited protonated form hardly does. So, in acidic conditions when YFP exists mainly in the protonated state, not much fluorescence is emitted. Furthermore, binding of halides to YFP has been shown to increase the  $pK_a$  by destabilisation of the deprotonated state, causing a drop in emitted fluorescence (Jayaraman et al., 2000).

The H148Q mutation increases the  $pK_a$  of protonation from 5.5 (Mcananey et al., 2005; Wachter & Remington, 1999) to 7.1, which makes this variant more sensitive to halides at a cytoplasmic pH (Jayaraman et al., 2000; Wachter et al., 2000). The I152L mutation greatly improves the sensitivity of YFP(H148Q) to  $I^-$ , decreasing the  $K_d$  of  $I^-$  from 11 mM to 1.9 mM (Galiotta et al., 2001b). The  $K_d$  for  $Cl^-$  on the other hand, is many times higher and stays roughly the same (85 mM) in the H148Q/I152L variant. Therefore, at the low millimolar physiological levels of  $Cl^-$  (the level of  $I^-$  is extremely low in most cell types), the anion binding site is largely unoccupied and the fluorescence of YFP(H148Q/I152L) is high.

The increase in  $I^-$  sensitivity allows the quantification of  $I^-$  transport through CFTR. Function of CFTR has been quantified by co-expressing YFP(H148Q/I152L) with CFTR and adding  $I^-$  to the

extracellular buffer. When CFTR is activated,  $I^-$  enters the cell and its intracellular concentration rapidly increases. Inside the cell  $I^-$  binds to the cytosolic YFP(H148Q/I152L), stabilizing its protonated state. The corresponding drop in fluorescence can be measured to quantify CFTR function (Galiotta et al., 2002; Pedemonte et al., 2005a; Trzcińska-Daneluti et al., 2009; Yang et al., 2003). Langron et al. (2017) constructed an assay in which YFP(H148Q/I152L) is fused to the N-terminal of CFTR. Normalisation, by the fluorescence intensity before  $I^-$  addition, reduced the variability in estimated function of different CFTR variants, the latter mainly due to unequal expression ratios of cytosolic YFP to CFTR.

### 3.2.2 mCherry

The first naturally occurring red fluorescent protein was isolated from corals of the genus *Discosoma* (Matz et al., 1999). This protein, initially called drFP583 and later referred to as DsRed, has been extensively studied and engineered (Baird et al., 2000; Campbell et al., 2002; Gross et al., 2000; Wall et al., 2000). DsRed forms an obligatory tetramer and has an emission wavelength shifted to the red compared to its primarily monomeric homologue GFP with which it has a modest sequence similarity but shares a common fold (Wachter et al., 2010). The maturation speed of DsRed was improved through mutagenesis (Bevis & Glick, 2002) and subsequently the first monomeric variant of DsRed, named mRFP1 (monomeric red fluorescent protein 1), was created (Campbell et al., 2002). Among the mRFPs that have been developed, the characteristics of mCherry are most desirable; it has a very good resistance to fluorescence variations due to fluctuations in pH, and of all the mRFPs it has the longest excitation and emission wavelengths, the highest photostability and it matures fastest (Shaner et al., 2004).

### 3.2.3 Bicistronic expression system

Simultaneous monitoring of multiple parameters in living cells with fluorescent proteins requires heterologous expression of the multiple encoding genes. There are various ways in which expression of multiple fluorescent probes can be achieved. It can be achieved by sequential or co- transfection of

cells with different plasmids, by transfection with polycistronic expression constructs, or by transfection with a single plasmid and subsequent (self)cleavage of a fusion protein. Alternatively, viral vectors can be used for (co)infection of cells. However, viral vectors are expensive and have other disadvantages including the requirement of additional biosafety measures and low packaging capacity (Kim & Eberwine, 2010). For this reason, they are usually not used for *in vitro* experiments where cell types are amenable to transfection with plasmids.

To achieve co-expression of YFP(H148Q/I152L)-CFTR (Langron et al., 2017) and soluble mCherry (Shaner et al., 2004) in HEK-293 cells, we made use of an Internal Ribosome Entry Site (IRES)-based bicistronic expression plasmid. In eukaryotes translation usually starts at the 5' cap of the mRNA so that only a single translation occurs for each mRNA. However, IRES sequences, first discovered in 1988 in the poliovirus (Pelletier & Sonenberg, 1988) and encephalomyocarditis virus (Jang et al., 1988), allow the initiation of translation in a cap-independent manner from an internal region of the mRNA. The IRES elements can be fused with target genes resulting in the co-expression of multiple proteins from the same mRNA (Attal et al., 1999; Gallardo et al., 1997; Martínez-Salas, 1999; Mountford & Smith, 1995). The efficiency of IRES-dependent second gene translation however, is often lower than that of the gene that directly follows the promoter (e.g. Al-Allaf et al., 2019; Mizuguchi et al., 2000).

### 3.3 The pIRES2-mCherry-YFPCFTR plasmid

Two sequential subcloning procedures (see section 2.1.1 *pIRES2-mCherry-YFPCFTR construction*) resulted in the pIRES2-mCherry-YFPCFTR plasmid, with the IRES2 of the encephalomyocarditis virus (ECMV) positioned between the two open reading frames for mCherry and YFP(H148Q/I152L)-CFTR; the YFP(H148Q/I152L)-CFTR fusion protein being translated by the canonical cap-dependent mechanism and the mCherry through the cap-independent mechanism (Hellen & Sarnow, 2001; Martínez-Salas, 1999; Mountford & Smith, 1995). This plasmid allows us to transiently transfect HEK-293 cells using cationic liposomes (lipofectamine), resulting in the co-expression of YFP(H148Q/I152L)-CFTR and cytosolic mCherry (**Figure 11a**). Images taken of transfected cells **Figure**

**11b)** show a homogenous distribution of mCherry inside the cells. On the other hand, the signal coming from the YFP(H148Q/I152L) linked to WT-CFTR shows a different distribution, forming bright rings around the border of the cells which corresponds to the location of the plasma membrane, and clusters within the cells probably representing the YFP(H148Q/I152L)-CFTR in the ER and Golgi.

**Figure 11c** shows two cells transfected with pIRES2-mCherry-YFPCFTR containing the WT-CFTR (left panels) or F508del-CFTR (right panels). Both cells have a similar uniformly distributed mCherry fluorescence signal coming from the cell interior. Again, in the cell expressing WT-CFTR in the left panels, a clear ring of YFP(H148Q/I152L) fluorescence is present on the edge of the cell, corresponding to CFTR located on or near the plasma membrane. The in the cell expressing F508del-CFTR in the right panels, shows a fluorescence profile typical for this genotype. In this cell fluorescence emitted by YFP(H148Q/I152L) is clustered within the cell with virtually no fluorescence on its edge, corresponding retention of F508del-CFTR in the internal vesicles of the cell. We exploited this difference in YFP(H148Q/I152L) profile to quantify the capacity of CFTR to escape the ER and reach the plasma membrane.

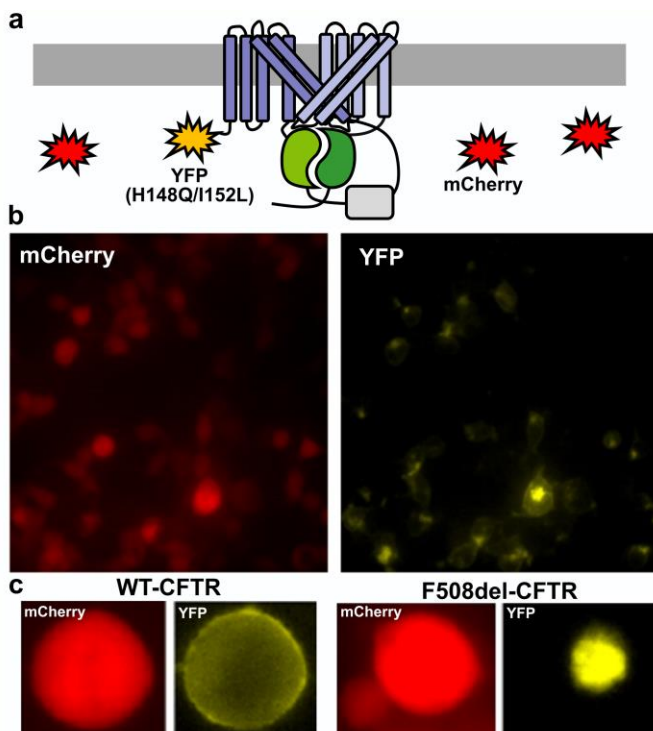


**Figure 11 Co-expression of soluble mCherry and YFP(H148Q/I152L)-CFTR**

a) A schematic representation of the YFP(H148Q/I152L)-CFTR fusion protein in a patch of membrane, and soluble mCherry proteins in the cytosol. b) The pIRES2-mCherry-YFPCFTR containing the WT variant of CFTR was expressed in HEK-293 cells. Images of mCherry (531 ± 20 nm excitation filter, and a 593 ± 20 nm emission filter) and YFP(H148Q/I152L)-CFTR (472 ± 30 nm excitation filter, and a 520 ± 35 nm emission filter) were taken using a 60X objective. c) mCherry and YFP(H148Q/I152L) fluorescence in a cell expressing WT-CFTR (left panels) and a cell expressing F508del-CFTR (right panels).

### 3.4 Quantification of CFTR Channel function

Construction of a YFP(H148Q/I152L)-CFTR fusion protein with the YFP(H148Q/I152L) tagged to the N terminal of CFTR reduced variability and enabled the rate of fluorescence quenching to more accurately represent CFTR ion channel function than using a cytosolic YFP(H148Q/I152L) (Langron et al., 2017). The pIRES2-mCherry-YFPCFTR allowed us to monitor CFTR function by means of methods already established using the same YFP(H148Q/I152L)-CFTR fusion protein (Langron et al., 2017, 2018).

Two different protocols were used: the *I<sup>-</sup> first protocol* during which  $I^-$  was added to the extracellular medium before activating CFTR with forskolin, and the *I<sup>-</sup> last protocol* during which CFTR reached steady state activation before  $I^-$  addition. The *I<sup>-</sup> first protocol* quantifies channel function by estimation of the maximal rate of  $I^-$  entry during CFTR activation. The *I<sup>-</sup> last protocol* on the other hand, estimates CFTR conductance and membrane potential during steady state activation of the channel, by fitting the experimental fluorescence quenching data to a mathematical model. While the first method allows faster data acquisition and a less computationally intensive analysis, the latter method gives a more rigorous estimate of CFTR conductance, unaffected by signal transduction kinetics, and accounts for changing membrane potential and altering concentrations of intracellular ions upon  $I^-$  addition. In both quantifications the observed YFP(H148Q/I152L) fluorescence quenching was corrected for variations in transfection efficiency, using the average mCherry fluorescence intensity within the cell selection relative to cells expressing WT-CFTR on the same plate.

#### 3.4.1 The *I<sup>-</sup> first protocol*: maximal rate of iodide entry

For the *I<sup>-</sup> first protocol*, the maximal observed rate of  $I^-$  entry was used as a measure of CFTR function. Since both  $I^-$  and  $Cl^-$  bind to YFP(H148Q/I152L),  $I^-$  with a much higher affinity than  $Cl^-$ , there will be some competition for the binding site. However, for the *I<sup>-</sup> first protocol* we simplified the system by not taking into account  $Cl^-$  competition in the analysis of the data, i.e. assuming that the amount of  $Cl^-$  bound YFP(H148Q/I152L) was negligible. The simplification can be justified since adjusting for competitive binding of YFP(H148Q/I152L) to  $Cl^-$  only causes very small discrepancies, given its

relatively low binding affinity and low cytosolic  $\text{Cl}^-$  concentration (Langron et al., 2017). Competitive binding of  $\text{Cl}^-$  has most likely also not been considered in previous work using the halide-sensitive YFP (Galiotta et al., 2001a; Pedemonte et al., 2005a).

To determine whether CFTR conductance was increased, the maximal rate of  $\text{I}^-$  entry after addition of forskolin, was compared to the maximal rate of  $\text{I}^-$  entry after addition of DMSO (control). An equation based on the Hill-Langmuir equation for receptor binding, allowed estimation of the free  $\text{I}^-$  concentration at the chromophore (Langron et al., 2017). The Hill-Langmuir equation is commonly expressed as follows:

$$\theta = \frac{[L]^{nH}}{K_d + [L]^{nH}} \quad (1)$$

where symbols have the following meaning:

$\theta$	fraction of ligand-bound macromolecules
$[L]$	free ligand concentration
$K_d$	equilibrium dissociation constant of the ligand to the macromolecule
$nH$	Hill coefficient

In our case the Hill-Langmuir equation expresses the fraction of anion-bound YFP(H148Q/I152L) as function of the free intracellular  $\text{I}^-$  concentration and the binding affinity of  $\text{I}^-$  to YFP(H148Q/I152L).

Because Galiotta and his colleagues (2001) found that there is very little or no cooperative binding of halides to YFP(H148Q/I152L), we will use  $nH = 1$ .

$$P_I = \frac{[\text{I}^-]_{in}}{K_I + [\text{I}^-]_{in}} \quad (2)$$

where:

$P_I$	fraction of $\text{I}^-$ -bound YFP(H148Q/I152L)
$[\text{I}^-]_{in}$	free intracellular $\text{I}^-$ concentration
$K_I$	dissociation equilibrium constant for the $\text{I}^-$ - YFP(H148Q/I152L) complex

The YFP(H148Q/I152L) fluorescence intensity was normalised to the timepoint before  $\text{I}^-$  was added.

With the assumption that  $\text{I}^-$  bound YFP(H148Q/I152L) is not fluorescent, and the approximation that the YFP(H148Q/I152L) with no  $\text{I}^-$  bound is maximally fluorescent, we can substitute  $1 - P_I$  by the normalised fluorescence intensity,  $f$ . In support of the assumption, before  $\text{I}^-$  is added during the experiments, the fraction of  $\text{I}^-$  bound YFP(H148Q/I152L) must be zero ( $P_I = 0$ ), and because the

YFP(H148Q/I152L) fluorescence intensity ( $f$ ) is normalised to the time point before  $I^-$  addition when it is maximal,  $f = 1$  (so  $f = 1$  when  $P_I = 0$ ). Moreover, in the presence of very high concentrations of  $I^-$ , a situation in which almost all YFP(H148Q/I152L) is bound to  $I^-$ , the measured fluorescence intensity was near zero (so  $f \approx 0$  when  $P_I \approx 1$ ) (Galiotta et al., 2001b; Rhoden et al., 2008). Furthermore, experimental data indicates that  $f$  is roughly proportional to  $1 - P_I$ ; when the proportion of unbound YFP(H148Q/I152L) increases a certain amount, the fluorescence intensity increases a similar amount (Rhoden et al., 2008). We can now say that  $f \approx 1 - P_I = 1 - \frac{[I^-]_{in}}{K_I + [I^-]_{in}}$ , which can be rearranged to express the free  $I^-$  concentration at the chromophore:

$$[I^-]_{in} = K_I \frac{(1-f)}{f}. \quad (3)$$

The published dissociation equilibrium constant for the  $I^-$ -YFP(H148Q/I152L) complex is 1.9 mM (Galiotta et al., 2001b), and the normalised fluorescence intensity can be determined experimentally. Using these values, the free  $I^-$  concentration at the chromophore can be estimated.

Data is collected every 2 seconds, therefore the rate of  $I^-$  entry per second ( $\frac{d[I^-]_{in}}{dt}$ ) can be estimated by subtracting the  $[I^-]_{in}$  at a certain timepoint ( $[I^-]_{in}(t)$ ), by the  $[I^-]_{in}$  at the subsequent timepoint  $[I^-]_{in}(t + 1)$  and dividing this by 2 s ( $\frac{d[I^-]_{in}}{dt} = \frac{[I^-]_{in}(t+1) - [I^-]_{in}(t)}{2 \text{ s}}$ ). The maximal observed rate of  $I^-$  entry is determined to quantify CFTR activation. This quantity is not just related to the open probability and single-channel conductance of YFP(H148Q/I152L)-CFTR, but is also a function of the proportion of YFP(H148Q/I152L)-CFTR at the membrane and of the driving force for  $I^-$  flux over time.

With help of Cato Hastings, I contributed implementing fast and automatic analysis of the images (using MATLAB) to determine the maximal observed rate of  $I^-$  entry.

### 3.4.2 The $I^-$ last protocol: estimation of $G$ and $V_m$

We can estimate the membrane potential ( $V_m$ ) and the CFTR mediated whole-cell  $Cl^-$  conductance ( $G_{CFTR-Cl}$ ; and after this chapter simply referred to as  $G$ ) in the presence of 140 mM symmetrical  $[Cl^-]$ , by fitting the fluorescence quenching curves to a mathematical model. The model was created by Dr Paola Vergani who had formalised it in GraphPad Prism. I programmed the model in MATLAB, which

enabled fast and automated fitting of the data. After this, small adjustments and improvements to the model were made by Dr Paola Vergani, Dr Emily Langron, and me.

Cells were modelled as 8.9  $\mu\text{m}$ -radius (half of the average cell dimension observed in images) spheres in the presence of intra- and extracellular  $\text{Cl}^-$ ,  $\text{K}^+$ , and  $\text{I}^-$  at 28  $^\circ\text{C}$  (301.15 Kelvin, temperature used for our measurements). Based on the initial conditions set, at each time point the following quantities can be calculated: the proportions of unbound,  $\text{Cl}^-$  bound and  $\text{I}^-$  bound YFP(H148Q/I152L), the intracellular concentrations of  $\text{Cl}^-$ ,  $\text{I}^-$  and  $\text{K}^+$ , the ionic currents of  $\text{Cl}^-$ ,  $\text{I}^-$  and  $\text{K}^+$ , and the  $V_m$ . In **Figure 12** the modelled variables are displayed together with three different observed YFP(H148Q/I152L) quenching traces (solid red circles). Cells were expressing WT-CFTR (**Figure 12a**) or

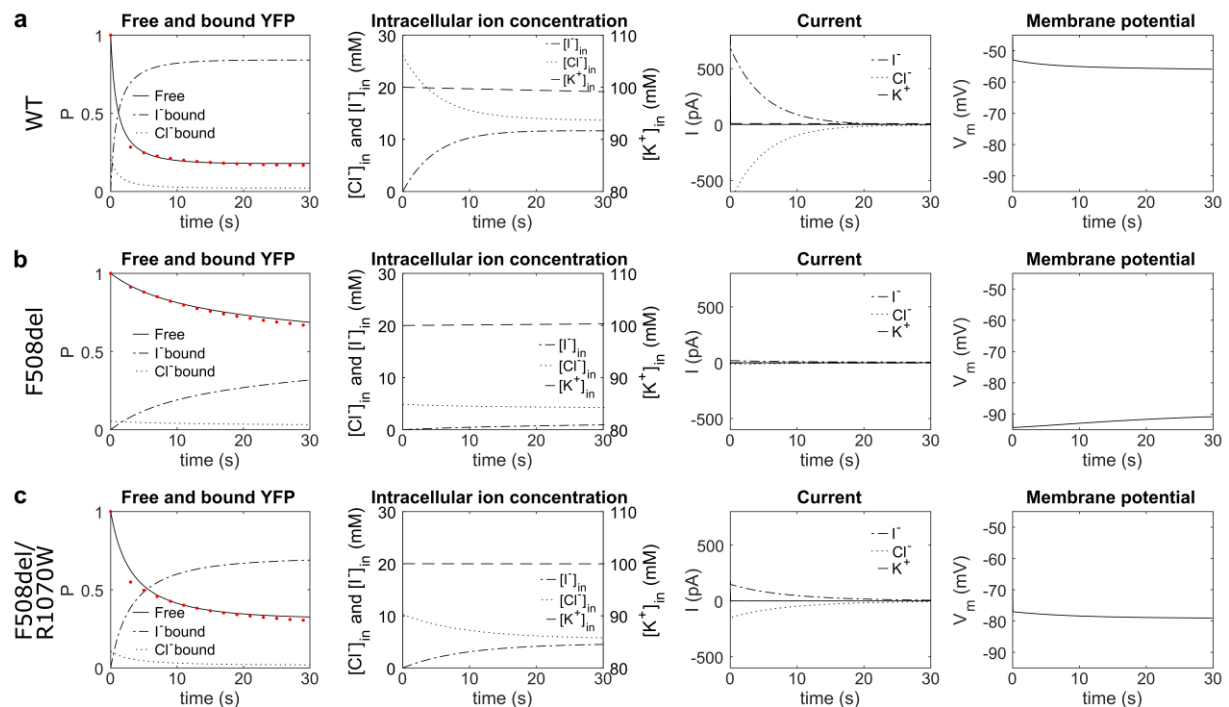


**Figure 12** Fitting of the fluorescence quenching to a simple mathematical model

Cells were transfected with pIRES2-mCherry-YFPCFTR containing the WT variant of CFTR (**a**), F508del-CFTR (**b**), or F508del/R1070W-CFTR (**c**). CFTR was activated with 10  $\mu\text{M}$  forskolin and allowed 230 s to reach steady state activation before  $\text{I}^-$  addition at timepoint 0. The first column of panels displays the measured normalised YFP(H148Q/I152L) fluorescence (solid red circles). These measurements were used to obtain fit parameters to model the proportions of anion-free (solid lines),  $\text{Cl}^-$  bound (dotted lines) and  $\text{I}^-$  bound (dot-dashed lines) YFP(H148Q/I152L). To relate the normalised fluorescence quenching time course (solid red circles) to the proportion of free YFP(H148Q/I152L) (solid line), the proportion of free YFP(H148Q/I152L) was also normalised to the timepoint just before addition of  $\text{I}^-$ . The second and third columns of panels show respectively the modelled intracellular ion concentrations and transmembrane ion currents carried by  $\text{Cl}^-$  (dotted lines),  $\text{I}^-$  (dot-dashed lines) and  $\text{K}^+$  (dashed lines). Finally, the fourth column shows the modelled potential difference across the membrane.

F508del-CFTR without (**Figure 12b**) and with the revertant mutation R1070W (**Figure 12c**). Measurements were obtained after activation with 10  $\mu$ M forskolin, followed by a 230 s preincubation (as described by Langron et al., 2018) during which CFTR activation occurred, and subsequent addition of 100 mM extracellular iodide at timepoint zero.

### *Equilibrium potentials*

The extracellular and intracellular concentrations of  $\text{Cl}^-$ , and  $\text{K}^+$  are assumed to be in equilibrium at the timepoint of  $\text{I}^-$  addition. The Nernst equation for a generic ion  $i$ , was used to calculate their equilibrium potentials.

$$E_i = \frac{RT}{z_i F} \ln \frac{[i]_{out}}{[i]_{in}} \quad (4)$$

where:

$E_i$	equilibrium potential for ion $i$
R	ideal gas constant ( $8.314 \text{ J}\cdot\text{K}^{-1}\cdot\text{mol}^{-1}$ )
T	absolute temperature in Kelvin (K)
$z_i$	valence of ion $i$
F	Faraday's constant ( $96485.332 \text{ C}\cdot\text{mol}^{-1}$ )
$[i]_{out}$	extracellular concentration of ion $i$
$[i]_{in}$	intracellular concentration of ion $i$

### *Ionic currents and conductance*

By convention, the direction of an electric current is defined as positive in the direction of movement of positive charge. The movement of cations across a cell membrane from the extracellular to intracellular space is regarded as an inward ionic current. On the other hand, when cations cross the cell membrane in the opposite direction (towards the extracellular space), the current is referred to as an outward current. For anions, which have a negative charge, the direction of the ion flux is opposite to the direction of the current. So, when anions cross the cell membrane, a movement from the extracellular to intracellular space corresponds to an outward ionic current, and a movement from the intracellular to the extracellular space corresponds to an inward ionic current. The convention is for outward ionic currents to be positive and inward ionic currents to be negative.

Goldman (1943) was the first to formulate equations for currents through and voltages across biological membranes and his formulation was subsequently applied by Hodgkin and Katz (1949). In

our model we use a derivation of the Goldman-Hodgkin-Katz current equation to estimate  $\text{Cl}^-$ ,  $\text{K}^+$ , and  $\text{I}^-$  currents at each timepoint (Johnston & Wu, 1995). The Goldman-Hodgkin-Katz flux equation for an ion  $i$  describes the ionic current ( $I_i$  in  $\text{A}\cdot\text{m}^{-2}$ ) across a cell membrane as a function of the membrane potential ( $V_m$ ), the permeability of the membrane to ion  $i$  ( $p_i$ ), the valency of ion  $i$  ( $z_i$ ), and the concentrations of the ion inside ( $[i]_{in}$ ) and outside ( $[i]_{out}$ ) of the cell.

$$I_i = \frac{p_i z_i^2 F^2}{RT} V_m \left( \frac{[i]_{in} - [i]_{out} e^{-z_i F V_m / RT}}{1 - e^{-z_i F V_m / RT}} \right) \quad (5)$$

In symmetrical solutions, where both extracellular and intracellular concentrations of ion  $i$  are  $[i]_{sym}$  (see Appendix A in Alvarez & Latorre, 2017) the conductance ( $G_i$ ) for ion  $i$  can be expressed as

$$G_i = \frac{p_i z_i^2 F^2 [i]_{sym}}{RT}, \text{ which can be rearranged as } \frac{G_i}{[i]_{sym}} = \frac{p_i z_i^2 F^2}{RT}. \text{ Now it is possible to express}$$

whole-cell ionic currents of ion  $i$  ( $I_i$ ) as follows:

$$I_i = \frac{G_i}{[i]_{sym}} V_m \left( \frac{[i]_{in} - [i]_{out} e^{-z_i F V_m / RT}}{1 - e^{-z_i F V_m / RT}} \right) \quad (6)$$

Using the maximal conductance values in 140 mM symmetrical solutions, whole-cell currents for  $\text{Cl}^-$ ,  $\text{K}^+$  and  $\text{I}^-$  were predicted in our experimental conditions.  $\text{K}^+$  currents ( $I_K$ ) are mediated by endogenous potassium channels. An endogenous leak conductance for  $\text{K}^+$  ( $G_{leak-K}$ ) was set to 2.5 nS (Rapedius et al., 2005) to predict  $\text{K}^+$  mediated currents ( $I_K$ ). The CFTR mediated  $\text{Cl}^-$  conductance ( $G_{CFTR-Cl}$ , after this chapter simply called G) was estimated by fitting the experimental data to the model. The parameter was constrained between 0 and 300 nS to avoid it taking on unphysiological values.

It has been shown that the permeability of WT-CFTR to  $\text{Cl}^-$  is slightly higher than its permeability to  $\text{I}^-$ ; the permeability to  $\text{I}^-$  over the permeability to  $\text{Cl}^-$  ( $p_I/p_{Cl}$ ) is 0.83 (Linsdell, 2001). Because  $\text{Cl}^-$  and  $\text{I}^-$  ions have the same valency ( $z_{Cl} = z_I$ ), in symmetrical solutions we can expect the relationship between CFTR-mediated  $\text{Cl}^-$  and  $\text{I}^-$  conductance ( $G_{CFTR-I}/G_{CFTR-Cl}$ ) to be the same. For this reason, the CFTR mediated  $\text{I}^-$  conductance ( $G_{CFTR-I}$ ) was set to be proportionate to the CFTR mediated  $\text{Cl}^-$  conductance ( $G_{CFTR-I} = 0.83 \cdot G_{CFTR-Cl}$ ).

A non-CFTR related transient anion conductance ( $G_{trans}$ ) had to be added to the model in order to describe the experimental data accurately. This small, CFTR unrelated and transient anion conductance was observed upon addition of  $I^-$  (Langron et al., 2018). We hypothesised that endogenous anion permeabilities of the HEK-293 underlie the transient conductance, possibly triggered by a small hyperpolarization of the cell membrane predicted by the model upon  $I^-$  addition. The time course of  $G_{trans}$  is described in the model as a single exponential decay characterised by a time constant ( $\tau_{trans}$ ) that represents the time in seconds after which the transient conductance is reduced to  $1/e$  ( $\approx 0.368$ ) times its initial value. For this transient conductance too, its whole-cell current was predicted at each timepoint and it was added to the estimated CFTR related  $Cl^-$  and  $I^-$  currents ( $I_{Cl}$  and  $I_I$ ).

$$I_K = \frac{G_{leak-K}}{[K^+]_{sym}} V_m \left( \frac{[K^+]_{in} - [K^+]_{out} e^{-z_i F V_m / RT}}{1 - e^{-z_i F V_m / RT}} \right) \quad (7)$$

$$I_{Cl} = \frac{G_{CFTR-Cl}}{[Cl^-]_{sym}} V_m \left( \frac{[Cl^-]_{in} - [Cl^-]_{out} e^{-z_i F V_m / RT}}{1 - e^{-z_i F V_m / RT}} \right) \quad (8)$$

$$+ \frac{G_{trans} e^{-t/\tau_{trans}}}{[Cl^-]_{sym}} V_m \left( \frac{[Cl^-]_{in} - [Cl^-]_{out} e^{-z_i F V_m / RT}}{1 - e^{-z_i F V_m / RT}} \right) \quad (9)$$

$$I_I = \frac{0.83 \cdot G_{CFTR-Cl}}{[I^-]_{sym}} V_m \left( \frac{[I^-]_{in} - [I^-]_{out} e^{-z_i F V_m / RT}}{1 - e^{-z_i F V_m / RT}} \right) + \frac{0.83 \cdot G_{trans} e^{-t/\tau_{trans}}}{[I^-]_{sym}} V_m \left( \frac{[I^-]_{in} - [I^-]_{out} e^{-z_i F V_m / RT}}{1 - e^{-z_i F V_m / RT}} \right)$$

### Intracellular ion concentrations

The model predicts how the intracellular concentration of  $Cl^-$ ,  $K^+$  and  $I^-$  changes over time. In the model, timepoint 0 represents the moment of iodide addition to the extracellular medium. At this moment CFTR has reached a steady-state, and  $[Cl^-]_{in}$  is assumed to have equilibrated with  $[Cl^-]_{out}$ .

The initial parameters at timepoint 0 are:

$[Cl^-]_{out}$	117.1 mM (corresponding to the extracellular $Cl^-$ concentration after $I^-$ addition)
$[Cl^-]_{in}$	$[Cl^-]_{out} / e^{\left(\frac{V_m}{RT/z_i F}\right)}$ where $[Cl^-]_{out}$ is 152 mM corresponding to the extracellular $Cl^-$ concentration before $I^-$ addition
$[K^+]_{out}$	4.7 mM
$[K^+]_{in}$	100.0 mM
$[I^-]_{out}$	100.0 mM
$[I^-]_{in}$	0.0 mM

Because current ( $I_i$ ) is characterised by the charge that moves across a section of circuit per second and the Faraday's constant ( $F$ ) represents the charge carried by 1 mole of electrons, the molar ion flux per second for ion  $i$  is given by  $\frac{I_i}{z_i F}$ . Because of the conventions described above,  $-\left(\frac{I_i}{z_i F}\right)$  describes the increase in intracellular ions due to inward movement (in moles per second) across the cell membrane as positive, and the outward molar flux as negative. To predict how, for a given current, the ion concentration inside the cell changes over time, the molar flux by the volume of our modelled cell ( $V_{cell}$ );  $\frac{d[i]_{in}}{dt} = \frac{-\left(\frac{I_i}{z_i F}\right)}{V_{cell}}$ , where  $V_{cell} = \frac{4}{3}\pi \cdot r^3$ . At time intervals ( $dt$ ) of 0.2 ms, intracellular concentrations at subsequent timepoints ( $[i]_{in}(t+1)$ ) were approximated as follows using the intracellular concentration of ion  $i$  at timepoint  $t$  ( $[i]_{in}(t)$ ) and the estimated ionic current of ion  $i$ :

$$[i]_{in}(t+1) = [i]_{in}(t) + dt \frac{-\left(\frac{I_i}{z_i F}\right)}{V_{cell}} \quad (10)$$

*The proportion of anion-bound and anion-free YFP(H148Q/I152L)*

The anion binding site on the YFP(H148Q/I152L) chromophore, can be unoccupied, occupied by  $I^-$  or occupied by  $Cl^-$ . While the *I<sup>-</sup> first protocol* does not take into account binding of YFP(H148Q/I152L) to  $Cl^-$ , for the *I<sup>-</sup> last protocol* we considered binding competition between the anions. The relative proportions of binding sites occupied by  $I^-$  and  $Cl^-$  depend on intracellular concentrations and affinities of the halides for the binding site. The equilibria of the anions binding to a receptor (in this case YFP(H148Q/I152L), represented by YFP) can be represented as follows:



According to the law of mass action, the rate of a chemical reaction is directly proportional to the concentrations of the reactants and the ratio between the concentration of reactants and the concentration of products is constant at equilibrium (Kenakin, 2016). By applying the law of mass action, the binding of  $I^-$  and  $Cl^-$  to YFP(H148Q/I152L) at equilibrium can be described as follows:

$$\begin{aligned} [YFP] \cdot [I^-] &= K_I [YFPI^-] \\ [YFP] \cdot [Cl^-] &= K_{Cl} [YFPCl^-] \end{aligned} \quad (12)$$

where  $K_I$  and  $K_{Cl}$  are the dissociation equilibrium constants for the  $I^-$ -bound and  $Cl^-$ -bound YFP(H148Q/I152L) complexes. To estimate the proportion of  $I^-$  bound ( $P_I$ ),  $Cl^-$  bound ( $P_{Cl}$ ), and anion-free YFP(H148Q/I152L) ( $P_{free}$ ) the equations are reformulated as follows:

$$P_{free} \cdot [I^-] = K_I P_I \quad (13)$$

$$P_{free} \cdot [Cl^-] = K_{Cl} P_{Cl}$$

To estimate  $P_I$ ,  $P_{free}$  and  $P_{Cl}$  are expressed as a function of  $P_I$ :

$$P_{free} = P_I \cdot \frac{K_I}{[I^-]} \quad (14)$$

$$P_{Cl} = P_{free} \cdot \frac{[Cl^-]}{K_{Cl}} = P_I \cdot \frac{K_I}{[I^-]} \cdot \frac{[Cl^-]}{K_{Cl}} \quad (15)$$

YFP(H148Q/I152L) is either anion-free, bound to  $I^-$ , or bound to  $Cl^-$ , therefore  $P_{free} + P_I + P_{Cl} = 1$ .

$P_I$  can be found by substituting  $P_{free}$  and  $P_{Cl}$  expressed as a function of  $P_I$ :

$$P_I \cdot \frac{K_I}{[I^-]} + P_I + P_I \cdot \frac{K_I}{[I^-]} \cdot \frac{[Cl^-]}{K_{Cl}} = 1 \quad (16)$$

Which can be rearranged as:

$$P_I = \frac{[I^-]}{K_I \left(1 + \frac{K_{Cl}}{[Cl^-]}\right) + [I^-]} \quad (17)$$

Similarly, to estimate  $P_{Cl}$ ,  $P_{free}$  and  $P_I$  can be expressed as a function of  $P_{Cl}$ :

$$P_{Cl} = \frac{[Cl^-]}{K_{Cl} \left(1 + \frac{[I^-]}{K_I}\right) + [Cl^-]} \quad (18)$$

The binding affinities of  $I^-$  and  $Cl^-$  to YFP(H148Q/I152L) are 1.9 mM and 85 mM respectively (Galiotta et al., 2001a) and the intracellular ion concentrations ( $[I^-]$  and  $[Cl^-]$ ) at every simulated timepoint are determined as described in the section above. With this information it is possible to estimate  $P_I$  and  $P_{Cl}$  at all timepoints in the simulation. Now  $P_{free}$  can now be estimated as follows:

$$P_{free} = 1 - (P_I + P_{Cl}) \quad (19)$$

The fluorescence intensity ( $f$ ) is normalised to that measured at the time point before  $I^-$  addition. To relate to the fluorescence quenching time course to  $P_{free}$ ,  $P_{free}$  was normalised to  $P_{free}$  at timepoint zero ( $t_0$ );  $\hat{P}_{free} = \frac{P_{free}}{P_{free}(t_0)}$ . Because only anion-free YFP(H148Q/I152L) is fluorescent in our

conditions (Langron et al., 2017), we can fit the  $\hat{P}_{free}$  predictions from the model to observed experimental fluorescence measurements to estimate the free parameters.

### *The membrane capacitance*

The membrane of cells acts as a capacitor that can store charge on its surface. The membrane capacitance ( $C_m$  in farads) is defined as the amount of charge ( $Q_m$  in coulombs) that can be stored by the membrane for a given transmembrane voltage,  $C_m = \frac{Q_m}{V_m}$ . The membrane capacitance is proportional to the cell surface area. It has been previously shown that, due to filopodia, the actual membrane surface area of HEK-293 cells is roughly 50 % larger than the surface area determined by the radius of the cell alone (Gentet et al., 2000). Therefore, the membrane surface area ( $A_m$ ) of HEK-293 cells was adjusted by adding 50 % to the value calculated from their radius ( $r$ ),  $A_m = 4\pi r^2 + \frac{1}{2}(4\pi r^2)$ . In our model we used a membrane capacitance of  $1 \mu F \cdot cm^{-2}$ , typically used for biological membranes, to estimate the membrane capacitance of the cell.

### *The membrane potential*

The membrane capacitance determines the rate at which the membrane potential changes in response to the charge that moves across the membrane. To estimate the change in membrane potential at each timepoint,  $C_m = \frac{Q_m}{V_m}$  was rearranged to  $V_m = \frac{Q_m}{C_m}$ , and  $V_m$  and  $Q_m$  were differentiated to describe the rate at which they change. The capacitance is constant over time, so  $\frac{dV_m}{dt} = \frac{(\frac{dQ_m}{dt})}{C_m}$ . Since whole cell membrane current is defined as the rate at which charge ( $Q_m$  in coulombs) moves across the membrane, the capacitive current ( $I_{cap}$ ) can be defined as  $I_{cap} = \frac{dQ_m}{dt}$  and therefore  $\frac{dV_m}{dt} = \frac{I_{cap}}{C_m}$ .

Kirchhoff's current law states that the total inward current at a junction (in our case a patch of cell membrane) is equal to the total outward current at that junction. In other words, the sum of all the currents at a junction must be equal to zero. The total membrane current is composed of two components, the capacitive current  $I_{cap}$  and the net ionic current  $I_{ion}$ . Because of conservation of

electrical charge (Kirchhoff's current law),  $I_{cap} + I_{ion} = 0$  and therefore  $I_{cap} = -I_{ion}$  and  $\frac{dV_m}{dt} = \frac{-I_{ion}}{C_m}$  (see Conradi Smith, 2019). In our model the net ionic current exists of a  $K^+$  leak current, and  $Cl^-$  and  $I^-$  currents with a CFTR and non-CFTR related component ( $I_{ion} = I_K + I_{Cl} + I_I$ ), therefore  $\frac{dV_m}{dt} = \frac{-(I_K + I_{Cl} + I_I)}{C_m}$ . To approximate the new membrane potential ( $V_{m(t+1)}$ ) at time intervals ( $dt$ ) of 0.2 ms, the following equation was used:

$$V_{m(t+1)} = V_m(t) + dt \frac{-(I_K + I_{Cl} + I_I)}{C_m} \quad (20)$$

The membrane potential estimates were constrained between -30 and -90 mV to avoid unphysiological values.

### 3.4.3 Normalisation to control for transfection efficiency

For quantification of CFTR function, cell selection based on an adaptive threshold, was used to calculate the average mCherry fluorescence intensity inside the cells ( $f_{mCherry\ cells}$ ). Because of a considerable variability in absolute fluorescence values between plates due to illumination/acquisition conditions (see **Figure 13** in section 3.5.1 *WT-CFTR: normalisation*), for every plate the average  $f_{mCherry\ cells}$  was normalised  $f_{mCherry\ cells}$  of WT-CFTR on the same plate. The normalised  $f_{mCherry\ cells}$  value, denoted as  $\hat{f}_{mCherry\ cells}$ , was used to further take into account some of the variability in transfection efficiency by normalising the maximal rate of iodide entry ( $d[I^-]/dt$ ) as well as conductance mediated by the expressed CFTR (G) to  $\hat{f}_{mCherry\ cells}$ .

## 3.5 CFTR membrane proximity

By co-expressing soluble mCherry with the YFP(H148Q/I152L)-CFTR fusion protein, our assay enables the characterisation of both CFTR function, and the amount of CFTR present in proximity of the plasma membrane ( $\rho$ ).

### 3.5.1 WT-CFTR: normalisation

Although the mCherry fluorescence intensity within each single cell ( $f_{mCherry\ cell}$ ) accounts for variations in mRNA levels between cells within plates, there are other factors that affect the measured

fluorescence intensity values of the fluorophores, such as the exact configuration of the imaging apparatus, illumination intensity, fluorophore bleaching etc. The between plate variation in fluorescence intensity profiles for mCherry is visible in **Figure 13a**. There does not seem to be a consistent pattern within the plates for the two CFTR genotypes (WT in transparent light gray and F508del in dark gray): sometimes the median  $f_{mCherry\ cell}$  is larger for WT (dotted lines) and sometimes for F508del-CFTR (dashed lines), but in most plates the difference is negligible.

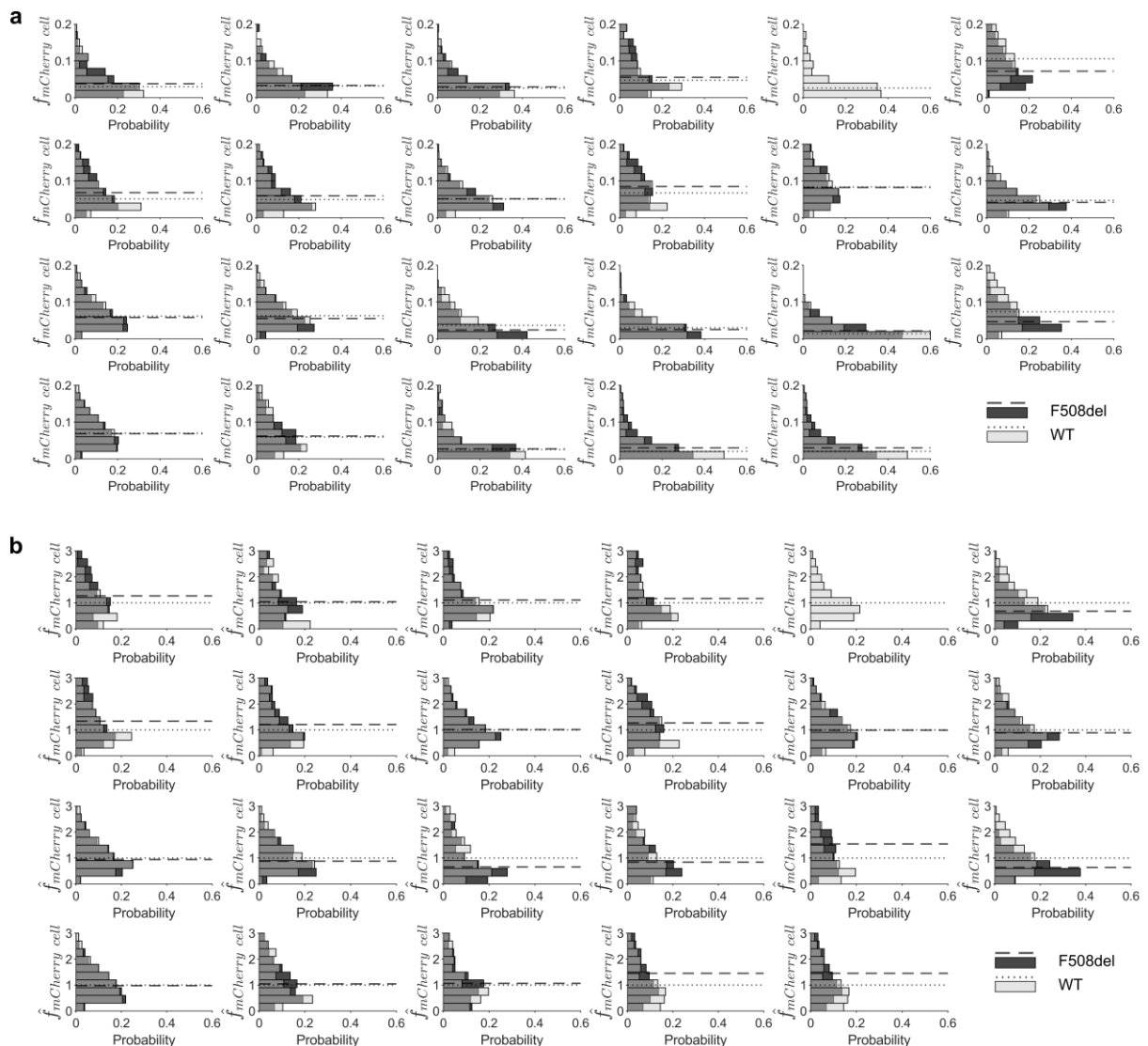


**Figure 13** Effect of normalisation on mCherry fluorescence

Probability distributions for mCherry fluorescence in individual cells ( $f_{mCherry\ cell}$ ) after background correction but before normalisation (**a**) and after normalisation ( $\hat{f}_{mCherry\ cell}$ ; **b**). For each plate, normalisation was performed by dividing  $f_{mCherry\ cell}$  by the median  $f_{mCherry\ cell}$  of cells expressing WT-CFTR. The lines represent the median  $f_{mCherry\ cell}$  (**a**) and  $\hat{f}_{mCherry\ cell}$  (**b**) in F508del-CFTR (dashed) and WT-CFTR (dotted). Each graph represents a separate plate.

However, visual inspection of the  $f_{\text{mCherry cell}}$  distributions among different plates reveals quite large between-plate differences. Some of the distributions are shifted down with median fluorescence intensities less than 0.05 AU whereas other distributions are shifted up with median fluorescence intensities over 0.1 AU. These differences are likely to reflect poorly controlled differences in settings during the image acquisition; a longer exposure time/higher intensity of incident light intensity is likely to result in an up shifted probability distribution. To minimise the between-plate variability we

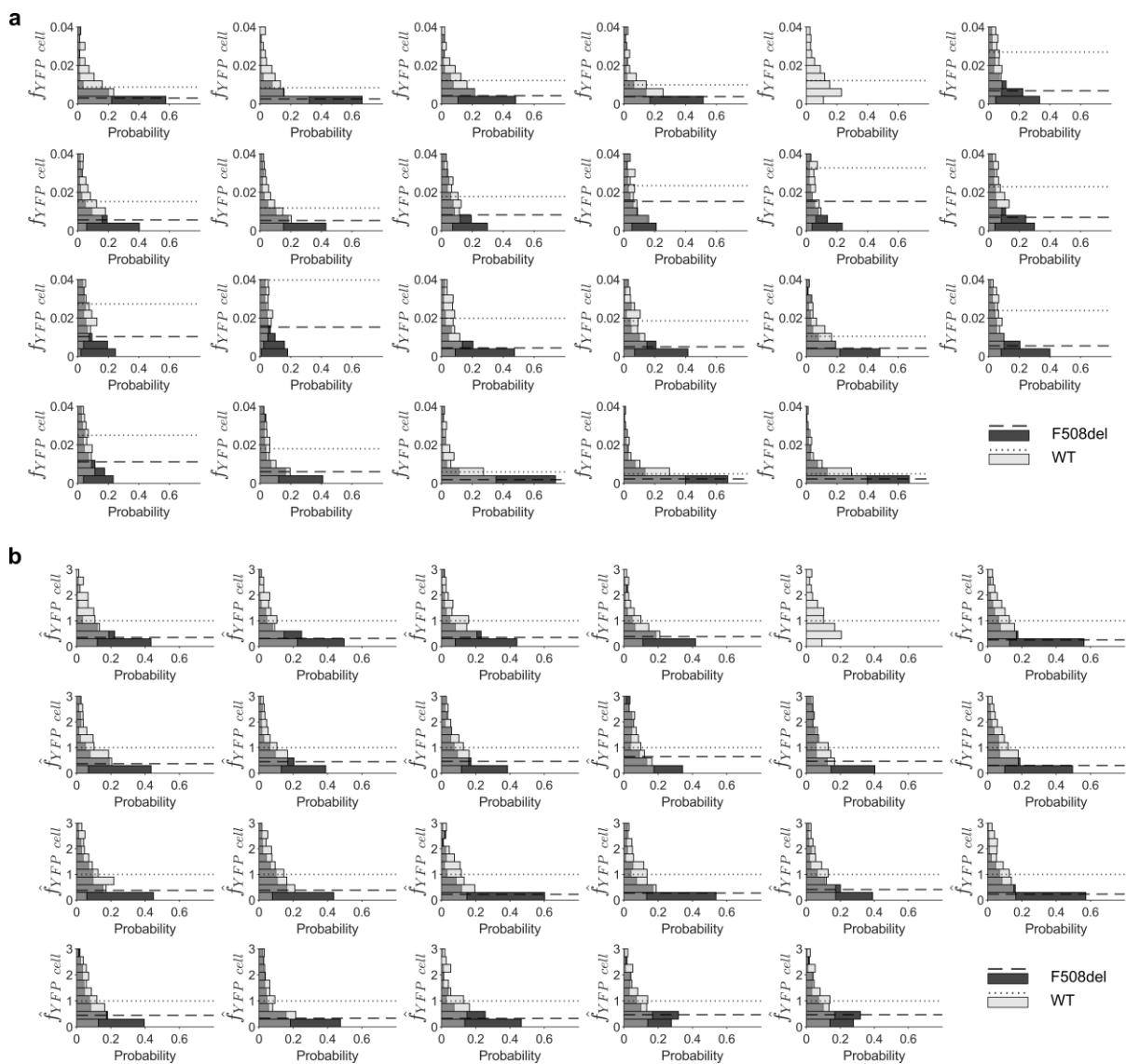


**Figure 14** Effect of normalisation on YFP(H148Q/I152L) fluorescence

Probability distributions for YFP(H148Q/I152L) fluorescence in individual cells ( $f_{\text{YFP cell}}$ ) after background correction but before normalisation (**a**) and after normalisation ( $\hat{f}_{\text{YFP cell}}$ ; **b**). For each plate, normalisation was performed by dividing  $f_{\text{YFP cell}}$  by the median  $f_{\text{YFP cell}}$  of cells expressing WT-CFTR. The lines represent the median  $f_{\text{YFP cell}}$  (**a**) and  $\hat{f}_{\text{YFP cell}}$  (**b**) in F508del-CFTR (dashed) and WT-CFTR (dotted). Each graph represents a separate plate.

decided to normalise  $f_{\text{mCherry cell}}$  to the median  $f_{\text{mCherry cell}}$  of WT-CFTR expressing cells within its plate (**Figure 13b**). The normalised mCherry fluorescence intensity is denoted as  $\hat{f}_{\text{mCherry cell}}$ .

**Figure 14** shows the probability distributions of the average YFP(H148Q/I152L) fluorescence intensity for each cell per plate. Before normalisation to the median  $f_{\text{YFP cell}}$  of WT-CFTR (**a**), and unlike the mCherry fluorescence intensity profiles, there is a clear pattern for the two genotypes. Within every plate the median  $f_{\text{YFP cell}}$  is larger in WT-CFTR compared to F508del-CFTR. This difference reflects the decreased metabolic stability of F508del-CFTR, and therefore of the tagged fluorophore. However, because of the between plate variation, some median  $f_{\text{YFP cell}}$  values of cells expressing F508del-CFTR appear higher than the  $f_{\text{YFP cell}}$  values of cells expressing the WT-CFTR on different plates. Again, to be able to better compare the data from different plates we decided to normalise the  $f_{\text{YFP cell}}$  to the median  $f_{\text{YFP cell}}$  of WT-CFTR expressing cells within that plate (**Figure 14b**). Here too, a circumflex was used to indicate the normalisation of YFP(H148Q/I152L) fluorescence intensity ( $\hat{f}_{\text{YFP cell}}$ ).

### 3.5.2 mCherry: membrane localisation and normalisation

The mCherry expression has two purposes. Firstly, it allows image segmentation and localization of the border of the cells, without depending on efficient YFP(H148Q/I152L)-CFTR membrane trafficking. The cell border corresponds to the location of the cell membrane and we have defined a  $\sim 1 \mu\text{m}$  wide band on the inside of a cell's border as the membrane proximal zone (**Figure 15a-b**). For each cell the average normalised YFP(H148Q/I152L) fluorescence intensity in the membrane proximal zone,  $\hat{f}_{\text{YFP membrane}}$ , is determined. Since the membrane is within this zone, the fluorescence intensity is related to the amount of CFTR on and in proximity of the plasma membrane. When the capacity of CFTR to escape the ER and reach the plasma membrane increases, higher YFP(H148Q/I152L)-CFTR fluorescence intensities in the membrane-proximal zone are to be expected.

The second function of mCherry is the correction for between-cell transfection efficiency within each plate.  $\hat{f}_{\text{mCherry cell}}$  serves as standard for the normalisation of YFP(H148Q/I152L) fluorescence intensity, reducing variability due to unequal transfection efficiency within the plates. The two proteins are expressed separately, but because they are translated from the same mRNA transcript,

the mCherry fluorescence intensity is proportional to the amount of YFP(H148Q/I152L)-CFTR expression and can be used to normalise YFP(H148Q/I152L)-CFTR fluorescence.

### 3.5.3 Defining CFTR membrane proximity ( $\rho$ )

**Figure 15** shows panels with cropped images of the mCherry and YFP(H148Q/I152L)-CFTR fluorescence of a segmented cell transfected with pIRES2-mCherry-YFPCFTR containing WT-CFTR (**a**) or F508del-CFTR (**b**), the panels with the binary image indicate the location and border of the cells as determined by the image segmentation based on the mCherry signal. In the lower panels, fluorescence intensity for mCherry ( $f_{\text{mCherry}}$ , red dashed line) and YFP(H148Q/I152L)-CFTR ( $f_{\text{YFP}}$ , yellow solid line) is plotted as a function of the distance from the cell border. Both cells follow a very similar

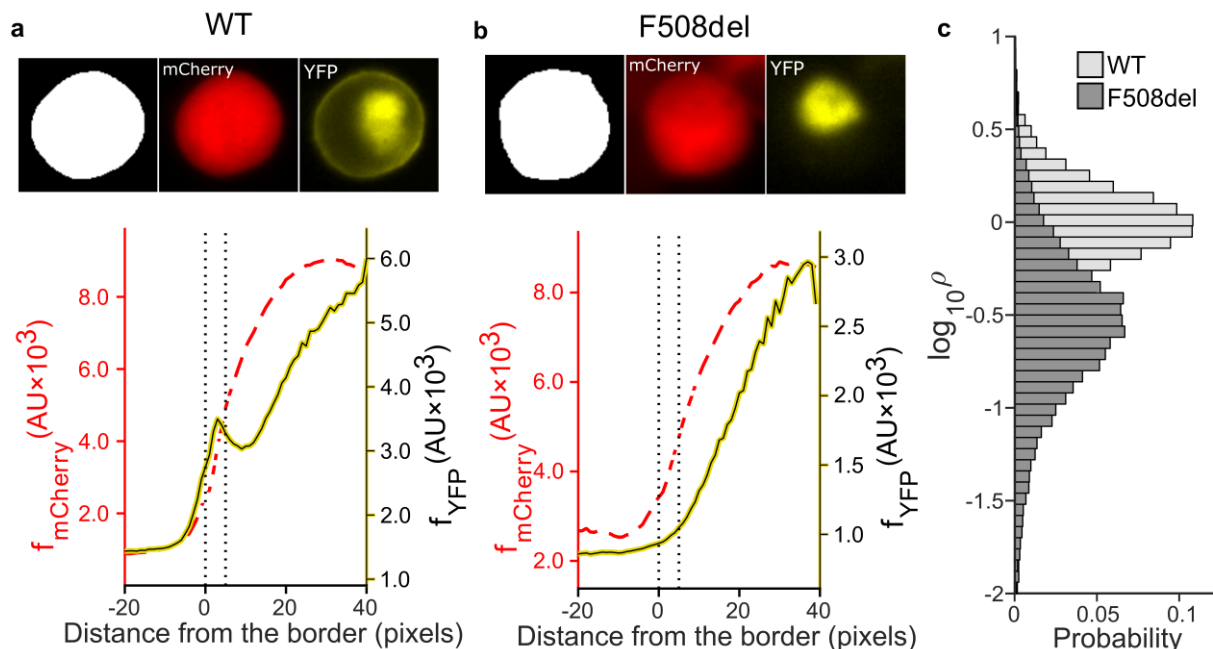


**Figure 15** Quantification of CFTR membrane proximity ( $\rho$ )

Image analysis of individual representative HEK-293 cells transfected with pIRES2-mCherry-YFPCFTR containing WT-CFTR (**a**), and pIRES2-mCherry-YFPCFTR containing F508del-CTR (**b**). Upper panels: boundary delimiting cell (white) from non-cell (black) is obtained from mCherry image (centre). CFTR cellular localization is obtained from YFP(H148Q/I152L) image (right). Lower panels: average mCherry fluorescence intensity ( $f_{\text{mCherry}}$ , red dashed line), and average YFP(H148Q/I152L) fluorescence intensity ( $f_{\text{YFP}}$ , solid yellow line), as a function of the distance from cell border. Positive distance values going to the inside (white area in binary image) of the cell and negative values going away outwards from the border (black area in binary image). Membrane proximity ( $\rho$ ) is defined as  $\hat{f}_{\text{YFP membrane}}/\hat{f}_{\text{mCherry cell}}$ , where  $\hat{f}_{\text{YFP membrane}}$  is the average fluorescence intensity within the membrane zone, set in the  $\sim 1 \mu\text{m}$  band at the cell border (between the dotted lines in bottom panels). **c**) Probability density distribution of  $\log_{10}\rho$  for cells expressing YFP(H148Q/I152L)-WT-CFTR (light grey), and YFP(H148Q/I152L)-F508del-CFTR (dark grey), incubated at 37 °C. For the WT cell shown,  $\rho = 1.60$ ; for the F508del cell,  $\rho = 0.25$ .

pattern for  $f_{mCherry}$ , however, comparing the  $f_{YFP}$  of the fluorescence plots, a small peak in fluorescence intensity in the membrane-proximal zone (delimited by vertical black dotted lines) is apparent for WT-CFTR but not for F508del-CFTR.

The fraction of YFP(H148Q/I152L)-CFTR in proximity to the membrane can be determined by dividing the average normalised YFP(H148Q/I152L)-CFTR fluorescence intensity within the membrane proximal zone by the average normalised YFP(H148Q/I152L)-CFTR fluorescence intensity over the entire cell ( $\hat{f}_{YFP\ membrane}/\hat{f}_{YFP\ cell}$ ). However, because the metabolic stability of YFP(H148Q/I152L)-CFTR can be affected by the CFTR genotype and appears to be an important determinant for how much of the CFTR finally reaches the plasma membrane, the magnitudes of YFP(H148Q/I152L)-CFTR on the membrane and over the entire cell are very strongly correlated. Moreover, minor imprecision in locating the membrane-proximal zone has a strong influence on the  $\hat{f}_{YFP\ membrane}/\hat{f}_{YFP\ cell}$ . We therefore decided to take into account the  $\hat{f}_{mCherry\ cell}$ . Unlike the metabolic stability of YFP(H148Q/I152L), the metabolic stability of mCherry is unaffected by CFTR genotype and modulator drugs and reflects the levels of mRNA transcript encoding both mCherry and YFP(H148Q/I152L)-CFTR. The fluorescence level of mCherry can thus be used as a yardstick, informing us about alterations in stability of YFP(H148Q/I152L)-CFTR; higher levels of YFP(H148Q/I152L)-CFTR fluorescence intensity relative to mCherry fluorescence intensity, indicate increased metabolic stability of CFTR.

We decided to estimate the density of CFTR in proximity of the membrane, denoted as  $\rho$ , by dividing the average normalised YFP(H148Q/I152L)-CFTR fluorescence intensity within the membrane proximal-zone by the average normalised mCherry fluorescence intensity over the entire cell ( $\hat{f}_{YFP\ membrane}/\hat{f}_{mCherry\ cell}$ ). In this way our measurement of CFTR membrane proximity not only considers the fraction of YFP(H148Q/I152L)-CFTR at the membrane but also the overall rates of biosynthesis versus degradation of the protein. The  $\rho$  metric can also be thought of as the product of the fraction of YFP(H148Q/I152L)-CFTR localized in proximity of the membrane, multiplied by the metabolic stability of YFP(H148Q/I152L)-CFTR with respect to mCherry.

The distributions of  $p$  are skewed and transforming the data with a  $\log_{10}$ -transformation normalises the distributions. **Figure 15c** shows the  $\log_{10}p$  probability distributions of a population of live HEK-293 cells expressing WT (light grey) or F508del-CFTR (dark grey) at 37 °C. The probability distributions show that there is a large heterogeneity among cells; the populations of  $\log_{10}p$  distributions are overlapping, with one tail of the distribution of F508del-CFTR expressing cells having a  $\log_{10}p$  measurement similar to, or higher than, the average WT-CFTR  $\log_{10}p$ . The automation of the image analysis has made it possible to rapidly quantify the membrane proximity of thousands of cells while minimising subjective bias of the researcher.

### 3.6 Discussion

We developed an assay that enables rapid and simultaneous assessment of two fundamental but distinct CFTR characteristics, channel function and membrane proximity, in live HEK-293 cells. The assay makes use of a bicistronic expression system for the expression of two fluorescent proteins, a soluble mCherry and a halide sensitive YFP, YFP(H148Q/I152L) (Galiotta, Haggie and Verkman, 2001), linked to the N-terminus of CFTR (Langron et al., 2017). To our knowledge this is the first assay in which CFTR channel function and biogenesis can be measured simultaneously within the same population of cells. Being able to simultaneously monitor these two key CFTR characteristics is clearly advantageous. Simultaneous screening obviously is much faster than sequential screening. But most importantly, obtaining both measurements simultaneously on the same cells, makes an accurate assessment of the relationship between them possible, providing a concise description of CFTR molecular characteristics.

#### 3.6.1 Membrane proximity

The  $\hat{f}_{\text{YFP membrane}}$  represents the amount of YFP(H148Q/I152L)-CFTR in the membrane proximal zone. Unlike methods that quantify CFTR surface expression using membrane impermeable molecules to activate tags located on CFTRs extracellular domains (see 1.5.2 *Biogenesis*, p. 40), we are not able to differentiate between the YFP(H148Q/I152L)-CFTR present at the surface of the membrane vs. those in proximity of the membrane. This is not dissimilar to what is usually measured by Western Blots

where CFTR maturation is typically assessed by distinguishing the amount of ER core-glycosylated from the amount of fully glycosylated CFTR. Unless combined with cell-surface biotinylation to separate CFTR on the cell surface from intracellular CFTR (Farinha et al., 2004), Western Blots cannot distinguish between fully glycosylated CFTR on the membrane surface or inside the cell. In addition to considering the amount of protein in the membrane proximal zone, the p metric takes into account the metabolic stability of YFP(H148Q/I152L)-CFTR. This decreases variability within plates, but also provides a more meaningful description of CFTR's ability to reach the plasma membrane.

### 3.6.2 pH sensitivity YFP(H148Q/I152L)

The properties of fluorophores can be altered by the intracellular environment, and their affinity for ions may vary depending on the environment. mCherry fluorescence is not dependent on pH and mCherry performs well under a wide range of physiological pH conditions (Doherty et al., 2010; Stoddard & Rolland, 2019). YFP(H148Q/I152L) on the other hand, like other YFPs, is sensitive to changes in pH with lower pH values decreasing its fluorescence and increasing iodide affinity (Rhoden et al., 2007) because of a positive cooperativity between halide and proton binding (Wachter et al., 2000). Because the halide-sensing mechanism of YFP(H148Q/I152L) involves a shift in  $pK_a$  (Jayaraman et al., 2000), the sensitivity of this fluorophore to pH is unavoidable.

Galiotta and colleagues found that the cytoplasmic pH dropped from 7.35 to 7.20 during the CFTR activation protocol (Galiotta et al., 2001c). Rhoden and colleagues (2007) estimated that at a pH of 7.0, a 0.2 unit change in pH upon extracellular iodide addition is at most responsible for a 15 % change in the degree of YFP(H148Q/I152L) quenching in FRTL-5 cells. Furthermore, it has been estimated that a drop in pH from 7.35 to 7.20 accounts for less than 1 % of the quenching upon maximal activation of YFP(H148Q/I152L) tagged CFTR in HEK-293-cells and a decrease to pH 6 only would induce only around 5 % quenching of YFP(H148Q/I152L)-CFTR (Langron, 2016).

Taking all of this in consideration, we can assume that the pH changes during the CFTR activation protocol are small and not expected to strongly affect fluorescence quenching. Moreover, the pH dependent change in fluorescence is likely to affect YFP(H148Q/I152L)-CFTR quenching

similarly for the different conditions/genotypes tested and therefore is unlikely to alter conclusions based on comparisons of the latter.

### 3.6.3 $K_i$

At pH 7.35, purified YFP(H148Q/I152L) has a ~45-fold selectivity for iodide compared to chloride with a dissociation equilibrium constant for iodide of 1.9 mM and of 85 mM for chloride, but at pH 7.50 the selectivity for iodide versus chloride was reduced, with equilibrium constants for iodide of 3.0 mM and of 88 mM for chloride (Galiotta et al., 2001b). Other studies reported affinities of YFP(H148Q/I152L) for iodide ranging from 1.4 mM to 7.4 mM, all affected by pH, while maintaining ~20-fold selectivity for iodide versus chloride (Rhoden et al., 2007, 2008)

In our research group, steady state fluorescence at increasing concentrations of extracellular iodide was measured in HEK-293 cells expressing YFP(H148Q/I152L) tagged CFTR (Langron et al., 2017). The extracellular iodide concentration at which half of the total fluorescence was quenched was 41.4 mM (Langron et al., 2017). To estimate the intracellular iodide concentration at equilibrium with 41.4 mM extracellular iodide, the Nernst equation (see Equation (4), p. 71) can be rearranged:

$$[i]_{in} = \frac{[i]_{out}}{e^{\frac{E_i z_i F}{RT}}} \quad \text{where } [i] = [I^-] \text{ and } z_i = z_I \quad (21)$$

The average estimated membrane potential at steady state activation for cells expressing WT-CFTR was -51.7 mV (SD = 7.75, N = 17; **Table 7**, p. 137). At a temperature of 28 °C (T = 301.15 K) and a membrane potential of -51.7 mV ( $E_i$ ), an extracellular concentration of 41.4 mM ( $[i]_{out}$ ) is in equilibrium with 5.7 mM intracellular iodide ( $[i]_{in}$ ) and would thus correspond to a  $K_i$  of 5.7 mM for YFP(H148Q/I152L) in our system. This is very similar to the 6.1 mM affinity of iodide to YFP(H148Q/I152L) at a pH of 7.4 reported by Rhoden and colleagues (Rhoden et al., 2008).

It must be noted however, that the expression system used to estimate the half-maximal extracellular iodide concentration (pcDNA3.1; Langron et al., 2017), differed from the expression system used in the current study (pIRES2) to obtain membrane potential estimates for cells expressing YFP(H148Q/I152L)-CFTR. It is possible that this estimate for the affinity of iodide to YFP(H148Q/I152L)

is an underestimate. A relatively low expression of YFP(H148Q/I152L)-CFTR in the pcDNA3.1 system would result in a more hyperpolarized membrane potential than that measured for the pIRES system, thus an extracellular  $[I^-_{out}] = 41.4$  mM would be in equilibrium with a lower  $[I^-_{in}]$ , at the chromophore. To get a more accurate estimate of  $K_i$  in our system, steady state YFP(H148Q/I152L)-CFTR fluorescence at increasing concentrations of extracellular iodide could be measured in cells expressing pIRES2-mCherry-YFPCFTR.

### 3.6.4 Relevance

For most patients with cystic fibrosis, rescue of either CFTR channel function or the number of CFTR molecules on the membrane, is not enough for effective treatment (Clancy et al., 2012; Flume et al., 2012). For this reason, therapies combining correctors that promote correct positioning of CFTR at the cell membrane, and potentiators that restore CFTR channel function, are now seen as most promising (Holguin, 2018). The recent focus on these combination therapies, highlights how an assay capable of discriminating between improvements in CFTR membrane proximity vs. improvements in its gating and permeation characteristics could better inform the drug development process, starting at early stages. Moreover, the fact that several potentiators have been shown to have detrimental effects on F508del-CFTR membrane stability (Cholon et al., 2014; Meng et al., 2017; Veit et al., 2014), further demonstrates the importance of being able to discriminate between CFTR function (gating/permeation) and the capacity of CFTR to reach the plasma membrane. Currently most cystic fibrosis drug discovery strategies involve separate functional assays to screen for potentiators and correctors. It has been pointed out however, that the conventional sharp distinction between compounds that potentiate and those that correct could hamper discovery of compounds with dual activity (Rowe & Verkman, 2013).

Finally, CFTR plays a central role in the control of fluid secretion and homeostasis in several types of epithelia (Frizzell & Hanrahan, 2012; Saint-Criq & Gray, 2017) and has been implicated in a number of conditions other than cystic fibrosis including chronic obstructive pulmonary disease (COPD) (Fernandez Fernandez et al., 2018; Solomon et al., 2017; Zhao et al., 2014), secretory diarrhoeas

(Moon et al., 2015; Thiagarajah et al., 2015), polycystic kidney disease (Chapin & Caplan, 2010; Li et al., 2012) and other conditions (Solymosi et al., 2013; Wen et al., 2007; Zhang et al., 2018a). Given the complexity of CFTR folding (Farinha & Canato, 2017; Lukacs & Verkman, 2012), many CFTR targeting compounds are likely to target cellular processing (e.g. Clunes et al., 2012), suggesting that the assay could also be deployed in drug development programs for these conditions.

## 4. Validating the mCherry-YFPCFTR assay

### 4.1 Introduction

We modified the YFP-CFTR assay (Langron et al., 2017) to enable simultaneous measurement of CFTR function (quantified by CFTR-mediated rate of  $I^-$  entry) and CFTR's ability to reach the plasma membrane (quantified by  $\rho$ ). To validate the new mCherry-YFPCFTR assay, we transfected HEK-293 cells with pIRES2-mCherry-YFPCFTR containing WT-CFTR, F508del-CFTR or F508del/R1070W-CFTR and assessed whether different experimental conditions resulted in the expected changes in CFTR mediated rate of  $I^-$  entry and  $\rho$ . The conditions we used were incubation at low temperature (Denning et al., 1992a; Rennolds et al., 2008; Varga et al., 2008; Wang et al., 2008; Yang et al., 2003), treatment with the corrector VX-809 (He et al., 2013; Okiyoneda et al., 2013), combination treatment with VX-809 and VX-770 (Cholon et al., 2014; Veit et al., 2014), and addition of revertant mutation R1070W (Farinha et al., 2013; Okiyoneda et al., 2013; Thibodeau et al., 2010).

The experiments described in this chapter investigating chronic (24 h) VX-770 incubation on VX-809 rescued F508del-CFTR (**Figure 17c**) were planned and performed by Dr Emily Langron (EL). Furthermore, Cato Hastings (CH) helped me with the collection of data on the effect of R1070W at 37 °C (**Figure 17b**, left panels; **Figure 18d**, left panel), and Emily Hill (EH) helped me with collection of data on the effect of R1070W at 37 °C as well as 28 °C (**Figure 17b**; **Figure 18d**). All image analysis and further analysis of the data was performed by me. Most of the findings described in this chapter will be published in the *Journal of Biological Chemistry* (Prins et al., 2020).

## 4.2 Results

### 4.2.1 mCherry accounts for variability due to unequal transfection efficiency

Because YFP(H148Q/I152L)-WT-CFTR and mCherry are translated from the same mRNA transcript, their fluorescence intensity is expected to be proportional to each other. When quantifying membrane proximity ( $\rho$ ), the normalised mCherry fluorescence intensity ( $\hat{f}_{\text{mCherry cell}}$ ) is used to account for between-cell differences in the number of mRNA transcripts caused by variation in transfection efficiency. So,  $\hat{f}_{\text{mCherry cell}}$  and  $\rho$  are not expected to correlate. **Figure 16** displays scatterplots that show the relationship between  $\hat{f}_{\text{mCherry cell}}$  and  $\hat{f}_{\text{YFP cell}}$ ,  $\hat{f}_{\text{YFP membrane}}$ , and  $\rho$ . To investigate the relationship between these variables, Spearman correlation coefficients were computed. While there were strong positive correlations between  $\hat{f}_{\text{mCherry cell}}$  and  $\hat{f}_{\text{YFP cell}}$  ( $r_s = 0.82$ ,  $N = 11741$ ,  $P < 0.0001$ ), and between  $\hat{f}_{\text{mCherry cell}}$  and  $\hat{f}_{\text{YFP membrane}}$  ( $r_s = 0.80$ ,  $N = 11741$ ,  $P < 0.0001$ ), there was no significant correlation between  $\hat{f}_{\text{mCherry cell}}$  and  $\rho$  ( $r_s = 0.01$ ,  $N = 11741$ ,  $P = 0.13$ ). These results show that mCherry fluorescence intensity corresponds very well to the level of YFP(H148Q/I152L)-WT-CFTR and can be effectively used to account for within-plate variations in transfection efficiency.

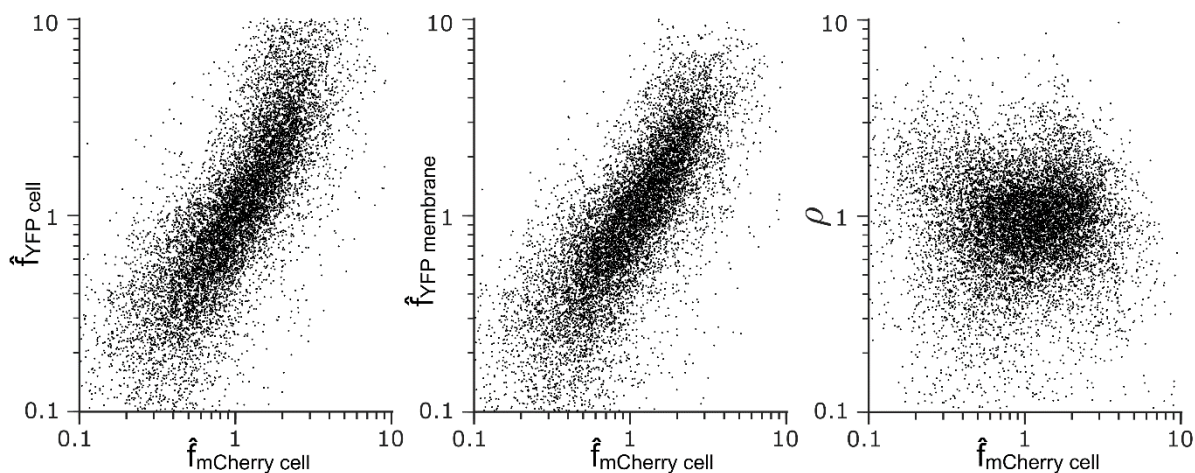


**Figure 16** The relationship between  $\hat{f}_{\text{mCherry cell}}$  and  $\hat{f}_{\text{YFP cell}}$ ,  $\hat{f}_{\text{YFP membrane}}$ , and  $\rho$

The scatterplots show the relationship between  $\hat{f}_{\text{mCherry cell}}$  on the x-axis and  $\hat{f}_{\text{YFP cell}}$  (first panel),  $\hat{f}_{\text{YFP membrane}}$ , (second panel) and  $\rho$  (third panel) on the y-axis, in 11741 cells expressing WT-CFTR at 37 °C, pooled from seven different plates. Logarithmic scales were used to better visualize the full range of the measurements.

#### 4.2.2 Ability to reach the membrane

The effects of incubation at low temperature, chronic incubation with modulator drugs (corrector VX-809, alone or co-administered with potentiator VX-770) and introduction of revertant mutation R1070W, on the ability of CFTR to reach the plasma membrane ( $\rho$ ) are summarized in **Figure 17** (see also **Table 2**, p. 133).

##### *VX-809*

HEK-293 cells expressing pIRES2-mCherry-YFPCFTR were incubated with 10  $\mu$ M VX-809 for 24 hours before image acquisition. In the control conditions, only DMSO (vehicle used for VX-809) was added to the cells. The temperature and VX-809 concentration, were kept constant during image acquisition. Plate  $\log_{10}\rho$  averages of cells expressing F508del-CFTR treated with or without VX-809 were matched and paired t-tests were performed on the matched pairs (**Table 2**). At 37 °C, 24-hour incubation with VX-809 modestly but significantly increased in  $\log_{10}\rho$  of F508del-CFTR (**Figure 17a**, left panel). The effect is small but could be picked up with the paired t-test because it is consistent in size and direction. A significant increase in membrane proximity was also measured when cells were incubated at 28 °C for 24 hours with VX-809 (**Figure 17a**, right panel). At low temperature, the increase in  $\log_{10}\rho$  due to VX-809 incubation was more pronounced than at 37 °C.

##### *Rescue by R1070W*

To investigate whether the assay could pick up F508del-CFTR rescue by introduction of R1070W, HEK-293 cells were transfected with pIRES2-mCherry-YFPCFTR containing the F508del-CFTR variant with or without the revertant R1070W mutation. Paired t-tests were performed on the matched plate  $\log_{10}\rho$  averages of cells expressing F508del-CFTR or F508del/R1070W-CFTR (**Table 2**). Introduction of the R1070W had a small but significant effect on  $\log_{10}\rho$  of cells expressing F508del-CFTR at 37 °C, increasing the  $\log_{10}\rho$  from -0.58 to -0.53 (**Figure 17a**, left panel). At 28 °C (**Figure 17a**, left panel) too, R1070W significantly increased the  $\log_{10}\rho$  and again the magnitude of the effect was larger at low temperature.

## VX-770 destabilisation

Chronic VX-770 treatment has been shown to reverse VX-809-mediated CFTR correction of F508del-CFTR (Cholon et al., 2014; Veit et al., 2014). HEK-293 cells expressing F508del-CFTR, incubated for 24 hours with 10  $\mu$ M VX-809 alone were compared to cells incubated with both 10  $\mu$ M VX-809 and 10  $\mu$ M VX-770 (paired t-tests; **Table 2**). At 37  $^{\circ}$ C, there was a small but significant decrease in  $\log_{10}\rho$  when cells were incubated with both compounds (**Figure 17c**, left panel). At low temperature too, there was a significant decrease in  $\log_{10}\rho$  in the F508del-CFTR expressing cells treated with VX-770 in addition to VX-809. Again, at 28  $^{\circ}$ C the difference was more pronounced than at 37  $^{\circ}$ C (**Figure 17c**, right panel).

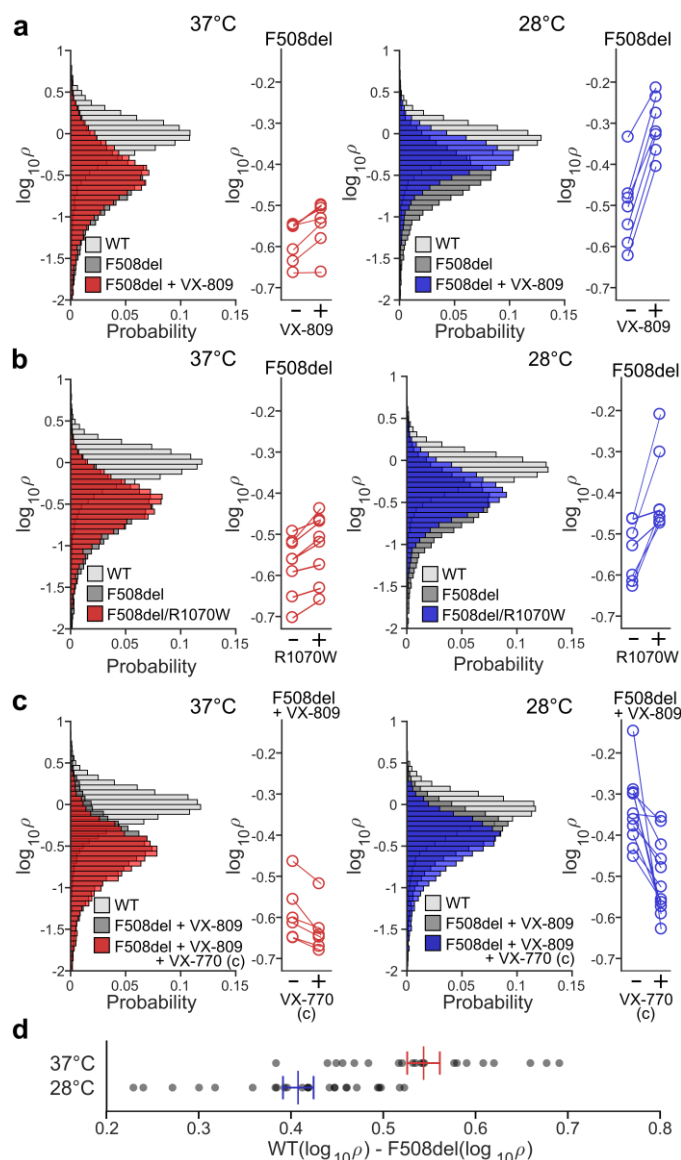


## Figure 17 WT-CFTR, F508del-CFTR, and F508del/R1070W-CFTR membrane proximity in various experimental conditions

Effects of chronic treatment with 10  $\mu$ M VX-809 (**a**), R1070W rescue (**b**), and chronic treatment with 10  $\mu$ M VX-809  $\pm$  10  $\mu$ M VX-770 (**c**), on  $\log_{10}\rho$  at 37  $^{\circ}$ C (left, red) and 28  $^{\circ}$ C (right, blue). Conditions of final incubation were maintained during image acquisition. The probability distributions in the panels on the left, contain  $\log_{10}\rho$  measurements from thousands of cells, pooled from all experiments. For statistical analysis, mean  $\log_{10}\rho$  values determined in independent experiments, and paired per plate, were used (displayed in panels on the right; **d**) Before imaging, plates were incubated at 37  $^{\circ}$ C, or 28  $^{\circ}$ C for 24 hours. For each plate, the difference between mean  $\log_{10}\rho$  for WT-CFTR and F508del-CFTR was calculated (WT( $\log_{10}\rho$ ) - F508del( $\log_{10}\rho$ ), grey dots). Red (37  $^{\circ}$ C) and blue (28  $^{\circ}$ C) lines show mean  $\pm$  SEM, calculated from 21 (37  $^{\circ}$ C) and 25 (28  $^{\circ}$ C) within-plate difference estimates. CH and EH helped with the collection of data on R1070W rescue (**b**), and EL collected the data on and chronic treatment with 10  $\mu$ M VX-809  $\pm$  10  $\mu$ M VX-770 (**c**).

### *Temperature rescue*

Although there is a considerable amount of variability in the  $p$  measurements between plates, the within plate differences seem to be consistent across the experiments. For this reason,  $\log_{10}p$  averages of cells in the experimental condition were matched with those in the control condition on the same plate to evaluate the effects of treatment with VX-809 with or without VX-770, and the R1070W rescue mutation. However, to evaluate the effect of temperature correction, plates were either incubated at 37 °C or at 28 °C making it impossible to match temperature corrected and uncorrected pairs per plate. Moreover, for each condition  $p$  values were normalised to those obtained from cells expressing WT-CFTR grown on the same plate. Therefore, the estimated  $p$  varies depending on the measured  $p$  for WT (which might be affected by temperature too). It would not have been legitimate to directly compare  $p$  measurements obtained on different plates to assess the effect of incubation temperature on F508del-CFTR. Instead, we compared the difference between the mean  $\log_{10}p$  of WT-CFTR and that of F508del-CFTR measured within each plate. In this way the effect of low temperature on  $p$  could be assessed without directly comparing measurements on different plates. A smaller difference at 28 °C between the mean  $\log_{10}p$  of WT-CFTR and of F508del-CFTR suggests that the reduced membrane proximity of F508del-CFTR becomes more similar to that of WT-CFTR, and therefore is partially rescued, after incubation at the lower temperature. An independent t-test showed that the difference in  $\log_{10}p$  of F508del-CFTR and WT-CFTR was indeed significantly smaller at 28 °C compared to 37 °C (**Figure 17d; Table 2**) and confirms that the assay can detect the effect of low-temperature correction.

### 4.2.3 CFTR function

For this set of experiments CFTR function was quantified as the maximal rate of  $I^-$  entry (as described in 3.4.1 *The  $I^-$  first protocol: maximal rate of iodide entry*, p. 67). In the negative control conditions, following addition of extracellular 100 mM  $I^-$ , the maximal rate of  $I^-$  entry was quantified after the addition of DMSO (the vehicle used for dissolving forskolin with or without VX-770). In the test conditions, after addition of 100 mM extracellular  $I^-$ , CFTR was activated by 10  $\mu$ M forskolin alone, or by a combination of 10  $\mu$ M forskolin and 10  $\mu$ M VX-770. To avoid confusion, we defined the

potentiation with VX-770 in these experiments as an acute (a) treatment (see labels in **Figure 18**), as opposed to the 24-hour chronic (c) incubation with VX-770 that was used as experimental condition in the experiments in section

#### 4.2.1 *mCherry accounts for variability due to unequal transfection efficiency*

Because YFP(H148Q/I152L)-WT-CFTR and mCherry are translated from the same mRNA transcript, their fluorescence intensity is expected to be proportional to each other. When quantifying membrane proximity ( $\rho$ ), the normalised mCherry fluorescence intensity ( $\hat{m}Cherry_{cell}$ ) is used to account for between-cell differences in the number of mRNA transcripts caused by variation in transfection efficiency. So,  $\hat{m}Cherry_{cell}$  and  $\rho$  are not expected to correlate. **Figure 16** displays scatterplots that show the relationship between  $\hat{m}Cherry_{cell}$  and  $\hat{YFP}_{cell}$ ,  $\hat{YFP}_{membrane}$ , and  $\rho$ . To investigate the relationship between these variables, Spearman correlation coefficients were computed. While there were strong positive correlations between  $\hat{m}Cherry_{cell}$  and  $\hat{YFP}_{cell}$  ( $r_s = 0.82$ ,  $N = 11741$ ,  $P < 0.0001$ ), and between  $\hat{m}Cherry_{cell}$  and  $\hat{YFP}_{membrane}$  ( $r_s = 0.80$ ,  $N = 11741$ ,  $P < 0.0001$ ), there was no significant correlation between  $\hat{m}Cherry_{cell}$  and  $\rho$  ( $r_s = 0.01$ ,  $N = 11741$ ,  $P = 0.13$ ). These results show that mCherry fluorescence intensity corresponds very well to the level of YFP(H148Q/I152L)-WT-CFTR and can be effectively used to account for within-plate variations in transfection efficiency.

4.2.2 Ability to reach the membrane. For each well (up to four wells per condition per plate), the fluorescence quenching timeline was determined. These were then averaged across all wells in a plate, before calculating the maximal rate of  $I^-$  entry for each condition. The measurements obtained from each plate were considered single independent measurements.

In addition to potentiation with VX-770 (a), we assessed how chronic incubation with VX-809 and introduction of the R1070W revertant mutation, affected the maximal rate of  $I^-$  entry in HEK-293 cells expressing F508del-CFTR. Furthermore, the effect of temperature correction on CFTR function was investigated by incubating plates at 37 °C or at 28 °C for 24 hours prior to the experiments. To test whether there was functional CFTR on the membrane in the different experimental conditions, we used independent t-tests to compare the maximal rate of  $I^-$  entry after addition of forskolin with

the maximal rate of I<sup>-</sup> entry after addition of DMSO (**Table 4**, p. 134). Furthermore, the maximal rate of I<sup>-</sup> entry after forskolin activation was compared between different experimental conditions (**Table 5**, p. 135). The results of the experiments are summarised in **Figure 18**.

#### *DMSO control*

In the negative control conditions, DMSO (vehicle) was added instead of forskolin or forskolin + VX-770. To test whether there was a difference between the maximal rate of I<sup>-</sup> entry among the different genotypes and chronic treatment groups in the control condition (**Table 3**, p. 133), a one-way ANOVA was performed. As expected, there was no significant difference between the groups in the DMSO control condition,  $F(7,58) = 1.82$ ,  $p = .10$ .

#### *WT-CFTR*

As expected, at both 37 °C and 28 °C the maximal rate of I<sup>-</sup> entry in cells expressing WT-CFTR was significantly higher after activation with 10 µM forskolin compared to control (DMSO), even without additional potentiation with VX-770 (a) (**Table 4**, p. 134; **Figure 18a** and **Figure 18e**). Potentiation of WT-CFTR with 10 µM VX-770 (a) on top of activation with 10 µM forskolin, appears to increase the maximal rate of I<sup>-</sup> entry at 37 °C as well as 28 °C. Furthermore, the maximal rate of I<sup>-</sup> entry in cells expressing WT-CFTR appears to be somewhat lower after incubation at low temperature (**Figure 18a** and **Figure 18e**). However, independent t-tests were conducted and, after the Bonferroni correction for multiple comparisons was applied, the changes caused by the presence of 10 µM VX-770 (a) or by the lower temperature on maximal rate of I<sup>-</sup> entry after forskolin addition (**Table 5**, p. 135) were not large enough to reach statistical significance.

#### *F508del-CFTR: VX-770 potentiation*

At 37 °C as well as 28 °C, the maximal rate of I<sup>-</sup> entry in F508del-CFTR expressing cells that had received no pharmacological correction (chronic incubation with DMSO vehicle only), was not significantly different after activation with 10 µM forskolin alone than after the addition of DMSO (**Figure 18b** and **e**, **Table 4**). Similarly, at 37 °C, when F508del-CFTR expressing cells were further potentiated

with 10  $\mu\text{M}$  VX-770 (a) no significant difference in the maximal rate of  $\text{I}^-$  entry was detected. If chronic incubation occurred at 28  $^\circ\text{C}$ , however, activation with forskolin and VX-770 (a) resulted in a significantly increased maximal rate of  $\text{I}^-$  entry with compared to DMSO vehicle control (**Table 4**).

### F508del-CFTR: VX-809 correction

When cells were incubated with 10  $\mu\text{M}$  VX-809 at 37  $^\circ\text{C}$ , there was a significant increase in the maximal rate of  $\text{I}^-$  entry after the addition of 10  $\mu\text{M}$  forskolin in the presence of 10  $\mu\text{M}$  VX-770 (a) compared to

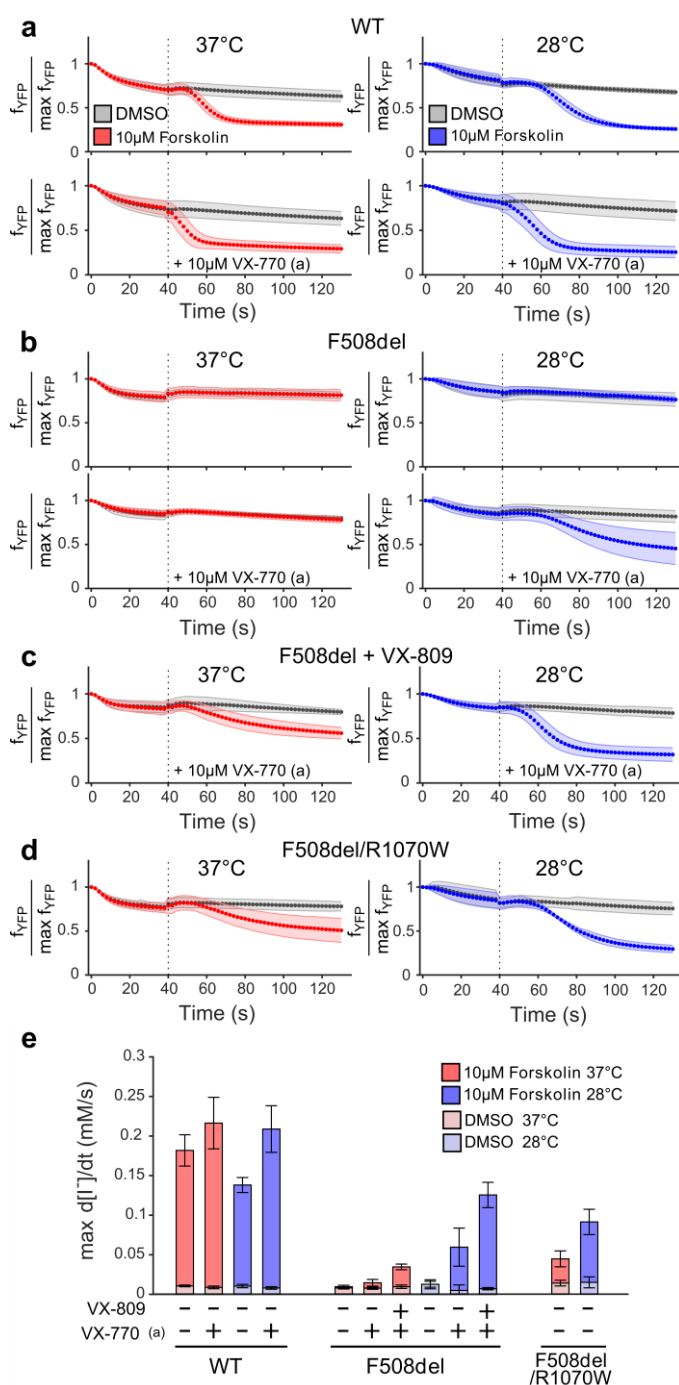


**Figure 18** Effect of temperature, genotype, acute potentiation with VX-770 and chronic VX-809 treatment on the rate of iodide entry. Quenching of normalised YFP fluorescence ( $f_{\text{YFP}}/\text{max } f_{\text{YFP}}$ ) in HEK-293 cells expressing WT-CFTR (a), F508del-CFTR treated with DMSO (b) or after 24-h treatment with 10  $\mu\text{M}$  VX-809 (c), and R1070W/F508del-CFTR (d). Prior to imaging plates were incubated for 24 hours, at 37  $^\circ\text{C}$  (left panels, red) or 28  $^\circ\text{C}$  (right panels, blue). This incubation temperature was maintained throughout image acquisition. At time point 0 s,  $\text{I}^-$  was added to the extracellular medium to achieve a final concentration of 100 mM. At time point 40 s DMSO, forskolin or forskolin + VX-770 (acute, a), as indicated, were added (dotted line) to the extracellular medium. The baseline fluorescence before addition of  $\text{I}^-$  ( $\text{max } f_{\text{YFP}}$ ) was used to normalize YFP fluorescence intensity. (e) The maximal rate of  $\text{I}^-$  entry ( $d[\text{I}^-]/dt$ ) was normalised for expression level against  $\hat{f}_{\text{mCherry}}$  cells and is used to summarize CFTR function for genotypes and conditions shown in (a-d). CH and EH helped with the collection of data on R1070W rescue (d; summarized in e bar 11 and 12)

control (**Table 4**). At low temperature too, activation of VX-809 treated cells expressing F508del-CFTR with 10  $\mu$ M forskolin and 10  $\mu$ M VX-770 (a) significantly increased the maximal rate of  $I^-$  entry compared to the control condition in which VX-809 treated cells were exposed to DMSO. The maximal rate of  $I^-$  entry after the addition forskolin and VX-770 (a) in F508del-CFTR expressing, VX-809 treated, cells was also compared at the different temperatures: at 28 °C the maximal rate of  $I^-$  entry was significantly higher than at 37 °C (**Figure 18c**; **Figure 18e**, F508del bar 6 vs. 3; **Table 5**).

#### *F508del-CFTR: Rescue by R1070W*

In cells expressing F508del/R1070W-CFTR, the maximal rate of  $I^-$  entry after the addition of forskolin (alone) was compared to the maximal rate of  $I^-$  entry without activation. At 37 °C as well as 28 °C, activation with 10  $\mu$ M forskolin significantly increased F508del/R1070W-CFTR channel activity (**Figure 18d**; **Table 4**). Again, the maximal rate of  $I^-$  entry was significantly higher at 28 °C compared to 37 °C (**Figure 18e** F508del/R1070W; **Table 5**).

#### *F508del-CFTR: Temperature rescue*

The severe gating deficit of F508del-CFTR is reflected by the finding that even after incubation at 28 °C, activation with 10  $\mu$ M forskolin was not sufficient to significantly increase the maximal rate of  $I^-$  entry in untreated cells (**Figure 18b** top; **Figure 18e** F508del bars 1 and 4; **Table 4**). The effect of low temperature on F508del-CFTR biogenesis could be observed only when F508del-CFTR was activated by 10  $\mu$ M forskolin together with 10  $\mu$ M VX-770 (a). Following potentiated activation, an increased maximal rate of  $I^-$  entry was observed after incubation at 28 °C, but not at 37 °C. Moreover, low temperature incubation enhanced the effects of VX-809 correction and of revertant mutation R1070W (**Figure 18e**; **Table 5**).

### 4.3 Relationship between channel function and membrane proximity

Data on maximum rate of  $I^-$  entry can be plotted against the corresponding  $p$  values, measured for experimental conditions employing different F508del-CFTR rescue strategies (**Figure 19**). A linear interpolation between data points for uncorrected F508del-CFTR (red squares, **Figure 19a**, used to

approximate an internal  $p$ -axis intercept, assuming virtually no channels reach the membrane for this genotype/condition) and WT-CFTR activated by 10  $\mu$ M forskolin (red circles, **Figure 19a**), describes the ion channel function expected from cells with increasing  $p$  values, assuming open probability ( $P_o$ ) and single channel conductance ( $\gamma$ ) of baseline-activated WT-CFTR and a linear relationship between  $p$  and channel function (Prins et al., 2020, see also **Figure 20**). The interpolation allows us to make inferences about how the gating and permeation characteristics of F508del-CFTR vary for different types of rescue.

Our results suggest that introduction of the R1070W revertant mutation is particularly effective in improving channel function of F508del-CFTR. The mutation increases the maximal rate of  $I^-$  entry more than would be expected based solely on increase in  $p$  (**Figure 19**). Comparing the effect of R1070W at 37 °C (**Figure 19**, empty red square) with temperature correction of F508del-CFTR (**Figure 19**, empty blue five-pointed star), shows how both conditions result in a similar increase in membrane proximity but how temperature-corrected F508del-CFTR has a much lower channel function unless acutely potentiated with VX-770 (filled blue five-pointed star). The data suggests that F508del/R1070W channels that reach the membrane have gating and/or permeation properties equal to, or even better than those of WT-CFTR. This is consistent with single channel patch-clamp recordings indicating that F508del/R1070W-CFTR channel characteristics like  $P_o$ , mean burst duration and interburst interval, were similar to those of WT-CFTR (Liu et al., 2018).

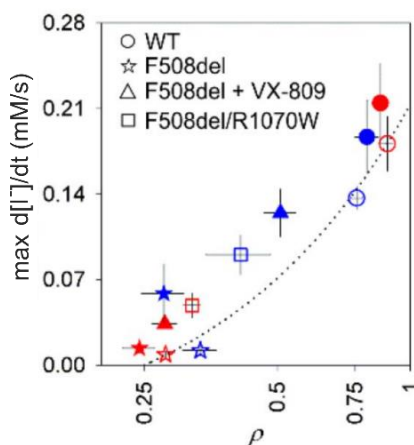


**Figure 19 Relationship between  $p$  and the maximal rate of iodide entry**  
 Relationship between the  $p$  and the maximal rate of  $I^-$  influx ( $d[I^-]/dt$ ) after activation with 10  $\mu$ M forskolin in HEK-293 cells expressing WT-CFTR, F508del-CFTR, and F508del/R1070W-CFTR, at 37 °C (red) and 28 °C (blue). In some conditions there was further potentiation with 10  $\mu$ M VX-770 (filled symbols) in addition to forskolin. The dotted line represents the linear regression between measurements obtained at 37 °C for uncorrected F508del-CFTR (empty red five-pointed star) and WT-CFTR (empty red circle), both without VX-770 (a) potentiation; slope = 0.284, constant = -0.071, resulting in an x-axis intercept at  $p = 0.25$ . CH and EH helped with the collection of data on R1070W rescue.

## 4.4 Discussion

### 4.4.1 Validation of membrane proximity quantification

Our results demonstrate that the mCherry-YFPCFTR assay can accurately detect small changes in membrane proximity of CFTR, even when there is a large heterogeneity among cells. To validate our assay, we tested the effect of chronic treatment with VX-809 with or without VX-770, the second-site mutation R1070W, and low temperature rescue. Although our assay cannot directly quantify the CFTR surface density (see 3.6.1 *Membrane proximity*, p. 83), the effects of our manipulations are similar in magnitude and direction as has been reported by other groups.

VX-809 increases maturation and membrane density of F508del-CFTR (e.g. Carlile et al., 2018; He et al., 2013; Okiyoneda et al., 2013, 2018; Van Goor et al., 2011). Although van Goor and colleagues (2011) report a very pronounced effect of VX-809 at 37 °C, others have combined VX-809 treatment with low temperature correction or revertant mutations in order to measure its effects (Okiyoneda et al., 2013). Consistent with the results of others (He et al., 2013), the increase in F508del-CFTR membrane proximity detected by our assay in response to chronic VX-809 treatment, is very small at 37 °C and a lot larger at 28 °C. Furthermore, in agreement with other studies (Cholon et al., 2014; Veit et al., 2014) we observed a small but significant decrease in membrane proximity of VX-809-treated cells following chronic incubation with VX-770 consistent with the idea that VX-770 destabilises F508del-CFTR. In agreement with the findings of others (Farinha et al., 2013; Mendoza et al., 2012; Okiyoneda et al., 2013; Rabeh et al., 2012; Thibodeau et al., 2010) we showed that R1070W increased F508del-CFTR membrane proximity. Last but not least, our assay was able to verify the effects of low temperature on the membrane proximity of F508del-CFTR (Denning et al., 1992a; He et al., 2013; Rennolds et al., 2008; Wang et al., 2008).

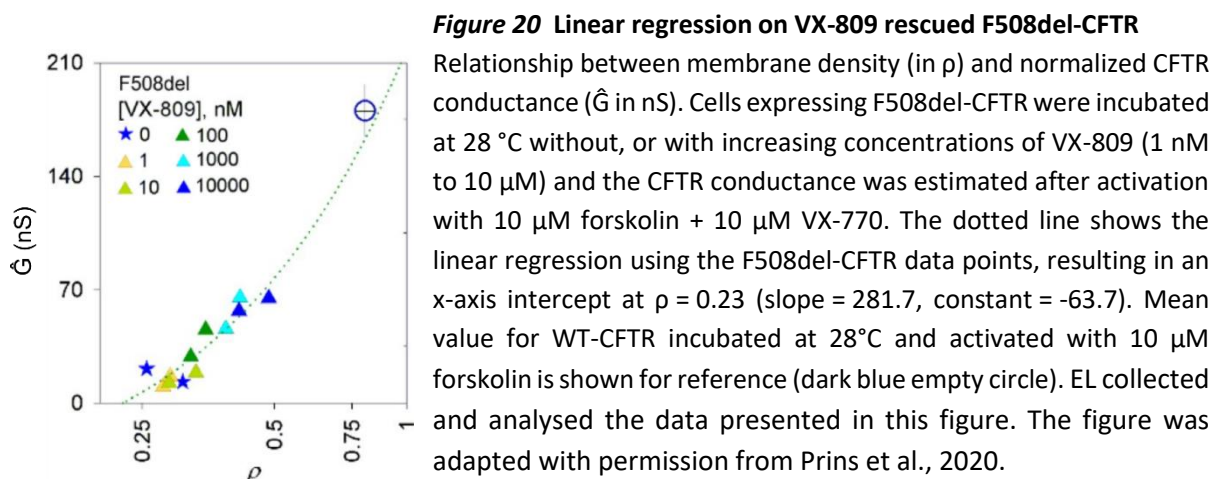
### 4.4.2 Background noise in $\rho$ measurements

Even when virtually no CFTR is present at the membrane, for example in cells expressing F508del-CFTR at 37 °C, the value of  $\rho$  does not fall to zero. The mean  $\log_{10}\rho$  for F508del-CFTR at 37 °C is -0.59 (SD = 0.05), corresponding to a  $\rho$  of 0.26. Considering the  $\rho$  value that corresponds to WT-CFTR at

37 °C, which is 1.12 ( $\log_{10}\rho = -0.05$ ,  $SD = 0.03$ ,  $N = 21$ ), the mean  $\rho$  of F508del-CFTR is higher than would be expected if it is assumed that a  $\rho$  of zero would mean that there is no CFTR on the membrane. There could be several reasons why the  $\rho$  does not approach zero in conditions in which there is practically no CFTR at the membrane.

There inevitably is some inaccuracy in segmentation of the images leading to erroneous localisation of the membrane proximal zone. Misidentification of the cell's edge increases the chance that fluorescence from YFP(H148Q/I152L)-CFTR localised in the internal vesicles will be detected within the membrane proximal zone, leading to noise in the signal and a  $\rho$  above zero. On top of this, because we are using wide-field microscopy, there will be stray light from out-of-focus planes, adding more noise to the signal. Implementing the assay using a confocal or a higher resolution microscope could improve this latter aspect in the future.

To investigate the relationship between CFTR conductance and  $\rho$ , Dr. Emily Langron treated cells expressing F508del-CFTR with increasing concentrations of VX-809 (**Figure 20**), improving both CFTR membrane proximity and conductance in a roughly linear way (Prins et al., 2020). Linear extrapolation allowed an accurate positioning of the x-axis intercept at  $\rho = 0.23$ . A linear regression on our data points obtained at 37 °C for uncorrected F508del-CFTR and WT-CFTR, results in a very similar x-axis intercept at  $\rho = 0.25$  (**Figure 19**). These results suggest that, a  $\rho$  of between 0.23 and 0.25 corresponds to a situation in which almost no channels are being present in close proximity of the membrane.



#### 4.4.3 Channel function: upper limit of the dynamic range

Besides membrane proximity, our assay is capable of quantifying CFTR ion channel function by a previously established method that relies on monitoring the time course of YFP(H148Q/I152L)-CFTR quenching (Langron et al., 2017, 2018). The maximal rate of  $I^-$  entry during CFTR activation, accurately quantifies small differences in the low CFTR function which is typically seen in mutants. The conditions we used in our study were optimised to measure activity of F508del-CFTR which has a severely impaired function. However, they are not ideal for the quantification of differences in activity of WT-CFTR, which has a much higher single-channel conductance. Due to its high activity, the rate of iodide influx, and therefore the YFP(H148Q/I152L) quenching rate, is very high. In some measurements, the fluorescence quenches faster than our acquisition frequency can follow. In these conditions the upper limit of the dynamic range of the assay is reached, resulting in a poor differentiation between conditions with high CFTR activity.

Optimisation of the assay for measurement of differences in WT or high-conducting mutants can very likely be achieved by lowering the concentration of iodide that is added to the extracellular medium. This will lower the driving force for iodide influx and slow down the YFP(H148Q/I152L) quenching rate possibly allowing detection of small differences in rate of iodide entry between high-conducting CFTR variants.

#### 4.4.4 Channel function: $I^-$ first protocol

For the experiments described in this chapter we decided to use the  $I^-$  first protocol in which activation of CFTR with forskolin takes place after addition of extracellular iodide. Compared to the  $I^-$  last protocol, in which forskolin is added first – allowing CFTR activation to reach steady state before iodide is added – the  $I^-$  first protocol requires a less computationally intensive analysis. However, changes in the rate at which CFTR activation occurs, affecting any one of multiple sequential steps following forskolin permeation and ultimately resulting in CFTR phosphorylation, could result in a change in the maximal rate of iodide influx. By contrast, the  $I^-$  last protocol is not affected by the signal transduction kinetics. This reduces the number of parameters which affect the quenching time course, and

therefore makes it possible to fit observed fluorescence values to a simple mathematical model with a small number of free parameters allowing a more direct assessment of CFTR conductance.

#### 4.4.5 Simultaneous assessment of membrane proximity and channel function for pharmacology

Being able to simultaneously assess CFTR ion channel function and membrane proximity, gives more accurate information on the gating and permeation properties of the CFTR. By considering the changes in CFTR function taking into account the changes in CFTR membrane proximity, a more accurate inference on CFTR channel function can be made than by looking at both aspects separately (see for instance, discussion in section *4.3 Relationship between channel function and membrane proximity*, p. 95).

So far, CFTR-targeting drugs have been classified as either correctors or potentiators, and their search has involved separate screening techniques assessing CFTR's capacity to reach the cell membrane, or channel function. Others have pointed out that because of the interrelatedness of CFTR function and biogenesis – both depending on CFTR folding – the artificial separation of compounds into classes of potentiators and correctors might hamper the discovery of compounds with dual potentiator and corrector activity (Rowe & Verkman, 2013). Moreover, evidence suggests that potentiators can negatively interfere with the action of corrector compounds (Cholon et al., 2014; Meng et al., 2017; Veit et al., 2014).

Further complicating drug development, each cystic fibrosis causing mutation alters CFTR differently, and for this reason not only compound action but also compound interference is genotype specific. Taken together, this highlights the relevance of being able to simultaneously quantify CFTR membrane proximity and function. Implementing the assay at early stages of drug discovery programmes could better inform drug development.

#### 4.4.6 Correlation results rare mutant panel with existing datasets

Dr Emily Langron used the mCherry-YFPCFTR assay to characterise a panel of 61 rare cystic fibrosis causing mutations and their response to VX-770 (Prins et al., 2020). Describing each mutant with two

coordinates ( $\rho$  and  $\hat{G}$ ) is a concise and informative way of characterizing the mutants and the effects that compounds have on them. For very rare cystic fibrosis causing mutations, clinical trials are not feasible because the patient populations are so small. For these genotypes the FDA has, in one case, provided licensing based on the results of *in vitro* data obtained using FRT cells (Ratner, 2017). The data we collected on membrane proximity and channel function reproduces the findings of other studies in which rare mutants are characterised in FRT cells (Sosnay et al., 2013; Van Goor et al., 2014; Yu et al., 2012). Although our expression system and metrics differ from the ones used in the other studies, there is a good correlation between our dataset, and two published datasets (Prins et al., 2020).

While the correlation between the published datasets using the same expression system and metric is  $r^2 = 0.48$ , correlations between our  $\rho$  and the proportion of CFTR acquiring complex glycosylation are  $r^2 = 0.74$  (Sosnay et al., 2013),  $r^2 = 0.53$  (Van Goor et al., 2014; Yu et al., 2012), and  $r^2 = 0.67$  using average values for mutants from the datasets (Prins et al., 2020). Western Blot measurements obtained with FRT cell lines stably expressing CFTR are known to have *in vivo* predictive value for cystic fibrosis (Han et al., 2018; Sosnay et al., 2013). Our study thus validates the use of HEK-293 cells for molecular characterization of CFTR biogenesis. Furthermore, although HEK-293 cells do not form monolayers required for transepithelial current measurements, our results for CFTR channel function ( $\hat{G}$ ) correlate well with published short-circuit Ussing Chamber measurements using cell monolayers:  $r^2 = 0.68$  (Van Goor et al., 2014),  $r^2 = 0.61$  (Sosnay et al., 2013; Yu et al., 2012), and  $r^2 = 0.60$  using average values for mutants (Prins et al., 2020).

## 5. Second-site mutations in *cis* with F508del

### 5.1 Introduction

F508del-CFTR biogenesis and function can be rescued by introduction of second-site mutations in *cis* with F508del. One of these rescue mutations is R1070W. R1070W is located in the ICL4 and corrects both function and trafficking of F508del-CFTR (Mendoza et al., 2013; Rabeh et al., 2012; Thibodeau et

al., 2010). In this study two sets of second-site mutations in *cis* with F508del were tested using the mCherry-YFPCFTR assay: 64 second-site mutations in the ICL4 and two second-site mutations (A141S and R1097T) that were chosen based on studies in F670del-Yor1 (Louie et al., 2012; Pagant et al., 2010). The effects of these mutations on membrane proximity and channel function (assessed using the  $I^-$  last protocol, see 3.4.2 *The  $I^-$  last protocol: estimation of  $G$  and  $V_m$* ) are discussed in this chapter.

### 5.1.1 ICL4

#### *The TMD-NBD interfaces*

CFTR gating is regulated by ATP binding to the NBDs, and by phosphorylation of the R domain. The NBDs interact with four short helices in the intracellular domains, the coupling helices (CHs), which are part of the cytosol-exposed parts of the TMDs, here referred to as intracellular loops (ICLs). The interaction between the ICLs and NBDs is believed to be critical for the transmission of regulatory changes of the NBDs to the rest of the channel. Similar to other ABC transporters, ICL2 (between TM4 and TM5 of TMD1) and ICL4 (between TM10 and TM11 in TMD2) are buried in the NBD2 and NBD1 respectively, while ICL1 (between TM2 and TM3 of TMD1) and ICL3 (between TM8 and TM9 of TMD2) have more superficial contacts with the NBDs (Hwang et al., 2018). Some functional and molecular dynamics data suggests that the ICL4-NBD1 and ICL2-NBD2 interfaces might move synchronously as rigid bodies during the gating cycle (He et al., 2008; Odera et al., 2018).

#### *Flexibility of the ICL-NBD interfaces*

Interestingly, a recent study indicates that the NBD1-ICL4 and the NBD2-ICL2 interfaces are less rigid than previously thought. Crystal structures of NBD1-nanobody complexes suggest that CFTR must adopt, at least transiently, a conformation that differs significantly from the published cryo-EM structures; involving undocking of NBD1 to allow binding of the nanobodies at a binding site located at the ICL4-NBD1 interface (Sigoillot et al., 2019). The authors argue that CFTR could have evolved to allow undocking of NBD1 for a functional reason. In agreement with the idea that the NBD1 domain can undock from the ICL4, it has been shown that cysteines at position 508 in the NBD1 and at positions in the ICL4 can be covalently linked using crosslinkers with spacer arms ranging from 3.9 Å

to 24.7 Å, indicating considerable flexibility in the positioning of each member of the cysteine pair with respect to the other (Serohijos et al., 2008). Moreover, the observation that channel gating was completely inhibited by cross-linking of cysteines on opposite sides of the NBD1-ICL4 or the NBD2-ICL2 interfaces, suggests that NBD and TMDs might not move as rigid-body, fixed units, but rather, that some relative domain movement is actually required for channel gating (Serohijos et al., 2008). Furthermore, it is becoming increasingly clear that other members of the ABC transporter family too, might not operate according to the rigid body motion first proposed based on their structure (Ward et al., 2007) but instead have an unexpected flexibility during which the NBDs must come loose from the ICLs (Mehmood et al., 2012).

#### *Role of the ICL4-NBD1 interface*

The ICL4-NBD1 interface seems to be particularly important in the gating and maturation processes of CFTR, with several CF-causing mutations located in the ICL4 (Cotten et al., 1996; Seibert et al., 1996) and on the NBD1 face of this “ball-and-socket” joint. The most common CF-causing mutation, F508del, had been predicted to be within the ICL4-NBD1 interface by CFTR homology models (e.g. Dalton et al., 2012; Mornon et al., 2008; Serohijos et al., 2008); a prediction that was confirmed by the observation that F508C can be cross-linked to cysteines introduced at sites L1065, F1068, G1069, and F1074 (Serohijos et al., 2008) and later also by the resolved molecular structures of zebrafish and human CFTR (Liu et al., 2017; Zhang et al., 2017; Zhang & Chen, 2016). Molecular Dynamics simulations using atom coordinates from a homology model have suggested that deletion of F508 not only disrupts a hydrophobic cluster located at the NBD1-ICL4 interface, but could also affect NBD1-NBD2 dimerization (Hoffmann et al., 2018; Odera et al., 2018).

#### *F508del-CFTR rescue by targeting the ICL4*

Second-site revertant mutations, also called rescue or suppressor mutations, are mutations that alleviate or revert the phenotypic effects of an existing mutation. A small number of second-site revertant mutations for F508del-CFTR have been identified outside the NBD1. One of these is R1070W (Thibodeau et al., 2010), located in the ICL4 at its interface with the NBD1. R1070W partially corrects

the function of F508del-CFTR (Mendoza et al., 2013; Rabeh et al., 2012; Thibodeau et al., 2010). It has been suggested that it does so by enhancing hydrophobic interactions at the ICL4-NBD1 interface (Chong et al., 2015). Identification of effective suppressor mutations for F508del-CFTR and subsequent mechanistic characterisation of their effects, could provide insights for drug discovery. We set out to investigate whether there are second-site mutations in the ICL4, in addition the known revertant R1070W, capable of rescuing F508del-CFTR function. We scanned the ICL4 by systematically introducing second-site mutations, replacing ten residues in a stretch of F508del-CFTRs ICL4 at its interface with the NBD1.

### 5.1.2 F670del-Yor1 revertants

#### *Yeast models*

The study of model organisms like bakers' yeast *Saccharomyces cerevisiae* has been invaluable for our understanding of fundamental properties of living cells (Fields & Johnston, 2005). Yeast has long been a valuable tool in basic biomedical research and its use extends from the field of diagnostics to drug discovery. For example, a yeast-based assay has been developed for assessing the functionality of the tumour suppressor gene p53 in cancer patients (Ishioka et al., 1993), informing about the most appropriate treatment options. Furthermore, yeast-based assays have been developed as high throughput drug screening platforms for inherited mitochondrial diseases (Couplan et al., 2011), prion diseases (Bach et al., 2003) and Huntington's disease (Zhang et al., 2005).

Yeast models have also been used in CFTR research. A STE6-CFTR chimera, which contains the yeast STE6 a-factor transporter with the NBD1 domain of CFTR has been used to identify second-site revertant mutations for F508del-CFTR (Decarvalho et al., 2002; Teem et al., 1993, 1996). Recently, the joint effort by the group of Professor Elizabeth Miller and the group of Professor John Hartman has led to the validation of a phenomic yeast model for the most common form of cystic fibrosis (Louie et al., 2012). They showed that cellular pathways and genes similar to the ones known to modulate biogenesis of F508del-CFTR are involved in the disrupted processing of F670del-Yor1p which is a yeast homolog of CFTR with a mutation equivalent to F508del.

### *F670del-Yor1p*

The sequence of the yeast genome predicts the existence of 29 yeast ABC transporters and although no ortholog of CFTR exists in yeast, there are six genes encoding proteins homologous to members of the ABCC human subfamily that includes CFTR (Decottignies & Goffeau, 1997). Of these six homologs only Yor1p localizes to the plasma membrane; the others are localised to the vacuolar membrane which is the yeast equivalent of the lysosomal membrane in mammalian cells (Paumi et al., 2009). Yor1p, which stands for yeast oligomycin resistance protein, is a multidrug transporter required for growth in the presence of the mitochondrial poison oligomycin (Cui et al., 1996; Katzmann et al., 1995). Yor1p has a similar quaternary structure to CFTR, with domain swapping creating an ICL1-ICL4 unit that interacts with the NBD1 and an ICL2-ICL3 unit that interacts with NBD2 (Pagant et al., 2008). Deletion of the highly conserved F670 residue in Yor1p, equivalent to the F508del mutation in CFTR, causes misfolding, ER retention and degradation, similar to F508del (Pagant et al., 2007).

### *Rescue of F670del-Yor1p by second site-mutations*

Several second-site mutations that partially rescue F670del-Yor1p folding or increase its transport efficiency have been identified. In one study, the ICL1-ICL4-NBD1 interface of Yor1p was perturbed by the introduction of a mutation in the ICL1 (G278R) or in the ICL4 (I1084P); like F670del-Yor1p, G278R-Yor1p and I1084P-Yor1p did not allow growth in the presence of oligomycin, suggesting that the function and/or the biogenesis of Yor1p is impaired by all these mutations (Pagant et al., 2010). The XL1-red *Escherichia coli* mutator strain was used to produce a randomly mutagenized plasmid library after which the plasmids were transformed in a yeast strain lacking the gene encoding Yor1p.

Out of ~300,000 mutagenized plasmids screened, 2 second-site revertant mutations for I1084P-Yor1 that allowed growth in the presence of oligomycin were identified: R1168M and F270S. The effect of R1168M was stronger than that of F270S when incubated in the presence of oligomycin for two days, but both mutations had comparable effects when incubation was performed for four days. The authors introduced the second-site mutations in F670del-YOR1 (equivalent to F508del-CFTR) and G278R-Yor1. The effect of the second-site mutations in the ICL1 mutant,

G278R-Yor1, was similar to their effect on ICL4 mutant I1084P-Yor1p. Although the introduction of either F270S or R1168M in F670del-YOR1 had little to no effect on oligomycin sensitivity of F670del-Yor1p expressing yeast, introduction of F270S and R1168M together substantially suppresses oligomycin sensitivity, likely as a result of rescued folding and trafficking mediated through stabilization of the hydrophobic transmembrane domains (Pagant et al., 2010).

In a different study, an intragenic suppressor screen was performed in F670del-Yor1. 5,000 double mutants were screened, leading to the identification of R1116T (Louie et al., 2012). While the intracellular processing defects of the F670del/R1116T-Yor1p mutant were similar to those exhibited by the single F670del-Yor1p mutant, the oligomycin growth phenotype associated with F670del/R1116T-Yor1p was between that of F670del-Yor1p and WT Yor1p, suggesting that this second-site mutation boosts F670del-Yor1p pump function.

We tested whether mutations in F508del-CFTR (A141S and R1097T) corresponding to the second-site revertant mutations in F670del-YOR1 (F270S and R1116T respectively) were capable of rescuing F508del-CFTR membrane proximity and/or channel function.

## 5.2 Results

We evaluated how the mutations in *cis* with F508del affected the membrane proximity and channel function of F508del-CFTR, using the mCherry-YFPCFTR assay. A panel of 65 pIRES2-mCherry-YFPCFTR (see 2.1.1 *pIRES2-mCherry-YFPCFTR construction*) plasmids, encoding F508del-CFTR with or without second-site mutations, and including WT-CFTR as a reference for normalisation, was used to transfect HEK-293 cells. To see whether mutations in the ICL4, other than R1070W, could improve the disrupted dynamics of the ICL4-NBD1 interface in F508del-CFTR, we introduced 61 second-site mutations in the ICL4. These mutations replaced residues at site 1064-1074 (ICL4) with tryptophan (W), histidine (H), tyrosine (Y), phenylalanine (F), methionine (M) and glutamine (Q). Moreover, we introduced the equivalents to the F670del-Yor1p revertants F270S (Pagant et al., 2010) and R1116T (Louie et al., 2012) in *cis* with F508del.

Because we wanted to maximize the chance of picking up effects, even when they are small, of the second-site mutations on F508del-CFTR function, we conducted our experiments at 28 °C as low temperatures increase the proportion of F508del-CFTR on the membrane (Denning et al., 1992a); an improvement that is additive with F508del-CFTR rescue by other second-site mutations (Farinha et al., 2013).

### 5.2.1 The CFTR equivalents to the F670del-Yor1p revertants

We aligned the sequences of asymmetric ABC-transporters (Szollosi et al., 2011) and found that F270, R1116 and R1168 in YOR1, correspond to A141, R1097 and N1148 in CFTR respectively. The regions in which A141 and N1148 are located are poorly conserved, but R1097 is located in a highly conserved region. The positions corresponding to A141, R1097 and N1148 in YOR1 are shown on the cryo-EM structures of dephosphorylated human CFTR, 5UAK (Liu et al., 2017) and phosphorylated, ATP-bound human CFTR, 6MSM (Z. Zhang, Liu, & Chen, 2018); **Figure 21a** and **Figure 21b** respectively. All sites are located in close proximity to each other (within 16Å) at the interface between the cytosol and the membrane (**Figure 21**).

Interestingly, R1097 is located in TM11 which is part of the domain-swapped portion of TMD2 that enables the ICL4 (connecting TM10 and TM11) to make contact with the NBD1. A recent *in silico* study using the cryo-EM structure of phosphorylated, ATP-bound zebrafish CFTR (PDBID: 5W81; Z. Zhang et al., 2017) predicts that R1097 is one of the positively charged amino acids lining the pore that chloride ions spend more time in close proximity to (Farkas et al., 2019). A141 is located in TM2 which is part of TMD1 and is connected to the ICL1; in turn, the ICL1 has been shown to interact with NBD1 (He et al., 2008, 2010). Results of a study in which a cysteine scan of TM12 was performed, indicated that N1148, which is located in TM12, is exposed to the aqueous medium in the inner vestibule of the pore of CFTR (Bai et al., 2011).

### 5.2.2 mCherry fluorescence

While changing the independent variable, genotype, we tried keep other conditions unchanged. However, it is possible that some conditions have been modified unintentionally while creating the

different genotypes. The mCherry fluorescence is an indicator of the amount of plasmid mRNA compared to WT for each condition within that plate. Unlike YFP(H148Q/I152L) which is fused to CFTR, the amount of mCherry is expected not to depend on CFTR genotype. Changes in mCherry

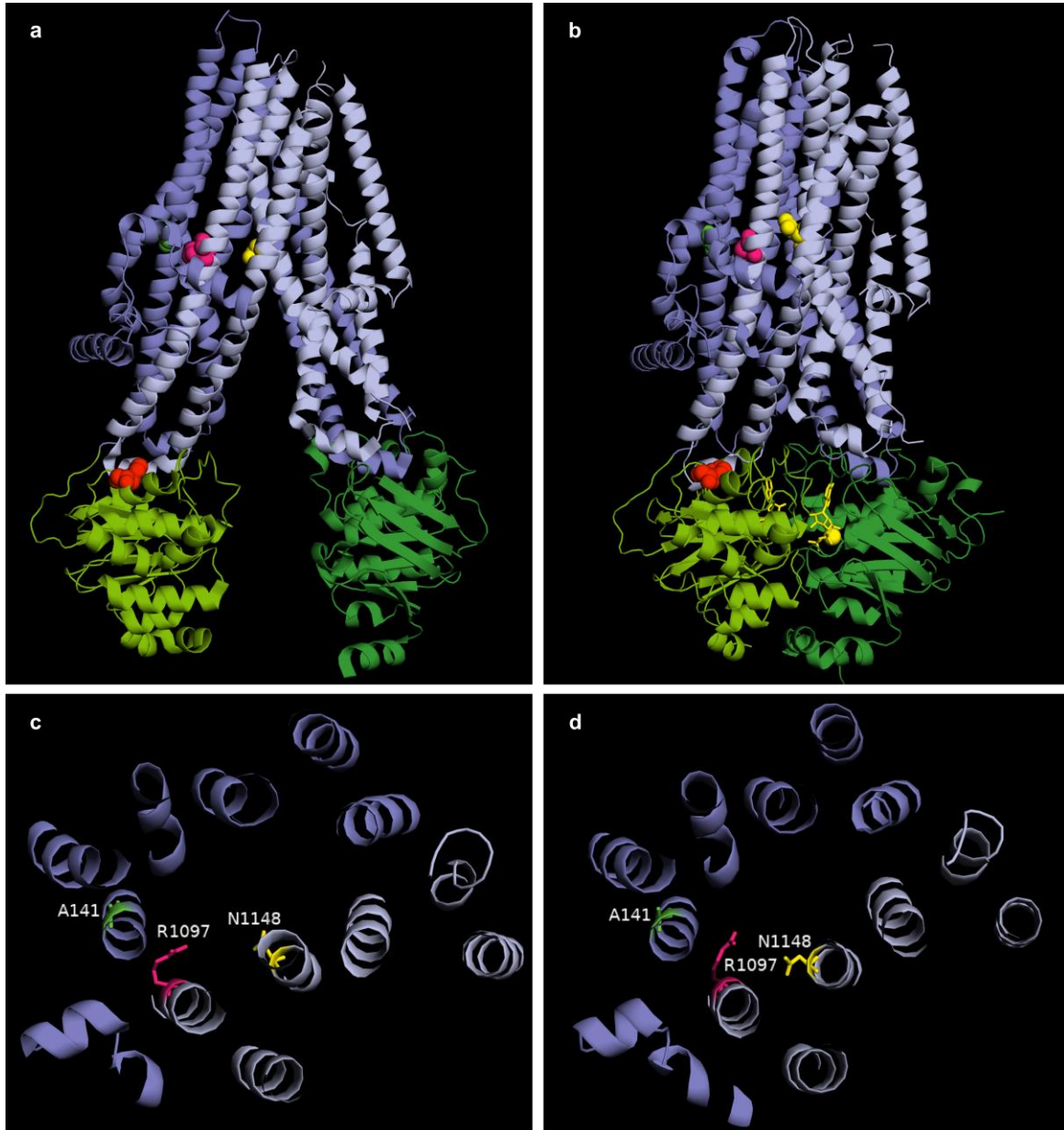


**Figure 21** Positions of F508, A141, R1097 and N1148 in CFTR molecular models

The cryo-EM structures of dephosphorylated human CFTR, 5UAK (a) and phosphorylated, ATP-bound human CFTR, 6MSM (b). TMD1 and TMD2 are coloured in dark purple and light purple respectively, and NBD1 and NBD2 are coloured in light green and dark green respectively. The red spheres represent F508. A141 (TM2, green), R1097 (TM11, magenta) and N1148 (TM12, yellow) are highlighted as spheres (upper panels) or sticks (lower panels). c and d show a slab of the transmembrane helices turned 90 ° towards the viewer relative to the structures in the upper panels (5UAK, c; 6MSM, d). The distances between alpha carbon atoms of A141 and R1097, R1097 and N1148 and A141 and N1148 are 7.1 Å, 7.9 Å, and 16 Å respectively in 5UAK (a) and 7.0 Å, 7.4 Å, and 14.7 Å respectively in 6MSM (b).

fluorescence that appear to be dependent on genotype could indicate a consistently low expression of that genotype due to impurities in the plasmid preparation or off-site mutations in mCherry or IRES.

We wanted to check whether there were genotype related differences in normalised mCherry fluorescence intensity of cells expressing F508del-CFTR with or without second-site mutations. Mean normalised mCherry fluorescence per plate was measured in two different ways for each genotype: using the images collected with the I<sup>-</sup> first (quenching) protocol and using the images collected for with the membrane proximity protocol (**Figure 22; Table 6**, p. 136). For the quenching protocol the normalised mCherry fluorescence,  $\hat{f}_{\text{mCherry cells}}$ , was determined by dividing the average mCherry fluorescence inside the cell selection to the average mCherry fluorescence inside the cell selection of WT-CFTR expressing cells (see 3.4.3 *Normalisation to control for transfection efficiency*, p. 77). For images collected to determine membrane proximity, the average mCherry fluorescence for each cell was determined ( $f_{\text{mCherry cell}}$ ), after which each cell value was divided by the median  $f_{\text{mCherry cell}}$  of cells expressing WT-CFTR within that plate (resulting in  $\hat{f}_{\text{mCherry cell}}$ ). For analysis, the  $\hat{f}_{\text{mCherry cell}}$  plate means ( $\overline{\hat{f}_{\text{mCherry cell}}}$ ) were used.

Measurements collected with the quenching protocol as well as the membrane proximity protocol, did not approximate a normal distribution and displayed heteroscedasticity. For the measurements collected with the quenching protocol, the non-parametric Kruskal-Wallis test indicated that there was a statistically significant difference in normalised mCherry fluorescence intensity ( $\hat{f}_{\text{mCherry cells}}$ ) between the different genotypes,  $\chi^2(64) = 113.05$ ,  $p = 0.0002$ . Pairwise comparisons between all groups indicated that for F508del/Q1071F,  $\hat{f}_{\text{mCherry cells}}$  had a significantly lower mean rank compared to the following ten genotypes: F508del, F508del/A1067F, F508del/A1067M, F508del/G1069H, F508del/G1069W, F508del/R1070M, F508de/Q1071W, F508de/Y1073M, F508del/F1074H and F508del/F1074M.

After performing a cube root transformation on  $\overline{\hat{f}_{\text{mCherry cell}}}$ , the mCherry fluorescence measurements collected with the membrane proximity protocol met the assumptions for parametric testing. An ANOVA test indicated that here too, there was a difference between groups,  $F(64) = 1.65$ ,

$p = 0.0025$ . Pairwise comparisons between all groups showed that F508del/Q1071F had a significantly lower cube root  $\sqrt[3]{\hat{f}_{\text{mCherry cell}}}$  compared to the following nine genotypes: F508del, F508del/G1069W, F508del/Q1071M, F508del/Y1073H, F508del/Y1073M, F508del/F1074H, F508del/F1074Q, F508del/F1074W and F508del/F1074Y. Moreover, F508del/A1067Q had a significantly lower cube root  $\sqrt[3]{\hat{f}_{\text{mCherry cell}}}$  compared to F508del/F1074H.

We had noticed already that mCherry fluorescence in cells expressing F508del/Q1071F-CFTR was low for all measurements. We first reasoned that impurities in the DNA preparation could cause the transfection efficiency for certain genotypes to be consistently low, but also after doing additional measurements with a new DNA preparation, the normalised mCherry fluorescence intensity stayed very low for this genotype. The fluorescence intensity of mCherry, but not the YFP(H148Q/I152L) intensity, was extremely low for this mutant, resulting in very high  $p$  values while hardly any YFP(H148Q/I152L) could be observed in the membrane proximal zone. It seems likely that an unwanted off-target mutation in the sequence of mCherry or the IRES, introduced during the

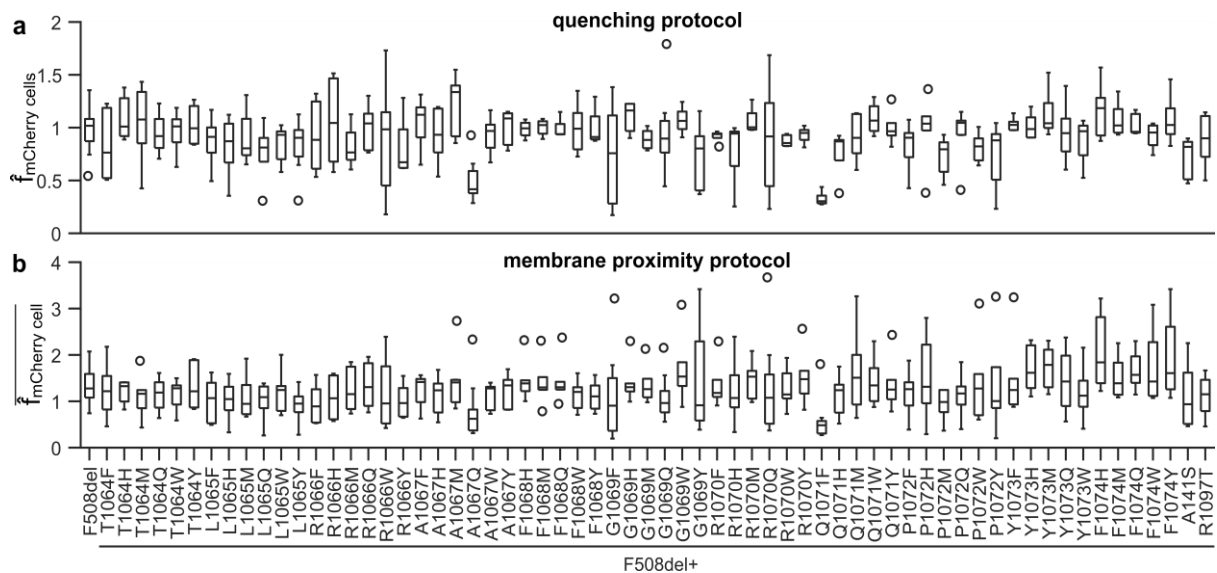


**Figure 22** Boxplots of the normalised mCherry fluorescence intensity

The normalised mCherry fluorescence intensity was determined for each genotype. For each plate of measurements obtained in the quenching protocol (a) the normalised mCherry fluorescence,  $\hat{f}_{\text{mCherry cells}}$ , was determined by normalising the average mCherry fluorescence inside the cell selection to the average mCherry fluorescence inside the cell selection of WT-CFTR expressing cells. In the membrane proximity protocol (b), the mCherry fluorescence,  $f_{\text{mCherry cell}}$ , was obtained for each cell separately, after which it was normalised to the median  $f_{\text{mCherry cell}}$  of cells expressing WT-CFTR on the same plate. This results in  $\hat{f}_{\text{mCherry cell}}$  of which the plate means were taken for this boxplot (denoted as  $\sqrt[3]{\hat{f}_{\text{mCherry cell}}}$ ).

site-directed mutagenesis, could be the cause of the low mCherry fluorescence intensity. These results suggest that the readouts of F508del/Q1071F-CFTR are probably unreliable, we therefore decided to remove this mutant from the dataset that was used for further analysis.

### 5.2.3 Membrane proximity

For assessment of the CFTR membrane proximity of cells expressing F508del-CFTR with or without second-site mutations, collected images were processed as described in sections 2.3.2 *MetaXpress image acquisition protocols – CFTR membrane proximity* and 2.5.1 *Membrane proximity*. Membrane proximity was described by the  $\rho$  metric which was calculated for each cell as described in section 3.5.3 *Defining CFTR membrane proximity ( $\rho$ )*. The  $\rho$  measurements approximated a lognormal distribution and were  $\log_{10}$  transformed before determining plate means for each genotype. The distribution of  $\log_{10}\rho$  means approximated a normal distribution and there was homogeneity of variances. To evaluate whether second-site mutations significantly improved F508del-CFTR membrane proximity, paired t-tests were performed between the mean  $\log_{10}\rho$  of cells expressing F508del-CFTR with or without second-site mutation pairing measurements obtained within plates (see **Figure 23; Table 7**, p. 137). Substitution of the arginine (R) at site 1070 with tryptophan (W) or methionine (M), as well as substitution of the phenylalanine (F) at site 1074 methionine (M), significantly increased the mean  $\log_{10}\rho$  of F508del-CFTR. R1070Y too, appears to increase  $\log_{10}\rho$ , but this effect was not significant. Mean  $\log_{10}\rho$  of F508del-CFTR was significantly decreased by 25 substitutions at sites T1064, L1065, R1066, A1067, F1068, G1069, Q1071, P1072 and F1074 (**Table 8**, p. 138).

### 5.2.4 Channel function

To assess how second-site mutations in *cis* with F508del affect the function of the channel, YFP(H148Q/I152L)-CFTR fluorescence quenching experiments were carried out. The quenching time course was fitted to a mathematical model (see 3.4.2 *The  $I^-$  last protocol: estimation of  $G$  and  $V_m$* ). At 28 °C, the estimated transient endogenous anion conductance in the control (DMSO) conditions decayed slower than in previous estimates at 37 °C (Langron et al., 2018). Because the transient

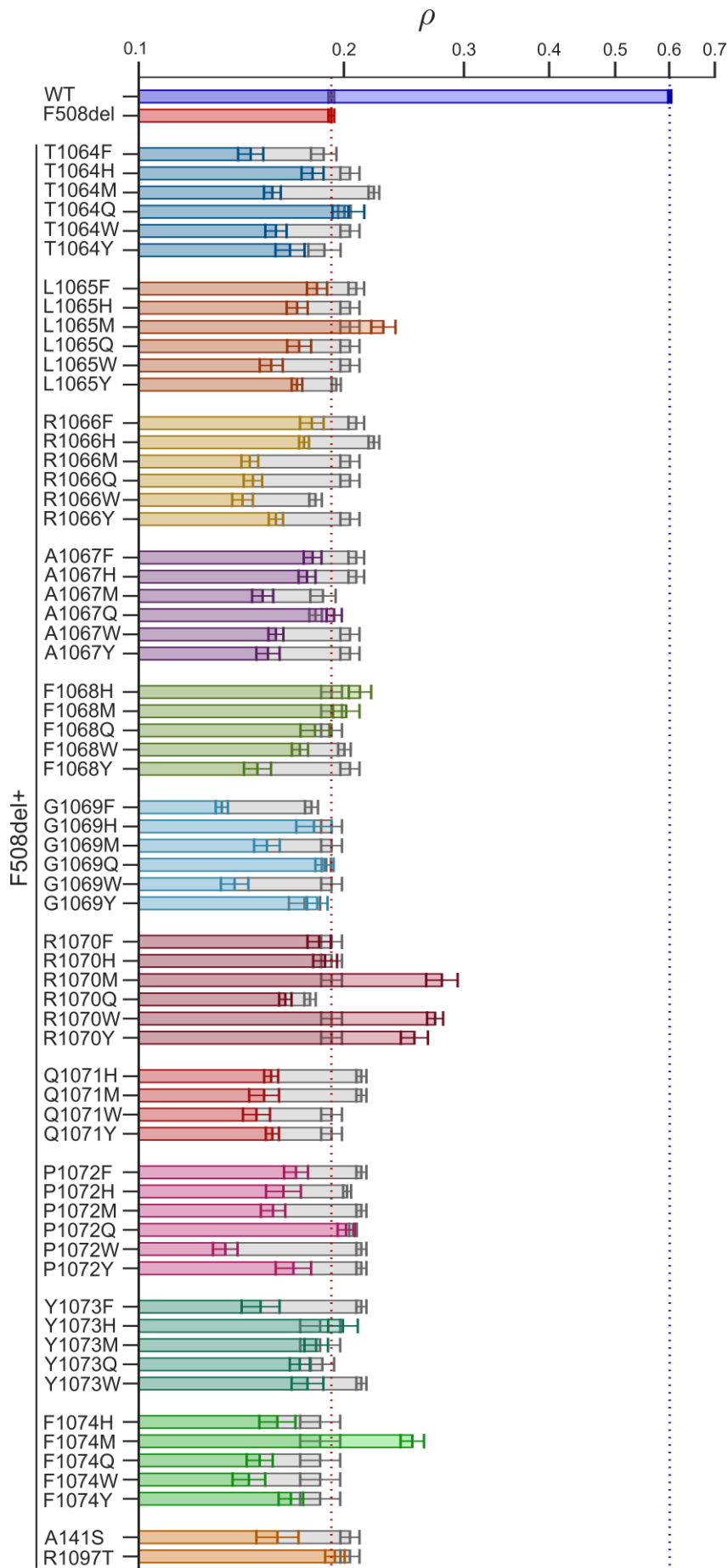


**Figure 23 Effect of ICL4 mutations in cis with F508del on membrane proximity**

The capacity of CFTR to reach the plasma membrane was assessed in HEK-293 cells expressing WT-CFTR and F508del-CFTR with or without second-site mutation.  $\rho$  values, quantifying membrane proximity, were  $\log_{10}$  transformed before doing statistical analysis. This figure shows the back transformed mean  $\log_{10}\rho \pm$  the back transformed values for the upper and lower limits of the SEM. Each coloured bar represents a different CFTR genotype (specified on the y-tick label left of the y-axis). The coloured bars overlap grey bars that represents F508del-CFTR without second-site mutation, plate-matched to mutant on the y-tick label (statistical analysis was performed on these plate-matched pairs by means of paired t-tests). The dashed horizontal reference lines indicate the  $\rho$  values back transformed from mean  $\log_{10}\rho$  for WT (blue;  $\rho = 0.60$ ) and F508del (red;  $\rho = 0.19$ ).

current overlapped more with the slower CFTR-related current than at 37 °C, it was not possible to reliably estimate the values describing the transient current. For this reason, we decided to repeat the analysis constraining  $G_{\text{trans}}$  and  $\tau_{\text{trans}}$  to the average values obtained from the negative (DMSO) controls (9 nS and 11.4 s respectively). The maximal CFTR conductance ( $G$  in nS) and membrane potential before addition of iodide ( $V_m$  in mV); summarised in **Table 7**. Conductance was normalised to mCherry fluorescence (denoted as  $\hat{G}$ ), taking into account genotype specific small variations in transfection efficiency (see 3.4.3 Normalisation to control for transfection efficiency).

### Conductance

#### DMSO controls

In the control condition, the mutants with the F508del-background typically had an average  $\hat{G}$  estimate around 1 nS ( $M = 0.97$  nS,  $SD = 1.29$ ,  $N = 64$ ), consistent with a small anion permeability reflecting mainly endogenous, non-CFTR mediated conductances. A Kruskal-Wallis test indicated that there were genotype dependent differences in  $\hat{G}$  after the addition of DMSO,  $\chi^2(63) = 108.79$ ,  $p = 0.0003$ . However, we were unable to identify which groups differed from each other as no significant differences were found when *post hoc* pairwise comparisons between the group mean ranks were performed.

**Figure 24** shows boxplots of the  $\hat{G}$  after the addition of DMSO in nS (**a**) and ranks (**b**). Although F508del/Y1073F appears to have an increased  $\hat{G}$  in the DMSO control ( $M = 8.13$  nS,  $SD = 9.13$ ,  $N = 5$ ),

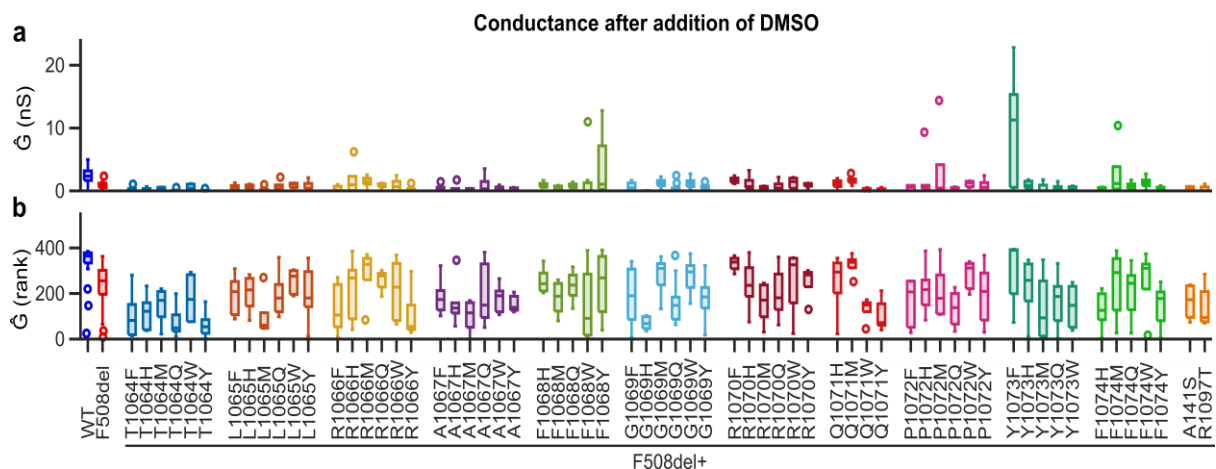


**Figure 24** Effect of ranking on normalised conductance distributions in the control condition

Boxplots of the normalised conductance ( $\hat{G}$ ) in the control (DMSO) condition before (a) and after ranking (b).

compared to the other mutants (**Table 7**), after the data is ranked (**b**) this difference is no longer obvious. There is a high variability in the F508del/Y1073F measurements: while three out of five measurements range from 11 to 23 nS, two measurements are below 1 nS. The two low conductance measurements have been collected on the same day while the three high conductance measurements have all been collected on different days. It is therefore more likely that the low conductance measurements, rather than the high measurements, are unreliable. Given these results it is likely that  $\hat{G}$  after the addition of DMSO is increased in F508del/Y1073F. Possibly Y1073F attenuates the phosphorylation dependency of CFTR activity. Additional experiments are required to confirm whether or not Y1073F increases  $\hat{G}$  after the addition of DMSO compared to genotypes. If it turns out that non-activated F508del/Y1073F indeed has an increased conductance compared to other mutants with a F508del background, it would be interesting to test the effect of Y1073F in a WT background too.

#### forskolin vs. DMSO

**Figure 25** shows boxplots of the  $\hat{G}$  and  $V_m$  estimates after addition of DMSO (gray boxes) and 10  $\mu$ M forskolin (coloured boxes). To determine whether activation of CFTR through the cAMP pathway resulted in a measurable increase in anion conductance, we conducted one-tailed Wilcoxon ranking tests (**Table 9**, p. 139). As expected, the  $\hat{G}$  estimate for WT-CFTR was significantly higher after addition of forskolin ( $Mdn = 117.70$  nS,  $N = 17$ ) compared to DMSO ( $Mdn = 2.35$  nS,  $N = 20$ ). For F508del-CFTR too, we observed a significant, albeit modest, increase in  $\hat{G}$  after addition of forskolin ( $Mdn = 5.7$  nS,  $N = 18$ ) compared to the control condition ( $Mdn = 0.86$  nS,  $N = 19$ ). Furthermore, increased conductance after addition of forskolin compared to DMSO was observed in 24 mutants with second-site mutations in *cis* with F508del: T1064H/F/Y, L1065M, A1067W, F1068H/M/Q, G1069H, R1070H/F/M/Q/W/Y, P1072W/M/Q/Y, Y1073Q/H, F1074M, A141S and R1097T (**Table 9**). Mutations at site 1071 and 1066 appear to abolish forskolin induced conductance in F508del-CFTR; for none of these mutants  $\hat{G}$  after addition of forskolin was significantly increased compared to the control condition.

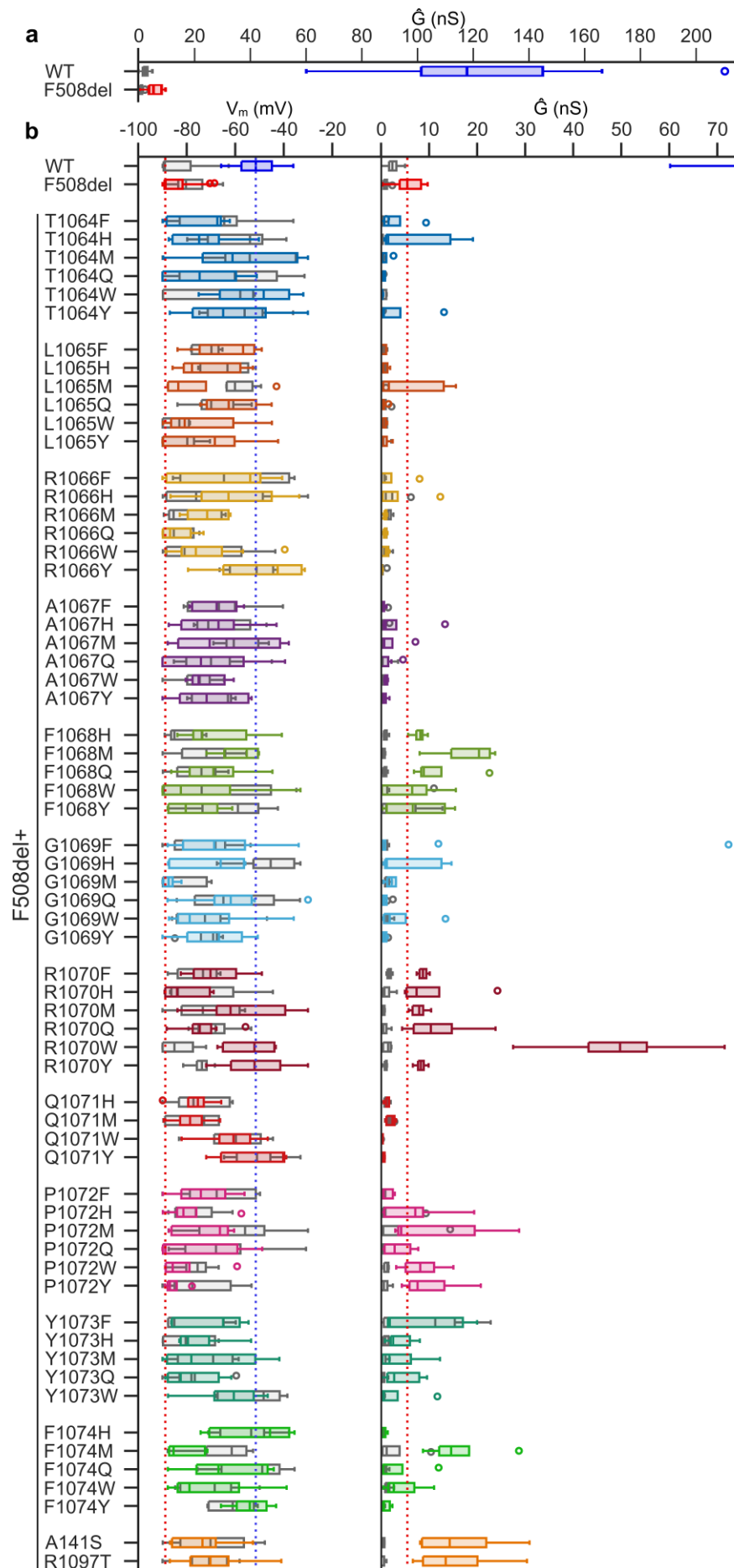


**Figure 25** Effect of second-site mutations in *cis* with F508del on CFTR conductance and membrane potential

Boxplots summarising  $\hat{G}$  (nS; **a** and **b**) and  $V_m$  (mV; **b**) estimates in HEK-293 cells expressing WT-CFTR, F508del-CFTR, or F508del-CFTR with second-site mutations. The grey boxes represent the measurements in the control (DMSO) conditions, while the coloured boxes represent the measurements after addition of 10  $\mu$ M forskolin. The dotted reference lines indicate the median  $V_m$  for WT (blue; -51.51 mV) and the median  $V_m$  and  $\hat{G}$  for F508del (red; -88.69 mV and 5.45 nS respectively), all after forskolin mediated steady state activation. WT  $\hat{G}$  (and F508del for comparison) was displayed on an axis with a large x-axis range in **a**.

### Effect of second-site mutations in *cis* with F508del

To investigate whether introduction of any of the introduced second-site mutations resulted in a change in F508del-CFTR channel function, we conducted Wilcoxon Rank Sum tests on the  $\hat{G}$  after addition of 10  $\mu\text{M}$  forskolin (**Table 10**, p. 140). More than half of the 63 tested second-site mutations significantly affected F508del-CFTR conductance. In particular, substitutions of T1064, L1065, R1066, A1067, G1069 and Q1071 severely perturbed F508del-CFTR: at least half of the substitutions at these sites significantly decreased  $\hat{G}$ . P1072F and F1074H/Y too, significantly decreased conductance.

While many mutations impacted F508del-CFTR channel function adversely, a few of them significantly rescued F508del-CFTR. R1070W ( $Mdn = 49.76$  nS,  $N = 5$ ), was particularly effective, increasing F508del-CFTR conductance significantly to nearly half of the value measured for WT-CFTR. Substitutions of arginine (R) at site 1070 with glutamine or phenylalanine (F) also significantly increased  $\hat{G}$ . Second to R1070W, the most successful revertant mutation was F1068M ( $Mdn = 20.39$  nS,  $N = 5$ ), followed by F1074M ( $Mdn = 14.58$  nS,  $N = 5$ ), A141S ( $Mdn = 14.29$  nS,  $N = 5$ ), R1097T ( $Mdn = 13.46$  nS,  $N = 5$ ), R1070Q ( $Mdn = 10.36$  nS,  $N = 10$ ), F1068Q ( $Mdn = 8.89$  nS,  $N = 5$ ) and R1070F ( $Mdn = 8.71$  nS,  $N = 5$ ) respectively.

### *Membrane potential*

#### DMSO controls

In the control condition, the mutants with the F508del-background had an estimated average  $V_m$  ranging between -45 and -90 mV ( $M = -69.87$  mV,  $SD = 10.60$ ,  $N = 64$ ; **Table 7**). Although a Kruskal-Wallis test indicated that there were genotype dependent differences in  $V_m$  after the addition of DMSO,  $\chi^2(63) = 108.79$ ,  $p = 0.0003$ , no significant differences were found when *post hoc* pairwise comparisons between the group mean ranks were performed.

#### forskolin vs. DMSO

Increased anion conductance through activation of CFTR will bring the membrane potential ( $V_m$  at steady-state CFTR activation and before addition of iodide), closer to the Nernst equilibrium for chloride and thus depolarise the membrane potential. To determine whether there was a significant

depolarisation of the membrane potential after activation of CFTR with forskolin, we conducted one-tailed Wilcoxon ranking tests (**Table 9**). The  $V_m$  estimate for WT-CFTR was significantly higher after addition of forskolin ( $Mdn = -51.51$  mV,  $N = 17$ ) compared to DMSO ( $Mdn = -88.99$  mV,  $N = 20$ ). Also for F508del/R1070W ( $Mdn = -52.07$  mV,  $N = 6$  vs.  $Mdn = -85.07$  mV,  $N = 5$ ), F508del/R1070Y ( $Mdn = -51.52$  mV,  $N = 6$  vs.  $Mdn = -73.72$  mV,  $N = 5$ ) and F508del/F1068M ( $Mdn = -55.26$  mV,  $N = 6$  vs.  $Mdn = -71.90$  mV,  $N = 5$ ) the membrane potential was significantly more depolarised after addition of forskolin compared to DMSO.

#### Effect of second-site mutations in *cis* with F508del

We conducted Wilcoxon Rank Sum tests on the  $V_m$  after addition of 10  $\mu$ M forskolin to examine whether any of the second-site mutations resulted in a change in F508del-CFTR membrane potential (**Table 10**). The majority of mutations significantly depolarised F508del-CFTR membrane potential at steady state activation of CFTR. Y1073 was the only mutation site that was not affected by any of the amino acid substitutions.

#### 5.2.5 Relating ion channel function and membrane proximity

To determine the  $p$  value at which there are no channels, or very few channels, on the membrane, mutants were selected with a very low average conductance ( $\hat{G} < 1$  nS) and a very low average  $p$  ( $\log_{10}p < -0.8$ ); see **Table 7**. The average  $p$  of these very impaired mutants (T1064M, R1066M, R1066Q, R1066W, R1066Y, R1067Y, Q1071W, Q1071Y) was 0.15. A restrained linear regression was performed on the  $G$ - $p$  measurements of WT-CFTR after basal activation with 10  $\mu$ M forskolin (blue solid circles, **Figure 26a**), forcing the regression through the x-axis intercept at  $p = 0.15$ . The conductance is expected to increase with the number of channels on the membrane in a roughly linear fashion; see **Figure 20**, p. 98 and Prins et al., 2020. Therefore, the regression line describes conductance as a function of membrane proximity, assuming the product of open probability ( $P_o$ ) and single channel conductance ( $\gamma$ ) is that of WT-CFTR after basal activation.

Data points falling above the line suggest a  $P_o \cdot \gamma$  that is higher than that of WT-CFTR. On the other hand, when data points fall below the line, channel activity is below what is expected for

WT-CFTR channels at that membrane proximity. In this way we can make better inferences about how second-site mutations affect gating and permeation characteristics of F508del-CFTR considering each mutant's characteristic  $p$  value. Conductance estimates ( $\hat{G}$ ) were plotted against membrane proximity ( $p$ ) for the mutants that, in *cis* with F508del, had amino acid substitutions at site F1068 (**Figure 26b**), R1070 (**Figure 26c**), F1074 (**Figure 26d**), or mutations A141S and R1097T (**Figure 26e**).

#### *F1068 substitutions*

Both F1068Q (green triangle) and F1068M (orange five-point star) significantly improve the conductance of F508del-CFTR (**Figure 26b**) but have different positions in the  $\hat{G}$ - $p$  plot (**Figure 26b**). While, relative to F508del, F508del/F1068Q has a similar position on the  $p$  axis, it has moved up on the  $\hat{G}$ -axis, suggesting that the increase in conductance is a result of an increase in channel gating and/or permeation rather than an increase of the number of channels on the membrane. On the other hand, F508del/F1068M has not only moved up on the  $\hat{G}$ -axis relative to F508del, but also has moved to the right on the  $p$ -axis, suggesting that part of the increase in  $\hat{G}$  is due to an increase in the number of channels on the membrane. Both F508del/F1068M and F508del/F1068Q fall on the regression line, suggesting that although F508del/F1068M is positioned higher on the  $\hat{G}$ -axis, both mutants have similar  $P_o \cdot \gamma$  characteristics, close to those measured for WT.

#### *R1070 substitutions*

F508del/R1070W (red circle) falls above the regression line, suggesting that it reaches a  $P_o \cdot \gamma$  level comparable to, or even slightly higher than, that of WT-CFTR (**Figure 26c**); consistent with published single-channel recordings (Liu et al., 2018). While the average F508del/R1070M (orange 5-point star), F508del/R1070Y (blue asterisk), F508del/R1070F (pink 6-point star) and F508del/R1070H (purple square) all have a roughly similar position on the  $\hat{G}$ -axis, F508del/R1070M and F508del/R1070Y are shifted to the right on the  $p$ -axis compared to F508del and their distance from the regression line has increased (**Figure 26c**). So R1070F and R1070H appear to rescue  $P_o \cdot \gamma$  of F508del-CFTR (only R1070F affects F508del-CFTR  $\hat{G}$  significantly; **Table 10**, p. 140), whereas R1070M and R1070Y only rescue biogenesis (only R1070M does so significantly; **Table 10**). R1070Q (green triangle) is shifted to the left

on the  $\rho$ -axis compared to F508del but shifted up on the  $\hat{G}$ -axis. So, despite a reduction in membrane proximity, whole cell conductance in cells expressing F508del/R1070Q-CFTR has increased. The mutant falls above the regression line, suggesting that R1070Q may rescue  $P_o \cdot \gamma$  to above WT level.

### F1074 substitutions

All substitutions at site F1074, except for methionine (M; orange 5-point star), decrease the position on the  $\hat{G}$ -axis as well as on the  $\rho$ -axis (**Figure 26d**). F508del/F1074M was one of the three mutants that significantly increased membrane proximity of F508del-CFTR. While the position of the mutant has

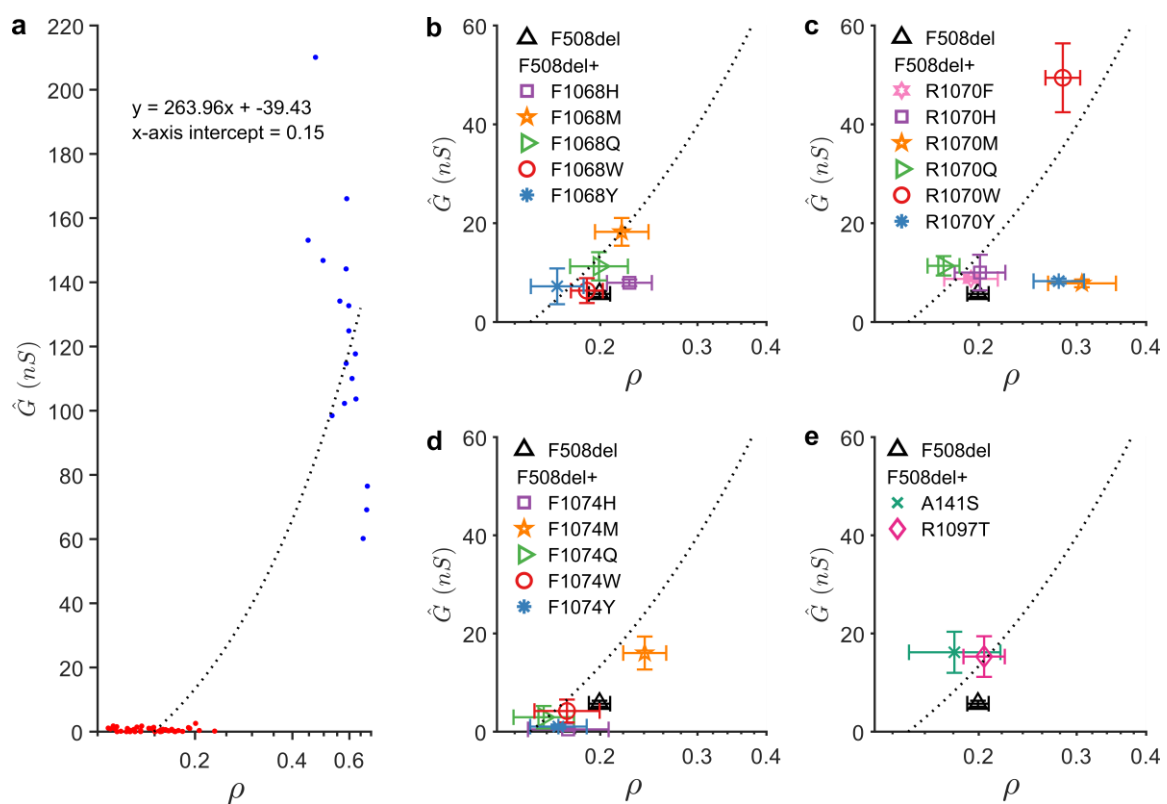


**Figure 26 Relationship between conductance and membrane proximity in genotypes with second-site mutations that alleviate F508del related impairments**

For every plate the  $\hat{G}$  estimates (in nS) were plotted as a function of membrane proximity ( $\rho$ ), obtained by back transformation of mean  $\log_{10}\rho$ . **a** The  $\hat{G}$ - $\rho$  pairs for WT-CFTR (red solid circles) and for mutants that had both a very low mean normalised conductance after addition of 10  $\mu$ M forskolin ( $G < 1$  nS) and a very low mean  $\rho$  ( $\log_{10}\rho < -0.80$ ) were selected (blue dots; T1064M, R1066M, R1066Q, R1066W, R1066Y, R1067Y, Q1071W, Q1071Y) and a restrained linear regression was performed on the WT data points forcing the regression through the average  $\rho$  of the very impaired mutants ( $\rho = 0.15$ ). The other panels show  $\hat{G}$ - $\rho$  pairs for F508del-CFTR with or without second site mutations at site F1068 (**b**), R1070 (**c**), and F1074 (**d**), or F508del/A141S-CFTR and F508del/R1097T-CFTR (**e**). Markers and error bars represent the mean  $G \pm$  SEM (y-axis) and back transformed mean  $\rho \pm$  upper and lower limits of the SEM (x-axis)

shifted on both axes, the distance from the regression line has stayed largely unchanged, suggesting that F1074M increases whole cell conductance primarily by increasing the number of channels on the membrane and not by increasing  $P_o$  and/or  $\gamma$  properties of the channel.

#### *A141S and R1097T*

A141S (green cross) and R1097T (pink diamond) move up on the  $\hat{G}$ -axis relative to F508del (**Figure 26e**), both significantly improving the conductance of F508del-CFTR (**Table 10**). Although they roughly have the same position on the  $\hat{G}$ -axis, F508del/A141S has shifted a bit to the left on the  $\rho$ -axis and falls above the regression line.

### 5.3 Discussion

We evaluated how mutations in *cis* with F508del affected the membrane proximity and channel function of F508del-CFTR. While many second-site mutations worsened F508del-CFTR membrane proximity and/or function, some mutations significantly improved defects associated with F508del. R1070W and F1074M were the only mutations that significantly increased membrane proximity as well as channel function. The only other mutation that significantly increased F508del-CFTR membrane proximity was R1070M. Mutations that significantly improved conductance but did not significantly affect membrane proximity were: F1068M/Q, R1070F/Q, A141S, and R1097T. While F508del-CFTR membrane potential after addition of forskolin appears to be particularly hyperpolarised, for most mutants membrane potential after addition of forskolin is significantly depolarised compared to F508del-CFTR, and only for WT, F508del/R1070W, F508del/R1070Y and F508del/F1068M, membrane potential after addition of forskolin was significantly depolarised compared to control.

#### 5.3.1 R1070Y

Although membrane proximity and conductance of F508del/R1070Y are not statistically different from F508del, the  $p$  values of the comparisons are very close to the critical values ( $q$ ) that are used to determine significance (**Table 10**). Considering the finding that R1070Y membrane potential is

significantly depolarised after forskolin compared to DMSO, an effect only observed in WT and two mutants with rescued F508del-CFTR function, it seems likely that the outcomes of the statistical tests on membrane proximity and conductance for this mutant are false negatives. While our results do not ubiquitously show that R1070Y rescues F508del-CFTR function, in this discussion we will leave the possibility open that R1070Y improves F508del-CFTR function.

### 5.3.2 Why is R1070W such an effective rescue mutation?

Although membrane proximity and/or function was modestly increased in several mutants, R1070W had by far the largest impact. In agreement with published results (Liu et al., 2018) and our measurements using the  $I^-$  first protocol (see 4. Validating the mCherry-YFPCFTR assay), the results reported in this chapter show that R1070W significantly increases membrane proximity and may rescue single channel activity to WT-levels or above. Substitutions of R1070 with other hydrophobic aromatic amino acids, phenylalanine (F) and tyrosine (Y) had a modest effect on F508del-CFTR function, but these substitutions could not rescue function to the same extent as tryptophan (W).

In **Figure 27**, a close-up of the ICL4-NBD1 interface in the cryo-EM structures of ATP-bound phosphorylated human CFTR (6MSM, **a**; Z. Zhang, Liu, & Chen, 2018) and dephosphorylated human CFTR (5UAK, **b**; F. Liu et al., 2017a) are shown with residues E504, F508, F1068, R1070, and F1074 highlighted. Interestingly, tryptophan is the only amino acid that has an indole ring with a nitrogen atom able to act as a hydrogen-bond donor. The indole nitrogen of tryptophan is positioned roughly at the same distance from the  $\alpha$ -carbon as one of the nitrogen atoms of the guanidino group in arginine. It could be that this nitrogen is important functionally.

One possibility is that the indole nitrogen acts as a donor for a hydrogen bond, possibly to a backbone carbonyl oxygen in the F508 loop in NBD1 (the backbone carbonyl of F508 is only 3.2 Å away in 6MSM) or to the  $\delta$ -Carbon in E504 (Hoffmann et al., 2018). In the F508del mutant the tryptophan might thus both provide an appropriately positioned hydrogen bond donor and fill the cavity left void at site F508 with an aromatic ring, capable of hydrophobic contacts. Furthermore, tryptophan is the bulkiest amino acid and therefore may have the potential to make most molecular contacts with the

NBD1 thereby restoring structural interactions at the ICL4-NBD1 interface better compared to the other bulky amino acids we tested.

### 5.3.3 Window for optimal ICL4-NBD1 interface flexibility

There is evidence suggesting that the ICL4-NBD1 interface might be highly dynamic (Sigoillot et al., 2019). Gating of CFTR is abolished when cysteines are cross-linked on either side of the ICL4-NBD1 interface, highlighting the importance of mobility that allows dynamic reconfiguration at the interface (Serohijos et al., 2008). The amount of F508del-CFTR rescue as a function of stabilisation of the ICL4-NBD1 interface might follow a steep bell-shaped curve with an optimal amount of face to face mobility required for successful rescue of CFTR conductance. Small deviations from this optimal amount of stabilisation, causing the interface to be too fixed or too mobile, may have a big effect on channel function. A small window of optimal flexibility for channel function might explain why none of the substitutions that we introduced in the ICL4 had a big effect on conductance.

Of all the mutations we introduced only three of them (1070W, R1070Y and R1070M) significantly increased F508del-CFTR membrane proximity. Although they all restore F508del-CFTR membrane proximity to similar levels, R1070W had a way larger effect on channel function (**Figure 26c**). As was pointed out by others (Rowe & Verkman, 2013), CFTR gating and biogenesis are expected to be interrelated processes that both depend on protein folding. Our results demonstrate that structural changes responsible for improving F508del-CFTR biogenesis do not necessarily contribute

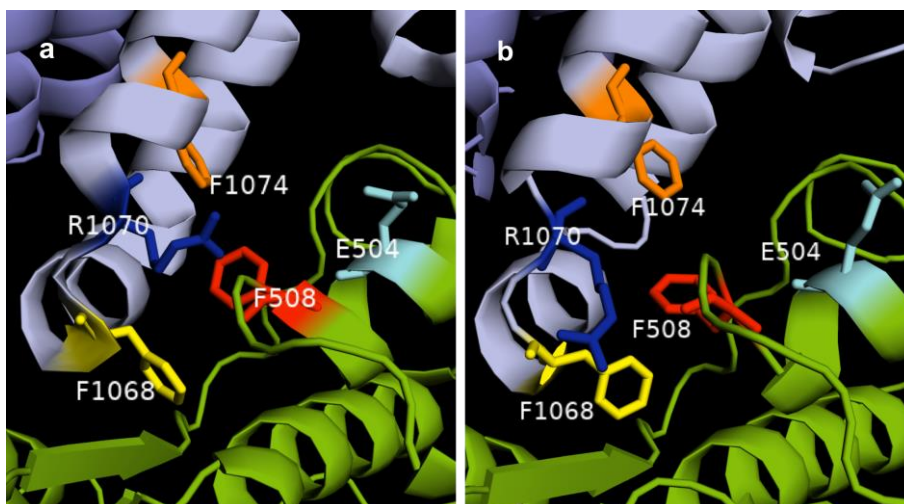


**Figure 27 ICL4-NBD1 interface**

A close-up of the ICL4-NBD1 interface in ATP-bound human CFTR, 6MSM (a) and in dephosphorylated human CFTR, 5UAK (b). with E504 (cyan), F508 (red), F1068 (yellow), R1070 (blue) and F1074 (orange) highlighted as sticks.

to channel function rescue to the extent that would be expected if F508del-CFTR function and biogenesis would be entirely correlated. Could it be that a tyrosine (Y) or methionine (M) at site R1070 increase the stability of the ICI4-NBD1 interface to an extent that decreases the folding defect of F508del-CFTR, thus increasing F508del-CFTR membrane proximity, but causes the interface to be too rigid for optimal gating/permeation?

It might be possible to further investigate this hypothesis experimentally. For example, with cysteine cross-linking experiments in Cys-less F508del-CFTR containing a V510C/G1069C Cys-pair. It has been shown that cross linking between V510C and G1069C in Cys-less WT-CFTR can be mediated by cross-linkers of varying lengths indicating flexibility in the positioning of these residues with respect to each other (Serohijos et al., 2008). Introduction of R1070W would be expected to allow cysteine cross linkers with spacer arms of different lengths to bind. However, if it is true that R1070Y and R1070M increase stability too much, decreasing flexibility necessary for proper channel gating, introduction of these mutations would only allow the shorter cysteine cross linkers to mediate V510C/G1069C cross linking.

A disadvantage of cysteine cross-linking is that the disulphide bonds can form between usually distant cysteine side chains during very rare and transient channel conformations. Because the disulphide bonds are irreversible in non-reducing conditions, the channel may get trapped in these transient conformations. An alternative approach is to use weaker cadmium ( $\text{Cd}^{2+}$ ) bridges. Two or more cysteines in close proximity can tightly bind metal ions such as  $\text{Cd}^{2+}$ . The metal bridges are reversible and their formation is strongly dependent on stable protein conformations instead of transient ones (Linsdell, 2015). When  $\text{Cd}^{2+}$  bridges form they stabilize the protein conformation and the affinity and impact of the  $\text{Cd}^{2+}$  bridges on CFTR gating can be measured in different conditions (see El Hiani & Linsdell, 2014).

### 5.3.4 Methionine substitutions at sites F1068 and F1074 partially rescue F508del-CFTR

Excluding R1070W, the most effective suppressor mutations are F1068M and F1074M. In a study on the permeation pathway of the Fluc-Ec2 ion channel, one of the critical phenylalanines could only be functionally replaced by methionine (Last et al., 2017). The authors argue that methionine's electron-withdrawing sulfur can be expected to produce a partial positive charge on the  $\gamma$ -methylene and terminal methyl groups, either of which could act as an electrostatic substitute for the weak positive charge on the edge of the aromatic ring of phenylalanine. Alternatively the sulfur atom itself might form relatively stable  $S/\pi$  interactions (particularly common in known protein structures, see Newberry & Raines, 2019). It is interesting that molecular dynamics simulations have suggested that an upward movement of the loop including F508 with respect to ICL4 might be important for stabilizing an open channel conformation. A network of interactions including a hydrogen bond between R1070 and E504 and several hydrophobic interactions locally stabilize this loop in simulations using WT-CFTR (Hoffmann et al., 2018). Alternative contacts between R1070W-E504, F1068M-R560, and F1074M-N505 might be important in stabilizing F508del-CFTR, carrying the revertant mutations.

### 5.3.5 F670del-Yor1p revertants

#### *A141S*

When F270S (Yor1p equivalent to A141S in CFTR) was introduced in G278R-Yor1p or I1084P-Yor1p (G278R (ICL1) and I1084P (ICL4) destabilise the ICL1-ICL4-NBD1 module), oligomycin resistance was increased as a result of partial restoration of folding and trafficking (Pagant et al., 2010). In contrast, introduction of F270S in F670del-Yor1p (the yeast equivalent to F508del-CFTR), resulted in little to no rescue of drug resistance. F670del/F270S-Yor1p had a proteolysis profile similar to F670del-Yor1p and remained poorly incorporated into COPII vesicles involved in trafficking proteins from the ER to the Golgi. Only when F270S was introduced together with another suppressor mutation, R1168M, there was rescue of drug resistance. F670del/F270S/R1168M-Yor1p showed increased resistance to proteolysis with trypsin and increased cooperation in COPII vesicles, indicating rescue of the

F670del-Yor1p folding and trafficking defects. Although F270S alone had no effect on F670del-Yor1p function, A141S was able to rescue function of F508del-CFTR without introduction of additional suppressor mutations. While the rescue of drug resistance by F270S in G278R-Yor1p and I1084P-Yor1p, and in F670del-Yor1p when introduced together with R1168M, was attributed to restoration of folding and biogenesis defects, our data shows that A141S increased F508del-CFTR conductance by rescuing the ion channel function rather than through effects on stability or trafficking of the protein (**Figure 26e**).

### *R1097T*

Introduction of R1116T in F670del-Yor1p results in an increased oligomycin resistance in yeast (Louie et al., 2012). Louie and colleagues (2012) show that while the biogenesis of the R1116T/F670del-Yor1p mutant appears to be identical to that of the F670del-Yor1p, R1116T increases F670del-Yor1p pump function in the rhodamine exclusion assay. These results indicate that instead of rescuing folding and ER export, R1116T increases pump function of the F670del-Yor1p, boosting the function of the little F670del-Yor1p that reaches the plasma membrane.

Recent studies have indicated that the transition from the outward facing state to inward facing state, is the rate limiting step in the transport cycles of ABC-transporters like the P-glycoprotein (Barsony et al., 2016), TmrAB (Hofmann et al., 2019), TM287/288 (Hutter et al., 2019), and MRP1 (Wang et al., 2020). If Yor1p has a similar kinetic profile, the boost in F670del-Yor1p pump function caused by R1116T likely reflects an increased transition rate from outward facing conformation to inward facing conformation. Interestingly, because CFTR is believed to adopt an inward-facing conformation in the closed and an outward-facing conformation in the open state, so in CFTR a faster transition from outward facing to inward facing would correspond to an increased closing rate.

In F508del-CFTR, the equivalent to R1116T in Yor1p, R1097T, significantly increased conductance ( $\hat{G}$ ) by affecting  $P_o$  and/or  $\gamma$  properties (**Figure 26e**). It is hard to see how modification of permeation properties or the substrate binding site can improve F670del-Yor1p pumping. R1116T possibly acts by speeding up the transition of the inward facing conformation to the outward

conformation which is the rate-limiting step in the pumping cycle of other ABC-transporters. However, a similar change in CFTR would increase the closing rate and result in a decreased  $P_o$  which is exactly the opposite of what our data suggests the effect of R1097T is. While both R1116T and R1097T appear to increase the activity of Yor1p and CFTR respectively, they likely do so through different mechanisms. Maybe this is not surprising since in the CFTR gating cycle seems to follow different kinetics than the transport cycle other ABC-proteins like MRP1 (Wang et al., 2020). For CFTR, the rate-limiting step for opening of the pore is the formation of the NBD-dimerized outward facing conformation (Vergani et al., 2003). Furthermore, while ATP hydrolysis is a rate-limiting step for the closure of CFTR (Baukrowitz et al., 1994; Carson et al., 1995; Gunderson & Kopito, 1994, 1995; Hwang et al., 1994; Zeltwanger et al., 1999), ATP hydrolysis appears to be a fast step in the outward facing state to inward facing state transition in ATP-transporters like TmrAB (Hofmann et al., 2019) and MRP1 (Wang et al., 2020). It is difficult to make inferences on the mechanism by which R1116T and R1097T affect pump and channel function respectively, especially since the rate-limiting step for the cycle might be different in mutants.

## 6. Conclusion

### 6.1 Assay development

Currently, only multi-assay approaches have been implemented for parallel assessment of channel function and membrane proximity. We developed and validated a new assay that allows rapid and simultaneous quantification of CFTR function as well as CFTR membrane proximity in live HEK-293 cells. Replication of well-characterized effects of the following experimental conditions: incubation at low temperature, treatment with VX-809 with and without VX-770, and addition of revertant mutation R1070W in *cis* with F508del, all manipulations resulted in the expected changes in measured F508del-CFTR function and membrane proximity. The assay successfully detects small changes in membrane density of CFTR, even when the heterogeneity among cells is large. For example, the effect of VX-809 on F508del-CFTR membrane density at 37 °C is small and often combined with temperature rescue or revertant mutations for easier detection, but our assay can pick up the minute difference in

average membrane proximity between untreated and VX-809 treated HEK-293 cells incubated at 37 °C. Moreover, membrane density measurements on a panel of rare cystic fibrosis causing mutations done in our group by Dr Emily Langron (Prins et al., 2020) correlate very well with published results (Sosnay et al., 2013; Van Goor et al., 2014). All these results validate our assay as a powerful tool for high-content CFTR screening. Furthermore, because CFTR is emerging as a potential target for other conditions too, e.g. COPD, polycystic kidney disease, diarrhoea, constipation, cardiogenic pulmonary oedema (de Hostos et al., 2011; Snyder et al., 2011; Solomon et al., 2017; Solymosi et al., 2013; Thiagarajah et al., 2015), the assay we developed could be used in drug discovery programmes beyond cystic fibrosis.

## 6.2 F508del-CFTR revertant mutations

Understanding why certain second-site mutations, like R1070W, are effective in improving F508del-CFTR biogenesis and function, could help us understand the basic defects that underlie cystic fibrosis for most patients, and help guide development of improved pharmacotherapy.

### 6.2.1 ICL4

Once the assay was validated, we used the method to search for revertant mutations in *cis* with F508del. Systematic scanning of the ICL4 validates R1070W (Thibodeau et al., 2010) as a particularly effective revertant; at 28 °C introduction of R1070W increased F508del-CFTR conductance approximately 9-fold and increased membrane proximity ~3-fold. Other substitutions at site R1070 resulted in significant rescue of F508del-CFTR membrane proximity and/or conductance too. Introduction of methionine (M) increased membrane proximity ~3-fold and resulted in a ~1.5-fold increase in conductance, and R1070F significantly increased conductance ~1.6-fold. Some mutations at F1068 also partially revert defects caused by F508del. F1068M and F1068Q increased F508del-CFTR conductance ~3.7-fold and ~1.6-fold respectively. Furthermore, although all other substitutions at site F1074 failed to rescue defects of F508del-CFTR, F1074M significantly increased F508del-CFTR conductance ~2.7-fold and membrane proximity ~2.5-fold

## 6.2.2 F670del-Yor1p revertants in F508del-CFTR

Deletion of F670 residue in CFTR yeast homologue Yor1p, causes defects equivalent to the F508del mutation in CFTR (Pagant et al., 2007). We tested equivalents of the F670del-Yor1p revertant mutations R1116T (Louie et al., 2012) and F270S (Pagant et al., 2010), A141S and R1097T respectively, in human CFTR. While F270S only was able to rescue of F670del-Yor1p when combined with another rescue mutation, we show that A141S on its own significantly rescues F508del-CFTR conductance. Furthermore, introduction of R1097T in *cis* with F508del, resulted in a significant increase of channel function.

## 6.3 Limitations of our study

### 6.3.1 Expression system

The effects of potentiators appears to be largely independent of the cell system used for testing (Pedemonte et al., 2010) and VX-770 is effective in diverse expression systems ranging from oocytes (e.g. Csanády & Töröcsik, 2019) to primary human bronchial epithelia (e.g. Raju et al., 2017). Corrector action on the other hand is often strongly affected by cell type, with in extreme cases correctors working in one cell type but being ineffective in another (Pedemonte et al., 2010). There are potential concerns for the use of any cell line as even immortalized cell lines derived from human bronchial epithelia (such as CFBE) are not always predictive of corrector activity in primary cultures (Phuan et al., 2014).

We chose to implement our assay in the HEK-293 heterologous expression system, even though this system has some limitations. The system does not recapitulate the epithelial environment in which CFTR is typically expressed and because HEK-293 do not form monolayers they cannot be used for studying transepithelial ion transport. Nevertheless, HEK-293 cells also offer clear advantages over more native cell lines, including the much greater ease of culture and manipulation. Furthermore, they are widely used in the study of both CFTR biogenesis and its function (e.g. Domingue et al., 2014 and references therein; Ehrhardt et al., 2016; Hildebrandt et al., 2015; Wang et al., 2016), providing a useful system for characterization of CFTR. Results using our assay, profiling membrane proximity and

conductance on CFTR with rare cystic fibrosis causing mutations (see 4.4.6 *Correlation results rare mutant panel with existing datasets* ), correlate well with published data obtained with FRT cell lines (Sosnay et al., 2013; Van Goor et al., 2014), further validating the HEK-293 heterologous expression system as a valuable tool for investigation of CFTR molecular characterisation and pharmacology.

### 6.3.2 Image acquisition system

In our assay, quantification of membrane proximity relies on an automated image acquisition and analysis protocols. However, our approach has some limitations. The image acquisition system we used (see 2.3.1 *ImageXpress*) is equipped with an widefield fluorescence microscope. The use of widefield optics results in stray light from out-of-focus planes reaching the photomultiplier, causing noise in the image. Confocal images have a better signal-to-noise ratio and would allow the location of the cell border and of the CFTR proteins to be estimated more accurately. Currently we have no access to a confocal microscope that allows automated fluid additions, but our group hopes to test the assay in this setting in the future. Despite the low-resolution optics that we used, our membrane proximity estimates correlate well with published data, which shows promise for further improvements in accuracy. One other drawback of our method is that the image acquisition system we rely on might be not readily available to many researchers, limiting the ability of our assay to be implemented in other research groups.

### 6.3.3 Inability to directly measure CFTR surface expression

Unlike our assay for CFTR membrane proximity, CFTR surface expression assays using extracellular tags that react to membrane impermeable molecules (see 1.5.2 *Biogenesis*) can differentiate between intracellular CFTR and membrane bound CFTR. While most of these CFTR surface expression assays only permit the amount of membrane bound CFTR to be quantified, Botelho and colleagues (2015) developed an assay that enables detection of the total amount of CFTR too. The inability of our assay to directly differentiate between these two groups of proteins is a clear limitation. Western blot technique is widely used for assessing CFTR biogenesis and allows interferences to be made about the capacity of the protein to escape the ER, by quantifying the post-translational modifications made in

the Golgi (see *Western blot*, p. 40). However, like our assay, this method neither directly assess the amount of CFTR that eventually reaches the cell membrane.

#### 6.3.4 Unwanted secondary mutations

Second-site mutations in *cis* with F508del were introduced using site-directed mutagenesis (see *Site directed mutagenesis*, p. 46). To confirm introduction of the desired mutations, we have sequenced the stretch of DNA containing the site of the mutation. Although the chance is low, it is possible that unwanted secondary mutations are introduced during the site-directed mutagenesis protocol. Unwanted secondary mutations in the CFTR gene could affect CFTR function and processing, but also unwanted secondary mutations in the IRES-containing bicistronic vector or the genes encoding YFP(H148Q/I152L) or mCherry, could affect the measurements of CFTR function, but especially membrane proximity. We actually suspect that an unwanted secondary mutation was introduced in one of our plasmids (containing F508del/Q1071F-CFTR, see 5.2.2 *mCherry fluorescence*).

In case further evaluation of some of the mutants investigated in this study is planned, it would be a good idea to introduce the mutation independently with different primers. In case particular results with a mutant in this study have been caused by an unwanted secondary mutation, the chance is extremely low that the same unwanted secondary mutation, or one with a similar effect, will be introduced again. Alternatively, the full plasmid could be sequenced and analysed to identify unexpected mutations.

### 6.4 Future directions

#### 6.4.1 Single cell analysis for CFTR function

The image analysis for membrane density readouts involves segmentation of images to calculate  $\rho$  for each individual cell. The image analysis for CFTR channel function on the other hand, involves cell selection by means of thresholding and estimates maximal rate of iodide influx or CFTR conductance averaging background-subtracted, within-cell fluorescence over each well. Combination of the two types of analysis to obtain CFTR channel function readouts for individual cells too, would make the assay more informative, allowing each cell's quenching time course to be normalised based on

mCherry expression in the specific cell. Single cell analysis for CFTR function can be achieved by modification of the image analysis scripts and the protocols used for image collection. The only drawback could be the additional computational time it would take to analyse the images. Currently the fitting of the data takes just over a minute for each well, requiring ~2 hours for the analysis of one plate in a typical experiment. But images of each well usually contain several hundreds of cells and implementation of single cell conductance analysis without changing the efficiency of the analysis process would mean that the analysis time of a typical experiment could increase to up to two weeks. Implementation of the single cell conductance analysis will require improving the efficiency of this process and/or use of specialist platforms for high throughput computing.

#### 6.4.2 R1070W rescue mechanism

Why does substitution of the arginine at site 1070 with a tryptophan rescue F508del-CFTR biogenesis and function, while substitution with other hydrophobic aromatic amino acids, such as phenylalanine and tyrosine have only a minor effect on F508del-CFTR function? To further investigate why R1070W is such a potent revertant, molecular dynamics simulations were set up by Dr Valentina Corradi (in the group of Professor Peter Tieleman, University of Calgary). Several homology models were generated, using the coordinates of structure 6MSM of phosphorylated, ATP-bound human CFTR (Zhang et al., 2018b) but replacing its NBD1 with that from structure 2PZF containing the F508del mutation (Atwell et al., 2010). Mutations were then generated at the R1070 position and simulations of F508del-CFTR, F508del/R1070F-CFTR and F508del/R1070W-CFTR were run for 2  $\mu$ s, each system embedded in a phospholipid bilayer.

Preliminary analyses suggest that the ICL4 in F508del/R1070W-CFTR moves closer to the NBD1 Q-loop (which includes the  $\gamma$ -phosphate sensing glutamine, Q493; Urbatsch, Gimi, Wilke-Mounts, & Senior, 2000) compared to the F508del-CFTR and F508del/R1070F-CFTR systems. It has been shown that the Q-loops of CFTR NBD1 and NBD2 form contacts with ICL4 and ICL2, respectively (He et al., 2008) and Q493 is thought to play a role in coupling ATP binding and hydrolysis to channel opening (Berger et al., 2002).

Interestingly, a recent molecular dynamics study, using models of the full WT protein embedded in a lipid bilayer, shows an upward movement of the NBD1 segment containing the Q-loop, is characteristic for the open, outward-facing conformation of the CFTR channel (Hoffmann et al., 2018). The authors draw parallels with ABC importers like MJ1267, in which a movement of the  $\alpha$ -helical NBD subdomain causes a loss of the molecular contacts between the ADP molecule and the glutamine of the Q loop, likely facilitating ADP release after hydrolysis (Karpowich et al., 2001). Comparison of the ADP-bound structure of MJ1267 to the ATP-bound structure of HisP (Hung et al., 1998), suggests that ATP binding locks the  $\alpha$ -helical NBD subdomain in close proximity to the active site. Results of an NMR study investigating the conformational dynamics of MJ1267, suggest that the Q loop is highly flexible in both apo and ADP bound proteins (Wang et al., 2004). The authors hypothesise that loss of flexibility of key motifs, like the Q loop, upon ATP binding as a result of the interaction between the  $\gamma$ -phosphate and the ATP molecule, may be crucial for mechanochemical energy transduction in ABC transporters.

The Q loop is highly conserved among ABC proteins (Locher, 2016), and transitions between flexibility and rigidity of the Q-loop may be an important aspect of CFTR function too. A molecular dynamics study found that F508del destabilizes NBD1 residues 492–499 containing the Q-loop, causing this segment to dissociate from the rest of the domain (Wieczorek & Zielenkiewicz, 2008). Could it be that R1070W but not R1070F decreases the destabilisation of the Q-loop caused by the deletion of F508 and thereby promote channel function? In the molecular dynamics study by Wieczorek and Zielenkiewicz (2008) the simulations were performed in submerged in TIP4P water molecules using structures of isolated NBD domains. The situation is likely very different in a full-length protein embedded in the membrane. A more detailed analysis of the simulation data and possibly cross-linking experiments involving Q493 and R1070, R1070W or R1070F, could provide us with mechanistic insights about F508del-CFTR rescue by R1070W.

## Supplementary information

**Table 2 Assay validation: Statistical test results  $\log_{10}\rho$**

Paired sample t-tests comparing the  $\log_{10}\rho$  of F508del-CFTR or F508del/R1070W-CFTR after a variety of chronic incubation conditions. An independent t-test was performed to assess the significance of the difference in  $\log_{10}\rho$  of WT-CFTR and F508del-CFTR at 37 °C and 28 °C. P-values were Bonferroni adjusted to account for multiple comparisons.

		M	SD	SD for the MD	df	T	P	Adjusted P
37 °C	F508del	-0.59	0.05	0.02	6	-4.64	3.56E-03	0.01
	F508del + VX-809	-0.55	0.06					
	F508del + VX-809	-0.59	0.07	0.02	5	4.22	8.34E-03	0.02
	F508del + VX-809 + VX-770 (c)	-0.63	0.06					
	F508del	-0.58	0.07	0.02	7	-5.78	6.70E-04	2.01E-03
	F508del/R1070W	-0.53	0.08					
28 °C	F508del	-0.51	0.09	0.04	6	-12.23	2.00E-05	6.00E-05
	F508del + VX-809	-0.31	0.07					
	F508del + VX-809	-0.34	0.08	0.20	10	4.06	2.27E-03	4.54E-03
	F508del + VX-809 + VX-770 (c)	-0.50	0.09					
	F508del	-0.54	0.07	0.13	6	-4.73	3.22E-03	0.01
	F508del/R1070W	-0.40	0.10					
temperature correction	37 °C (WT - F508del)	0.54	0.08	NA	44	5.59	1.35E-06	4.05E-06
	28 °C (WT - F508del)	0.41	0.08					

**Table 3 Assay validation:  $d[I^-]/dt$  in the control condition**

Maximal rate of  $I^-$  entry after addition of DMSO (control). HEK-293 cells expressed WT-CFTR, F508del-CFTR with or without 24-h VX-809 (10  $\mu$ M) incubation or F508del/R1070W-CFTR.

	N	M	SD
F508del 28 °C	10	0.0075	0.0063
F508del 37 °C	12	0.0079	0.0033
F508del + VX-809 28 °C	6	0.0065	0.0039
F508del + VX-809 37 °C	6	0.0131	0.0038
F508del/R1070W 28 °C	4	0.0149	0.0142
F508del/R1070W 37 °C	7	0.0136	0.0093
WT 28 °C	9	0.0089	0.0045
WT 37 °C	12	0.0096	0.0024

**Table 4 Assay validation: statistical test results  $d[I^-]/dt$  (Forskolin vs. DMSO)**

Independent t-tests comparing the maximal rate of  $I^-$  entry after addition of 10  $\mu$ M forskolin vs. after DMSO (control). Cells were transfected with WT-CFTR, F508del-CFTR, or F508del/R1070W-CFTR and incubated at either 37 °C or 28 °C, with or without 10  $\mu$ M VX-809, 24 hours before imaging. In some conditions the potentiator VX-770 (10  $\mu$ M) was added acutely together with forskolin.

		VX-809	VX-770 (a)		M	SD	df	T	P
WT	37 °C	-	-	Forskolin	0.180	0.059	16	8.65	1.99E-07
				DMSO	0.010	0.003			
		-	+	Forskolin	0.214	0.056	4	6.36	3.13E-03
				DMSO	0.008	0.003			
	28 °C	-	-	Forskolin	0.137	0.023	10	13.18	1.20E-07
				DMSO	0.010	0.005			
		-	+	Forskolin	0.214	0.056	5	6.36	3.13E-03
				DMSO	0.008	0.003			
F508del	37 °C	-	-	Forskolin	0.009	0.005	15	0.71	0.49
				DMSO	0.007	0.004			
		-	+	Forskolin	0.014	0.007	4	1.50	0.21
				DMSO	0.007	0.002			
	+	+	Forskolin	0.034	0.008	9	5.72	2.87E-04	
			DMSO	0.013	0.004				
	28 °C	-	-	Forskolin	0.012	0.009	10	0.00	1.00
				DMSO	0.012	0.014			
		-	+	Forskolin	0.059	0.042	5	2.71	0.04
				DMSO	0.004	0.001			
+		+	Forskolin	0.124	0.039	9	6.67	9.12E-05	
			DMSO	0.007	0.004				
F508del/ R1070W	37 °C	-	-	Forskolin	0.044	0.026	12	2.87	0.01
				DMSO	0.014	0.010			
	28 °C	-	-	Forskolin	0.090	0.032	6	4.38	4.68E-03
				DMSO	0.015	0.014			

**Table 5 Assay validation: statistical test results  $d[I^-]/dt$  after addition of forskolin**

Independent t-tests comparing the maximal rate of  $I^-$  entry after addition of 10  $\mu$ M forskolin in varying conditions.

	<b>M</b>	<b>SD</b>	<b>df</b>	<b>T</b>	<b>P</b>	<b>adjusted P</b>
WT 37 °C	0.180	0.059	10	0.88	0.40	0.80
WT + VX-770 (a) 37 °C	0.214	0.056				
WT 28 °C	0.137	0.023	8	2.71	0.03	0.05
WT + VX-770 (a) 28 °C	0.207	0.058				
WT 37 °C	0.180	0.059	13	1.70	0.11	0.22
WT 28 °C	0.137	0.023				
WT + VX-770 (a) 37 °C	0.214	0.056	5	0.17	0.87	1.00
WT + VX-770 (a) 28 °C	0.207	0.058				
F508del + VX-770 (a) 37 °C	0.014	0.007	6	3.52	0.01	0.02
F508del + VX-770 (a) + VX-809 37 °C	0.034	0.008				
F508del + VX-770 (a) 28 °C	0.059	0.042	7	2.34	0.05	0.10
F508del + VX-770 (a) + VX-809 28 °C	0.124	0.039				
F508del + VX-770 (a) + VX-809 37 °C	0.034	0.008	9	5.06	6.77E-04	1.35E-03
F508del + VX-770 (a) + VX-809 28 °C	0.124	0.039				
F508del 37 °C	0.009	0.005	13	-3.70	2.69E-03	0.01
F508del/R1070W 37 °C	0.044	0.026				
F508del/R1070W 37 °C	0.044	0.026	9	-2.62	0.03	0.06
F508del/R1070W 28 °C	0.090	0.032				

**Table 6 Descriptive statistics: normalised mCherry fluorescence intensity**

On every plate the mean mCherry fluorescence intensity for each genotype was determined for measurements obtained in the quenching protocol and the membrane proximity protocol.

	quenching				membrane proximity			
	N	M	Mdn	SD	N	M	Mdn	SD
WT	20	1.00	1.00	0.00	23	1.33	1.25	0.19
F508del	19	0.98	1.02	0.18	22	1.35	1.28	0.38
F508del + T1064F	6	0.83	0.76	0.32	6	1.24	1.22	0.59
F508del + T1064H	5	1.09	1.01	0.21	6	1.21	1.33	0.25
F508del + T1064M	5	1.05	1.08	0.39	6	1.12	1.16	0.48
F508del + T1064Q	7	0.94	0.92	0.18	8	1.15	1.19	0.35
F508del + T1064W	5	0.96	1.01	0.21	6	1.15	1.28	0.34
F508del + T1064Y	5	1.03	0.99	0.19	6	1.32	1.22	0.48
F508del + L1065F	5	0.87	0.91	0.24	6	1.03	1.07	0.46
F508del + L1065H	5	0.83	0.87	0.29	6	1.02	1.05	0.45
F508del + L1065M	5	0.91	0.80	0.26	6	1.09	0.94	0.48
F508del + L1065Q	5	0.77	0.81	0.28	6	1.00	1.09	0.41
F508del + L1065W	5	0.84	0.93	0.18	6	1.22	1.24	0.46
F508del + L1065Y	10	0.83	0.90	0.23	11	0.94	0.95	0.30
F508del + R1066F	6	0.91	0.88	0.32	6	0.95	0.89	0.41
F508del + R1066H	5	1.06	1.04	0.42	6	1.08	1.07	0.45
F508del + R1066M	5	0.82	0.77	0.20	6	1.24	1.15	0.47
F508del + R1066Q	5	0.99	1.04	0.22	6	1.34	1.31	0.48
F508del + R1066W	9	0.87	0.98	0.48	11	1.13	0.95	0.70
F508del + R1066Y	5	0.81	0.67	0.28	6	1.01	0.96	0.37
F508del + A1067F	6	1.05	1.12	0.24	7	1.23	1.42	0.35
F508del + A1067H	6	0.92	0.93	0.25	7	1.10	1.24	0.41
F508del + A1067M	5	1.21	1.34	0.30	7	1.44	1.41	0.63
F508del + A1067Q	10	0.48	0.42	0.20	11	0.77	0.62	0.59
F508del + A1067W	5	0.93	0.97	0.18	6	1.13	1.28	0.29
F508del + A1067Y	5	1.00	1.09	0.17	6	1.25	1.34	0.35
F508del + F1068H	5	0.99	0.99	0.08	6	1.46	1.39	0.45
F508del + F1068M	5	1.00	1.02	0.08	6	1.41	1.30	0.50
F508del + F1068Q	5	0.99	0.94	0.09	6	1.43	1.30	0.49
F508del + F1068W	7	0.99	0.99	0.22	8	1.13	1.20	0.31
F508del + F1068Y	4	1.00	0.91	0.20	6	1.11	1.11	0.33
F508del + G1069F	10	0.73	0.76	0.45	10	1.11	0.91	0.90
F508del + G1069H	5	1.10	1.16	0.15	6	1.42	1.30	0.45
F508del + G1069M	5	0.89	0.88	0.10	6	1.37	1.26	0.42
F508del + G1069Q	10	0.95	0.90	0.36	11	1.07	0.96	0.46
F508del + G1069W	5	1.07	1.06	0.12	6	1.70	1.53	0.75
F508del + G1069Y	5	0.72	0.80	0.33	5	1.46	0.91	1.24
F508del + R1070F	5	0.92	0.94	0.06	6	1.35	1.18	0.49
F508del + R1070H	5	0.78	0.94	0.31	6	1.22	1.07	0.70
F508del + R1070M	5	1.06	1.00	0.12	6	1.47	1.53	0.41
F508del + R1070Q	11	0.87	0.92	0.48	11	1.29	1.08	0.96
F508del + R1070W	5	0.87	0.85	0.06	6	1.27	1.15	0.43
F508del + R1070Y	5	0.93	0.95	0.08	6	1.53	1.48	0.59
F508del + Q1071F	11	0.32	0.30	0.05	12	0.55	0.48	0.41
F508del + Q1071H	5	0.77	0.87	0.22	6	1.14	1.24	0.44
F508del + Q1071M	5	0.92	0.90	0.23	6	1.64	1.51	0.93
F508del + Q1071W	5	1.09	1.07	0.15	6	1.43	1.34	0.52
F508del + Q1071Y	5	1.00	0.97	0.16	6	1.37	1.25	0.57
F508del + P1072F	5	0.83	0.90	0.24	6	1.18	1.26	0.50
F508del + P1072H	6	0.98	1.04	0.33	7	1.52	1.31	0.86
F508del + P1072M	5	0.73	0.80	0.19	6	1.41	0.98	1.35
F508del + P1072Q	7	0.94	1.05	0.25	8	1.13	1.17	0.42
F508del + P1072W	5	0.81	0.82	0.14	6	1.43	1.28	0.91
F508del + P1072Y	5	0.73	0.88	0.32	6	1.34	1.00	1.06
F508del + Y1073F	5	1.03	1.03	0.07	6	1.51	1.24	0.89
F508del + Y1073H	5	1.01	0.99	0.12	6	1.69	1.61	0.53
F508del + Y1073M	5	1.13	1.04	0.23	6	1.74	1.79	0.48
F508del + Y1073Q	7	0.96	0.95	0.26	8	1.44	1.43	0.65
F508del + Y1073W	5	0.87	0.97	0.22	6	1.19	1.12	0.59
F508del + F1074H	5	1.15	1.18	0.27	6	2.05	1.84	0.80
F508del + F1074M	5	1.08	1.02	0.17	6	1.51	1.39	0.45
F508del + F1074Q	5	1.03	0.96	0.10	6	1.66	1.57	0.42
F508del + F1074W	5	0.92	0.95	0.12	6	1.73	1.43	0.79
F508del + F1074Y	5	1.08	1.03	0.23	6	1.93	1.61	0.91
F508del + A141S	5	0.71	0.82	0.20	6	1.12	0.94	0.70

**Table 7** Descriptive statistics: assay readouts for WT-CFTR and F508del-CFTR with and without second-site mutations

	Membrane proximity				After addition of FSK						After addition of DMSO							
	$(\log_{10}p)$				$\hat{G}$ (nS)				$V_m$ (mV)		$\hat{G}$ (nS)				$V_m$ (mV)			
	N	M	Mdn	SD	N	M	Mdn	SD	M	Mdn	SD	N	M	Mdn	SD	M	Mdn	SD
WT	23	-0.22	-0.21	0.05	17	121.45	117.70	37.27	-51.74	-51.51	7.75	20	2.46	2.35	1.38	-84.06	-88.99	8.59
F508del	22	-0.72	-0.70	0.09	18	5.70	5.45	2.57	-84.41	-88.69	7.63	19	0.86	0.88	0.61	-78.61	-80.31	7.86
F508del +																		
T1064F	6	-0.84	-0.87	0.11	5	2.79	1.55	3.76	-74.88	-67.38	12.90	6	0.29	0.16	0.41	-66.23	-64.54	19.01
T1064H	6	-0.74	-0.72	0.10	5	7.05	1.48	8.47	-74.03	-74.88	14.81	5	0.23	0.20	0.29	-58.65	-53.93	15.79
T1064M	6	-0.80	-0.80	0.07	5	0.75	0.25	1.04	-56.93	-61.11	24.40	5	0.36	0.40	0.25	-53.22	-54.01	23.27
T1064Q	8	-0.69	-0.73	0.19	6	0.46	0.51	0.38	-73.36	-74.68	16.55	7	0.10	0.00	0.20	-60.52	-60.15	22.74
T1064W	6	-0.80	-0.78	0.09	5	0.18	0.14	0.17	-51.68	-48.27	17.53	5	0.53	0.43	0.56	-68.47	-57.93	19.64
T1064Y	6	-0.78	-0.76	0.13	5	3.04	0.57	5.63	-61.93	-64.97	21.71	5	0.08	0.00	0.17	-58.03	-56.13	15.31
L1065F	6	-0.74	-0.73	0.09	5	0.44	0.00	0.60	-62.88	-56.75	14.47	5	0.54	0.56	0.51	-71.72	-69.82	5.99
L1065H	6	-0.77	-0.74	0.09	5	0.77	0.43	0.73	-71.14	-77.83	14.19	5	0.60	0.60	0.43	-63.95	-63.20	10.64
L1065M	6	-0.64	-0.61	0.11	5	6.04	1.62	7.28	-76.74	-83.48	19.05	5	0.20	0.00	0.45	-58.13	-60.10	6.26
L1065Q	6	-0.76	-0.73	0.11	5	0.40	0.17	0.65	-61.27	-62.68	12.15	5	0.69	0.46	0.85	-68.16	-69.92	11.20
L1065W	6	-0.81	-0.83	0.10	5	0.60	0.36	0.46	-73.38	-80.84	18.25	5	0.91	1.04	0.37	-84.15	-83.02	5.53
L1065Y	11	-0.77	-0.75	0.09	10	0.76	0.36	0.78	-69.75	-68.40	17.06	10	0.71	0.45	0.64	-81.71	-79.77	7.60
R1066F	6	-0.75	-0.76	0.10	5	1.64	0.00	3.56	-64.99	-53.84	22.47	6	0.32	0.10	0.44	-61.83	-64.65	21.70
R1066H	6	-0.76	-0.76	0.04	5	2.63	0.32	5.42	-60.28	-62.77	20.22	5	1.66	0.97	2.59	-67.75	-76.12	25.28
R1066M	6	-0.84	-0.84	0.07	5	0.86	0.99	0.49	-71.59	-71.57	9.23	5	1.46	1.48	0.93	-78.31	-85.41	12.21
R1066Q	6	-0.83	-0.83	0.08	5	0.84	0.87	0.38	-83.96	-86.85	7.29	5	0.92	1.04	0.31	-83.55	-85.32	6.88
R1066W	11	-0.85	-0.89	0.17	9	0.85	1.00	0.69	-71.64	-76.23	15.47	9	0.85	0.66	0.87	-74.92	-80.91	17.46
R1066Y	6	-0.80	-0.78	0.06	5	0.11	0.05	0.15	-49.29	-42.53	20.36	5	0.25	0.00	0.53	-53.18	-51.20	10.24
A1067F	7	-0.74	-0.75	0.09	6	0.37	0.21	0.44	-67.98	-67.67	9.96	6	0.53	0.42	0.49	-65.78	-66.72	15.43
A1067H	7	-0.75	-0.73	0.09	6	3.15	0.96	5.10	-67.84	-66.91	16.00	6	0.46	0.27	0.64	-65.98	-71.13	12.44
A1067M	7	-0.82	-0.80	0.11	5	1.75	0.66	3.04	-64.22	-70.55	22.76	5	0.18	0.17	0.19	-57.89	-60.61	8.94
A1067Q	11	-0.71	-0.74	0.12	10	0.92	0.00	1.50	-70.67	-74.14	17.81	10	0.99	0.32	1.27	-69.66	-69.99	12.28
A1067W	6	-0.80	-0.82	0.07	5	1.06	1.18	0.34	-71.69	-75.10	8.24	5	0.45	0.50	0.34	-75.63	-74.61	9.19
A1067Y	6	-0.81	-0.82	0.10	5	0.63	0.50	0.69	-70.10	-71.79	15.95	5	0.35	0.29	0.16	-68.46	-63.01	9.32
F1068H	6	-0.68	-0.66	0.10	5	7.94	8.18	1.48	-66.73	-73.57	16.77	5	0.92	0.76	0.46	-81.21	-85.08	7.56
F1068M	6	-0.70	-0.65	0.12	5	18.25	20.39	6.28	-58.02	-55.26	9.07	5	0.48	0.48	0.35	-72.71	-71.90	12.94
F1068Q	6	-0.74	-0.70	0.13	5	11.27	8.89	6.38	-68.50	-69.00	15.44	5	0.79	0.71	0.44	-75.69	-73.92	10.51
F1068W	8	-0.76	-0.75	0.09	6	6.36	6.47	6.15	-73.34	-82.41	22.42	7	1.83	0.01	4.09	-67.94	-73.85	23.55
F1068Y	6	-0.83	-0.82	0.12	4	7.22	6.62	7.24	-77.46	-80.39	12.71	4	3.72	1.05	6.08	-61.99	-58.89	18.87
G1069F	10	-0.88	-0.89	0.09	10	8.63	0.33	22.69	-66.90	-68.68	16.98	10	0.63	0.49	0.66	-72.16	-68.15	12.32
G1069H	6	-0.74	-0.78	0.16	5	5.84	1.20	6.86	-70.64	-66.00	15.81	5	0.02	0.00	0.03	-46.01	-45.38	13.45
G1069M	6	-0.81	-0.85	0.11	5	2.09	2.21	1.09	-87.21	-87.47	3.09	5	1.26	1.30	0.72	-82.34	-89.75	10.32
G1069Q	11	-0.73	-0.74	0.15	10	0.62	0.64	0.45	-60.81	-61.86	14.84	10	0.54	0.33	0.76	-61.45	-64.88	18.14
G1069W	6	-0.86	-0.87	0.12	5	3.69	1.79	5.50	-71.16	-78.77	20.55	5	1.26	1.17	0.89	-72.28	-72.49	15.47
G1069Y	5	-0.74	-0.76	0.08	4	0.67	0.62	0.61	-68.51	-66.67	16.36	5	0.58	0.47	0.54	-71.60	-69.11	7.69
R1070F	6	-0.74	-0.76	0.10	5	8.73	8.71	1.02	-68.03	-70.21	12.76	5	1.68	1.57	0.50	-75.56	-73.29	9.30
R1070H	6	-0.73	-0.74	0.11	5	10.01	7.39	8.06	-80.35	-83.96	9.74	5	1.15	0.70	1.25	-73.47	-83.64	18.28
R1070M	6	-0.56	-0.56	0.14	5	7.83	7.93	1.75	-56.11	-61.95	20.66	5	0.42	0.41	0.33	-71.55	-73.34	14.22
R1070Q	11	-0.78	-0.75	0.10	10	11.37	10.36	6.19	-73.72	-74.61	8.41	11	0.78	0.46	0.73	-69.09	-68.11	7.80
R1070W	6	-0.57	-0.57	0.07	5	49.42	49.76	15.58	-54.21	-52.07	11.21	5	1.23	1.47	0.93	-83.25	-85.07	7.68
R1070Y	6	-0.60	-0.58	0.12	5	8.27	8.27	1.17	-51.52	-52.03	15.57	5	0.93	1.06	0.40	-74.08	-73.72	4.70
Q1071H	6	-0.81	-0.82	0.06	5	1.34	1.64	0.49	-76.46	-75.39	8.63	5	1.12	1.17	0.74	-74.38	-77.23	12.35
Q1071M	6	-0.82	-0.82	0.13	5	2.05	2.36	0.97	-78.21	-78.61	8.34	5	1.66	1.57	0.70	-76.91	-72.85	11.46
Q1071W	6	-0.83	-0.80	0.12	5	0.22	0.35	0.19	-61.41	-60.72	12.99	5	0.29	0.33	0.16	-60.47	-59.73	14.77
Q1071Y	6	-0.80	-0.79	0.06	5	0.40	0.35	0.35	-51.01	-40.23	15.69	5	0.17	0.00	0.25	-51.20	-51.02	11.74
P1072F	6	-0.77	-0.74	0.11	5	1.24	0.53	1.26	-73.33	-74.17	12.77	5	0.46	0.56	0.44	-66.88	-67.65	16.67
P1072H	7	-0.79	-0.87	0.18	6	7.17	7.12	7.06	-78.34	-81.35	11.17	6	1.97	0.63	3.62	-75.93	-76.27	9.82
P1072M	6	-0.80	-0.78	0.11	5	11.21	4.20	11.27	-72.78	-66.30	12.83	5	3.16	0.45	6.28	-59.59	-55.95	21.31
P1072Q	8	-0.70	-0.66	0.10	7	3.53	2.82	3.03	-75.37	-88.77	18.12	7	0.27	0.29	0.28	-66.97	-67.93	19.30
P1072W	6	-0.87	-0.88	0.11	5	8.36	8.15	4.49	-81.58	-85.79	12.60	5	1.12	1.31	0.49	-76.44	-75.51	7.89
P1072Y	6	-0.77	-0.77	0.16	5	9.95	7.60	6.46	-85.49	-86.91	4.40	5	0.81	0.57	1.00	-73.83	-77.71	14.76
Y1073F	6	-0.82	-0.85	0.17	5	8.13	1.81	9.13	-70.26	-65.00	15.02	5	9.54	11.3	9.47	-77.35	-85.11	13.22
Y1073H	6	-0.70	-0.68	0.13	5	3.82	2.51	2.88	-74.97	-79.50	12.30	5	0.95	0.89	0.71	-79.13	-80.40	11.05
Y1073M	6	-0.74	-0.71	0.10	5	3.70	1.72	5.06	-70.47	-78.09	21.15	5	0.49	0.01	0.78	-72.22	-69.10	13.27
Y1073Q	8	-0.76	-0.74	0.12	7	4.27	2.72	3.82	-77.80	-82.48	11.57	6	0.53	0.49	0.56	-77.56	-78.06	10.11
Y1073W	6	-0.75	-0.73	0.14	5	2.66	0.58	5.07	-62.28	-60.58	15.48	5	0.35	0.33	0.36	-52.90	-48.30	13.77
F1074H	6	-0.80	-0.77	0.16	5	0.46	0.19	0.60	-52.69	-45.66	17.99	5	0.30	0.23	0.26	-55.67	-53.42	12.81
F1074M	6	-0.60	-0.61	0.10	5	16.02	14.58	7.50	-80.86	-85.43	8.01	5	2.72	1.16	4.34	-64.94	-61.44	13.83
F1074Q	6	-0.82	-0.81	0.11	5	2.94	0.40	5.11	-63.67	-66.92	18.06	5	0.76	0.78	0.65	-53.		

**Table 8 Paired t-tests comparing log<sub>10</sub>p of F508del without vs. with second-site mutations**

The Benjamini-Hochberg procedure with a false discovery rate of 10 % was applied to control for the family wise error rate. Arrows indicate the mutants for which the mean log<sub>10</sub>p was higher than the mean log<sub>10</sub>p of F508del-CFTR. P-values below the critical value (Q) are considered significant.

	Difference		↑	Test statistics			
	M	SD		T	df	P	Q
F508del + Q1071H	-0.13	0.05		6.44	5	0.001	0.002
F508del + R1066M	-0.15	0.06		5.81	5	0.002	0.003
F508del + F1068Y	-0.14	0.06		5.79	5	0.002	0.005
F508del + A1067F	-0.06	0.03		4.86	6	0.003	0.006
F508del + R1066Y	-0.11	0.05		5.26	5	0.003	0.008
F508del + G1069F	-0.15	0.12		3.94	9	0.003	0.010
F508del + R1066Q	-0.14	0.07		5.05	5	0.004	0.011
F508del + A1067Y	-0.12	0.06		5.04	5	0.004	0.013
F508del + P1072W	-0.20	0.10		4.84	5	0.005	0.014
F508del + A1067M	-0.09	0.05		4.34	6	0.005	0.016
F508del + T1064W	-0.11	0.06		4.56	5	0.006	0.017
F508del + R1066H	-0.10	0.06		4.37	5	0.007	0.019
F508del + R1070W	0.15	0.09	↑	-4.26	5	0.008	0.021
F508del + Q1071Y	-0.09	0.05		4.21	5	0.008	0.022
F508del + T1064M	-0.15	0.09		3.97	5	0.011	0.024
F508del + F1074Q	-0.09	0.05		4.11	4	0.015	0.025
F508del + L1065W	-0.12	0.08		3.55	5	0.016	0.027
F508del + F1074M	0.15	0.08	↑	-3.98	4	0.016	0.029
F508del + L1065Y	-0.06	0.07		2.87	10	0.017	0.030
F508del + A1067H	-0.07	0.06		3.22	6	0.018	0.032
F508del + L1065F	-0.07	0.05		3.39	5	0.019	0.033
F508del + A1067W	-0.11	0.08		3.25	5	0.023	0.035
F508del + P1072M	-0.13	0.10		3.20	5	0.024	0.037
F508del + R1070M	0.16	0.13	↑	-3.09	5	0.027	0.038
F508del + P1072F	-0.10	0.08		2.95	5	0.032	0.040
F508del + Q1071W	-0.11	0.09		2.92	5	0.033	0.041
F508del + G1069W	-0.14	0.12		2.91	5	0.033	0.043
F508del + Q1071M	-0.14	0.13		2.79	5	0.038	0.044
F508del + R1070Y	0.12	0.12	↑	-2.58	5	0.049	0.046
F508del + F1068W	-0.07	0.08		2.36	7	0.051	0.048
F508del + L1065Q	-0.07	0.07		2.52	5	0.053	0.049
F508del + T1064F	-0.09	0.09		2.49	5	0.055	0.051
F508del + L1065M	0.05	0.05	↑	-2.47	5	0.057	0.052
F508del + Y1073F	-0.15	0.16		2.32	5	0.068	0.054
F508del + G1069M	-0.09	0.10		2.30	5	0.070	0.056
F508del + T1064H	-0.05	0.06		2.28	5	0.072	0.057
F508del + L1065H	-0.08	0.08		2.28	5	0.072	0.059
F508del + R1066V	-0.11	0.19		1.86	10	0.093	0.060
F508del + T1064Y	-0.05	0.07		1.78	5	0.135	0.062
F508del + R1070Q	-0.06	0.12		1.57	10	0.147	0.063
F508del + P1072H	-0.09	0.15		1.66	6	0.147	0.065
F508del + R1066F	-0.09	0.13		1.71	5	0.148	0.067
F508del + A141S	-0.11	0.16		1.66	5	0.157	0.068
F508del + P1072Y	-0.10	0.16		1.56	5	0.179	0.070
F508del + F1074W	-0.10	0.15		1.60	4	0.185	0.071
F508del + Y1073W	-0.08	0.13		1.47	5	0.201	0.073
F508del + F1074Y	-0.05	0.07		1.40	4	0.233	0.075
F508del + F1068H	0.04	0.08	↑	-1.26	5	0.264	0.076
F508del + Y1073Q	-0.04	0.08		1.19	6	0.278	0.078
F508del + F1074H	-0.05	0.10		1.13	4	0.322	0.079
F508del + R1097T	-0.02	0.05		1.10	5	0.322	0.081
F508del + F1068Q	-0.02	0.09		0.69	5	0.520	0.083
F508del + F1068M	0.02	0.08	↑	-0.66	5	0.538	0.084
F508del + A1067Q	-0.03	0.15	↑	-0.60	10	0.563	0.086
F508del + G1069H	-0.03	0.13		0.48	5	0.649	0.087
F508del + G1069Y	-0.02	0.11		0.48	4	0.655	0.089
F508del + R1070F	-0.02	0.10		0.45	5	0.670	0.090
F508del + Y1073H	0.01	0.08	↑	-0.41	4	0.700	0.092
F508del + P1072Q	-0.01	0.08		0.38	7	0.713	0.094
F508del + Y1073M	-0.01	0.09		0.21	4	0.843	0.095
F508del + R1070H	-0.01	0.11		0.20	5	0.847	0.097
F508del + T1064Q	0.01	0.20	↑	-0.08	7	0.938	0.098
F508del + G1069Q	0.00	0.15		0.06	10	0.957	0.100

**Table 9 One-tailed Wilcoxon Rank Sum tests (DMSO vs. forskolin)**

For every genotype the test assessed whether conductance ( $\hat{G}$ ) was significantly increased and/or whether the membrane potential ( $V_m$ ) was significantly depolarised after addition of 10  $\mu$ M forskolin compared to the DMSO control condition

	$\hat{G}$				$V_m$			
	W	z	P	sig	W	z	P	sig
WT	210	-5.17	1.20E-07	****	211	-5.14	1.41E-07	****
F508del	206	-4.69	1.33E-06	****	426	1.99	0.977	
F508del + T1064F	25	-1.92	0.028	*	41	1.00	0.842	
F508del + T1064H	16	-2.30	0.011	*	34	1.46	0.928	
F508del + T1064M	27	0.00	0.500		29	0.42	0.662	
F508del + T1064Q	37	-1.64	0.050		56	1.07	0.858	
F508del + T1064W	31	0.63	0.798		21	-1.25	0.105	
F508del + T1064Y	17	-2.09	0.018	*	29	0.42	0.662	
F508del + L1065F	32	0.84	0.852		23	-0.84	0.202	
F508del + L1065H	26	-0.21	0.417		33	1.25	0.895	
F508del + L1065M	17	-2.09	0.018	*	35	1.67	0.953	
F508del + L1065Q	33	1.04	0.895		25	-0.42	0.338	
F508del + L1065W	33	1.04	0.895		23	-0.84	0.202	
F508del + L1065Y	109	0.26	0.633		84	-1.55	0.061	
F508del + R1066F	37	0.09	0.608		39	0.64	0.739	
F508del + R1066H	29	0.21	0.662		24	-0.63	0.265	
F508del + R1066M	35	1.46	0.953		21	-1.25	0.105	
F508del + R1066Q	30	0.42	0.735		29	0.42	0.662	
F508del + R1066W	82	-0.26	0.396		74	-0.97	0.166	
F508del + R1066Y	26	-0.21	0.417		24	-0.63	0.265	
F508del + A1067F	44	0.72	0.811		38	-0.08	0.468	
F508del + A1067H	30	-1.36	0.087		39	0.08	0.532	
F508del + A1067M	21	-1.25	0.105		30	0.63	0.735	
F508del + A1067Q	120	1.10	0.879		108	0.26	0.604	
F508del + A1067W	17	-2.09	0.018	*	27	0.00	0.500	
F508del + A1067Y	26	-0.21	0.417		28	0.21	0.583	
F508del + F1068H	15	-2.51	0.006	**	20	-1.46	0.072	
F508del + F1068M	15	-2.51	0.006	**	18	-1.88	0.030	*
F508del + F1068Q	15	-2.51	0.006	**	24	-0.63	0.265	
F508del + F1068W	39	-1.36	0.087		50	0.21	0.585	
F508del + F1068Y	15	-0.72	0.235		23	1.59	0.944	
F508del + G1069F	108	0.19	0.604		97	-0.57	0.285	
F508del + G1069H	15	-2.51	0.006	**	37	2.09	0.982	
F508del + G1069M	21	-1.25	0.105		27	0.00	0.500	
F508del + G1069Q	92	-0.94	0.172		103	-0.11	0.455	
F508del + G1069W	26	-0.21	0.417		27	0.00	0.500	
F508del + G1069Y	25	0.00	0.549		23	-0.37	0.357	
F508del + R1070F	15	-2.51	0.006	**	24	-0.63	0.265	
F508del + R1070H	15	-2.51	0.006	**	32	1.04	0.852	
F508del + R1070M	15	-2.51	0.006	**	23	-0.84	0.202	
F508del + R1070Q	66	-3.84	6.21E-05	****	138	1.23	0.891	
F508del + R1070W	15	-2.51	0.006	**	15	-2.51	0.006	**
F508del + R1070Y	15	-2.51	0.006	**	16	-2.30	0.011	*
F508del + Q1071H	24	-0.63	0.265		27	0.00	0.500	
F508del + Q1071M	25	-0.42	0.338		28	0.21	0.583	
F508del + Q1071W	27	0.00	0.500		28	0.21	0.583	
F508del + Q1071Y	20	-1.46	0.072		27	0.00	0.500	
F508del + P1072F	24	-0.63	0.265		30	0.63	0.735	
F508del + P1072H	33	-0.88	0.189		42	0.56	0.712	
F508del + P1072M	18	-1.88	0.030	*	32	1.04	0.852	
F508del + P1072Q	38	-1.79	0.037	*	61	1.15	0.875	
F508del + P1072W	15	-2.51	0.006	**	32	1.04	0.852	
F508del + P1072Y	15	-2.51	0.006	**	34	1.46	0.928	
F508del + Y1073F	26	-0.21	0.417		22	-1.04	0.148	
F508del + Y1073H	18	-1.88	0.030	*	25	-0.42	0.338	
F508del + Y1073M	21	-1.25	0.105		26	-0.21	0.417	
F508del + Y1073Q	27	-2.07	0.019	*	43	0.21	0.585	
F508del + Y1073W	24	-0.63	0.265		31	0.84	0.798	
F508del + F1074H	26	-0.21	0.417		26	-0.21	0.417	
F508del + F1074M	16	-2.30	0.011	*	35	1.67	0.953	
F508del + F1074Q	26	-0.21	0.417		32	1.04	0.852	
F508del + F1074W	20	-1.10	0.135		26	0.37	0.643	
F508del + F1074Y	21	-1.25	0.105		22	-1.04	0.148	
F508del + A141S	10	-2.33	0.010	**	21	0.37	0.643	
F508del + R1097T	15	-2.51	0.006	**	27	0.00	0.500	

**Table 10** Two-tailed Wilcoxon Rank Sum tests comparing F508del without vs. with second-site mutations

Median  $\hat{G}$  and  $V_m$  after addition of 10  $\mu$ M forskolin in cells expressing F508del-CFTR with vs. without second-site mutations were compared. Arrows indicate the mutants for which the median  $\hat{G}$  /  $V_m$  was higher / more depolarised compared to the median  $\hat{G}$  /  $V_m$  of F508del-CFTR. The Benjamini-Hochberg procedure with a false discovery rate of 10 % was applied to control for family wise error rate. P-values below the critical (Q) value were considered significant.

	$\hat{G}$					$V_m$					
	W	z	P	Q	↑	W	z	P	Q	↑	
F508del + L1065Y	343	3.91	9.32E-05	0.002		F508del + G1069Q	179	-3.91	9.32E-05	0.002	↑
F508del + G1069Q	343	3.91	9.32E-05	0.003		F508del + R1070W	171	-3.32	0.001	0.003	↑
F508del + R1066W	327	3.83	1.27E-04	0.005		F508del + F1074Y	171	-3.32	0.001	0.005	↑
F508del + A1067Q	341	3.81	1.38E-04	0.006		F508del + G1069F	193	-3.24	0.001	0.006	↑
F508del + A1067F	277	3.43	0.001	0.008		F508del + F1068M	174	-3.09	0.002	0.008	↑
F508del + R1070W	171	-3.32	0.001	0.010	↑	F508del + R1070Y	174	-3.09	0.002	0.010	↑
F508del + T1064Q	275	3.30	0.001	0.011		F508del + Q1071Y	174	-3.09	0.002	0.011	↑
F508del + T1064W	260	3.24	0.001	0.013		F508del + T1064W	175	-3.02	0.003	0.013	↑
F508del + R1066Y	260	3.24	0.001	0.014		F508del + R1066Y	175	-3.02	0.003	0.014	↑
F508del + L1065F	259	3.17	0.002	0.016		F508del + R1070M	176	-2.94	0.003	0.016	↑
F508del + L1065Q	259	3.17	0.002	0.017		F508del + Q1071W	176	-2.94	0.003	0.017	↑
F508del + F1074H	259	3.17	0.002	0.019		F508del + F1074H	176	-2.94	0.003	0.019	↑
F508del + T1064M	258	3.09	0.002	0.021		F508del + R1070Q	200	-2.90	0.004	0.021	↑
F508del + L1065W	258	3.09	0.002	0.022		F508del + L1065Q	177	-2.87	0.004	0.022	↑
F508del + A1067Y	258	3.09	0.002	0.024		F508del + Y1073W	177	-2.87	0.004	0.024	↑
F508del + Q1071W	258	3.09	0.002	0.025		F508del + A1067F	182	-2.83	0.005	0.025	↑
F508del + Q1071Y	258	3.09	0.002	0.027		F508del + R1066H	178	-2.80	0.005	0.027	↑
F508del + F1074M	174	-3.09	0.002	0.029	↑	F508del + A1067H	183	-2.77	0.006	0.029	↑
F508del + L1065H	257	3.02	0.003	0.030		F508del + L1065F	179	-2.72	0.007	0.030	↑
F508del + R1066M	257	3.02	0.003	0.032		F508del + R1066W	199	-2.70	0.007	0.032	↑
F508del + R1066Q	256	2.94	0.003	0.033		F508del + F1074Q	180	-2.65	0.008	0.033	↑
F508del + A1067W	256	2.94	0.003	0.035		F508del + T1064Y	181	-2.57	0.010	0.035	↑
F508del + F1068M	176	-2.94	0.003	0.037	↑	F508del + R1070F	181	-2.57	0.010	0.037	↑
F508del + Q1071H	256	2.94	0.003	0.038		F508del + F1068Q	182	-2.50	0.013	0.038	↑
F508del + F1074Y	256	2.94	0.003	0.040		F508del + R1066M	183	-2.42	0.015	0.040	↑
F508del + P1072F	255	2.87	0.004	0.041		F508del + A1067W	183	-2.42	0.015	0.041	↑
F508del + R1097T	178	-2.80	0.005	0.043	↑	F508del + F1068H	183	-2.42	0.015	0.043	↑
F508del + G1069Y	240	2.77	0.006	0.044		F508del + G1069H	183	-2.42	0.015	0.044	↑
F508del + G1069M	253	2.72	0.007	0.046		F508del + P1072M	183	-2.42	0.015	0.046	↑
F508del + Q1071M	253	2.72	0.007	0.048		F508del + Y1073F	183	-2.42	0.015	0.048	↑
F508del + A141S	179	-2.72	0.007	0.049	↑	F508del + R1097T	183	-2.42	0.015	0.049	↑
F508del + R1070Q	208	-2.52	0.012	0.051	↑	F508del + A1067M	184	-2.35	0.019	0.051	↑
F508del + F1068Q	183	-2.42	0.015	0.052	↑	F508del + L1065H	185	-2.27	0.023	0.052	↑
F508del + G1069F	311	2.37	0.018	0.054		F508del + T1064M	188	-2.05	0.040	0.054	↑
F508del + R1066F	248	2.35	0.019	0.056		F508del + Y1073Q	200	-2.03	0.043	0.056	↑
F508del + R1070F	185	-2.27	0.023	0.057	↑	F508del + G1069W	189	-1.98	0.048	0.057	↑
F508del + A1067M	246	2.20	0.028	0.059		F508del + Y1073H	189	-1.98	0.048	0.059	↑
F508del + A1067H	256	2.03	0.042	0.060		F508del + A141S	189	-1.98	0.048	0.060	↑
F508del + R1066H	241	1.83	0.068	0.062		F508del + T1064H	190	-1.90	0.057	0.062	↑
F508del + R1070Y	191	-1.83	0.068	0.063	↑	F508del + F1074W	185	-1.83	0.067	0.063	↑
F508del + T1064F	240	1.75	0.080	0.065		F508del + F1068Y	186	-1.75	0.081	0.065	↑
F508del + T1064Y	240	1.75	0.080	0.067		F508del + L1065M	193	-1.68	0.094	0.067	↑
F508del + Y1073W	240	1.75	0.080	0.068		F508del + T1064F	194	-1.60	0.109	0.068	↑
F508del + F1074Q	240	1.75	0.080	0.070		F508del + R1066F	195	-1.53	0.127	0.070	↑
F508del + F1068H	193	-1.68	0.094	0.071	↑	F508del + P1072F	195	-1.53	0.127	0.071	↑
F508del + G1069W	239	1.68	0.094	0.073		F508del + F1074M	195	-1.53	0.127	0.073	↑
F508del + R1070M	193	-1.68	0.094	0.075	↑	F508del + L1065Y	229	-1.51	0.131	0.075	↑
F508del + P1072Q	259	1.48	0.138	0.076		F508del + A1067Y	196	-1.45	0.146	0.076	↑
F508del + P1072Y	196	-1.45	0.146	0.078	↑	F508del + G1069Y	190	-1.40	0.160	0.078	↑
F508del + Y1073H	236	1.45	0.146	0.079		F508del + L1065W	198	-1.30	0.192	0.079	↑
F508del + Y1073M	236	1.45	0.146	0.081		F508del + Y1073M	198	-1.30	0.192	0.081	↑
F508del + P1072W	200	-1.16	0.248	0.083	↑	F508del + A1067Q	234	-1.27	0.204	0.083	↑
F508del + R1070H	201	-1.08	0.280	0.084	↑	F508del + P1072H	206	-1.23	0.217	0.084	↑
F508del + F1074W	220	1.06	0.287	0.086		F508del + Q1071M	199	-1.23	0.219	0.086	↑
F508del + Y1073Q	251	1.00	0.318	0.087		F508del + Q1071H	200	-1.16	0.248	0.087	↑
F508del + T1064H	222	0.41	0.682	0.089		F508del + R1070H	201	-1.08	0.280	0.089	↑
F508del + L1065M	222	0.41	0.682	0.090		F508del + P1072W	202	-1.01	0.314	0.090	↑
F508del + G1069H	222	0.41	0.682	0.092		F508del + P1072Y	204	-0.86	0.391	0.092	↑
F508del + Y1073F	222	0.41	0.682	0.094		F508del + T1064Q	212	-0.83	0.405	0.094	↑
F508del + P1072H	220	-0.30	0.764	0.095	↑	F508del + F1068W	216	-0.57	0.571	0.095	↑
F508del + F1068Y	206	-0.04	0.966	0.097	↑	F508del + G1069M	221	0.34	0.737	0.097	↑
F508del + P1072M	215	-0.04	0.970	0.098	↑	F508del + R1066Q	218	0.11	0.911	0.098	↑
F508del + F1068W	224	-0.03	0.973	0.100	↑	F508del + P1072Q	232	-0.09	0.928	0.100	↑

## References

- Abou Alaiwa, M. H., Beer, A. M., Pezzulo, A. A., Launspach, J. L., Horan, R. A., Stoltz, D. A., Starner, T. D., Welsh, M. J., & Zabner, J. (2014). Neonates with cystic fibrosis have a reduced nasal liquid pH; A small pilot study. *Journal of Cystic Fibrosis*. <https://doi.org/10.1016/j.jcf.2013.12.006>
- Abu-Arish, A., Pandzic, E., Goepp, J., Matthes, E., Hanrahan, J. W., & Wiseman, P. W. (2015). Cholesterol Modulates CFTR Confinement in the Plasma Membrane of Primary Epithelial Cells. *Biophysical Journal*. <https://doi.org/10.1016/j.bpj.2015.04.042>
- Al-Allaf, F. A., Abduljaleel, Z., Athar, M., Taher, M. M., Khan, W., Mehmet, H., Colakogullari, M., Apostolidou, S., Bigger, B., Waddington, S., Coutelle, C., Themis, M., Al-Ahdal, M. N., Al-Mohanna, F. A., Al-Hassnan, Z. N., & Bouazzaoui, A. (2019). Modifying inter-cistronic sequence significantly enhances IRES dependent second gene expression in bicistronic vector: Construction of optimised cassette for gene therapy of familial hypercholesterolemia. *Non-Coding RNA Research*. <https://doi.org/10.1016/j.ncrna.2018.11.005>
- Alasbahi, R. H., & Melzig, M. F. (2010). *Plectranthus barbatus*: A review of phytochemistry, ethnobotanical uses and pharmacology part 1. In *Planta Medica*. <https://doi.org/10.1055/s-0029-1240898>
- Aleksandrov, L., Aleksandrov, A. A., Chang, X. B., & Riordan, J. R. (2002). The first nucleotide binding domain of cystic fibrosis transmembrane conductance regulator is a site of stable nucleotide interaction, whereas the second is a site of rapid turnover. *Journal of Biological Chemistry*. <https://doi.org/10.1074/jbc.M111713200>
- Aller, S. G., Yu, J., Ward, A., Weng, Y., Chittaboina, S., Zhuo, R., Harrell, P. M., Trinh, Y. T., Zhang, Q., Urbatsch, I. L., & Chang, G. (2009). Structure of P-glycoprotein reveals a molecular basis for poly-specific drug binding. *Science*. <https://doi.org/10.1126/science.1168750>
- Alvarez, O., & Latorre, R. (2017). The enduring legacy of the “constant-field equation” in membrane ion transport. *The Journal of General Physiology*. <https://doi.org/10.1085/jgp.201711839>
- Anderson, M. P., Berger, H. A., Rich, D. P., Gregory, R. J., Smith, A. E., & Welsh, M. J. (1991). Nucleoside

- triphosphates are required to open the CFTR chloride channel. *Cell*.  
[https://doi.org/10.1016/0092-8674\(91\)90072-7](https://doi.org/10.1016/0092-8674(91)90072-7)
- Attal, J., Théron, M. C., & Houdebine, L. M. (1999). The optimal use of IRES (internal ribosome entry site) in expression vectors. *Genetic Analysis - Biomolecular Engineering*.  
[https://doi.org/10.1016/S1050-3862\(99\)00021-2](https://doi.org/10.1016/S1050-3862(99)00021-2)
- Atwell, S., Brouillette, C. G., Conners, K., Emtage, S., Gheyi, T., Guggino, W. B., Hendle, J., Hunt, J. F., Lewis, H. A., Lu, F., Protasevich, I. I., Rodgers, L. A., Romero, R., Wasserman, S. R., Weber, P. C., Wetmore, D., Zhang, F. F., & Zhao, X. (2010). Structures of a minimal human CFTR first nucleotide-binding domain as a monomer, head-to-tail homodimer, and pathogenic mutant. *Protein Engineering, Design and Selection*. <https://doi.org/10.1093/protein/gzq004>
- Bach, S., Talarek, N., Andrieu, T., Vierfond, J. M., Mettey, Y., Galons, H., Dormont, D., Meijer, L., Cullin, C., & Blondel, M. (2003). Isolation of drugs active against mammalian prions using a yeast-based screening assay. *Nature Biotechnology*. <https://doi.org/10.1038/nbt855>
- Bai, Y., Li, M., & Hwang, T. C. (2010). Dual roles of the sixth transmembrane segment of the CFTR chloride channel in gating and permeation. *Journal of General Physiology*.  
<https://doi.org/10.1085/jgp.201010480>
- Bai, Y., Li, M., & Hwang, T. C. (2011). Structural basis for the channel function of a degraded ABC transporter, CFTR (ABCC7). *Journal of General Physiology*.  
<https://doi.org/10.1085/jgp.201110705>
- Baird, G. S., Zacharias, D. A., & Tsien, R. Y. (2000). Biochemistry, mutagenesis, and oligomerization of DsRed, a red fluorescent protein from coral. *Proceedings of the National Academy of Sciences of the United States of America*. <https://doi.org/10.1073/pnas.97.22.11984>
- Bajmocz, M., Gadjeva, M., Alper, S. L., Pier, G. B., & Golan, D. E. (2009). Cystic fibrosis transmembrane conductance regulator and caveolin-1 regulate epithelial cell internalization of *Pseudomonas aeruginosa*. *American Journal of Physiology - Cell Physiology*.  
<https://doi.org/10.1152/ajpcell.00527.2008>

- Baldwin, T. O. (2013). Chemiluminescence and Bioluminescence. In *Encyclopedia of Biological Chemistry: Second Edition*. <https://doi.org/10.1016/B978-0-12-378630-2.00006-2>
- Barriere, H., Bagdany, M., Bossard, F., Okiyoneda, T., Wojewodka, G., Gruenert, D., Radzioch, D., & Lukacs, G. L. (2009). Revisiting the role of cystic fibrosis transmembrane conductance regulator and counterion permeability in the pH regulation of endocytic organelles. *Molecular Biology of the Cell*. <https://doi.org/10.1091/mbc.E09-01-0061>
- Barsony, O., Szaloki, G., Turk, D., Tarapcsak, S., Gutay-Toth, Z., Bacso, Z., Holb, I. J., Szekvolgyi, L., Szabo, G., Csanady, L., Szakacs, G., & Goda, K. (2016). A single active catalytic site is sufficient to promote transport in P-glycoprotein. *Scientific Reports*. <https://doi.org/10.1038/srep24810>
- Bass, J. J., Wilkinson, D. J., Rankin, D., Phillips, B. E., Szewczyk, N. J., Smith, K., & Atherton, P. J. (2017). An overview of technical considerations for Western blotting applications to physiological research. In *Scandinavian Journal of Medicine and Science in Sports*. <https://doi.org/10.1111/sms.12702>
- Basso, C., Vergani, P., Nairn, A. C., & Gadsby, D. C. (2003). Prolonged nonhydrolytic interaction of nucleotide with CFTR's NH 2-terminal nucleotide binding domain and its role in channel gating. *Journal of General Physiology*. <https://doi.org/10.1085/jgp.200308798>
- Baukrowitz, T., Hwang, T. C., Nairn, A. C., & Gadsby, D. C. (1994). Coupling of CFTR Cl<sup>-</sup> channel gating to an ATP hydrolysis Cycle. *Neuron*. [https://doi.org/10.1016/0896-6273\(94\)90206-2](https://doi.org/10.1016/0896-6273(94)90206-2)
- Bear, C. E., Li, C., Kartner, N., Bridges, R. J., Jensen, T. J., Ramjeesingh, M., & Riordan, J. R. (1992). Purification and functional reconstitution of the cystic fibrosis transmembrane conductance regulator (CFTR). *Cell*. [https://doi.org/10.1016/0092-8674\(92\)90155-6](https://doi.org/10.1016/0092-8674(92)90155-6)
- Beck, E. J., Yang, Y., Yaemsiri, S., & Raghuram, V. (2008). Conformational changes in a pore-lining helix coupled to cystic fibrosis transmembrane conductance regulator channel gating. *Journal of Biological Chemistry*. <https://doi.org/10.1074/jbc.M702235200>
- Becq, F., Mettey, Y., Gray, M. A., Galletta, L. J. V., Dormer, R. L., Merten, M., Métayé, T., Chappe, V., Marvingt-Mounir, C., Zegarra-Moran, O., Tarran, R., Bulteau, L., Dérand, R., Pereira, M. M. C.,

- McPherson, M. A., Rogier, C., Joffre, M., ... Vierfond, J. M. (1999). Development of substituted benzo[c]quinolizinium compounds as novel activators of the cystic fibrosis chloride channel. *Journal of Biological Chemistry*. <https://doi.org/10.1074/jbc.274.39.27415>
- Berger, A. L., Ikuma, M., Hunt, J. F., Thomas, P. J., & Welsh, M. J. (2002). Mutations that change the position of the putative  $\gamma$ -phosphate linker in the nucleotide binding domains of CFTR alter channel gating. *Journal of Biological Chemistry*. <https://doi.org/10.1074/jbc.M109539200>
- Berger, H. A., Anderson, M. P., Gregory, R. J., Thompson, S., Howard, P. W., Maurer, R. A., Mulligan, R., Smith, A. E., & Welsh, M. J. (1991). Identification and regulation of the cystic fibrosis transmembrane conductance regulator-generated chloride channel. *Journal of Clinical Investigation*. <https://doi.org/10.1172/JCI115450>
- Berger, H. A., Travis, S. M., & Welsh, M. J. (1993). Regulation of the cystic fibrosis transmembrane conductance regulator Cl<sup>-</sup> channel by specific protein kinases and protein phosphatases. *Journal of Biological Chemistry*.
- Bevis, B. J., & Glick, B. S. (2002). Rapidly maturing variants of the *Discosoma* red fluorescent protein (DsRed). *Nature Biotechnology*. <https://doi.org/10.1038/nbt0102-83>
- Billet, A., Froux, L., Hanrahan, J. W., & Becq, F. (2017). Development of automated patch clamp technique to investigate CFTR chloride channel function. *Frontiers in Pharmacology*, *8*(195), 1–10. <https://doi.org/10.3389/fphar.2017.00195>
- Botelho, H. M., Uliyakina, I., Awatade, N. T., Proença, M. C., Tischer, C., Sirianant, L., Kunzelmann, K., Pepperkok, R., & Amaral, M. D. (2015). Protein Traffic Disorders: An Effective High-Throughput Fluorescence Microscopy Pipeline for Drug Discovery. *Scientific Reports*, *5*, 1–8. <https://doi.org/10.1038/srep09038>
- Boucher, R. C. (2007). Airway Surface Dehydration in Cystic Fibrosis: Pathogenesis and Therapy. *Annual Review of Medicine*, *58*, 157–170. <https://doi.org/10.1146/annurev.med.58.071905.105316>
- Bush, A., Alton, E. W. F. W., Davies, J. C., Griesenbach, U., & Jaffe, A. (2005). Cystic Fibrosis in the 21st

- Century. In *Progress in Respiratory Research* (Vol. 34). <https://doi.org/10.1159/isbn.978-3-318-01240-8>
- Butler, T. A. J., Paul, J. W., Chan, E. C., Smith, R., & Tolosa, J. M. (2019). Misleading westerns: Common quantification mistakes in western blot densitometry and proposed corrective measures. *BioMed Research International*. <https://doi.org/10.1155/2019/5214821>
- Cai, Z., & Sheppard, D. N. (2002). Phloxine B interacts with the cystic fibrosis transmembrane conductance regulator at multiple sites to modulate channel activity. *Journal of Biological Chemistry*, 277(22), 19546–19553. <https://doi.org/10.1074/jbc.M108023200>
- Cai, Z. W., Liu, J., Li, H. Y., & Sheppard, D. N. (2011). Targeting F508del-CFTR to develop rational new therapies for cystic fibrosis. *Acta Pharmacologica Sinica*. <https://doi.org/10.1038/aps.2011.71>
- Campbell, R. E., Tour, O., Palmer, A. E., Steinbach, P. A., Baird, G. S., Zacharias, D. A., & Tsien, R. Y. (2002). A monomeric red fluorescent protein. *Proceedings of the National Academy of Sciences of the United States of America*. <https://doi.org/10.1073/pnas.082243699>
- Carlile, G. W., Robert, R., Zhang, D., Teske, K. A., Luo, Y., Hanrahan, J. W., & Thomas, D. Y. (2007). Correctors of protein trafficking defects identified by a novel high-throughput screening assay. *ChemBioChem*, 8(9), 1012–1020. <https://doi.org/10.1002/cbic.200700027>
- Carlile, G. W., Yang, Q., Matthes, E., Liao, J., Radinovic, S., Miyamoto, C., Robert, R., Hanrahan, J. W., & Thomas, D. Y. (2018). A novel triple combination of pharmacological chaperones improves F508del-CFTR correction. *Scientific Reports*. <https://doi.org/10.1038/s41598-018-29276-y>
- Carson, M. R., Travis, S. M., & Welsh, M. J. (1995). The two nucleotide-binding domains of cystic fibrosis transmembrane conductance regulator (CFTR) have distinct functions in controlling channel activity. *Journal of Biological Chemistry*. <https://doi.org/10.1074/jbc.270.4.1711>
- Chalfie, M., Tu, Y., Euskirchen, G., Ward, W. W., & Prasher, D. C. (1994). Green fluorescent protein as a marker for gene expression. *Science*. <https://doi.org/10.1126/science.8303295>
- Chang, X. B., Hou, Y. X., Jensen, T. J., & Riordan, J. R. (1994). Mapping of cystic fibrosis transmembrane conductance regulator membrane topology by glycosylation site insertion. *Journal of Biological*

*Chemistry.*

- Chapin, H. C., & Caplan, M. J. (2010). The cell biology of polycystic kidney disease. In *Journal of Cell Biology*. <https://doi.org/10.1083/jcb.201006173>
- Chappe, V., Hinkson, D. A., Zhu, T., Chang, X. B., Riordan, J. R., & Hanrahan, J. W. (2003). Phosphorylation of protein kinase C sites in NBD1 and the R domain control CFTR channel activation by PKA. In *Journal of Physiology*. <https://doi.org/10.1113/jphysiol.2002.035790>
- Cheng, S. H., Gregory, R. J., Marshall, J., Paul, S., Souza, D. W., White, G. A., O'Riordan, C. R., & Smith, A. E. (1990). Defective intracellular transport and processing of CFTR is the molecular basis of most cystic fibrosis. *Cell*, *63*(4), 827–834. [https://doi.org/10.1016/0092-8674\(90\)90148-8](https://doi.org/10.1016/0092-8674(90)90148-8)
- Cholon, D. M., Quinney, N. L., Fulcher, M. L., Jr, C. R. E., Das, J., Dokholyan, N. V, Randell, S. H., Boucher, R. C., & Gentsch, M. (2014). Potentiator ivacaftor abrogates pharmacological correction of D F508 CFTR in cystic fibrosis. *Science Translational Medicine*, *6*(246), 1–11.
- Chong, P. A., Farber, P. J., Vernon, R. M., Hudson, R. P., Mittermaier, A. K., & Forman-kay, J. D. (2015). Deletion of Phenylalanine 508 in the First Nucleotide-binding Domain of the Cystic Fibrosis Transmembrane Conductance Regulator Increases Conformational Exchange and Inhibits. *Journal of Biological Chemistry*, *290*(38), 22862–22878. <https://doi.org/10.1074/jbc.M115.641134>
- Choudhury, H. G., Tong, Z., Mathavan, I., Li, Y., Iwata, S., Zirah, S., Rebuffat, S., Van Veen, H. W., & Beis, K. (2014). Structure of an antibacterial peptide ATP-binding cassette transporter in a novel outward occluded state. *Proceedings of the National Academy of Sciences of the United States of America*. <https://doi.org/10.1073/pnas.1320506111>
- Clancy, J. P., Rowe, S. M., Accurso, F. J., Aitken, M. L., Amin, R. S., Ashlock, M. A., Ballmann, M., Boyle, M. P., Bronsveld, I., Campbell, P. W., De Boeck, K., Donaldson, S. H., Dorkin, H. L., Dunitz, J. M., Durie, P. R., Jain, M., Leonard, A., ... Konstan, M. W. (2012). Results of a phase IIa study of VX-809, an investigational CFTR corrector compound, in subjects with cystic fibrosis homozygous for the F508del-CFTR mutation. *Thorax*, *67*(1), 12–18. <https://doi.org/10.1136/thoraxjnl-2011->

- Clunes, L. A., Davies, C. M., Coakley, R. D., Aleksandrov, A. A., Henderson, A. G., Zeman, K. L., Worthington, E. N., Gentzsch, M., Kreda, S. M., Cholon, D., Bennett, W. D., Riordan, J. R., Boucher, R. C., & Tarran, R. (2012). Cigarette smoke exposure induces CFTR internalization and insolubility, leading to airway surface liquid dehydration. *The FASEB Journal*. <https://doi.org/10.1096/fj.11-192377>
- Coakley, R. D., Grubb, B. R., Paradiso, A. M., Gatzky, J. T., Johnson, L. G., Kreda, S. M., O'Neal, W. K., & Boucher, R. C. (2003). Abnormal surface liquid pH regulation by cultured cystic fibrosis bronchial epithelium. *Proceedings of the National Academy of Sciences of the United States of America*, *100*(26), 16083–16088. <https://doi.org/10.1073/pnas.2634339100>
- Conradi Smith, G. (2019). The Current Balance Equation. In *Cellular Biophysics and Modeling: A Primer on the Computational Biology of Excitable Cells*. (pp. 132–153). Cambridge: Cambridge University Press. <https://doi.org/10.1017/9780511793905.011>
- Corradi, V., Vergani, P., & Tieleman, D. P. (2015). Cystic fibrosis transmembrane conductance regulator (CFTR):closedandopenstate channelmodels. *Journal of Biological Chemistry*. <https://doi.org/10.1074/jbc.M115.665125>
- Cotten, J. F., Ostedgaard, L. S., Carson, M. R., & Welsh, M. J. (1996). Effect of cystic fibrosis-associated mutations in the fourth intracellular loop of cystic fibrosis transmembrane conductance regulator. *Journal of Biological Chemistry*. <https://doi.org/10.1074/jbc.271.35.21279>
- Couplan, E., Aiyar, R. S., Kucharczyk, R., Kabala, A., Ezkurdia, N., Gagneur, J., St. Onge, R. P., Salin, B., Soubigou, F., Le Cann, M., Steinmetz, L. M., Di Rago, J. P., & Blondel, M. (2011). A yeast-based assay identifies drugs active against human mitochondrial disorders. *Proceedings of the National Academy of Sciences of the United States of America*. <https://doi.org/10.1073/pnas.1101478108>
- Csanády, L., Chan, K. W., Seto-Young, D., Kopsco, D. C., Nairn, A. C., & Gadsby, D. C. (2000). Severed channels probe regulation of gating of cystic fibrosis transmembrane conductance regulator by its cytoplasmic domains. *Journal of General Physiology*. <https://doi.org/10.1085/jgp.116.3.477>

- Csanády, L., & Töröcsik, B. (2019). Cystic fibrosis drug ivacaftor stimulates CFTR channels at picomolar concentrations. *ELife*. <https://doi.org/10.7554/eLife.46450>
- Csanády, L., Vergani, P., & Gadsby, D. C. (2019). Structure, Gating, and Regulation of the Cftr Anion Channel. *Physiological Reviews*, *99*(1), 707–738. <https://doi.org/10.1152/physrev.00007.2018>
- Csanády, L., Vergani, P., Gadsby, D. C., Csanady, L., Vergani, P., & Gadsby, D. C. (2010). Strict coupling between CFTR's catalytic cycle and gating of its Cl<sup>-</sup> ion pore revealed by distributions of open channel burst durations. *Proceedings of the National Academy of Sciences*, *107*(3), 1241–1246. <https://doi.org/10.1073/pnas.0911061107>
- Cui, Z., Hirata, D., Tsuchiya, E., Osada, H., & Miyakawa, T. (1996). The multidrug resistance-associated protein (MRP) subfamily (Yrs1/Yor1) of *Saccharomyces cerevisiae* is important for the tolerance to a broad range of organic anions. *Journal of Biological Chemistry*. <https://doi.org/10.1074/jbc.271.25.14712>
- Cystic Fibrosis Foundation. (2013). Cystic Fibrosis Foundation Patient Registry 2014 Annual Data Report. In *Cystic Fibrosis Foundation Patient Registry Annual Data Report. Bethesda (MD)*. <https://doi.org/10.1183/09031936.00196314.2>
- Dalemans, W., Barbry, P., Champigny, G., Jallat, S., Dott, K., Dreyer, D., Crystal, R. G., Pavirani, A., Lecocq, J. P., & Lazdunski, M. (1991). Altered chloride ion channel kinetics associated with the  $\Delta F508$  cystic fibrosis mutation. *Nature*, *354*(6354), 526–528. <https://doi.org/10.1038/354526a0>
- Dalton, J., Kalid, O., Schushan, M., Ben-Tal, N., & Villà-Freixa, J. (2012). New model of cystic fibrosis transmembrane conductance regulator proposes active channel-like conformation. *Journal of Chemical Information and Modeling*. <https://doi.org/10.1021/ci2005884>
- Davidson, A. L., & Chen, J. (2004). ATP-Binding Cassette Transporters in Bacteria. *Annual Review of Biochemistry*. <https://doi.org/10.1146/annurev.biochem.73.011303.073626>
- Davidson, A. L., Dassa, E., Orelle, C., & Chen, J. (2008). Structure, Function, and Evolution of Bacterial ATP-Binding Cassette Systems. *Microbiology and Molecular Biology Reviews*. <https://doi.org/10.1128/mnbr.00031-07>

- Davies, J. C., Alton, E. W. F. W., & Bush, A. (2007). Cystic fibrosis. In *British Medical Journal*.  
<https://doi.org/10.1136/bmj.39391.713229.AD>
- Davies, J. C., Van de Steen, O., van Koningsbruggen-Rietschel, S., Drevinek, P., Derichs, N., McKone, E. F., Kanters, D., Allamassey, L., Namour, F., de Kock, H., & Conrath, K. (2019). GLPG1837, a CFTR potentiator, in p.Gly551Asp (G551D)-CF patients: An open-label, single-arm, phase 2a study (SAPHIRA1). *Journal of Cystic Fibrosis*. <https://doi.org/10.1016/j.jcf.2019.05.006>
- Dawson, R. J. P., & Locher, K. P. (2006). Structure of a bacterial multidrug ABC transporter. *Nature*.  
<https://doi.org/10.1038/nature05155>
- Dawson, R. J. P., & Locher, K. P. (2007). Structure of the multidrug ABC transporter Sav1866 from *Staphylococcus aureus* in complex with AMP-PNP. *FEBS Letters*.  
<https://doi.org/10.1016/j.febslet.2007.01.073>
- de Hostos, E. L., Choy, R. K. M., & Nguyen, T. (2011). Developing novel antisecretory drugs to treat infectious diarrhea. In *Future medicinal chemistry*. <https://doi.org/10.4155/fmc.11.87>
- Dean, M., & Annilo, T. (2005). Evolution of the ATP-binding Cassette (ABC) Transporter Superfamily in Vertebrates. *Annual Review of Genomics and Human Genetics*.  
<https://doi.org/10.1146/annurev.genom.6.080604.162122>
- Dean, M., Rzhetsky, A., & Allikmets, R. (2001). The human ATP-binding cassette (ABC) transporter superfamily. In *Genome Research*. <https://doi.org/10.1101/gr.GR-1649R>
- Decarvalho, A. C. V., Gansheroff, L. J., & Teem, J. L. (2002). Mutations in the Nucleotide Binding Domain 1 Signature Motif Region Rescue Processing and Functional Defects of Cystic Fibrosis Transmembrane Conductance Regulator  $\Delta F508$ . *Journal of Biological Chemistry*, 277(39), 35896–35905. <https://doi.org/10.1074/jbc.M205644200>
- Decottignies, A., & Goffeau, A. (1997). Complete inventory of the yeast ABC proteins. *Nature Genetics*.  
<https://doi.org/10.1038/ng0297-137>
- Dekkers, J. F., Berkers, G., Kruisselbrink, E., Vonk, A., De Jonge, H. R., Janssens, H. M., Bronsveld, I., Van De Graaf, E. A., Nieuwenhuis, E. E. S., Houwen, R. H. J., Vleggaar, F. P., Escher, J. C., De Rijke,

- Y. B., Majoor, C. J., Heijerman, H. G. M., De Winter-De Groot, K. M., Clevers, H., ... Beekman, J. M. (2016). Characterizing responses to CFTR-modulating drugs using rectal organoids derived from subjects with cystic fibrosis. *Science Translational Medicine*. <https://doi.org/10.1126/scitranslmed.aad8278>
- Dekkers, J. F., Wiegerinck, C. L., De Jonge, H. R., Bronsveld, I., Janssens, H. M., De Winter-De Groot, K. M., Brandsma, A. M., De Jong, N. W. M., Bijvelds, M. J. C., Scholte, B. J., Nieuwenhuis, E. E. S., Van Den Brink, S., Clevers, H., Van Der Ent, C. K., Middendorp, S., & Beekman, J. M. (2013). A functional CFTR assay using primary cystic fibrosis intestinal organoids. *Nature Medicine*. <https://doi.org/10.1038/nm.3201>
- Denning, G. M., Anderson, M. P., Amara, J. F., Marshall, J., Smith, A. E., & Welsh, M. J. (1992a). Processing of mutant cystic fibrosis transmembrane conductance regulator is temperature-sensitive. *Nature*, *358*(6389), 761–764. <https://doi.org/10.1038/355242a0>
- Denning, G. M., Ostedgaard, L. S., & Welsh, M. J. (1992b). Abnormal localization of cystic fibrosis transmembrane conductance regulator in primary cultures of cystic fibrosis airway epithelia. *Journal of Cell Biology*. <https://doi.org/10.1083/jcb.118.3.551>
- Doherty, G. P., Bailey, K., & Lewis, P. J. (2010). Stage-specific fluorescence intensity of GFP and mCherry during sporulation in *Bacillus Subtilis*. *BMC Research Notes*. <https://doi.org/10.1186/1756-0500-3-303>
- Domingue, J. C., Ao, M., Sarathy, J., George, A., Alrefai, W. A., Nelson, D. J., & Rao, M. C. (2014). HEK-293 cells expressing the cystic fibrosis transmembrane conductance regulator (CFTR): A model for studying regulation of Cl<sup>-</sup> transport. *Physiological Reports*. <https://doi.org/10.14814/phy2.12158>
- Dormer, R. L., Dérand, R., McNeilly, C. M., Mettey, Y., Bulteau-Pignoux, L., Métafé, T., Vierfond, J. M., Gray, M. A., Galiotta, L. J. V., Morris, M. R., Pereira, M. M., Doull, L. J. M., Becq, F., & McPherson, M. A. (2001). Correction of delF508-CFTR activity with benzo(c)quinolizinium compounds through facilitation of its processing in cystic fibrosis airway cells. *Journal of Cell Science*.

- Dudez, T., Borot, F., Huang, S., Kwak, B. R., Bacchetta, M., Ollero, M., Stanton, B. A., & Chanson, M. (2008). CFTR in a lipid raft-TNFR1 complex modulates gap junctional intercellular communication and IL-8 secretion. *Biochimica et Biophysica Acta - Molecular Cell Research*. <https://doi.org/10.1016/j.bbamcr.2008.01.007>
- Ehrhardt, A., Chung, W. J., Pyle, L. C., Wang, W., Nowotarski, K., Mulvihill, C. M., Ramjeesingh, M., Hong, J., Velu, S. E., Lewis, H. A., Atwell, S., Aller, S., Bear, C. E., Lukacs, G. L., Kirk, K. L., & Sorscher, E. J. (2016). Channel gating regulation by the cystic fibrosis transmembrane conductance regulator (CFTR) first cytosolic loop. *Journal of Biological Chemistry*. <https://doi.org/10.1074/jbc.M115.704809>
- El Hiani, Y., & Linsdell, P. (2010). Changes in accessibility of cytoplasmic substances to the pore associated with activation of the cystic fibrosis transmembrane conductance regulator chloride channel. *Journal of Biological Chemistry*. <https://doi.org/10.1074/jbc.M110.113332>
- El Hiani, Y., & Linsdell, P. (2014). Metal bridges illuminate transmembrane domain movements during gating of the cystic fibrosis transmembrane conductance regulator chloride channel. *Journal of Biological Chemistry*. <https://doi.org/10.1074/jbc.M114.593103>
- Engelhardt, J. F., Yankaskas, J. R., Ernst, S. a, Yang, Y., Marino, C. R., Boucher, R. C., Cohn, J. a, & Wilson, J. M. (1992). Submucosal glands are the predominant site of CFTR expression in the human bronchus. *Nature Genetics*, 2(3), 240–248. <https://doi.org/10.1038/ng1192-240>
- Farinha, C. M., & Canato, S. (2017). From the endoplasmic reticulum to the plasma membrane: mechanisms of CFTR folding and trafficking. In *Cellular and Molecular Life Sciences*. <https://doi.org/10.1007/s00018-016-2387-7>
- Farinha, C. M., King-Underwood, J., Sousa, M., Correia, A. R., Henriques, B. J., Roxo-Rosa, M., Da Paula, A. C., Williams, J., Hirst, S., Gomes, C. M., & Amaral, M. D. (2013). Revertants, low temperature, and correctors reveal the mechanism of F508del-CFTR rescue by VX-809 and suggest multiple agents for full correction. *Chemistry and Biology*, 20(7), 943–955. <https://doi.org/10.1016/j.chembiol.2013.06.004>

- Farinha, C. M., Penque, D., Roxo-Rosa, M., Lukacs, G., Dormer, R., McPherson, M., Pereira, M., Bot, A. G. M., Jorna, H., Willemsen, R., De Jonge, H., Heda, G. D., Marino, C. R., Fanen, P., Hinzpeter, A., Lipecka, J., Fritsch, J., ... Amaral, M. D. (2004). Biochemical methods to assess CFTR expression and membrane localization. *Journal of Cystic Fibrosis*. <https://doi.org/10.1016/j.jcf.2004.05.017>
- Farkas, B., Tordai, H., Padányi, R., Tordai, A., Gera, J., Paragi, G., & Hegedűs, T. (2019). Discovering the chloride pathway in the CFTR channel. *Cellular and Molecular Life Sciences*. <https://doi.org/10.1007/s00018-019-03211-4>
- Fatehi, M., & Linsdell, P. (2009). Novel residues lining the CFTR Chloride channel pore identified by functional modification of introduced cysteines. *Journal of Membrane Biology*. <https://doi.org/10.1007/s00232-009-9167-3>
- Favia, M., Mancini, M. T., Bezzerri, V., Guerra, L., Laselva, O., Abbattiscianni, A. C., Debellis, L., Reshkin, S. J., Gambari, R., Cabrini, G., & Casavola, V. (2014). Trimethylangelicin promotes the functional rescue of mutant F508del CFTR protein in cystic fibrosis airway cells. *American Journal of Physiology - Lung Cellular and Molecular Physiology*. <https://doi.org/10.1152/ajplung.00305.2013>
- Fay, J. F., Aleksandrov, L. A., Jensen, T. J., Cui, L. L., Kousouros, J. N., He, L., Aleksandrov, A. A., Gingerich, D. S., Riordan, J. R., & Chen, J. Z. (2018). Cryo-EM Visualization of an Active High Open Probability CFTR Anion Channel. *Biochemistry*. <https://doi.org/10.1021/acs.biochem.8b00763>
- Fernandez Fernandez, E., De Santi, C., De Rose, V., & Greene, C. M. (2018). CFTR dysfunction in cystic fibrosis and chronic obstructive pulmonary disease. In *Expert Review of Respiratory Medicine*. <https://doi.org/10.1080/17476348.2018.1475235>
- Fields, S., & Johnston, M. (2005). Whither model organism research? In *Science*. <https://doi.org/10.1126/science.1108872>
- Flume, P. A., Liou, T. G., Borowitz, D. S., Li, H., Yen, K., Ordoñez, C. L., & Geller, D. E. (2012). Ivacaftor in subjects with cystic fibrosis who are homozygous for the F508del-CFTR mutation. *Chest*, 142(3), 718–724. <https://doi.org/10.1378/chest.11-2672>

- Frizzell, R. A., & Hanrahan, J. W. (2012). Physiology of epithelial chloride and fluid secretion. *Cold Spring Harbor Perspectives in Medicine*. <https://doi.org/10.1101/cshperspect.a009563>
- Frizzell, R. A., Rechkemmer, G., & Shoemaker, R. L. (1986). Altered regulation of airway epithelial cell chloride channels in cystic fibrosis. *Science*. <https://doi.org/10.1126/science.2425436>
- Galiotta, L. J. V., Jayaraman, S., & Verkman, A. S. (2002). *Cell-based assay for high-throughput quantitative screening of CFTR chloride transport agonists*. *0521*, 197–201.
- Galiotta, L. J. V., Springsteel, M. F., Eda, M., Niedzinski, E. J., By, K., Haddadin, M. J., Kurth, M. J., Nantz, M. H., & Verkman, A. S. (2001a). Novel CFTR Chloride Channel Activators Identified by Screening of Combinatorial Libraries Based on Flavone and Benzoquinolinium Lead Compounds. *Journal of Biological Chemistry*, *276*(23), 19723–19728. <https://doi.org/10.1074/jbc.M101892200>
- Galiotta, L. J. V., Haggie, P. M., & Verkman, A. S. (2001b). Green fluorescent protein-based halide indicators with improved chloride and iodide affinities. *FEBS Letters*, *499*(3), 220–224. [https://doi.org/10.1016/S0014-5793\(01\)02561-3](https://doi.org/10.1016/S0014-5793(01)02561-3)
- Galiotta, L. V., Jayaraman, S., & Verkman, A. S. (2001c). Cell-based assay for high-throughput quantitative screening of CFTR chloride transport agonists. *American Journal of Physiology. Cell Physiology*, *281*(5), C1734-42.
- Gallardo, H. F., Tan, C., & Sadelain, M. (1997). The internal ribosomal entry site of the encephalomyocarditis virus enables reliable coexpression of two transgenes in human primary T lymphocytes. *Gene Therapy*. <https://doi.org/10.1038/sj.gt.3300506>
- Gao, X., Bai, Y., & Hwang, T. C. (2013). Cysteine scanning of CFTR's first transmembrane segment reveals its plausible roles in gating and permeation. *Biophysical Journal*. <https://doi.org/10.1016/j.bpj.2012.12.048>
- Gao, X., & Hwang, T. C. (2015). Localizing a gate in CFTR. *Proceedings of the National Academy of Sciences of the United States of America*. <https://doi.org/10.1073/pnas.1420676112>
- Garland, A. L., Walton, W. G., Coakley, R. D., Tan, C. D., Gilmore, R. C., Hobbs, C. A., Tripathy, A., Clunes, L. A., Bencharit, S., Stutts, M. J., Betts, L., Redinbo, M. R., & Tarran, R. (2013). Molecular basis for

- pH-dependent mucosal dehydration in cystic fibrosis airways. *Proceedings of the National Academy of Sciences of the United States of America*, 110(40), 15973–15978.  
<https://doi.org/10.1073/pnas.1311999110>
- Ge, N., Muisei, C. N., Gong, X., & Linsdell, P. (2004). Direct comparison of the functional roles played by different transmembrane regions in the cystic fibrosis transmembrane conductance regulator chloride channel pore. *Journal of Biological Chemistry*. <https://doi.org/10.1074/jbc.M411935200>
- Gees, M., Musch, S., Van Der Plas, S., Wesse, A. S., Vandeveld, A., Verdonck, K., Mammoliti, O., Hwang, T. C., Sonck, K., Stouten, P., Swensen, A. M., Jans, M., Van Der Schueren, J., Nelles, L., Andrews, M., & Conrath, K. (2018). Identification and characterization of novel CFTR potentiators. *Frontiers in Pharmacology*. <https://doi.org/10.3389/fphar.2018.01221>
- Gentet, L. J., Stuart, G. J., & Clements, J. D. (2000). Direct measurement of specific membrane capacitance in neurons. *Biophysical Journal*. [https://doi.org/10.1016/S0006-3495\(00\)76293-X](https://doi.org/10.1016/S0006-3495(00)76293-X)
- Gentzsch, M., & Mall, M. A. (2018). Ion Channel Modulators in Cystic Fibrosis. *Chest*, 154(2), 383–393.  
<https://doi.org/10.1016/j.chest.2018.04.036>
- Glozman, R., Okiyoned, T., Mulvihill, C. M., Rini, J. M., Barriere, H., & Lukacs, G. L. (2009). N-glycans are direct determinants of CFTR folding and stability in secretory and endocytic membrane traffic. *Journal of Cell Biology*. <https://doi.org/10.1083/jcb.200808124>
- Goldman, D. E. (1943). Potential, impedance, and rectification in membranes. *Journal of General Physiology*. <https://doi.org/10.1085/jgp.27.1.37>
- Gomes-Alves, P., Neves, S., Coelho, A. V., & Penque, D. (2009). Low temperature restoring effect on F508del-CFTR misprocessing: A proteomic approach. *Journal of Proteomics*.  
<https://doi.org/10.1016/j.jprot.2009.09.001>
- González, J. E., Oades, K., Leychkis, Y., Harootunian, A., & Negulescu, P. A. (1999). Cell-based assays and instrumentation for screening ion-channel targets. In *Drug Discovery Today*.  
[https://doi.org/10.1016/S1359-6446\(99\)01383-5](https://doi.org/10.1016/S1359-6446(99)01383-5)
- Graham, F. L., Smiley, J., Russell, W. C., & Nairn, R. (1977). Characteristics of a human cell line

- transformed by DNA from human adenovirus type 5. *Journal of General Virology*.  
<https://doi.org/10.1099/0022-1317-36-1-59>
- Gross, L. A., Baird, G. S., Hoffman, R. C., Baldrige, K. K., & Tsien, R. Y. (2000). The structure of the chromophore within DsRed, a red fluorescent protein from coral. *Proceedings of the National Academy of Sciences of the United States of America*. <https://doi.org/10.1073/pnas.97.22.11990>
- Gunderson, K. L., & Kopito, R. R. (1994). Effects of pyrophosphate and nucleotide analogs suggest a role for ATP hydrolysis in cystic fibrosis transmembrane regulator channel gating. *Journal of Biological Chemistry*.
- Gunderson, K. L., & Kopito, R. R. (1995). Conformational states of CFTR associated with channel gating: The role of ATP binding and hydrolysis. *Cell*. [https://doi.org/10.1016/0092-8674\(95\)90310-0](https://doi.org/10.1016/0092-8674(95)90310-0)
- Guo, Y., Su, M., Su, M., McNutt, M. A., & Gu, J. (2009). Expression and distribution of cystic fibrosis transmembrane conductance regulator in neurons of the spinal cord. *Journal of Neuroscience Research*, 87(16), 3611–3619. <https://doi.org/10.1002/jnr.22154>
- Han, S. T., Rab, A., Pellicore, M. J., Davis, E. F., McCague, A. F., Evans, T. A., Joynt, A. T., Lu, Z., Cai, Z., Raraigh, K. S., Hong, J. S., Sheppard, D. N., Sorscher, E. J., & Cutting, G. R. (2018). Residual function of cystic fibrosis mutants predicts response to small molecule CFTR modulators. *JCI Insight*. <https://doi.org/10.1172/jci.insight.121159>
- Hanahan, D. (1983). Studies on transformation of Escherichia coli with plasmids. *Journal of Molecular Biology*. [https://doi.org/10.1016/S0022-2836\(83\)80284-8](https://doi.org/10.1016/S0022-2836(83)80284-8)
- Hanaoka, K., & Guggino, W. B. (2000). cAMP regulates cell proliferation and cyst formation in autosomal polycystic kidney disease cells. *Journal of the American Society of Nephrology*.
- Haws, C. M., Nepomuceno, I. B., Krouse, M. E., Wakelee, H., Law, T., Xia, Y., Nguyen, H., & Wine, J. J. (1996). Delta F508-CFTR channels: kinetics, activation by forskolin, and potentiation by xanthines. *The American Journal of Physiology*, 270, C1544–C1555.
- He, L., Aleksandrov, A. A., Serohijos, A. W. R., Hegedus, T., Aleksandrov, L. A., Cui, L., Dokholyan, N. V., & Riordan, J. R. (2008). Multiple membrane-cytoplasmic domain contacts in the cystic fibrosis

- transmembrane conductance regulator (CFTR) mediate regulation of channel gating. *Journal of Biological Chemistry*. <https://doi.org/10.1074/jbc.M803894200>
- He, L., Aleksandrov, L. A., Cui, L., Jensen, T. J., Nesbitt, K. L., & Riordan, J. R. (2010). Restoration of domain folding and interdomain assembly by second-site suppressors of the  $\Delta F508$  mutation in CFTR. *FASEB Journal: Official Publication of the Federation of American Societies for Experimental Biology*, 24(8), 3103–3112. <https://doi.org/10.1096/fj.09-141788>
- He, L., Kota, P., Aleksandrov, A. a., Cui, L., Jensen, T., Dokholyan, N. V., & Riordan, J. R. (2013). Correctors of  $\delta F508$  CFTR restore global conformational maturation without thermally stabilizing the mutant protein. *FASEB Journal*, 27(2), 536–545. <https://doi.org/10.1096/fj.12-216119>
- Heijerman, H. G. M., McKone, E. F., Downey, D. G., Van Braeckel, E., Rowe, S. M., Tullis, E., Mall, M. A., Welter, J. J., Ramsey, B. W., McKee, C. M., Marigowda, G., Moskowitz, S. M., Waltz, D., Sosnay, P. R., Simard, C., Ahluwalia, N., Xuan, F., ... Majoor, C. (2019). Efficacy and safety of the elexacaftor plus tezacaftor plus ivacaftor combination regimen in people with cystic fibrosis homozygous for the F508del mutation: a double-blind, randomised, phase 3 trial. *The Lancet*. [https://doi.org/10.1016/S0140-6736\(19\)32597-8](https://doi.org/10.1016/S0140-6736(19)32597-8)
- Hellen, U. T. C., & Sarnow, P. (2001). Internal ribosome entry sites in eukaryotic mRNA molecules  
Internal ribosome entry sites in eukaryotic mRNA molecules. *Journal of Virology*, 85(3), 49–63. <https://doi.org/10.1128/JVI.02656-12>
- Hildebrandt, E., Ding, H., Mulky, A., Dai, Q., Aleksandrov, A. A., Bajrami, B., Diego, P. A., Wu, X., Ray, M., Naren, A. P., Riordan, J. R., Yao, X., DeLucas, L. J., Urbatsch, I. L., & Kappes, J. C. (2015). A Stable Human-Cell System Overexpressing Cystic Fibrosis Transmembrane Conductance Regulator Recombinant Protein at the Cell Surface. *Molecular Biotechnology*. <https://doi.org/10.1007/s12033-014-9830-5>
- Hodgkin, A. L., & Katz, B. (1949). The effect of sodium ions on the electrical activity of the giant axon of the squid. *The Journal of Physiology*. <https://doi.org/10.1113/jphysiol.1949.sp004310>
- Hoffmann, B., Elbahnsi, A., Lehn, P., Décout, J. L., Pietrucci, F., Mornon, J. P., & Callebaut, I. (2018).

- Combining theoretical and experimental data to decipher CFTR 3D structures and functions. *Cellular and Molecular Life Sciences*. <https://doi.org/10.1007/s00018-018-2835-7>
- Hofmann, S., Janulienė, D., Mehdipour, A. R., Thomas, C., Stefan, E., Brüchert, S., Kuhn, B. T., Geertsma, E. R., Hummer, G., Tampé, R., & Moeller, A. (2019). Conformation space of a heterodimeric ABC exporter under turnover conditions. *Nature*. <https://doi.org/10.1038/s41586-019-1391-0>
- Hohl, M., Briand, C., Grütter, M. G., & Seeger, M. A. (2012). Crystal structure of a heterodimeric ABC transporter in its inward-facing conformation. *Nature Structural and Molecular Biology*. <https://doi.org/10.1038/nsmb.2267>
- Holguin, F. (2018). Triple CFTR Modulator Therapy for Cystic Fibrosis. *The New Engl and Journal of Medicine*, 379(17), 1671–1672. <https://doi.org/10.1056/NEJMe1811996>
- Hollenstein, K., Dawson, R. J., & Locher, K. P. (2007). Structure and mechanism of ABC transporter proteins. In *Current Opinion in Structural Biology*. <https://doi.org/10.1016/j.sbi.2007.07.003>
- Holleran, J. P., Glover, M. L., Peters, K. W., Bertrand, C. a, Watkins, S. C., Jarvik, J. W., & Frizzell, R. a. (2012). Pharmacological rescue of the mutant cystic fibrosis transmembrane conductance regulator (CFTR) detected by use of a novel fluorescence platform. *Molecular Medicine (Cambridge, Mass.)*, 18(1), 685–696. <https://doi.org/10.2119/molmed.2012.00001>
- Howard, M., DuVall, M. D., Devor, D. C., Dong, J. Y., Henze, K., & Frizzell, R. a. (1995). Epitope tagging permits cell surface detection of functional CFTR. *The American Journal of Physiology*, 269(6 Pt 1), C1565-76.
- Hung, L. W., Wang, I. X., Nikaido, K., Liu, P. Q., Ames, G. F. L., & Kim, S. H. (1998). Crystal structure of the ATP-binding subunit of an ABC transporter. *Nature*. <https://doi.org/10.1038/25393>
- Hutter, C. A. J., Timachi, M. H., Hürlimann, L. M., Zimmermann, I., Egloff, P., Göddeke, H., Kucher, S., Štefanić, S., Karttunen, M., Schäfer, L. V., Bordignon, E., & Seeger, M. A. (2019). The extracellular gate shapes the energy profile of an ABC exporter. *Nature Communications*. <https://doi.org/10.1038/s41467-019-09892-6>

- Hwang, T. C., Nagel, G., Nairn, A. C., & Gadsby, D. C. (1994). Regulation of the gating of cystic fibrosis transmembrane conductance regulator Cl channels by phosphorylation and ATP hydrolysis. *Proceedings of the National Academy of Sciences of the United States of America*.  
<https://doi.org/10.1073/pnas.91.11.4698>
- Hwang, T. C., Wang, F., Yang, I. C. H., & Reenstra, W. W. (1997). Genistein potentiates wild-type and  $\Delta F508$ -CFTR channel activity. *American Journal of Physiology*.  
<https://doi.org/10.1152/ajpcell.1997.273.3.c988>
- Hwang, T. C., Yeh, J. T., Zhang, J., Yu, Y. C., Yeh, H. I., & Destefano, S. (2018). Structural mechanisms of CFTR function and dysfunction. In *Journal of General Physiology*.  
<https://doi.org/10.1085/jgp.201711946>
- Hyde, S. C., Emsley, P., Hartshorn, M. J., Mimmack, M. M., Gileadi, U., Pearce, S. R., Gallagher, M. P., Gill, D. R., Hubbard, R. E., & Higgins, C. F. (1990). Structural model of ATP-binding proteing associated with cystic fibrosis, multidrug resistance and bacterial transport. *Nature*.  
<https://doi.org/10.1038/346362a0>
- Ishioka, C., Frebourg, T., Yan, Y. X., Vidal, M., Friend, S. H., Schmidt, S., & Iggo, R. (1993). Screening patients for heterozygous p53 mutations using a functional assay in yeast. *Nature Genetics*.  
<https://doi.org/10.1038/ng1093-124>
- Jang, S. K., Kräusslich, H. G., Nicklin, M. J., Duke, G. M., Palmenberg, A. C., & Wimmer, E. (1988). A segment of the 5' nontranslated region of encephalomyocarditis virus RNA directs internal entry of ribosomes during in vitro translation. *Journal of Virology*.
- Jayaraman, S., Haggie, P., Wachter, R. M., Remington, S. J., & Verkman, A. S. (2000). Mechanism and cellular applications of a green fluorescent protein-based halide sensor. *Journal of Biological Chemistry*, 275(9), 6047–6050. <https://doi.org/10.1074/jbc.275.9.6047>
- Jia, Y., Mathews, C. J., & Hanrahan, J. W. (1997). Phosphorylation by protein kinase C is required for acute activation of cystic fibrosis transmembrane conductance regulator by protein kinase A. *Journal of Biological Chemistry*. <https://doi.org/10.1074/jbc.272.8.4978>

- Johnston, & Wu. (1995). Foundations of cellular neurophysiology. In *MIT Press*.  
<https://doi.org/10.1097/00004691-199703000-00009>
- Karpowich, N., Martsinkevich, O., Millen, L., Yuan, Y. R., Dai, P. L., MacVey, K., Thomas, P. J., & Hunt, J. F. (2001). Crystal structures of the MJ1267 ATP binding cassette reveal an induced-fit effect at the ATPase active site of an ABC transporter. *Structure*. [https://doi.org/10.1016/S0969-2126\(01\)00617-7](https://doi.org/10.1016/S0969-2126(01)00617-7)
- Kartner, N., Augustinas, O., Jensen, T. J., Naismith, a L., & Riordan, J. R. (1992). Mislocalization of delta F508 CFTR in cystic fibrosis sweat gland. *Nature Genetics*, 1(5), 321–327.  
<https://doi.org/10.1038/ng0892-321>
- Katzmann, D. J., Hallstrom, T. C., Voet, M., Wysock, W., Golin, J., Volckaert, G., & Moye-Rowley, W. S. (1995). Expression of an ATP-binding cassette transporter-encoding gene (YOR1) is required for oligomycin resistance in *Saccharomyces cerevisiae*. *Molecular and Cellular Biology*.  
<https://doi.org/10.1128/mcb.15.12.6875>
- Kenakin, T. (2016). The mass action equation in pharmacology. *British Journal of Clinical Pharmacology*. <https://doi.org/10.1111/bcp.12810>
- Kim, T. K., & Eberwine, J. H. (2010). Mammalian cell transfection: The present and the future. *Analytical and Bioanalytical Chemistry*. <https://doi.org/10.1007/s00216-010-3821-6>
- Knapp, J. M., Wood, A. B., Phuan, P. W., Lodewyk, M. W., Tantillo, D. J., Verkman, A. S., & Kurth, M. J. (2012). Structure-activity relationships of cyanoquinolines with corrector-potentiator activity in Δf508 cystic fibrosis transmembrane conductance regulator protein. *Journal of Medicinal Chemistry*. <https://doi.org/10.1021/jm201372q>
- Knowles, M. R., & Boucher, R. C. (2002). Mucus clearance as a primary innate defense mechanism for mammalian airways. *Journal of Clinical Investigation*. <https://doi.org/10.1172/jci15217>
- Kopeikin, Z., Yuksek, Z., Yang, H. Y., & Bompadre, S. G. (2014). Combined effects of VX-770 and VX-809 on several functional abnormalities of F508del-CFTR channels. *Journal of Cystic Fibrosis*.  
<https://doi.org/10.1016/j.jcf.2014.04.003>

- Kowalski, M. P., & Pier, G. B. (2004). Localization of Cystic Fibrosis Transmembrane Conductance Regulator to Lipid Rafts of Epithelial Cells Is Required for *Pseudomonas aeruginosa* -Induced Cellular Activation . *The Journal of Immunology*. <https://doi.org/10.4049/jimmunol.172.1.418>
- Kulaksiz, H., Schlenker, T., Rost, D., Stiehl, A., Volkmann, M., Lehnert, T., Cetin, Y., & Stremmel, W. (2004). Guanylin Regulates Chloride Secretion in the Human Gallbladder Via the Bile Fluid. *Gastroenterology*, *126*(3), 732–740. <https://doi.org/10.1053/j.gastro.2003.11.053>
- Lakowicz, J. R. (2006). Principles of fluorescence spectroscopy. In *Principles of Fluorescence Spectroscopy*. <https://doi.org/10.1007/978-0-387-46312-4>
- Lancaster, M. A., & Knoblich, J. A. (2014). Organogenesis in a dish: Modeling development and disease using organoid technologies. In *Science*. <https://doi.org/10.1126/science.1247125>
- Langron, E. (2016). *Drug-discovery tools for cystic fibrosis : optical probes to quantify gating and trafficking of  $\Delta F508$ -CFTR* [University College London]. <https://discovery.ucl.ac.uk/id/eprint/1538676/>
- Langron, E., Prins, S., & Vergani, P. (2018). Potentiation of the cystic fibrosis transmembrane conductance regulator by VX-770 involves stabilization of the pre-hydrolytic, O 1 state. *British Journal of Pharmacology*, *175*(20), 3990–4002. <https://doi.org/10.1111/bph.14475>
- Langron, E., Simone, M. I., Delalande, C. M. S., Reymond, J. L., Selwood, D. L., & Vergani, P. (2017). Improved fluorescence assays to measure the defects associated with F508del-CFTR allow identification of new active compounds. *British Journal of Pharmacology*, *174*(7), 525–539. <https://doi.org/10.1111/bph.13715>
- Larsen, M. B., Hu, J., Frizzell, R. A., Watkins, S. C., Breum, M., Hu, J., Frizzell, R. A., Watkins, S. C., Larsen, M. B., Hu, J., Frizzell, R. A., & Watkins, S. C. (2016). Simple image-based no-wash method for quantitative detection of surface expressed CFTR. *Methods*, *96*, 40–45. <https://doi.org/10.1016/j.ymeth.2015.09.006>
- Last, N. B., Sun, S., Pham, M. C., & Miller, C. (2017). Molecular determinants of permeation in a fluoride-specific ion channel. *ELife*. <https://doi.org/10.7554/eLife.31259>

- Levental, I., Levental, K. R., & Heberle, F. A. (2020). Lipid Rafts: Controversies Resolved, Mysteries Remain. In *Trends in Cell Biology*. <https://doi.org/10.1016/j.tcb.2020.01.009>
- Lewis, H. A. A., Wang, C., Zhao, X., Hamuro, Y., Conners, K., Kearins, M. C. C., Lu, F., Sauder, J. M. M., Molnar, K. S. S., Coales, S. J. J., Maloney, P. C. C., Guggino, W. B. B., Wetmore, D. R. R., Weber, P. C. C., & Hunt, J. F. F. (2010). Structure and Dynamics of NBD1 from CFTR Characterized Using Crystallography and Hydrogen/Deuterium Exchange Mass Spectrometry. *Journal of Molecular Biology*, *396*(2), 406–430. <https://doi.org/10.1016/j.jmb.2009.11.051>
- Li, C., Ramjeesingh, M., Wang, W., Garami, E., Hewryk, M., Lee, D., Rommens, J. M., Galley, K., & Bear, C. E. (1996). ATPase activity of the cystic fibrosis transmembrane conductance regulator. *Journal of Biological Chemistry*. <https://doi.org/10.1074/jbc.271.45.28463>
- Li, H., Sheppard, D. N., & Hug, M. J. (2004). Transepithelial electrical measurements with the Ussing chamber. *Journal of Cystic Fibrosis*. <https://doi.org/10.1016/j.jcf.2004.05.026>
- Li, H., Yang, W., Mendes, F., Amaral, M. D., & Sheppard, D. N. (2012). Impact of the cystic fibrosis mutation F508del-CFTR on renal cyst formation and growth. *American Journal of Physiology - Renal Physiology*. <https://doi.org/10.1152/ajprenal.00130.2012>
- Li, M. S., Cowley, E. A., El Hiani, Y., & Linsdell, P. (2018). Functional organization of cytoplasmic portals controlling access to the cystic fibrosis transmembrane conductance regulator (CFTR) chloride channel pore. *Journal of Biological Chemistry*. <https://doi.org/10.1074/jbc.RA117.001373>
- Li, Y., & Tsien, R. W. (2012). PHTomato, a red, genetically encoded indicator that enables multiplex interrogation of synaptic activity. *Nature Neuroscience*. <https://doi.org/10.1038/nn.3126>
- Lin, S. C., Karoly, E. D., & Taatjes, D. J. (2013). The human  $\Delta$ Np53 isoform triggers metabolic and gene expression changes that activate mTOR and alter mitochondrial function. *Aging Cell*, *12*(5), 863–872. <https://doi.org/10.1111/accel.12108>
- Linsdell, P. (2001). Relationship between anion binding and anion permeability revealed by mutagenesis within the cystic fibrosis transmembrane conductance regulator chloride channel pore. *Journal of Physiology*. <https://doi.org/10.1111/j.1469-7793.2001.0051j.x>

- Linsdell, P. (2015). Metal bridges to probe membrane ion channel structure and function. In *Biomolecular Concepts*. <https://doi.org/10.1515/bmc-2015-0013>
- Linsdell, P. (2016). Anion conductance selectivity mechanism of the CFTR chloride channel. *Biochimica et Biophysica Acta (BBA) - Biomembranes*. <https://doi.org/10.1016/j.bbamem.2016.01.009>
- Linsdell, P., Evagelidis, A., & Hanrahan, J. W. (2000). Molecular determinants of anion selectivity in the cystic fibrosis transmembrane conductance regulator chloride channel pore. *Biophysical Journal*. [https://doi.org/10.1016/S0006-3495\(00\)76836-6](https://doi.org/10.1016/S0006-3495(00)76836-6)
- Linsdell, P., Tabcharani, J. a, Rommens, J. M., Hou, Y. X., Chang, X. B., Tsui, L. C., Riordan, J. R., & Hanrahan, J. W. (1997). Permeability of wild-type and mutant cystic fibrosis transmembrane conductance regulator chloride channels to polyatomic anions. *J.Gen.Physiol.*, *110*(4), 355–364.
- Liu, F., Zhang, Z., Csanády, L., Gadsby, D. C., & Chen, J. (2017). Molecular Structure of the Human CFTR Ion Channel. *Cell*, *169*(1), 85-95.e8. <https://doi.org/10.1016/j.cell.2017.02.024>
- Liu, F., Zhang, Z., Levit, A., Levring, J., Touhara, K. K., Shoichet, B. K., & Chen, J. (2019). Structural identification of a hotspot on CFTR for potentiation. *Science*. <https://doi.org/10.1126/science.aaw7611>
- Liu, J., Bihler, H., Farinha, C. M., Awatade, N. T., Romão, A. M., Mercadante, D., Cheng, Y., Musisi, I., Jantarajit, W., Wang, Y., Cai, Z., Amaral, M. D., Mense, M., & Sheppard, D. N. (2018). Partial rescue of F508del-cystic fibrosis transmembrane conductance regulator channel gating with modest improvement of protein processing, but not stability, by a dual-acting small molecule. *British Journal of Pharmacology*. <https://doi.org/10.1111/bph.14141>
- Locher, K. P. (2016). Mechanistic diversity in ATP-binding cassette (ABC) transporters. In *Nature Structural and Molecular Biology*. <https://doi.org/10.1038/nsmb.3216>
- Long, K. J., & Walsh, K. B. (1997). Iodide efflux measurements with an iodide-selective electrode: A non-radioactive procedure for monitoring cellular chloride transport. *Methods in Cell Science*. <https://doi.org/10.1023/A:1009766219974>
- Loo, T. W., Bartlett, M. C., & Clarke, D. M. (2010). The V510D suppressor mutation stabilizes DeltaF508-

- CFTR at the cell surface. *Biochemistry*, 49(30), 6352–6357. <https://doi.org/10.1021/bi100807h>
- Louie, R. J., Guo, J., Rodgers, J. W., White, R., Shah, N., Pagant, S., Kim, P., Livstone, M., Dolinski, K., McKinney, B. A., Hong, J., Sorscher, E. J., Bryan, J., Miller, E. A., & Hartman, J. L. (2012). A yeast phenomic model for the gene interaction network modulating CFTR- $\Delta$ F508 protein biogenesis. *Genome Medicine*, 4(12), 103. <https://doi.org/10.1186/gm404>
- Lukacs, G. L., Chang, X. B., Bear, C., Kartner, N., Mohamed, A., Riordan, J. R., & Grinstein, S. (1993). The  $\Delta$ F508 mutation decreases the stability of cystic fibrosis transmembrane conductance regulator in the plasma membrane: Determination of functional half-lives on transfected cells. *Journal of Biological Chemistry*, 268(29), 21592–21598.
- Lukacs, G. L., Mohamed, A., Kartner, N., Chang, X. B., Riordan, J. R., & Grinstein, S. (1994). Conformational maturation of CFTR but not its mutant counterpart ( $\Delta$ F508) occurs in the endoplasmic reticulum and requires ATP. *The EMBO Journal*, 13(24), 6076–6086. <https://doi.org/10.1002/j.1460-2075.1994.tb06954.x>
- Lukacs, G. L., & Verkman, A. S. (2012). CFTR: folding, misfolding and correcting the  $\Delta$ F508 conformational defect. *Trends in Molecular Medicine*, 18(2), 81–91. <https://doi.org/10.1016/j.molmed.2011.10.003>
- Ma, T., Thiagarajah, J. R., Yang, H., Sonawane, N. D., Folli, C., Galiotta, L. J. V., & Verkman, A. S. (2002). Thiazolidinone CFTR inhibitor identified by high-throughput screening blocks cholera toxin-induced intestinal fluid secretion. *Journal of Clinical Investigation*, 110(11), 1651–1658. <https://doi.org/10.1172/JCI0216112>
- MacKenzie, T., Gifford, A. H., Sabadosa, K. A., Quinton, H. B., Knapp, E. A., Goss, C. H., & Marshall, B. C. (2014). Longevity of patients with cystic fibrosis in 2000 to 2010 and beyond: Survival analysis of the Cystic Fibrosis Foundation Patient Registry. *Annals of Internal Medicine*. <https://doi.org/10.7326/M13-0636>
- Marshall, J., Fang, S., Ostedgaard, L. S., O’Riordan, C. R., Ferrara, D., Amara, J. F., Hoppe, H. th, Scheule, R. K., Welsh, M. J., Smith, A. E., & et al. (1994). Stoichiometry of recombinant cystic fibrosis

- transmembrane conductance regulator in epithelial cells and its functional reconstitution into cells in vitro. *J Biol Chem*, 269(4), 2987–2995. <http://www.ncbi.nlm.nih.gov/pubmed/7507932>
- Martínez-Salas, E. (1999). Internal ribosome entry site biology and its use in expression vectors. *Current Opinion in Biotechnology*, 10(5), 458–464. [https://doi.org/10.1016/S0958-1669\(99\)00010-5](https://doi.org/10.1016/S0958-1669(99)00010-5)
- Matz, M. V., Fradkov, A. F., Labas, Y. A., Savitsky, A. P., Zaraisky, A. G., Markelov, M. L., & Lukyanov, S. A. (1999). Fluorescent proteins from nonbioluminescent Anthozoa species. *Nature Biotechnology*. <https://doi.org/10.1038/13657>
- Mcananey, T. B., Zeng, W., Doe, C. F. E., Bhanji, N., Wakelin, S., Pearson, D. S., Abbyad, P., Shi, X., Boxer, S. G., & Bagshaw, C. R. (2005). Protonation , Photobleaching , and Photoactivation of Yellow Fluorescent Protein (YFP 10C): a unifying mechanism. 5510–5524.
- McCarty, N. A., & Zhang, Z. R. (2001). Identification of a region of strong discrimination in the pore of CFTR. *American Journal of Physiology - Lung Cellular and Molecular Physiology*. <https://doi.org/10.1152/ajplung.2001.281.4.l852>
- McShane, D., Davies, J. C., Davies, M. G., Bush, A., Geddes, D. M., & Alton, E. W. F. W. (2003). Airway surface pH in subjects with cystic fibrosis. *European Respiratory Journal*. <https://doi.org/10.1183/09031936.03.00027603>
- Mehmood, S., Domene, C., Forest, E., & Jault, J. M. (2012). Dynamics of a bacterial multidrug ABC transporter in the inward- and outward-facing conformations. *Proceedings of the National Academy of Sciences of the United States of America*. <https://doi.org/10.1073/pnas.1204067109>
- Mendoza, J. L., Schmidt, A., Li, Q., Caspa, E., Barrett, T., Robert, J., Feranchak, A. P., Brautigam, C. A., & Thomas, P. J. (2013). by Analyses of Evolved Sequences. 148(214), 164–174. <https://doi.org/10.1016/j.cell.2011.11.023>
- Mendoza, J. L., Schmidt, A., Li, Q., Nuvaga, E., Barrett, T., Bridges, R. J., Feranchak, A. P., Brautigam, C. A., & Thomas, P. J. (2012). Requirements for efficient correction of  $\Delta$ f508 CFTR revealed by analyses of evolved sequences. *Cell*. <https://doi.org/10.1016/j.cell.2011.11.023>

- Meng, X., Wang, Y., Wang, X., Wrennall, J. A., Rimington, T. L., Li, H., Cai, Z., Ford, R. C., & Sheppard, D. N. (2017). Two small molecules restore stability to a subpopulation of the cystic fibrosis transmembrane conductance regulator with the predominant disease-causing mutation. *Journal of Biological Chemistry*. <https://doi.org/10.1074/jbc.M116.751537>
- Mense, M., Vergani, P., White, D. M., Altberg, G., Nairn, A. C., & Gadsby, D. C. (2006). In vivo phosphorylation of CFTR promotes formation of a nucleotide-binding domain heterodimer. *EMBO Journal*. <https://doi.org/10.1038/sj.emboj.7601373>
- Middleton, P. G., Mall, M. A., Dřevínek, P., Lands, L. C., McKone, E. F., Polineni, D., Ramsey, B. W., Taylor-Cousar, J. L., Tullis, E., Vermeulen, F., Marigowda, G., McKee, C. M., Moskowitz, S. M., Nair, N., Savage, J., Simard, C., Tian, S., ... Jain, R. (2019). Elexacaftor-tezacaftor-ivacaftor for cystic fibrosis with a single Phe508del allele. *New England Journal of Medicine*. <https://doi.org/10.1056/NEJMoa1908639>
- Mizuguchi, H., Xu, Z., Ishii-Watabe, A., Uchida, E., & Hayakawa, T. (2000). IRES-Dependent Second Gene Expression Is Significantly Lower Than Cap-Dependent First Gene Expression in a Bicistronic Vector. *Molecular Therapy*. <https://doi.org/10.1006/mthe.2000.0050>
- Moon, C., Zhang, W., Sundaram, N., Yarlagadda, S., Reddy, V. S., Arora, K., Helmrath, M. A., & Naren, A. P. (2015). Drug-induced secretory diarrhea: A role for CFTR. In *Pharmacological Research*. <https://doi.org/10.1016/j.phrs.2015.08.024>
- Mornon, J. P., Hoffmann, B., Jonic, S., Lehn, P., & Callebaut, I. (2015). Full-open and closed CFTR channels, with lateral tunnels from the cytoplasm and an alternative position of the F508 region, as revealed by molecular dynamics. *Cellular and Molecular Life Sciences*. <https://doi.org/10.1007/s00018-014-1749-2>
- Mornon, J. P., Lehn, P., & Callebaut, I. (2008). Atomic model of human cystic fibrosis transmembrane conductance regulator: Membrane-spanning domains and coupling interfaces. *Cellular and Molecular Life Sciences*, 65(16), 2594–2612. <https://doi.org/10.1007/s00018-008-8249-1>
- Mountford, P. S., & Smith, A. G. (1995). Internal ribosome entry sites and dicistronic RNAs in

- mammalian transgenesis. *Trends in Genetics*, 11(5), 179–184. [https://doi.org/10.1016/S0168-9525\(00\)89040-X](https://doi.org/10.1016/S0168-9525(00)89040-X)
- Murphy, D. B., & Davidson, M. W. (2012). Fundamentals of Light Microscopy and Electronic Imaging: Second Edition. In *Fundamentals of Light Microscopy and Electronic Imaging: Second Edition*. <https://doi.org/10.1002/9781118382905>
- Negoda, A., El Hiani, Y., Cowley, E. A., & Linsdell, P. (2017). Contribution of a leucine residue in the first transmembrane segment to the selectivity filter region in the CFTR chloride channel. *Biochimica et Biophysica Acta - Biomembranes*. <https://doi.org/10.1016/j.bbamem.2017.02.014>
- Negoda, A., Hogan, M. S., Cowley, E. A., & Linsdell, P. (2019). Contribution of the eighth transmembrane segment to the function of the CFTR chloride channel pore. *Cellular and Molecular Life Sciences*. <https://doi.org/10.1007/s00018-019-03043-2>
- Neher, E., & Sakmann, B. (1976). Single-channel currents recorded from membrane of denervated frog muscle fibres. *Nature*. <https://doi.org/10.1038/260799a0>
- Newberry, R. W., & Raines, R. T. (2019). Secondary Forces in Protein Folding. *ACS Chemical Biology*. <https://doi.org/10.1021/acscchembio.9b00339>
- Nichols, D. P., & Chmiel, J. F. (2015). Inflammation and its genesis in cystic fibrosis. In *Pediatric Pulmonology*. <https://doi.org/10.1002/ppul.23242>
- Norez, C., Heda, G. D., Jensen, T., Kogan, I., Hughes, L. K., Auzanneau, C., Dérand, R., Bulteau-Pignoux, L., Li, C., Ramjeesingh, M., Li, H., Sheppard, D. N., Bear, C. E., Riordan, J. R., & Becq, F. (2004). Determination of CFTR chloride channel activity and pharmacology using radiotracer flux methods. *Journal of Cystic Fibrosis*. <https://doi.org/10.1016/j.jcf.2004.05.025>
- Odera, M., Furuta, T., Sohma, Y., & Sakurai, M. (2018). Molecular dynamics simulation study on the structural instability of the most common cystic fibrosis-associated mutant  $\Delta F508$ -CFTR. *Biophysics and Physicobiology*. [https://doi.org/10.2142/biophysico.15.0\\_33](https://doi.org/10.2142/biophysico.15.0_33)
- Okiyoneda, T., Veit, G., Dekkers, J. F., Bagdany, M., Soya, N., Xu, H., Roldan, A., Verkman, A. S., Kurth, M., Simon, A., Hegedus, T., Beekman, J. M., & Lukacs, G. L. (2013). Mechanism-based corrector

- combination restores  $\Delta$ F508-CFTR folding and function. *Nature Chemical Biology*, 9(7), 444–454.  
<https://doi.org/10.1038/nchembio.1253>
- Okiyoneda, T., Veit, G., Sakai, R., Aki, M., Fujihara, T., Higashi, M., Susuki-Miyata, S., Miyata, M., Fukuda, N., Yoshida, A., Xu, H., Apaja, P. M., & Lukacs, G. L. (2018). Chaperone-Independent Peripheral Quality Control of CFTR by RFFL E3 Ligase. *Developmental Cell*.  
<https://doi.org/10.1016/j.devcel.2018.02.001>
- Ormö, M., Cubitt, A. B., Kallio, K., Gross, L. A., Tsien, R. Y., & Remington, S. J. (1996). Crystal Structure of the Aequorea victoria Green Fluorescent Protein. *Science*, 273(1), 1392–1395.
- Oswald, C., Holland, I. B., & Schmitt, L. (2006). The motor domains of ABC-transporters: What can structures tell us? In *Naunyn-Schmiedeberg's Archives of Pharmacology*.  
<https://doi.org/10.1007/s00210-005-0031-4>
- Pagant, S., Brovman, E. Y., Halliday, J. J., & Miller, E. A. (2008). Mapping of interdomain interfaces required for the functional architecture of Yor1p, a eukaryotic ATP-binding cassette (ABC) transporter. *Journal of Biological Chemistry*, 283(39), 26444–26451.  
<https://doi.org/10.1074/jbc.M803912200>
- Pagant, S., Halliday, J. J., Kougentakis, C., & Miller, E. A. (2010). Intragenic suppressing mutations correct the folding and intracellular traffic of misfolded mutants of Yor1p, a eukaryotic drug transporter. *Journal of Biological Chemistry*, 285(47), 36304–36314.  
<https://doi.org/10.1074/jbc.M110.142760>
- Pagant, S., Kung, L., Dorrington, M., Lee, M. C. S., & Miller, E. A. (2007). Inhibiting Endoplasmic Reticulum (ER)-associated degradation of misfolded Yor1p does not permit ER export despite the presence of a diacidic sorting signal. *Molecular Biology of the Cell*.  
<https://doi.org/10.1091/mbc.E07-01-0046>
- Paumi, C. M., Chuk, M., Snider, J., Stagljar, I., & Michaelis, S. (2009). ABC Transporters in *Saccharomyces cerevisiae* and Their Interactors: New Technology Advances the Biology of the ABCC (MRP) Subfamily. *Microbiology and Molecular Biology Reviews*.

<https://doi.org/10.1128/membr.00020-09>

- Pedemonte, N., Lukacs, G. L., Du, K., Caci, E., Zegarra-moran, O., Galiotta, L. J. V., & Verkman, A. S. (2005a). Small-molecule correctors of defective  $\Delta$  F508-CFTR cellular processing identified by high-throughput screening. *The Journal of Clinical Investigation*, *115*(9), 2564–2571. <https://doi.org/10.1172/JCI24898DS1>
- Pedemonte, N., Sonawane, N. D., Taddei, A., Hu, J., Zegarra-moran, O., Suen, Y. F., Robins, L. I., Dicus, C. W., Willenbring, D., Nantz, M. H., Kurth, M. J., Galiotta, L. J. V., & Verkman, a S. (2005b). Phenylglycine and Sulfonamide Correctors of Defective  $\Delta$ F508 and G551D Cystic Fibrosis Transmembrane Conductance. *Molecular Pharmacology*, *67*(5), 1797–1807. <https://doi.org/10.1124/mol.105.010959.membrane>
- Pedemonte, N., Tomati, V., Sondo, E., Caci, E., Millo, E., Armirotti, A., Damonte, G., Zegarra-Moran, O., & Galiotta, L. J. V. (2011). Dual activity of aminoarylthiazoles on the trafficking and gating defects of the cystic fibrosis transmembrane conductance regulator chloride channel caused by cystic fibrosis mutations. *Journal of Biological Chemistry*. <https://doi.org/10.1074/jbc.M110.184267>
- Pedemonte, N., Tomati, V., Sondo, E., & Galiotta, L. J. V. (2010). Influence of cell background on pharmacological rescue of mutant CFTR. *American Journal of Physiology - Cell Physiology*. <https://doi.org/10.1152/ajpcell.00404.2009>
- Pelletier, J., & Sonenberg, N. (1988). Internal initiation of translation of eukaryotic mRNA directed by a sequence derived from poliovirus RNA. *Nature*. <https://doi.org/10.1038/334320a0>
- Pezzulo, A. A., Tang, X. X., Hoegger, M. J., Alaiwa, M. H. A., Ramachandran, S., Moninger, T. O., Karp, P. H., Wohlford-Lenane, C. L., Haagsman, H. P., van Eijk, M., Bánfi, B., Horswill, A. R., Stoltz, D. A., McCray, P. B., Welsh, M. J., Zabner, J., Abou Alaiwa, M. H., ... Zabner, J. (2012). Reduced airway surface pH impairs bacterial killing in the porcine cystic fibrosis lung. *Nature*, *487*(7405), 109–113. <https://doi.org/10.1038/nature11130>
- Phuan, P.-W., Veit, G., Tan, J. A., Finkbeiner, W. E., Lukacs, G. L., & Verkman, A. S. (2015). Potentiators of Defective  $\Delta$ F508-CFTR Gating that Do Not Interfere with Corrector Action. *Molecular*

*Pharmacology*, 88(4), 791–799. <https://doi.org/10.1124/mol.115.099689>

Phuan, P.-W. W., Veit, G., Tan, J., Roldan, A., Finkbeiner, W. E., Lukacs, G. L., & Verkman, A. S. (2014).

Synergy-Based Small-Molecule Screen Using a Human Lung Epithelial Cell Line Yields  $\Delta$ F508-CFTR Correctors That Augment VX-809 Maximal Efficacy *s. Molecular Pharmacology*, 86, 42–51. <https://doi.org/10.1124/mol.114.092478>

Phuan, P. W., Yang, B., Knapp, J. M., Wood, A. B., Lukacs, G. L., Kurth, M. J., & Verkman, A. S. (2011).

Cyanoquinolines with independent corrector and potentiator activities restore  $\Delta$ F508-cystic fibrosis transmembrane conductance regulator chloride channel function in cystic fibrosis. *Molecular Pharmacology*. <https://doi.org/10.1124/mol.111.073056>

Pind, S., Riordan, J. R., & Williams, D. B. (1994). Participation of the endoplasmic reticulum chaperone calnexin (p88, IP90) in the biogenesis of the cystic fibrosis transmembrane conductance regulator. *Journal of Biological Chemistry*, 269(17), 12784–12788.

Prasher, D. C., Eckenrode, V. K., Ward, W. W., Prendergast, F. G., & Cormier, M. J. (1992). Primary structure of the *Aequorea victoria* green-fluorescent protein. *Gene*. [https://doi.org/10.1016/0378-1119\(92\)90691-H](https://doi.org/10.1016/0378-1119(92)90691-H)

Prins, S., Langron, E., Hastings, C., Hill, E. J., Stefan, A. C., Griffin, L. D., & Vergani, P. (2020). Fluorescence assay for simultaneous quantification of CFTR ion-channel function and plasma membrane proximity. *Journal of Biological Chemistry*. <https://doi.org/10.1074/jbc.ra120.014061>

Procko, E., O'Mara, M. L., Drew Bennett, W. F., Peter Tieleman, D., & Gaudet, R. (2009). The mechanism of ABC transporters: General lessons from structural and functional studies of an antigenic peptide transporter. In *FASEB Journal*. <https://doi.org/10.1096/fj.08-121855>

Qian, F., El Hiani, Y., & Linsdell, P. (2011). Functional arrangement of the 12th transmembrane region in the CFTR chloride channel pore based on functional investigation of a cysteine-less CFTR variant. *Pflugers Archiv European Journal of Physiology*. <https://doi.org/10.1007/s00424-011-0998-2>

Rabeh, W. M., Bossard, F., Xu, H., Okiyoneda, T., Bagdany, M., Mulvihill, C. M., Du, K., Di Bernardo, S.,

- Liu, Y., Konermann, L., Roldan, A., & Lukacs, G. L. (2012). Correction of both NBD1 energetics and domain interface is required to restore  $\Delta F508$  CFTR folding and function. *Cell*, *148*(1–2), 150–163. <https://doi.org/10.1016/j.cell.2011.11.024>
- Raju, S. V., Lin, V. Y., Liu, L., McNicholas, C. M., Karki, S., Sloane, P. A., Tang, L., Jackson, P. L., Wang, W., Wilson, L., MacOn, K. J., Mazur, M., Kappes, J. C., DeLucas, L. J., Barnes, S., Kirk, K., Tearney, G. J., & Rowe, S. M. (2017). The cystic fibrosis transmembrane conductance regulator potentiator ivacaftor augments mucociliary clearance abrogating cystic fibrosis transmembrane conductance regulator inhibition by cigarette smoke. *American Journal of Respiratory Cell and Molecular Biology*. <https://doi.org/10.1165/rcmb.2016-0226OC>
- Rapedius, M., Soom, M., Shumilina, E., Schulze, D., Schönherr, R., Kirsch, C., Lang, F., Tucker, S. J., & Baukowitz, T. (2005). Long chain CoA esters as competitive antagonists of phosphatidylinositol 4,5-bisphosphate activation in Kir channels. *Journal of Biological Chemistry*. <https://doi.org/10.1074/jbc.M503503200>
- Ratner, M. (2017). FDA deems in vitro data on mutations sufficient to expand cystic fibrosis drug label. *Nature Biotechnology*. <https://doi.org/10.1038/nbt0717-606>
- Ren, H. Y., Grove, D. E., De La Rosa, O., Houck, S. A., Sopha, P., Van Goor, F., Hoffman, B. J., & Cyr, D. M. (2013). VX-809 corrects folding defects in cystic fibrosis transmembrane conductance regulator protein through action on membrane-spanning domain 1. *Molecular Biology of the Cell*, *24*(19), 3016–3024. <https://doi.org/10.1091/mbc.E13-05-0240>
- Rennolds, J., Boyaka, P. N., Bellis, S. L., & Cormet-Boyaka, E. (2008). Low temperature induces the delivery of mature and immature CFTR to the plasma membrane. *Biochemical and Biophysical Research Communications*, *366*(4), 1025–1029. <https://doi.org/10.1016/j.bbrc.2007.12.065>
- Rhoden, K. J., Cianchetta, S., Duchi, S., & Romeo, G. (2008). Fluorescence quantitation of thyrocyte iodide accumulation with the yellow fluorescent protein variant YFP-H148Q/I152L. *Analytical Biochemistry*, *373*(2), 239–246. <https://doi.org/10.1016/j.jab.2007.10.020>
- Rhoden, K. J., Cianchetta, S., Stivani, V., Portulano, C., Galiotta, L. J. V., & Romeo, G. (2007). Cell-based

- imaging of sodium iodide symporter activity with the yellow fluorescent protein variant YFP-H148Q/I152L. *American Journal of Physiology - Cell Physiology*.  
<https://doi.org/10.1152/ajpcell.00291.2006>
- Riordan, J. R., Rommens, J. M., Kerem, B. S., Alon, N. O. A. a, Rozmahel, R., Grzelczak, Z., Zielenski, J., Lok, S. I., Plavsic, N., Chou, J. L., Drumm, M. L., Iannuzzi, M. C., Collins, F. S., & Tsui, L. C. (1989). Identification the Cystic Fibrosis Gene : Cloning and Characterization of Complementary DNA. *Science*, 245, 1066–1073. <https://doi.org/10.1126/science.2475911>
- Roesch, E. A., Nichols, D. P., & Chmiel, J. F. (2018). Inflammation in cystic fibrosis: An update. In *Pediatric Pulmonology*. <https://doi.org/10.1002/ppul.24129>
- Rogers, C. S., Stoltz, D. A., Meyerholz, D. K., Ostedgaard, L. S., Rokhlina, T., Taft, P. J., Rogan, M. P., Pezzulo, A. A., Karp, P. H., Itani, O. A., Kabel, A. C., Wohlford-Lenane, C. L., Davis, G. J., Hanfland, R. A., Smith, T. L., Samuel, M., Wax, D., ... Welsh, M. J. (2008). Disruption of the CFTR gene produces a model of cystic fibrosis in newborn pigs. *Science*.  
<https://doi.org/10.1126/science.1163600>
- Rowe, S. M., Miller, S., & Sorscher, E. J. (2005). Cystic fibrosis. In *New England Journal of Medicine*.  
<https://doi.org/10.1056/NEJMra043184>
- Rowe, S. M., & Verkman, A. S. (2013). Cystic fibrosis transmembrane regulator correctors and potentiators. *Cold Spring Harbor Perspectives in Biology*.  
<https://doi.org/10.1101/cshperspect.a009761>
- Roxo-Rosa, M., Xu, Z., Schmidt, A., Neto, M., Cai, Z., Soares, C. M., Sheppard, D. N., & Amaral, M. D. (2006). Revertant mutants G550E and 4RK rescue cystic fibrosis mutants in the first nucleotide-binding domain of CFTR by different mechanisms. *Proceedings of the National Academy of Sciences of the United States of America*, 103(47), 17891–17896.  
<https://doi.org/10.1073/pnas.0608312103>
- Saint-Criq, V., & Gray, M. A. (2017). Role of CFTR in epithelial physiology. In *Cellular and Molecular Life Sciences*. <https://doi.org/10.1007/s00018-016-2391-y>

- Salas, P. J. I., Vega-Salas, D. E., Hochman, J., Rodriguez-Boulan, E., & Edidin, M. (1988). Selective anchoring in the specific plasma membrane domain: A role in epithelial cell polarity. *Journal of Cell Biology*. <https://doi.org/10.1083/jcb.107.6.2363>
- Sanderson, J. (2019). Understanding Light Microscopy. In *Understanding Light Microscopy*. <https://doi.org/10.1002/9781118696736>
- Schoumacher, R. A., Shoemaker, R. L., Halm, D. R., Tallant, E. A., Wallace, R. W., & Frizzell, R. A. (1987). Phosphorylation fails to activate chloride channels from cystic fibrosis airway cells. *Nature*. <https://doi.org/10.1038/330752a0>
- Schultz, B. D., Frizzell, R. A., & Bridges, R. J. (1999). Rescue of dysfunctional  $\Delta F508$ -CFTR chloride channel activity by IBMX. *Journal of Membrane Biology*. <https://doi.org/10.1007/s002329900537>
- Seamon, K. B., Padgett, W., & Daly, J. W. (1981). Forskolin: Unique diterpene activator of adenylate cyclase in membranes and in intact cells. *Proceedings of the National Academy of Sciences of the United States of America*. <https://doi.org/10.1073/pnas.78.6.3363>
- Seibert, F. S., Linsdell, P., Loo, T. W., Hanrahan, J. W., Clarke, D. M., & Riordan, J. R. (1996). Disease-associated mutations in the fourth cytoplasmic loop of cystic fibrosis transmembrane conductance regulator compromise biosynthetic processing and chloride channel activity. *Journal of Biological Chemistry*. <https://doi.org/10.1074/jbc.271.25.15139>
- Serohijos, A. W. R., Hegedus, T., Aleksandrov, A. A., He, L., Cui, L., Dokholyan, N. V., & Riordan, J. R. (2008). Phenylalanine-508 mediates a cytoplasmic-membrane domain contact in the CFTR 3D structure crucial to assembly and channel function. *Proceedings of the National Academy of Sciences of the United States of America*, *105*(9), 3256–3261. <https://doi.org/10.1073/pnas.0800254105>
- Shah, V. S., Meyerholz, D. K., Tang, X. X., Reznikov, L., Alaiwa, M. A., Ernst, S. E., Karp, P. H., Wohlford-Lenane, C. L., Heilmann, K. P., Leidinger, M. R., Allen, P. D., Zabner, J., McCray, P. B., Ostedgaard, L. S., Stoltz, D. A., Randak, C. O., & Welsh, M. J. (2016). Airway acidification initiates host defense

- abnormalities in cystic fibrosis mice. *Science*. <https://doi.org/10.1126/science.aad5589>
- Shan, J., Liao, J., Huang, J., Robert, R., Palmer, M. L., Fahrenkrug, S. C., O'Grady, S. M., & Hanrahan, J. W. (2012). Bicarbonate-dependent chloride transport drives fluid secretion by the human airway epithelial cell line Calu-3. *Journal of Physiology*. <https://doi.org/10.1113/jphysiol.2012.236893>
- Shaner, N. C., Campbell, R. E., Steinbach, P. A., Giepmans, B. N. G., Palmer, A. E., & Tsien, R. Y. (2004). Improved monomeric red, orange and yellow fluorescent proteins derived from *Discosoma* sp. red fluorescent protein. *Nature Biotechnology*. <https://doi.org/10.1038/nbt1037>
- Sharma, M., Pampinella, F., Nemes, C., Benharouga, M., So, J., Du, K., Bache, K. G., Papsin, B., Zerangue, N., Stenmark, H., & Lukacs, G. L. (2004). Misfolding diverts CFTR from recycling to degradation: Quality control at early endosomes. *Journal of Cell Biology*. <https://doi.org/10.1083/jcb.200312018>
- Shimomura, O., Johnson, F. H., & Saiga, Y. (1962). Extraction, Purification and Properties of Aequorin, a Bioluminescent Protein from the Luminous Hydromedusan, *Aequorea*. *Journal of Cellular and Comparative Physiology*. <https://doi.org/10.1002/jcp.1030590302>
- Shintre, C. A., Pike, A. C. W., Li, Q., Kim, J. I., Barr, A. J., Goubin, S., Shrestha, L., Yang, J., Berridge, G., Ross, J., Stansfeld, P. J., Sansom, M. S. P., Edward, A. M., Bountra, C., Marsden, B. D., Von Delft, F., Bullock, A. N., ... Carpenter, E. P. (2013). Structures of ABCB10, a human ATP-binding cassette transporter in apo- And nucleotide-bound states. *Proceedings of the National Academy of Sciences of the United States of America*. <https://doi.org/10.1073/pnas.1217042110>
- Sigoillot, M., Overtus, M., Grodecka, M., Scholl, D., Garcia-Pino, A., Laeremans, T., He, L., Pardon, E., Hildebrandt, E., Urbatsch, I., Steyaert, J., Riordan, J. R., & Govaerts, C. (2019). Domain-interface dynamics of CFTR revealed by stabilizing nanobodies. *Nature Communications*. <https://doi.org/10.1038/s41467-019-10714-y>
- Smith, S. S., Steinle, E. D., Meyerhoff, M. E., & Dawson, D. C. (1999). Cystic fibrosis transmembrane conductance regulator: Physical basis for lyotropic anion selectivity patterns. *Journal of General Physiology*. <https://doi.org/10.1085/jgp.114.6.799>

- Snyder, D. S., Tradtrantip, L., Yao, C., Kurth, M. J., & Verkman, A. S. (2011). Potent, metabolically stable benzopyrimido-pyrrolo-oxazine-dione (BPO) CFTR inhibitors for polycystic kidney disease. *Journal of Medicinal Chemistry*. <https://doi.org/10.1021/jm200505e>
- Solomon, G. M., Fu, L., Rowe, S. M., & Collawn, J. F. (2017). The therapeutic potential of CFTR modulators for COPD and other airway diseases. In *Current Opinion in Pharmacology*. <https://doi.org/10.1016/j.coph.2017.09.013>
- Solymosi, E. A., Kaestle-Gembardt, S. M., Vadász, I., Wang, L., Neye, N., Chupin, C. J. A., Rozowsky, S., Ruehl, R., Tabuchi, A., Schulz, H., Kapus, A., Morty, R. E., & Kuebler, W. M. (2013). Chloride transport-driven alveolar fluid secretion is a major contributor to cardiogenic lung edema. *Proceedings of the National Academy of Sciences of the United States of America*. <https://doi.org/10.1073/pnas.1216382110>
- Sosnay, P. R., Siklosi, K. R., Van Goor, F., Kaniecki, K., Yu, H., Sharma, N., Ramalho, A. S., Amaral, M. D., Dorfman, R., Zielenski, J., Masica, D. L., Karchin, R., Millen, L., Thomas, P. J., Patrinos, G. P., Corey, M., Lewis, M. H., ... Cutting, G. R. (2013). Defining the disease liability of variants in the cystic fibrosis transmembrane conductance regulator gene. *Nature Genetics*. <https://doi.org/10.1038/ng.2745>
- Stoddard, A., & Rolland, V. (2019). I see the light! Fluorescent proteins suitable for cell wall/apoplast targeting in *Nicotiana benthamiana* leaves. *Plant Direct*. <https://doi.org/10.1002/pld3.112>
- Stoltz, D. A., Meyerholz, D. K., Pezzulo, A. A., Ramachandran, S., Rogan, M. P., Davis, G. J., Hanfland, R. A., Wohlford-Lenane, C., Dohrn, C. L., Bartlett, J. A., Nelson IV, G. A., Eugene, C., Taft, P. J., Ludwig, P. S., Estin, M., Hornick, E. E., Launspach, J. L., ... Welsh, M. J. (2010). Cystic fibrosis pigs develop lung disease and exhibit defective bacterial eradication at birth. *Science Translational Medicine*, 2(29), 29ra31-29ra31. <https://doi.org/10.1126/scitranslmed.3000928>
- Szollosi, A., Muallem, D. R., Csanády, L., & Vergani, P. (2011). Mutant cycles at CFTR's non-canonical ATP-binding site support little interface separation during gating. *Journal of General Physiology*. <https://doi.org/10.1085/jgp.201110608>

- Tabcharani, J. A., Chang, X. B., Riordan, J. R., & Hanrahan, J. W. (1991). Phosphorylation-regulated Cl<sup>-</sup> channel in CHO cells stably expressing the cystic fibrosis gene. *Nature*.  
<https://doi.org/10.1038/352628a0>
- Teem, J. L., Berger, H. A., Ostedgaard, L. S., Rich, D. P., Tsui, L. C., & Welsh, M. J. (1993). Identification of revertants for the cystic fibrosis  $\Delta F508$  mutation using STE6-CFTR chimeras in yeast. *Cell*, 73(2), 335–346. [https://doi.org/10.1016/0092-8674\(93\)90233-G](https://doi.org/10.1016/0092-8674(93)90233-G)
- Teem, J. L., Carson, M. R., & Welsh, M. J. R. (1996). Mutation of R555 in CFTR- $\Delta F508$  enhances function and partially corrects defective processing. *Receptors and Channels*, 4(1), 63–72.
- Thiagarajah, J. R., Donowitz, M., & Verkman, A. S. (2015). Secretory diarrhoea: Mechanisms and emerging therapies. In *Nature Reviews Gastroenterology and Hepatology*.  
<https://doi.org/10.1038/nrgastro.2015.111>
- Thibodeau, P. H., Richardson, J. M., Wang, W., Millen, L., Watson, J., Mendoza, J. L., Du, K., Fischman, S., Senderowitz, H., Lukacs, G. L., Kirk, K., & Thomas, P. J. (2010). The Cystic Fibrosis-causing Mutation  $\Delta F508$  Affects Multiple Steps in Cystic Fibrosis Transmembrane Conductance Regulator Biogenesis. *Journal of Biological Chemistry*, 285(46), 35825–35835.  
<https://doi.org/10.1074/jbc.M110.131623>
- Thomas, P., & Smart, T. G. (2005). HEK293 cell line: A vehicle for the expression of recombinant proteins. *Journal of Pharmacological and Toxicological Methods*.  
<https://doi.org/10.1016/j.vascn.2004.08.014>
- Thorn, K. (2017). Genetically encoded fluorescent tags. In *Molecular Biology of the Cell*.  
<https://doi.org/10.1091/mbc.E16-07-0504>
- Tousson, a, Van Tine, B. a, Naren, a P., Shaw, G. M., & Schwiebert, L. M. (1998). Characterization of CFTR expression and chloride channel activity in human endothelia. *The American Journal of Physiology*, 275(6 Pt 1), C1555–C1564.
- Treize, A. E. O., & Buchwald, M. (1991). In vivo cell-specific expression of the cystic fibrosis transmembrane conductance receptor. *Letters to Nature*, 353, 434–437.

- Trzcińska-Daneluti, A. M., Ly, D., Huynh, L., Jiang, C., Fladd, C., & Rotin, D. (2009). High-content functional screen to identify proteins that correct F508del-CFTR function. *Molecular and Cellular Proteomics*. <https://doi.org/10.1074/mcp.M800268-MCP200>
- Tsai, M.-F., Li, M., & Hwang, T.-C. (2010). Stable ATP binding mediated by a partial NBD dimer of the CFTR chloride channel. *The Journal of General Physiology*, *135*(5), 399–414. <https://doi.org/10.1085/jgp.201010399>
- Urbatsch, I. L., Gimi, K., Wilke-Mounts, S., & Senior, A. E. (2000). Investigation of the role of glutamine-471 and glutamine-1114 in the two catalytic sites of P-glycoprotein. *Biochemistry*. <https://doi.org/10.1021/bi001220s>
- Ussing, H. H., & Zerahn, K. (1951). Active Transport of Sodium as the Source of Electric Current in the Short-circuited Isolated Frog Skin. *Acta Physiologica Scandinavica*. <https://doi.org/10.1111/j.1748-1716.1951.tb00800.x>
- Vachel, L., Norez, C., Becq, F., & Vandebrouck, C. (2013). Effect of VX-770 (Ivacaftor) and OAG on Ca<sup>2+</sup> influx and CFTR activity in G551D and F508del-CFTR expressing cells. *Journal of Cystic Fibrosis*. <https://doi.org/10.1016/j.jcf.2013.05.008>
- Van der Plas, S. E., Kelgtermans, H., De Munck, T., Martina, S. L. X., Dropsit, S., Quinton, E., De Blicck, A., Joannesse, C., Tomaskovic, L., Jans, M., Christophe, T., Van Der Aar, E., Borgonovi, M., Nelles, L., Gees, M., Stouten, P., Van der Schueren, J., ... Andrews, M. (2018). Discovery of N-(3-Carbamoyl-5,5,7,7-tetramethyl-5,7-dihydro-4H-thieno[2,3-c]pyran-2-yl)-1H-pyrazole-5-carboxamide (GLPG1837), a Novel Potentiator Which Can Open Class III Mutant Cystic Fibrosis Transmembrane Conductance Regulator (CFTR) Channels to a High. *Journal of Medicinal Chemistry*. <https://doi.org/10.1021/acs.jmedchem.7b01288>
- Van Goor, F., Hadida, S., Grootenhuis, P. D. J. J., Burton, B., Cao, D., Neuberger, T., Turnbull, A., Singh, A., Joubran, J., Hazlewood, A., Zhou, J., McCartney, J., Arumugam, V., Decker, C., Yang, J., Young, C., Olson, E. R., ... Negulescu, P. (2009). Rescue of CF airway epithelial cell function in vitro by a CFTR potentiator, VX-770. *Proceedings of the National Academy of Sciences*, *106*(44), 18825–

18830. <https://doi.org/10.1073/pnas.0904709106>

- Van Goor, F., Hadida, S., Grootenhuis, P. D. J. J., Burton, B., Stack, J. H., Straley, K. S., Decker, C. J., Miller, M., McCartney, J., Olson, E. R., Wine, J. J., Frizzell, R. A., Ashlock, M., & Negulescu, P. A. (2011). Correction of the F508del-CFTR protein processing defect in vitro by the investigational drug VX-809. *Proceedings of the National Academy of Sciences*, *108*(46), 18843–18848. <https://doi.org/10.1073/pnas.1105787108>
- Van Goor, F., Straley, K. S., Cao, D., González, J., Hadida, S., Hazlewood, A., Joubran, J., Knapp, T., Makings, L. R., Miller, M., Neuberger, T., Olson, E., Panchenko, V., Rader, J., Singh, A., Stack, J. H., Tung, R., ... Negulescu, P. (2006). Rescue of  $\Delta$ F508-CFTR trafficking and gating in human cystic fibrosis airway primary cultures by small molecules. *American Journal of Physiology. Lung Cellular and Molecular Physiology*, *290*(6), L1117-30. <https://doi.org/10.1152/ajplung.00169.2005>
- Van Goor, F., Yu, H., Burton, B., & Hoffman, B. J. (2014). Effect of ivacaftor on CFTR forms with missense mutations associated with defects in protein processing or function. *Journal of Cystic Fibrosis*. <https://doi.org/10.1016/j.jcf.2013.06.008>
- Varga, K., Goldstein, R. F., Jurkuvenaite, A., Chen, L., Matalon, S., Sorscher, E. J., Bebok, Z., & Collawn, J. F. (2008). Enhanced cell-surface stability of rescued  $\Delta$ F508 cystic fibrosis transmembrane conductance regulator (CFTR) by pharmacological chaperones. *The Biochemical Journal*, *410*(3), 555–564. <https://doi.org/10.1042/BJ20071420>
- Varga, K., Jurkuvenaite, A., Wakefield, J., Hong, J. S., Guimbellot, J. S., Venglarik, C. J., Niraj, A., Mazur, M., Sorscher, E. J., Collawn, J. F., & Bebok, Z. (2004). Efficient intracellular processing of the endogenous cystic fibrosis transmembrane conductance regulator in epithelial cell lines. *Journal of Biological Chemistry*, *279*(21), 22578–22584. <https://doi.org/10.1074/jbc.M401522200>
- Veit, G., Avramescu, R. G., Perdomo, D., Phuan, P.-W., Bagdany, M., Apaja, P. M., Borot, F., Szollosi, D., Wu, Y.-S., Finkbeiner, W. E., Hegedus, T., Verkman, a. S., & Lukacs, G. L. (2014). Some gating potentiators, including VX-770, diminish F508-CFTR functional expression. *Science Translational Medicine*, *6*(246), 246ra97-246ra97. <https://doi.org/10.1126/scitranslmed.3008889>

- Vergani, P., Lockless, S. W., Nairn, A. C., & Gadsby, D. C. (2005). CFTR channel opening by ATP-driven tight dimerization of its nucleotide-binding domains. *Nature*, *433*(7028), 876–880. <https://doi.org/10.1038/nature03313>
- Vergani, P., Nairn, A. C., & Gadsby, D. C. (2003). *On the Mechanism of MgATP-dependent Gating of CFTR Cl<sup>-</sup> Channels*. *120*(January). <https://doi.org/10.1085/jgp.20028673>
- Vij, N., Mazur, S., & Zeitlin, P. L. (2009). CFTR is a negative regulator of NFκB mediated innate immune response. *PLoS ONE*. <https://doi.org/10.1371/journal.pone.0004664>
- Wachter, R. M., Elsliger, M., Kallio, K., Hanson, G. T., & Remington, S. J. (1998). Structural basis of spectral shifts in the yellow-emission variants of green fluorescent protein. *Structure*, *6*(10), 1267–1277. [https://doi.org/10.1016/S0969-2126\(98\)00127-0](https://doi.org/10.1016/S0969-2126(98)00127-0)
- Wachter, R. M., & Remington, S. J. (1999). Sensitivity of the yellow variant of green fluorescent protein to halides and nitrate [2]. *Current Biology*, *9*(17), 628–629. [https://doi.org/10.1016/S0960-9822\(99\)80408-4](https://doi.org/10.1016/S0960-9822(99)80408-4)
- Wachter, R. M., Watkins, J. L., & Kim, H. (2010). Mechanistic diversity of red fluorescence acquisition by GFP-like proteins. *Biochemistry*. <https://doi.org/10.1021/bi100901h>
- Wachter, R. M., Yarbrough, D., Kallio, K., & Remington, S. J. (2000). Crystallographic and energetic analysis of binding of selected anions to the yellow variants of green fluorescent protein. *Journal of Molecular Biology*, *301*(1), 157–171. <https://doi.org/10.1006/jmbi.2000.3905>
- Wall, M. A., Socolich, M., & Ranganathan, R. (2000). The structural basis for red fluorescence in the tetrameric GFP homolog DsRed. *Nature Structural Biology*. <https://doi.org/10.1038/81992>
- Wang, C., Karpowich, N., Hunt, J. F., Rance, M., & Palmer, A. G. (2004). Dynamics of ATP-binding cassette contribute to allosteric control, nucleotide binding and energy transduction in ABC transporters. *Journal of Molecular Biology*. <https://doi.org/10.1016/j.jmb.2004.07.001>
- Wang, L., Johnson, Z. L., Wasserman, M. R., Levring, J., Chen, J., & Liu, S. (2020). Characterization of the kinetic cycle of an ABC transporter by single-molecule and cryo-EM analyses. *ELife*. <https://doi.org/10.7554/eLife.56451>

- Wang, W., El Hiani, Y., Rubaiy, H. N., & Linsdell, P. (2014). Relative contribution of different transmembrane segments to the CFTR chloride channel pore. *Pflugers Archiv European Journal of Physiology*. <https://doi.org/10.1007/s00424-013-1317-x>
- Wang, W., Hiani, Y. El, & Linsdell, P. (2011). Alignment of transmembrane regions in the cystic fibrosis transmembrane conductance regulator chloride channel pore. *Journal of General Physiology*. <https://doi.org/10.1085/jgp.201110605>
- Wang, W., Hong, J. S., Rab, A., Sorscher, E. J., & Kirk, K. L. (2016). Robust stimulation of W1282X-CFTR channel activity by a combination of allosteric modulators. *PLoS ONE*. <https://doi.org/10.1371/journal.pone.0152232>
- Wang, X., Koulov, A. V., Kellner, W. A., Riordan, J. R., & Balch, W. E. (2008). Chemical and Biological Folding Contribute to Temperature-Sensitive  $\Delta F508$  CFTR Trafficking. *Traffic*, *9*(11), 1878–1893. <https://doi.org/10.1111/j.1600-0854.2008.00806.x>
- Wang, Y., Cai, Z., Gosling, M., Sheppard, D. N., & Sheppard, X. D. N. (2018). Potentiation of the cystic fibrosis transmembrane conductance regulator Cl<sup>-</sup> channel by ivacaftor is temperature independent. *American Journal of Physiology - Lung Cellular and Molecular Physiology*, *315*, 846–857. <https://doi.org/10.1152/ajplung.00235.2018>
- Wang, Y., Loo, T. W., Bartlett, M. C., & Clarke, D. M. (2007). Correctors promote maturation of Cystic Fibrosis Transmembrane conductance Regulator (CFTR)-processing mutants by binding to the protein. *Journal of Biological Chemistry*, *282*(46), 33247–33251. <https://doi.org/10.1074/jbc.C700175200>
- Ward, A., Reyes, C. L., Yu, J., Roth, C. B., & Chang, G. (2007). Flexibility in the ABC transporter MsbA: Alternating access with a twist. *Proceedings of the National Academy of Sciences of the United States of America*. <https://doi.org/10.1073/pnas.0709388104>
- Ward, C. L., & Kopito, R. R. (1994). Intracellular turnover of cystic fibrosis transmembrane conductance regulator. Inefficient processing and rapid degradation of wild-type and mutant proteins. *Journal of Biological Chemistry*, *269*(41), 25710–25718.

- Ward, C. L., Omura, S., & Kopito, R. R. (1995). Degradation of CFTR by the ubiquitin-proteasome pathway. *Cell*, 83(1), 121–127. [https://doi.org/10.1016/0092-8674\(95\)90240-6](https://doi.org/10.1016/0092-8674(95)90240-6)
- Wei, S., Roessler, B. C., Icyuz, M., Chauvet, S., Tao, B., Hartman, J. L., & Kirk, K. L. (2016). Long-range coupling between the extracellular gates and the intracellular ATP binding domains of multidrug resistance protein pumps and cystic fibrosis transmembrane conductance regulator channels. *FASEB Journal*. <https://doi.org/10.1096/fj.15-278382>
- Welsh, M. J., & Liedtke, C. M. (1986). Chloride and potassium channels in cystic fibrosis airway epithelia. *Nature*. <https://doi.org/10.1038/322467a0>
- Wen, M. X., Qi, X. S., Wen, Y. C., Chen, X. Z., Ni, Y., Rowlands, D. K., Guo, Y. L., Zhu, H., Ze, G. M., Xiao, F. W., Zhang, H. C., Si, C. Z., Hong, S. D., Xiao, H. Z., Yiu, W. C., Yu, Y. Y., Wan, X. Y., & Hsiao, C. C. (2007). Cystic fibrosis transmembrane conductance regulator is vital to sperm fertilizing capacity and male fertility. *Proceedings of the National Academy of Sciences of the United States of America*. <https://doi.org/10.1073/pnas.0609253104>
- Wieczorek, G., & Zielenkiewicz, P. (2008).  $\Delta F508$  mutation increases conformational flexibility of CFTR protein. *Journal of Cystic Fibrosis*. <https://doi.org/10.1016/j.jcf.2007.11.008>
- Wills, N. K., Reuss, L., & Luis, S. A. (1996). *Epithelial transport : a guide to methods and experimental analysis* (1st ed). Chapman & Hall.
- Xu, S., & Hu, H. Y. (2018). Fluorogen-activating proteins: beyond classical fluorescent proteins. In *Acta Pharmaceutica Sinica B*. <https://doi.org/10.1016/j.apsb.2018.02.001>
- Yang, H., Shelat, A. A., Guy, R. K., Gopinath, V. S., Ma, T., Du, K., Lukacs, G. L., Taddei, A., Folli, C., Pedemonte, N., Galiotta, L. J. V., & Verkman, A. S. (2003). Nanomolar affinity small molecule correctors of defective  $\Delta F508$ -CFTR chloride channel gating. *Journal of Biological Chemistry*, 278(37), 35079–35085. <https://doi.org/10.1074/jbc.M303098200>
- Yang, Y., Raper, S. E., Cohn, J. A., Engelhardt, J. F., & Wilson, J. M. (1993). An approach for treating the hepatobiliary disease of cystic fibrosis by somatic gene transfer. *Proc.Natl.Acad.Sci.U.S.A.*, 90(10), 4601–4605.

- Yu, H., Burton, B., Huang, C. J., Worley, J., Cao, D., Johnson, J. P., Urrutia, A., Joubran, J., Seepersaud, S., Sussky, K., Hoffman, B. J., & Van Goor, F. (2012). Ivacaftor potentiation of multiple CFTR channels with gating mutations. *Journal of Cystic Fibrosis*. <https://doi.org/10.1016/j.jcf.2011.12.005>
- Zaidi, T., Bajmoczi, M., Zaidi, T., Golan, D. E., & Pier, G. B. (2008). Disruption of CFTR-dependent lipid rafts reduces bacterial levels and corneal disease in a murine model of pseudomonas aeruginosa keratitis. *Investigative Ophthalmology and Visual Science*. <https://doi.org/10.1167/iovs.07-0993>
- Zeltwanger, S., Wang, F., Wang, G. T., Gillis, K. D., & Hwang, T. C. (1999). Gating of cystic fibrosis transmembrane conductance regulator chloride channels by adenosine triphosphate hydrolysis: Quantitative analysis of a cyclic gating scheme. *Journal of General Physiology*. <https://doi.org/10.1085/jgp.113.4.541>
- Zhang, J., & Hwang, T. C. (2015). The Fifth Transmembrane Segment of Cystic Fibrosis Transmembrane Conductance Regulator Contributes to Its Anion Permeation Pathway. *Biochemistry*. <https://doi.org/10.1021/acs.biochem.5b00427>
- Zhang, J., Wang, Y., Jiang, X., & Chan, H. C. (2018a). Cystic fibrosis transmembrane conductance regulator—emerging regulator of cancer. In *Cellular and Molecular Life Sciences*. <https://doi.org/10.1007/s00018-018-2755-6>
- Zhang, W., Fujii, N., & Naren, A. P. (2012). Recent advances and new perspectives in targeting CFTR for therapy of cystic fibrosis and enterotoxin-induced secretory diarrheas. In *Future Medicinal Chemistry*. <https://doi.org/10.4155/fmc.12.1>
- Zhang, X., Smith, D. L., Meriin, A. B., Engemann, S., Russel, D. E., Roark, M., Washington, S. L., Maxwell, M. M., Lawrence Marsh, J., Thompson, L. M., Wanker, E. E., Young, A. B., Housman, D. E., Bates, G. P., Sherman, M. Y., & Kazantsev, A. G. (2005). A potent small molecule inhibits polyglutamine aggregation in Huntington's disease neurons and suppresses neurodegeneration in vivo. *Proceedings of the National Academy of Sciences of the United States of America*. <https://doi.org/10.1073/pnas.0408936102>

- Zhang, Z., & Chen, J. (2016). Atomic Structure of the Cystic Fibrosis Transmembrane Conductance Regulator. *Cell*, *167*, 1586–1597. <https://doi.org/10.1016/j.cell.2016.11.014>
- Zhang, Z., Liu, F., & Chen, J. (2017). Conformational Changes of CFTR upon Phosphorylation and ATP Binding. *Cell*. <https://doi.org/10.1016/j.cell.2017.06.041>
- Zhang, Z., Liu, F., & Chen, J. (2018b). Molecular structure of the ATP-bound, phosphorylated human CFTR. *Proceedings of the National Academy of Sciences of the United States of America*. <https://doi.org/10.1073/pnas.1815287115>
- Zhao, R., Liang, X., Zhao, M., Liu, S. L., Huang, Y., Idell, S., Li, X., & Ji, H. L. (2014). Correlation of apical fluid-regulating channel proteins with lung function in human COPD lungs. *PLoS ONE*. <https://doi.org/10.1371/journal.pone.0109725>